Technische Universität München
TUM School for Natural Sciences

Investigation of functional and structural divergence of the Hsp16 chaperone family in *Caenorhabditis elegans*

Yevheniia Bushman

Vollständiger Abdruck der von der TUM School of Natural Sciences der Technischen Universität München zur Erlangung einer

Doktorin der Naturwissenschaften (Dr. rer. Nat.)

genehmigten Dissertation.

Vorsitz: Prof. Dr. Matthias Feige

Prüfer*innen der Dissertation:

1. Prof. Dr. Johannes Buchner
2. Prof. Dr. Bernd Reif

Die Dissertation wurde am 26.09.2022 bei der Technischen Universität München eingereicht und durch die TUM School for Natural Sciences am 08.12.2022 angenommen.

“You have evolved from worm to man, but much within you is still worm”

by Friedrich Nietzsche

Contents

Abstract

The proteins are preserved in the cell via protein homeostasis. During a cellular stress, the integrity of the proteome is disturbed. The molecular chaperones, the ATP-dependent and ATP-independent, are the key players of a proteostasis. The roles of the ATP-dependent proteins, such as Hsp60, Hsp70, Hsp90, Hsp100, are well defined. Although we know that ATP-independent small heat shock proteins (sHsp) protect unfolding substrate proteins, the molecular mechanisms of their roles are yet elusive. In this study, a family of the highly homologous proteins of the Hsp16 family in *Caenorhabditis elegans* were analysed. They were investigated in regards of the structure and functions with a special interest in the high homology of up to 93% between these chaperones.

This study revealed that a homology of the Hsp16s has driven the functional and structural division of this family into the homologous pairs. Hsp16.1 and Hsp16.2, as well as, Hsp16.41 and Hsp16.48 show a pair-wise division in regards of their structure and a chaperone activity. For example, the sizes of the oligomers were similar within the pairs and each pair had either holdase or aggregase activity *in vitro*.

Using a proteomics approach, it was revealed that a temperature has shaped the interactomes of these molecular chaperones. The numerous interaction partners were different in their biological functions and cellular localisation. Thus, Hsp16s are involved in various proteostasis mechanisms and potentially other house-keeping events, such as metabolic processes, development and reproduction. The overlap of the interactors for each Hsp16 is high at the same elevated or permissive temperature, with many shared substrates. However, interactome shifts towards different interactors once temperature changes. Interestingly, the chaperone activity was not altered at permissive temperature and does not require dissociation of the

oligomers into smaller species. Moreover, the FRET experiments confirmed that Hsp16s communicate with each other *in vitro* as well as with the two members of Hsp12 family, implying that the last may modulate the activity of the Hsp16 family.

This study presents a detailed and systematic characterisation of the homologous family of the molecular chaperones – Hsp16s. It shows that Hsp16s evolved into a family of homologous and communicative proteins with to expand the interactome, thus, chaperone network.

Zusammenfassung

Die Proteine werden in der Zelle durch Proteinhomöostase erhalten. Während eines zellulären Stresses ist die Integrität des Proteoms gestört. Die molekularen Chaperone, die ATP-abhängigen und ATP-unabhängigen, sind die Hauptakteure der Proteostase. Die Rolle der ATP-abhängigen Proteine, wie Hsp60, Hsp70, Hsp90 und Hsp100, ist gut definiert. Obwohl wir wissen, dass ATP-unabhängige kleine Hitzeschockproteine (sHsp) die Entfaltung von Substratproteinen schützen, sind die molekularen Mechanismen ihrer Rolle noch nicht geklärt. In dieser Studie wurde eine Familie von hoch homologen Proteinen der Hsp16-Familie in Caenorhabditis elegans analysiert. Sie wurden im Hinblick auf ihre Struktur und Funktionen untersucht, wobei die hohe Homologie von bis zu 93 % zwischen diesen Chaperonen von besonderem Interesse war.

Diese Studie ergab, dass die Homologie der Hsp16 die funktionelle und strukturelle Aufteilung dieser Familie in homologe Paare bewirkt hat. Hsp16.1 und Hsp16.2 sowie Hsp16.41 und Hsp16.48 zeigen eine paarweise Aufteilung in Bezug auf ihre Struktur und Chaperonaktivität. So waren beispielsweise die Größen der Oligomere innerhalb der Paare ähnlich und jedes Paar hatte in vitro entweder Holdase- oder Aggregase-Aktivität.

Mithilfe eines Proteomics-Ansatzes wurde festgestellt, dass die Interaktome dieser molekularen Chaperone durch Temperatur definiert ist. Die zahlreichen Interaktionspartner unterschieden sich in ihren biologischen Funktionen und ihrer zellulären Lokalisierung. So sind die Hsp16 an verschiedenen Proteostasemechanismen und möglicherweise an anderen Haushaltsvorgängen wie Stoffwechselprozessen, Entwicklung und Fortpflanzung beteiligt. Die Überlappung der Interaktoren für jedes Hsp16 ist bei der gleichen erhöhten oder permissiven

Temperatur hoch, mit vielen gemeinsamen Substraten. Sobald sich jedoch die Temperatur ändert, verschiebt sich das Interaktom hin zu anderen Interaktionspartern. Interessanterweise wurde die Chaperonaktivität bei permissiver Temperatur nicht verändert und erfordert keine Dissoziation der Oligomere in kleinere Spezies. Darüber hinaus bestätigten die FRET-Experimente, dass Hsp16 in vitro sowohl miteinander als auch mit den beiden Mitgliedern der Hsp12-Familie kommunizieren, was darauf hindeutet, dass letztere die Aktivität der Hsp16-Familie modulieren können.

In dieser Studie wird eine detaillierte und systematische Charakterisierung der homologen Familie der molekularen Chaperone - Hsp16s - vorgestellt. Sie zeigt, dass sich die Hsp16s zu einer Familie homologer und kommunikativer Proteine entwickelt haben, die das Interaktom und damit das Chaperon-Netzwerk erweitern.

I. Introduction

Protein homeostasis

Proteostasis (protein homeostasis) is regulated by a sophisticated network of components that act to preserve proteins in the correct subcellular location, right concentration and confirmation. These aspects are achieved by the cooperative work of the network and results in the stability and functioning of the proteome (Clausen et al., 2019). The disturbance of proteome integrity is linked to disease development and aging (Calloni et al., 2020) as proteins participate in nearly all processes in the cell to preserve the cellular functions, healthspan and response to stress.

In all organisms the proteome is a dynamic equilibrium in which protein folding is balanced with degradation. Correct folding and protein stability are key aspects of the proteome balance (Balch et al., 2008). The amino acid sequence defines protein structure and function. This statement was supported by Afinsen's *in vitro* experiments on the folding of ribonuclease A (Anfinsen et al., 1961). To become fully functional, a protein has to obtain a native folded state. Such a state is highly dynamic as proteins continuously unfold and fold back (Sekhar and Kay, 2019).

In many cases, proteins can adopt several stable confirmations, which is often influenced by the environment. Such variability can impact biological processes in both positive and harmful ways. In such harmful cases, the "misfoded" state often results in aggregate (amorphous polymer) or amyloid (fibril polymer) (Dobson, 2001; Powers et al., 2009; Fox and Yamamoto, 2015; Whitney et al., 2019). Protein misfolding is linked to a variety of diseases, including neurodegenerative disorders, cancers, cardiovascular disease and type II diabetes. A major risk factor for many of these disorders is age (Balch et al., 2008; Feleciano et al., 2019). With the progress of

aging, the accumulation of toxic proteins introduces a challenge on proteostasis. During stress, the proteostasis network coordinates the clearance and disaggregation of protein aggregates to enable cells to cope with proteotoxicity especially during aging.

It is known that misfolded proteins usually expose hydrophobic patches, which is a target to cellular degradation and refolding machineries. To protect homeostasis, misfolded proteins must be either refolded or cleared via a sophisticated protein quality control (PQC) system (Samant and Frydman, 2019). It consists of degradation pathways and numerous molecular chaperones and co-chaperones, all working together on refolding or removal of dysfunctional proteins (Clausen et al., 2019). The folding of proteins is relatively challenging *in vivo*, as the environment in cell is extremely crowded (Ellis and Minton, 2006). It is likely that the need of chaperones initially arose due to the necessity to minimise protein degradation in crowded cells (Hart et al., 2011).

The clearance of toxic aggregates is executed through protein degradation pathways. It is mediated by ubiquitin-proteasome system (UPS) and the autophagosomal-lysosomal pathway (ALP). The UPS is the primary pathway for short-lived and misfolded proteins and takes part in several cellular functions, including cell survival and apoptosis. The ALP removes large and potentially dangerous protein aggregates (Dikic, 2017).

Before passing on the misfolded proteins to UPS for destruction, the chaperone system tries to rescue the proteins through disaggregation and refolding. This is performed by ATP-dependent chaperones, which mostly belong to the Hsp60, Hsp70, Hsp90 and AAA+ families (Bukau et al., 2006; Hartl et al., 2011; Mogk and Bukau, 2017; Feleciano et al., 2019). In addition, the families work in cooperation with co-chaperones, such as the Hsp40 family of co-chaperones and Hsp70 (Figure 1).

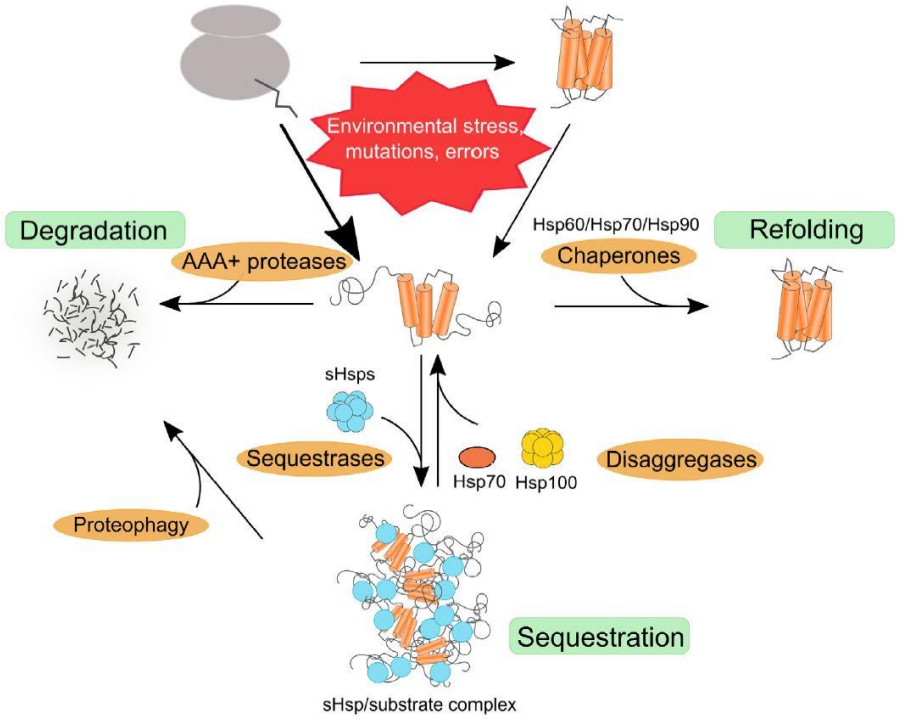

Figure 1. Proteostasis network and its components. *The misfolded proteins are either refolded by a chaperone network or degraded by AAA+ proteases. The misfolded proteins can be disaggregated by Hsp70/Hsp100 machinery or tageted to degradation (adapted from Reinle et al., 2022).*

Classes of molecular chaperones

ATP-dependent chaperones

Currently the information about molecular chaperones divides them into 5 major classes based on their molecular weight. They are named as the heat shock proteins (Hsp) based on their original discovery (Ritossa, 1962). Although the historical name of chaperones implies their dependence upon heat stress, they also are needed under non-stress cellular conditions. Hsps are generally ATP-hydrolysing Hsp60, Hsp70, Hsp90, Hsp100 families and the ATP-independent small heat shock proteins (sHsp) (Hayer-Hartl et al., 2016; Rosenzweig et al., 2019; Schopf et al., 2017; Sabil, 2013; Hasbeck and Vierling, 2015; Bascos and Landry, 2019; Dahiya and Buchner, 2019). The ATP cycle together with substrate recognition, binding and release are modulated by co-chaperones, such as Hsp10, Hsp40 (termed as J-proteins, DnaJ and Hsp70 co-chaperones), nucleotide exchange factors and many Hsp90 co-chaperones (Kampinga and Craig, 2010; Bracher and Verghese. 2015; Biebl and Buchner, 2019). Such sophisticated network implies flexible interaction and communication between chaperones and co-chaperones. For example, different Hsp40s may interact with the same Hsp70 to drive its substrate specificity (Kampinga and Craig, 2010). Likewise, Hop/Sti1 bridges both Hsp90 and Hsp70 (McClellan et al., 2005).

In general, Hsp60s are divided into two classes – Group I and Group II. The first group includes bacterial GroEL and Hsp60 found in mitochondria and chloroplasts. The second group includes chaperonins found in archaebacterial and eukaryotes, termed as TRIC/CCT (Hartl et al., 2011).

One of the most famous Hsp60s is its *E. coli* homolog – GroE, which consists of GroEL and GroES components (Fayet et al., 1989). GroEL (60 kDa) has a cylindrical structure that consists of seven subunit rings with a cavity in all of them (Figure 2, a). The subunits are divided in apical, intermediate and equatorial domains. The equatorial domain has an ATP-binding site (Thiyagarajan et al., 1996). Apical domain is able to bind substrate and GroES (Braig et al., 1993; Langer et al., 1992), which is required

for GroE function. GroES also has a ring structure that is formed by seven subunits with a molecular weight of 10 kDa each and can bind GroEL in the presence of nucleotide (Langer et al., 1992; Hunt et al., 1996). GroE is able to bind different confirmations of substrates and modulate their structure (Horst et a., 2005). The mechanism is such that substrates are trapped in the GroEL cavity and released upon ATP hydrolysis and GroES dissociation (Burston et al., 1995).

The Hsp70 family is comprised of 70 kDa large chaperones which hydrolyse ATP. They are involved in various cellular processes, such as unfolding and refolding, disaggregation, degradation and protein translocation (De Los Rios et al., 2006; Hu et al., 2006; Nillegoda et al., 2015; Fernández-Fernández et al., 2017; Craig, 2018). In eukaryotes, there is a constitutively expressed Hsc70 and heat stress induced Hsp70. In addition, there are two organelle-specific Hsp70s in the ER and mitochondrial (Behnke et al., 2015; Dutkiewicz et al., 2017).

Structurally, Hsp70s are comprised of an ATP-binding domain (NBD) and a substrate binding domain (SBD) (Figure 2, b). Upon interaction with a substrate, Hsp70 exhibits dynamic conformational changes that are initiated by ATP-hydrolysis. This leads to an ATP-bound closed conformation with low affinity towards substrate to switch to the ADP-bound open state upon ATP hydrolysis (Takeda and McKay, 1996). In the presence of ATP, substrate binding is mediated via interaction with the SBD (Srinivasan et al., 2012; Schneider et al., 2016). In addition, Hsp70 functions are regulated by Hsp40 co-chaperones (J-proteins) and nucleotide exchange factors (NEF).

Hsp40 proteins are a large and diverse group of chaperones that assist Hsp70s to fulfil their functions by binding to substrate proteins and effecting ATP-cycle (Laufen et al., 1999). They carry J-domain that was shown to directly interact with SBD of Hsp70 (Figure 2, c) and promote ATP hydrolysis (Kityk, et al., 2018). Release of hydrolysed ADP is promoted then by NEFs (Bracher and Verghese, 2015). In addition, NEFs were shown to stimulate the release of substrate by competing with it (Gowda et al., 2018). Release of the substrate allows spontaneous refolding of the protein. Alternatively,

the release of the substrate is followed by either its degradation or a handover to Hsp60 or Hsp90 for final maturation (Dahiya and Buchner, 2019).

Hsp90 is a class of conserved ATP-dependent chaperones found in many organisms from bacteria to human. The functional cycle of Hsp90 is impressively complex as it consists of cooperative effort between co-chaperones and Hsp70 system. Hsp90 is its constitutively expressed and its expression is increased upon stress. In addition, the chaperone targets of Hsp90 are limited to a specific pool of substrates, such as kinases, hormone receptors, transcriptional factors *etc*. (Taipale et al., 2010; Taipale et al., 2012). The clear molecular mechanisms of Hsp90 cycle are still elusive due to a large number of its components.

Hsp90 is a homo-dimer with each protomer carrying the N-terminal ATP-binding domain (NTD), the middle domain (MD) and the C-terminal dimerisation domain (CTD) (Figure 2, d). The Hsp90 homo-dimer can adopt open and closed conformations, which is regulated by ATP binding and hydrolysis. The transitions between Hsp90 conformation affect interaction with substrates and co-chaperones (Chadli et al., 2000; Richter et al., 2001; Shiau et al., 2006; Taipale et al., 2010).

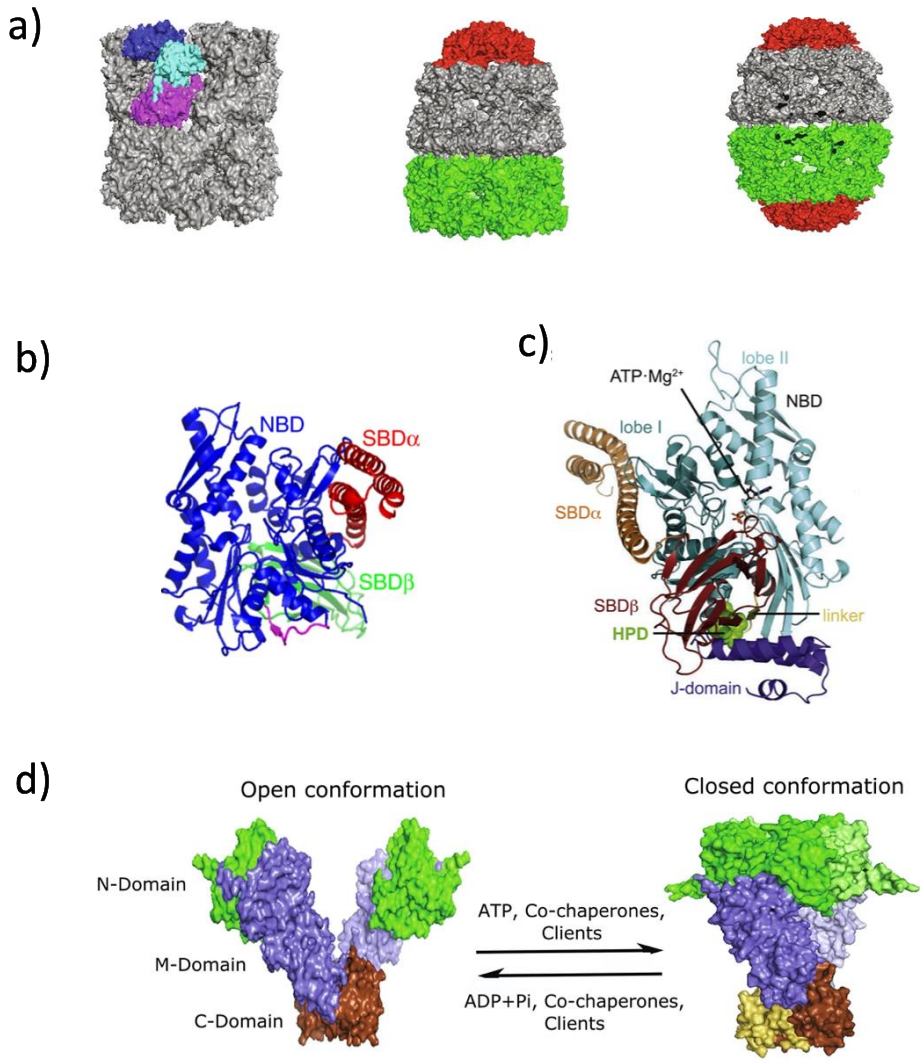

Figure 2. ATP-dependent chaperones*. a) Crystal structure of E. coli GroEL (PDB 1GRL). B) Crystal structure of ER-located Hsp70, BiP, in complex with ATP (PDB 6ASY). The nucleotide binding domain (NBD) and substrate binding domain (SBD) are illustrated. C) Structure of Hsp70 with ATP and J-domain of Hsp40 (PDB 5NRO). SBD, NBD, J-domain, HPD (His33-Pro34-Asp35) and linker between HSp70 and Hsp40 are shown. D) Crystal structures of open (left) and closed (right) states of Hsp90 (PDB 2IOQ, PDB 2CG9). N-terminal domain (NTD), middle domain (MD) and C-terminal domain (CTD) are illustrated. The conformational changes are modulated by ATP, co-chaperones and client (adapted from Braig et al., 1994; Yang et al., 2017; Kityk et al., 2018; Dahiya and Buchner, 2019).*

Co-chaperones of Hsp90 are a large subset of the chaperone network. Over 20 of them were identified in eukaryotic cells (Johnson and Brown, 2009). They have distinctive functions in a cell. For example, the largest group of co-chaperones,

termed tetratricopeptide or TPR co-chaperones, link Hsp70 and Hsp90 to assist in client binding. Among them is Hop (human) and its yeast homolog Sti1 (Kirschke et al., 2014; Richter et al., 2003; Röhl et al., 2015). Another TPR co-chaperones are the peptidyl-prolyl isomerases (PPIases). They catalyse cis-trans isomerisation in proteins (Schiene-Fischer, 2015) and might be involved in client hangover and activation (Dahiya and Buchner, 2019). Another type of co-chaperone, Cddc37 is specific to kinases and thus recruitment of kinase clients to Hsp90 (Keramisanou et al., 2016). In contrast, the p23 co-chaperone specifically targets a closed confirmation of Hsp90 to stabilise it and trap client proteins (McLaughlin et al., 2006).

The chaperone network has undergone expansion in the time course of evolution (Kampinga and Craig, 2010; Taipale et al., 2010; Kominek et al., 2013; Ramsøe et al., 2020). For example, Hsp40 family has evolved from only 3 members in *E. coli* to 18 in *C. elegans* and 49 in human (Kampinga and Craig, 2010; Frumkin et al., 2014; Shemesh et al., 2021). sHsp evolution is even more complex, as *C. elegans* and plants have more sHsps than human (Kriehuber et al., 2010; Frumkin et al., 2014).

The diversity, flexibility and resilience of the chaperone system is evident under conditions of stress, which leads to the up-regulation of some chaperones. Typically, overexpression of chaperones improves the folding facility, however, some chaperones were shown to disrupt folding upon overexpression (Coppinger et al., 2012; Blair et al., 2013). Similarly, downregulation of chaperones can lead to many diseases (Meister-Broekema et al., 2018).

Recently, large-scale studies on chaperone network aberrations were performed in the context of heat stress, cancer, aging and neurodegeneration (Brehme et al., 2014; Finka et al., 2015; Hadizadeh Esfahani et al., 2018). The disfunction of the chaperome occurs in all tissues or can be tissue-specific, like in a case of *C. elegans* HLH-1 (MYOD1 ortholog), a main transctiptional factor for muscle differentiation. It was shown to promote chaperone expression specifically in muscles (Bar-Lavan et al., 2016). Recent work by Shemesh et al (2021) identified a set of core chaperones that are ubiquitously expressed across all tissues. The authors present a website for searching

for the information on chaperones and their relationship and interaction across human tissues.

The roles of ATP-dependent chaperones are well-defined, while much less is known about the functions of the ATP-independent small heat shock proteins (sHsps). Thus, the further focus of the study will be laid on small heat shock proteins.

The world of small heat shock proteins

The class of small heat shock proteins is the most ubiquitous family of chaperones. They are present in all domains of life. sHsps act ATP-independently and serve as a first line of defence during cellular stress (Haslbeck and Vierling, 2015). They effectively bind a variety of non-native proteins and, therefore, are effective in preventing aggregation. Their primary role is to catch unfolding proteins before they approach the point of irreversible and uncontrolled aggregation. The process of refolding requires active cooperation with a chaperone network. The trapped substrates are, thus, passed over to ATP-dependent chaperones for refolding (Haslbeck et al., 2019; Reinle et al., 2022). For example, the Hsp70/Hsp40 system in the presence of ATP is effective in refolding the captured substrates (Ehrnsperger et al., 1997; Lee et al., 1997; Mogk et al., 2003).

Small Hsps are characterised by their low molecular weight ranging between 12-43 kDa. They consist of a typical three-part structure: a conserved α-crystallin domain (ACD), a flexible N-terminal region (NTR) and a short C-terminal region (CTR) (Caspers et al., 1995; Kriehuber et al., 2010; Haslbeck and Vierling, 2015).

ACD is a distinctive signature of sHsps. It is highly conserved and composed of a compact β-sheet-rich structure associated in an antiparallel fashion with hydrophobic grooves at each edge, predominantly at β4 and β8 and neighbouring strands (Figure 3) (Klevit, 2020). The structure of the domain differs across species. Bacterial ACDs consist of a distinct β6 strand, while mammals and non-plant higher eukaryotes have an extended β6+7 strand (Kim et al., 1998; van Montfort et al., 2001; Stamler et al., 2005).

The CTR of small Hsps is usually short, not longer than 20 amino acids (Kriehuber et al., 2010) and has an I-X-I/V motif. This three-residue patch is of structural and functional importance. It is reported to play a significant role in the oligomerisation of sHsps (Studer et al., 2002; Hayes et al., 2008; Delbecq et al., 2012).

Figure 3. Illustration of the organisation of α-crystallin domain in sHsps. *The mammalian and higher eukaryotic ACD (except plants) (left) differs from the bacterial ACD (right). Bacterial ACD consist of a distinct β6 strand, while mammalian strand is extended and referred as β6+7 strand (adapted from Haslbeck et al., 2019).*

The NTR is highly variable in sequence and length. It plays a role in oligomer formation and interaction with a substrate. As an extreme example Hsp42 from *Saccharomyces cerevisiae* carries a large NTR (247 residues) including a prion-like domain which is vital for its aggregase activity (Grousl et al., 2018). The smallest NTR composed of 24 residues is found in Hsp12.2 (Peter and Candido, 2002). The N-termini are rich in hydrophobic residues, phenylalanine and tryptophan residues are usually over-represented (Haslbeck et al., 2019). Notably, sHsp16 family consist of a very low number of aromatic amino acid residues, no tryptophan residues are found in Hsp16.1 and Hsp16.2.

The NTR is highly dynamic. Several studies reported high rates of hydrogen/deuterium exchange (Wintrode et al., 2003; Cheng et al., 2008). In addition, it is considered to be largely intrinsically disordered. Moreover, some patches of the NTR can adopt a secondary structure, such as in human αB-crystallin (Jehle et al., 2011).

The key feature of sHsps is their ability to form large oligomers that are composed of a varying number of subunits, typically in a range of 12-32-mers. However, there are exceptions to this rule, such as Hsp12.2 and Hsp12.3 that form tetramers (Kokke et al., 1998), human HspB6, Tsp36 from tapeworm and AtHsp18.5 from *Arabidopsis thaliana* that form dimers (Bukach et al., 2004; Kappé et al., 2004; Basha et al., 2013). The data correlates well with the properties of the NTRs and CTRs of the mentioned above proteins. The regions are either short or absent in the structure, the I-X-I/V motif is missing or the ACD lacks the β6 strand.

sHsp oligomers are formed predominantly by a weak interaction between the NTR/CTR and the ACD dimer. The ACD dimer serves a central frame for building high order structures. The dimer formation is driven by either interaction between β2/β6 antiparallel strands of each monomer or the extended β6+7 strands in the case of metazoans (Riedl et al., 2020). The ACD homodimer alone is usually not sufficient for building oligomers (Studer et al., 2002). Interaction of I-X-I/V motif of CTR or in rare cases of the NTR with the ACD dimer contributes to the oligomerisation. In addition, the NTR intermolecular contacts with either ACD or NTR of a neighbouring subunit promote assembly of oligomers (Jehle et al., 2011).

The variety of interaction modes leads to a structural plasticity of sHsps. The diverse and weak interactions between dimers grant the high dynamics and polydispersity to sHsp oligomers, termed quasi-ordered state (Clouser et al., 2019). Moreover, the complexity of the interactions is extended by a hetero-oligomerisation, which may play a role in chaperone activity and specificity (Baugman et al., 2020; Mymrikov et al., 2020). For example, in human, HspB2 and HspB3 are reported to form hetero-oligomers in muscle (Sugiyama et al., 2000). In addition, αA- and αB-crystallins, vital components of the eye lens, exist predominantly as hetero-oligomers in a 3:1 ratio (Haslbeck et al., 2016). Hetero-oligomer assembly not only activates the chaperone activity, it can also modulate it towards specific substrate, like in a case of human HspB1-HspB6 and HspB5-HspB6 hetero-oligomers. HspB6 acts as a negative or positive regulator of chaperone activity of its partner chaperone. In addition, hetero-oligomerisation can also lead to a reduced chaperone activity, for example, HspB1-HspB5 hetero-oligomers exhibit lower activity compared to the respective homo-oligomers (Mymrikov et al., 2020).

The described dynamics of sHsps keeps them in constant dissociation and association processes. This makes structural studies highly challenging.

sHsp oligomerisation is functionally important as it plays a role in the interaction of sHsps with a substrate. The high dynamics of sHsp assemblies is correlated with the substrate recognition and regulation of the chaperone activity (Basha et al., 2012). Usually, sHsp assemblies are sensitive to the environmental changes, such as pH,

temperature, post-translational modifications etc. These factors serve as an activation point for sHsp oligomers and often lead to conformational changes in the structure by shifting oligomeric assembles to smaller species (Haslbeck et al., 2019). The Hsp26 oligomers, for example, are activated by phosphorylation at permissive temperature. The post-translational modifications weaken the interaction between protein domains, which leads to the dissociation of the Hsp26 into small species, an active chaperone form (Mühlhofer et al., 2021).

The sHsp mechanism of action is directed towards isolating unfolding substrates. The interaction with a substrate is achieved via multiple sites in the NTR and ACD. Such interaction usually results in a formation of a large sHsp:substrate complex. These assemblies vary in size and composition, which depend upon various parameters, such as type of substrate, type of stress condition or sHsp:substrate ratio (Haslbeck et al., 2019; Reinle et al., 2022). The mechanism is such, that a partially unfolded substrate is bound to an activated sHsp ensemble, which is usually the smaller species (Figure 4). The activation can also be driven by the post-translational modifications, such as the mentioned above phosphorylation in the case of Hsp26 (Mühlhofer et al., 2021). The substrate is stabilized in a Hsp:substrate complex and can be further re-activated by the ATP-dependent chaperones.

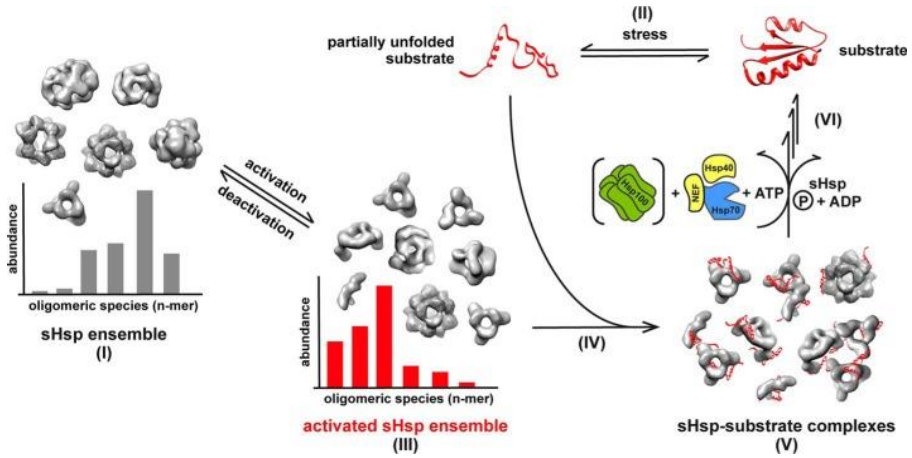

Figure 4. The mechanism of the chaperone function of sHsps. *I) sHsps are ensembled as oligomers; II) under stress, the substrates are destabilised; III) sHsps become activated and dissociate into smaller species; IV) a partially unfolded substrate is recruited by the activated sHsps and stabilised in a sHsp:substrate complex; V) substrates can be then re-activated by the ATP-dependent chaperones (Haslbeck et al., 2019).*

One of the models proposed is that the sHsp:substrate complexes are composed of a stable core and dynamic outer layer. According to the Reinle et al (2022), the core is made of substrate molecules and some sHsps, while outer part is composed of highly dynamic sHsps. The authours propose that the formation of such complexes starts from binding of sHsp molecules to unfolding substrate. This is followed by the recruitment of more sHsp molecules which leads to an increase of a sHsp:substrate complex size (Figure 5).

When sHsps exceed a substrate, the polydisperse soluble complexes of the Hsp:substrate are formed. When, the substrate proteins exceed, sHsps are incorporated in large amorphous aggregates of the substrates (Friedrich et al., 2004). The recruitment of sHsps in the insoluble aggregates was shown both *in vitro* (Haslbeck et al., 1999; Stromer et al., 2003) and *in vivo,* for example, in *C. elegans* during ageing (Walher et al., 2015) or yeast during heat stress (Specht et al., 2011).

It is reported that sHsps can have several substrate binding sites, which was confirmed by cross-linking mass spectrometry and peptide arrays (Haslbeck et al., 2019). For example, αB-crystallin binds Aβ(1–40) peptide mostly by the ACD, while lysozyme is bound to the disordered NTR (Mainz et al., 2015).

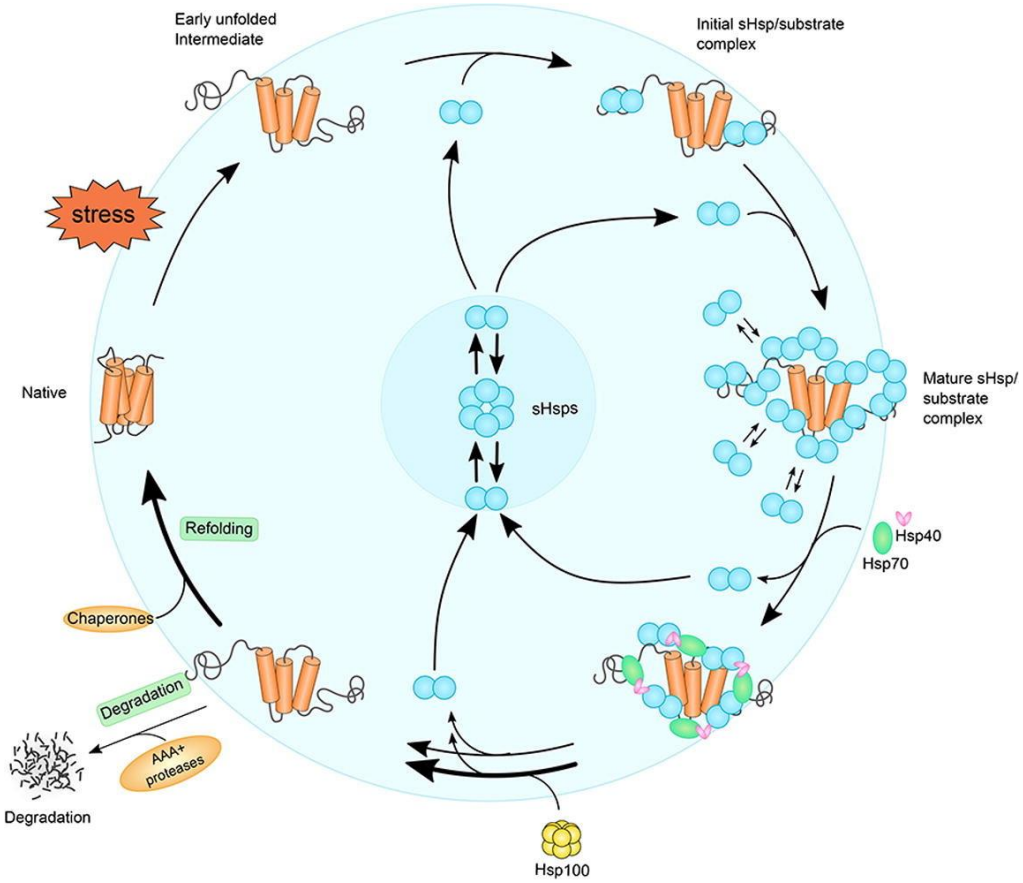

Figure 5. The illustration of the mechanism of action of sHsps. *sHsp:substrate complexes are formed via interaction of sHsps with early unfolding molecules. sHsps are further dragged into the complex resulting in its expansion. The Hsp70/40 machinery displaces sHsps and binds to the substrate hidden in the core. In yeast, Hsp100 disaggregases can catalyse the process. The substrate is then released and refolded. In some cases, the substrate can be partially degraded by the AAA+ degradation machinery (adapted from Reinle et al., 2022).*

Interestingly, sHsps can also interact with substrates that cannot be refolded. The recently reported feature of PQC system - a formation of cytosolic stress granules (SGs) - is shown to be controlled by sHsps (Molliex et al., 2015; Protter and Parker, 2016; Mackenzie et al., 2017; Alberti and Carra, 2018).

SGs are membrane-less deposits formed by liquid-liquid separation. They consist of mRNA, various RNA binding and non-binding proteins and translation factors. During severe cellular stress the misfolded proteins may be incorporated into SGs. This

triggers the formation of abnormal stress granules. The dynamics of this aberrant SGs is restored via granulostasis (Cherkasov et al., 2013; Grousl et al., 2018). Failure of this system is linked to the development of diverse diseases, such as cancer and neurodegeneration (Alberti and Carra, 2018). For example, human HspB1 and HspB8 were recently reported to maintain the functional properties of SGs formed by the protein fused in sarcoma (FUS) (Carra et al., 2019; Liu et al., 2020; Boczek et al., 2021). Additionally, HspB2 undergoes phase separation and forms nuclear membrane-less compartments to seize nuclear lamin-A (Morelli et al., 2017). This finding suggests that sHsps may not only act as “holdases” to keep the unfolding substrates from irreversible aggregation but may also exhibit “aggregase” activity. For example, Hsp42 was reported to drive chaperone-facilitated sequestration of misfolded substrates via its prion-like domain in NTR (Grousl et al., 2018). This protective mechanism is crucial for maintaining the cellular fitness during stress.

As seen from the above, sHsps have distinctive features that differentiate them from other chaperones, however, the functions and structure of sHsps also vary among different species. sHsps are ubiquitous and expressed in all kingdoms of life (Haslbeck et al., 2019). Single cell organisms usually have one or two sHsps, though some bacteria encode multiple sHsps, such as *Bradyrhizobium spp* that expresses eight of them. One of the highest numbers of sHsps was reported in plants, for example, in *Populus trichocarpa* (black cottonwood) there are 37 sHsps (Zhang et al., 2015; Li et al., 2016). In addition, sixteen members of the sHsp group were reported in *Caenorhabditis elegans*. Interestingly, there are only ten sHsps in humans (Haslbeck et al., 2019). The tendency shows that sHsps potentially evolved in the large groups in those species that are subjected to regular stress in the terrestrial environment (Waters and Vierling, 2020). As more genomes become available, it is possible to explore the evolutionary mechanisms that drove such sHsp diversification, especially in regards of their functions.

The ubiquitous source of a functional novelty, gene duplication, was firstly accounted in the 1930s (Bridges, 1936). The duplicated genes usually retain most of the ancestor’s sequence and structural features but can also diverge over time (Mallik et

al., 2022). Functional novelty is often complemented by structural ones, especially in case of oligomeric proteins (Hochberg et al., 2018). Protein diversification can lead to an existence of new oligomeric states, such as homomers, heteromers or hetero others (Figure 6) with novel functions. Although both scenarios, homo- and heteromers, are possible, a current study by Hochberfg and colleagues (2018) shows that most species of the two duplicated sHsps from *Pisum sativum* tend to form homomers. In *E. coli*, many diverged proteins exist as homomers (53%). In contrast, yeast have most of such proteins in a form of heteromers (32%). In total, whether two novel proteins form heteromers, depends upon the post-duplication changes in the protein structure (Mallik et al., 2022).

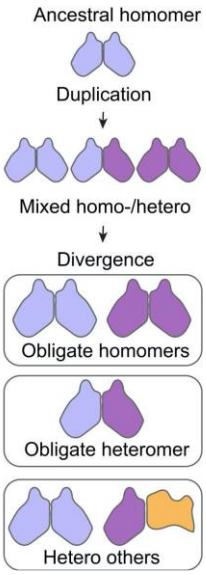

Figure 6. An illustration of the duplication of a gene that encodes a homomeric protein, which leads to a structural diversity. *An ancestral gene undergoes a duplication, which results in the two co-existing forms of a homomers and heteromers. After divergence of the two genes, three possible forms of the protein can exist: homomers, heteromers or hetero others (gain of a new interaction partner) (adapted from Mallik et al., 2022).*

In addition to the diversification of oligomeric structure, the novel oligomers can obtain new functions, or even subcellular localisation (Marques et al., 2008). For

example, yeast ALT1 (mitochondrial) and ALT2 (cytosolic) share the same initial function but localise in different cellular locations (Mallik et ak., 2022). In addition, duplication can also affect expression patterns of the related genes, like in case of *E. coli* LYSS and LYSU, which are constitutively expressed or heat-induced, respectively (Brevet et al., 1995).

sHsp implications in life

A large proportion of severe diseases is attributed to protein misfolding and aggregation. The sHsp field is of a high importance in this context, as sHsps are required in a variety of housekeeping functions in the cell. Malfunction of sHsps was thus reported to be implicated in the development of severe diseases, such as cancer, neurodegenerative and cardiovascular diseases (Sun and MacRae, 2005; Alberti and Carra, 2018; Carra et al., 2019; Vendredy et al., 2020). Specifically, HspB1 is implicated in cardiopulmonary diseases, which lead to the high rate of mortality worldwide (Guo et al., 2010).

Investigation of sHsps in model organisms is of advantage as such approaches allow to shed light on the molecular mechanisms behind their mode of action. For example, Hsp22 of *Drosophila melanogaster* localises to mitochondria during oxidative stress (Morrow et al., 2000). HspB8 was reported to be induced in the mouse model of amyotrophic lateral sclerosis (ALS), particularly in motor neurons and muscle (Rusmini et al., 2017; Cristofani et al., 2019). In a mouse model of motor neuropathy, HspB8 was identified as a key player in the disease development. Specifically, mutations in HspB8 were associated with the motor neuropathy, Charcot-Marie-Tooth disease and distal myopathy (Bouhy et al., 2018).

sHsps of *Caenorhabditis elegans*

Why *C. elegans*?

The focus of this study will be sHsps of *C. elegans*. 50 years ago, the nematode *Caenorhabditis elegans* was developed as a genetic model to unveil the mysteries of developmental biology and neurobiology (Brenner, 1974). These days, it is used as a model organism in over a thousand laboratories with more than a thousand research papers published a year (Corsi et al., 2015).

C. elegans is a small, free-living nematode spread worldwide. The microscopic size of adult nematodes of 1mm allows to easily investigate them under the microscope. Advantages to use this organism are its fast life cycle (Figure 7) and ease of genetic manipulation. They are usually maintained at 20°C, although they can live in a range of 12°C to 25°C. By manipulating the growth temperature, it is possible to influence the development of nematodes (Corsi et al., 2015).

The hermaphrodites can be either self-fertilised or fertilised by sperm from males. Once eggs are laid, they start development which culminates in a first stage (L1) larva. When the animals begin to eat, they continue their development through L1-L4 stages. When nematodes reach adulthood, they start laying eggs for 2-3 days. After this reproductive period is finished, hermaphrodites live up to several weeks more.

The ability to knock down gene activity by feeding RNAi is another advantage of this nematode. This technique together with the complete genomic sequence of *C. elegans* (*C. elegans* Sequencing Consortium, 1998) allows to study gene functions. Moreover, the protocols and current findings in *C. elegans* research of different forms are gathered in online databases. The reviews of nematode biology and methodology are located in WormBook database (http://www.wormbook.org/). Genomic data, including gene sequences, expression, phenotypes and genetic maps are provided in WormBase (http://www.wormbase.org/). Another tool, WormAtlas (https://www.wormatlas.org/), gives information on nematode anatomy and its methods, while WormImage (http://www.wormimage.org/) is an online database of

electron micrographs of nematode tissues. In addition, the scientific community made a useful tool to search current literature in the nematode field (https://celegans.textpresso.org/).Recent advances in *C. elegans* research include a whole-animal connectome, which contains the knowledge of connections between nervous system and end-organ across entire nematode (Cook et al., 2019).

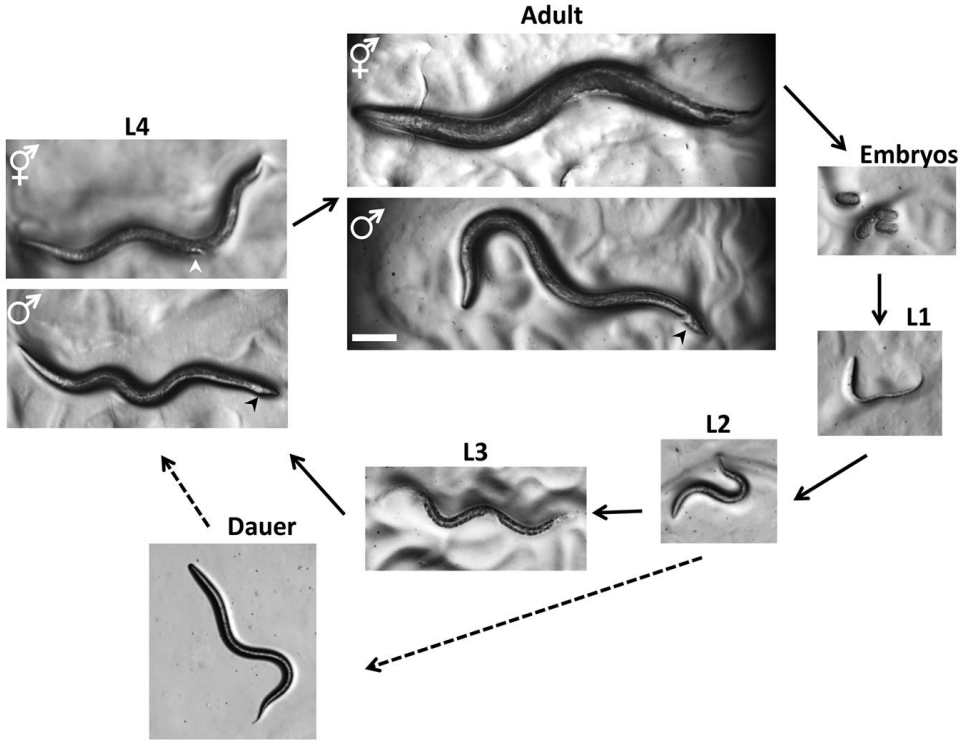

Figure 7. Life cycle of C. elegans. *The cycle starts from the embryo and develops through four larva stages. At L4 stage hermaphrodites have a developing vulva (white circle indicated by white arrow), which distinguishes them from males carrying a tapered tail (black arrow). At adult stage, male and hermaphrodite nematodes are well distinguished by their tails and size of the body. The dauer larvae is a protective mechanism during starvation (adapted from Corsi et al., 2015.*

In addition to its convenience for genetic analyses, *C. elegans* is advantageous as a model for eukaryotic biochemistry. In this study, nematodes are used as a model to study the heat shock response and molecular forces behind it. High level of orthologs between *C. elegans* and human genomes of up to 80% (Kaletta and Hengartner, 2006; Forslund et al., 2011; Shaye and Greenwald, 2011; Kim et al., 2018) makes it an important model to study conserved mechanisms and diseases. To understand such a complex network like chaperones, a manipulatable system that allows to

systematically unravel the molecular mechanisms involved is of a great use. By understanding the conserved mechanisms that mediate the stress response, we can relate the findings from nematode to a complex human network.

Components of chaperone network in *C. elegans*

Families of sHsp and Hsp proteins

The chaperone network in *C. elegans* is remarkably expansive and consists of 97 genes that encode a variety of chaperones and co-chaperones (Table 1). Those include the Hsp60 family, Hsp70 and their co-chaperones Hsp40/Dnaj, several nucleotide exchange factors, the Hsp90 group with Hsp90 co-chaperones and the sHsps.

The Hsp60/chaperonin family are ATP-dependent chaperones that are required for protein folding. It consists of the group of CCT proteins, Hsp60 and Hsp10. The many roles of 8 different CCT proteins remain elusive, however, it is known that they are required for a proper folding of tubulin and actin (Leroux and Candido, 1995; Horwich et al., 2007; Saegusa et al., 2014) and also have a broader cellular function, including misfolded protein degradation and neurodegeneration (Shen and Frydman, 2013; Gestaut et al., 2019). The Hsp60/Hsp10 chaperonin complex is involved in mitochondrial unfolded protein response and mediate a response to environmental stresses in nematodes (Bie et al., 2016). Hsp60 (Hsp60 human ortholog) chaperone is evolutionary conserved factor of mitochondria and contribute to such mechanisms in *C. elegans* as immunity (Jeong et al., 2017), response to oxygen deprivation (Peña et al., 2016) and even microgravity (Liu et al., 2019), which occurs during spaceflights.

Hsp70/Hsp40 is the largest family of the *C. elegans* chaperone network as it is encoded by 48 genes (Frumkin et al., 2014). They are active, conserved players of the heat shock response (HSR) (Zhang et al., 2013; Pagliuso et al., 2021; Schmauder et al., 2022). Hsc70 subclass is constitutively expressed, while in response to stress, several Hsc70 orthologs, termed Hsp70, are induced (Nikolaidis and Nei, 2004). In addition

to Hsp70 group, J-proteins, divided into three classes (A, B and C), assist in protein disaggregation and refolding. The Hsp40/DnaJs are co-chaperones of Hsp70s and may either target Hsp70's activity to clients or bind substrate directly to deliver it to Hsp70 (Kampinga and Craig 2010).

Hsp70s and J-proteins (Hsp40s) together were shown to have disaggregase function in *C. elegans* during stress and ageing. For example, it was reported that upon heat stress, constitutive Hsc70 is recruited by DnaJ proteins to disaggregate polyQ aggregates. This protective mechanism is handled by the interactive cooperation between A and B J-proteins (Kirstein et al., 2017). Mortalin (Hsp6), another member of Hsp70 family, is reported to be involved in senescence (Yokoyama et al., 2002; Zhang et al., 2022). Nowadays, it is a potential therapeutic target in cancer research, as it was reported to be enriched in several cancer types (Yoon et al., 2022). Additionally, Dnj-27, an ER-located protein, showed protective effects against human β-amyloid peptide (Aβ), α-synuclein (α-syn) and polyglutamine (polyQ) proteins in a *C. elegans* model of neurodegenerative diseases (Muñoz-Lobato et al., 2014). With these, the Hsp70/Hsp40 family is involved in numerous cytoprotective processes in *C. elegans*, including protein folding, translocation and degradation.

As was mentioned before, chaperones do not function in isolation. Indeed, the Hsp70 family not only cooperates with DnaJ co-chaperones, but works with members of the nucleotide exchange factor (NEF) group. They are predicted to exhibit ATP hydrolysis activity (Nillegoda et al., 2015; Tittelmeier, et al., 2020) and assist Hsp70 family in disaggregation. NEFs, such as the Bag proteins, compete with J-domain proteins and trigger nucleotide release (Sun et al., 2012; Papsdorf et al., 2014).

The most studied family of chaperones in worms is the Hsp90 family. In *C. elegans*, Hsp90 (daf-21) plays vital role in vulva development, maturation of gonads and oocyte as well as longevity (Inoue et al., 2006; Somogyvári et al., 2018). It is also reported to regulate HSR and innate immunity (Eckl et al., 2017). Depletion of Hsp90 leads to not only developmental arrest and weaker motility in larval stages, but also to specific transcriptional changes, such as dysregulation of Daf-16 targets (Schmauder and Richter, 2022).

Similar to the Hsp70 family, Hsp90s act together with almost 20 co-chaperones, which is an indication of a great expansion in evolution. One of the most studied Hsp90 co-chaperones is Unc-45. It is involved in Hsp90-dependent folding of the myosin motor domain (Barral et al., 2002; Srikakulam et al., 2008), which is why the knock-down of Unc-45 leads to a specific morphological change in *C. elegans*, such as paralysis and sterility (Gaiser et al., 2011). In addition, nematode Sti-1, Aha1 and p23 are required for the integrity of muscles (Frumkin et al., 2014).

The last family of *C. elegans* chaperone network is the sHsp group – a class of ATP-independent chaperones. It includes 16 proteins, which cannot disaggregase unfolding substrates, however they are able to prevent irreversible aggregation (Haslbeck and Vierling, 2015). The focus of this study will be concentrated specifically on this family of chaperones and the features of sHsps in *C. elegans* will be overviewed in the following chapter.

Table 1. List of chaperones in C. elegans. *The list includes in total 97 genes, 10 genes correspond to Hsp60 and Hsp10, 48 genes to Hsp70, Hsp40 and NEF, 21 genes to Hsp90 and co-chaperones, 18 genes to sHsps (adapted from Frumkin et al., 2014).*

	GENE NAME	OTHER NAME		GENE NAME	OTHER NAME
HSP60/CHAPERONIN	Cct- 1	TRiC/CCT	**NEF**	bag-1	BAG1
	Cct- 2	TRiC/CCT		unc-23	BAG2
	Cct- 3	TRiC/CCT		C34C12.8	GrpE
	Cct- 4	TRiC/CCT		Hsp110	Hsp110
	Cct- 5	TRiC/CCT		T24H7.2	Hsp110
	Cct- 6	TRiC/CCT		T14G8.3	Hsp110
	Cct- 7	TRiC/CCT	**Hsp90**	daf-21	Hsp90
	Cct- 8	TRiC/CCT		enpl-1	GRP94
	Hsp60	Hsp60		trap-1	mtHsp90
	Y22D7AL.10	Hsp10	**Hsp90 co-chaperones**	C01G10.8	AHA1
HSP70	Hsp1	Hsc70		sti-1	HOP/STI1
	F11F1.1	Hsc70		ZC395.10	P23
	Hsp3	BiP		fkb-6	FKBP
	Hsp4	BiP		cdc-37	CDC37
	stc-1	STCH		chn-1	CHIP
	Hsp6	Mortalin		pph-5	PP5
	Hsp70	Hsp70		sgt-1	SGT
	F44E5.5	Hsp70		Unc-45	UNC45
	F44E5.4	Hsp70		ZK370.8	TOM70
HSP40/DNAJ	dnj- 1			Y22D7AL.9	-
	dnj-2			hip-1	ST13
	dnj-3			C56C10.10	AIP1
	dnj-4			C34B2.5	TTC1
	dnj-5			C33H5.8	RAPAP3
	dnj-7			C17G10.2	TTC4
	dnj-8			C17G10.10	CNS1
	dnj-9			D1054.3	SGT
	dnj- 10		**sHSP**	Hsp12.1	
	dnj-11			Hsp12.2	
	dnj-12			Hsp12.3	
	dnj- 13			Hsp12.6	
	dnj- 14			Hsp16.1	
	dnj-15			Hsp16.11	
	dnj- 16			Hsp16.2	
	dnj-17			Hsp16.41	
	dnj-18			Hsp16.48	
	dnj-19			Hsp16.49	
	dnj-20			Hsp17	
	dnj-21			Hsp25	
	dnj-22			Hsp43	
	dnj-23			sip-1	
	dnj-24			ZK1128.7	
	dnj-25			Y55F3BR.6	
	dnj-26			F08H9.4	
	dnj-27			F08H9.3	
	dnj-28				
	dnj-29				
	dnj-30				
	rme-8				
	Y39C12A.9				
	K07F5.16				
	F54F2.9				

Molecular players of stress response

The stress-dependent expression of sHsps is a last point in the cascade of the sophisticated molecular events named insulin and insulin-like growth factor-1 (IGF-1) signalling (IIS) pathway. Together with other pathways, such as mTOR signalling, mitochondrial unfolded protein response and germline they form a longevity regulating pathway in nematodes (Figure 8). The cascade components are conserved in metazoans and play a role not only in response to stress, but also in system-wide functions, such as growth and aging (Piñero et al., 2009). It was discovered that the IIS pathway is one of the key players that regulates lifespan and can promote longevity in *C. elegans* (Kenyon et al., 1993).

The IIS pathway in *C. elegans* includes various components, such as insulin-like peptides (INS). One of them was reported to bind and activate human insulin receptor (Hsu et al., 2003; Morley and Morimoto, 2003). In nematodes, INS ligands activate the Daf-2 transmembrane receptor (insulin/IGF human ortholog) and start kinase phosphorylation cascade that culminates in the regulation of a transcription factor Daf-16 (ortholog of human FOXO). sHsp are direct targets of Daf-16 and their expression is regulated by it in response to various environmental stresses. For example, Hsp16.1 and Hsp16.48 were shown to be regulated by Daf16 and HSF-1 in *C. elegans* and contribute to a longevity (Hsu et al., 2003). Daf-16 is reported to promote longevity by translocating to the nucleus and binding DNA sites named Daf-16 binding elements (DBE).

Daf-16 is considered to be the key transcriptional output of IIS; however, heat shock in particular activates another IIS pathway - the HSR. It is mediated through transcriptional factor HSF-1 (heat shock factor-1) in *C. elegans*. It is essential for growth, development, regulation of longevity, and upon acute heat stress sHsps are direct targets of HSF-1. Additionally, HSF-1 is reported to direct transcriptional mechanisms different from HSR, such as the response to oxidative stress (Servello and Apfeld, 2020).

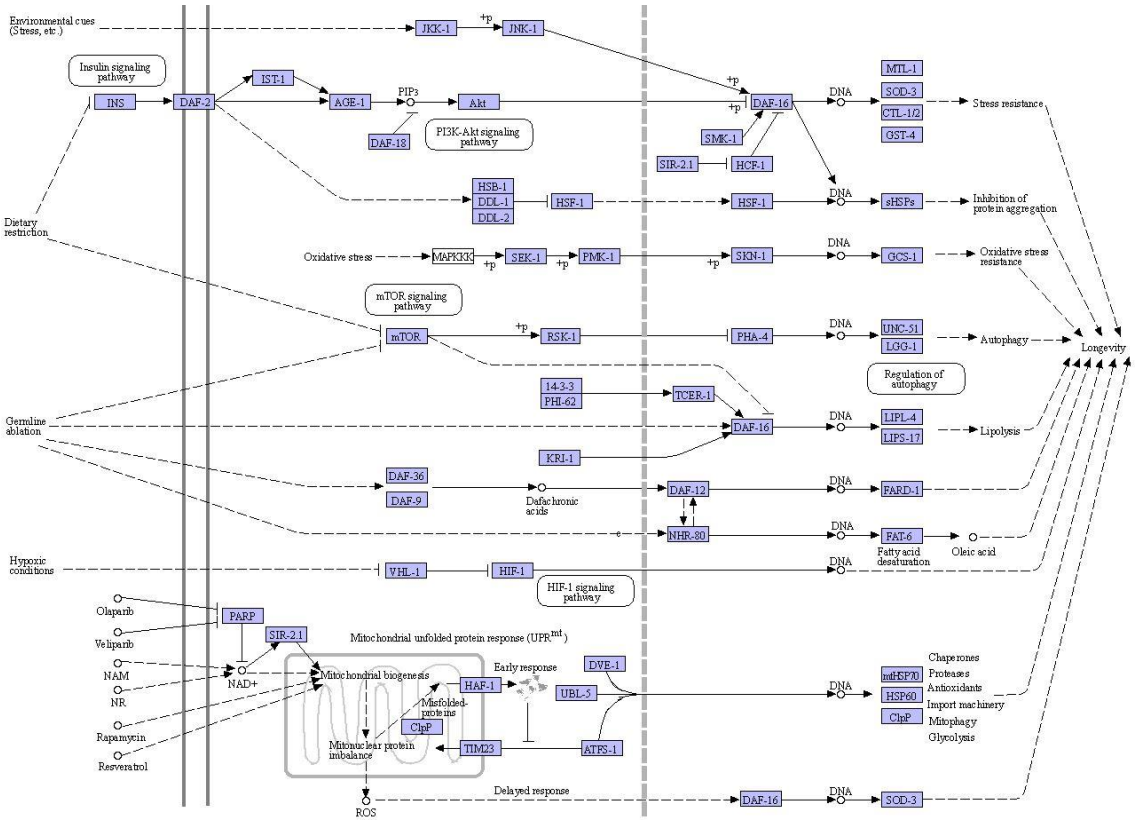

Figure 8. Longevity regulating pathway in nematodes. *The lifespan of the worms is influenced by over 70 genes with most of them involved in the IIS pathway. Together with mTOR signalling, mitochondrial respiration and germline, IIS belongs to the longevity regulating pathway. sHsps are members of IIS pathway and located at the very end of it. They are regulated by Daf16 and HSF-1 transcription factors (adapted from the KEGG database, Kanehisa et al., (2016)).*

In humans, HSF-1 is potentially implicated in cancer as it was shown to be constantly expressed in cancer cells (Mendillo et al., 2012). Under physiological conditions, HSF-1 exists as a monomeric protein, which activity is reported to be repressed by Hsp90-containing complexes (Voellmy and Boellmann, 2007).

HSF-1 is negatively regulated by the Daf-2 signalling cascade, in particular the DDL-1 containing HSF-1 inhibitory complex (DHIC) components (Figure 9), which retain HSF-1 in a monomeric state (Li et al., 2017; Sural et al., 2019). Upon upregulation, HSF-1 oligomerises into the complexes that translocate to the nucleus. They then become competent for DNA binding and target heat shock elements (HSE) located in the promoter region of Hsp and sHsp genes (Morley and Morimoto, 2003; Li et al., 2017).

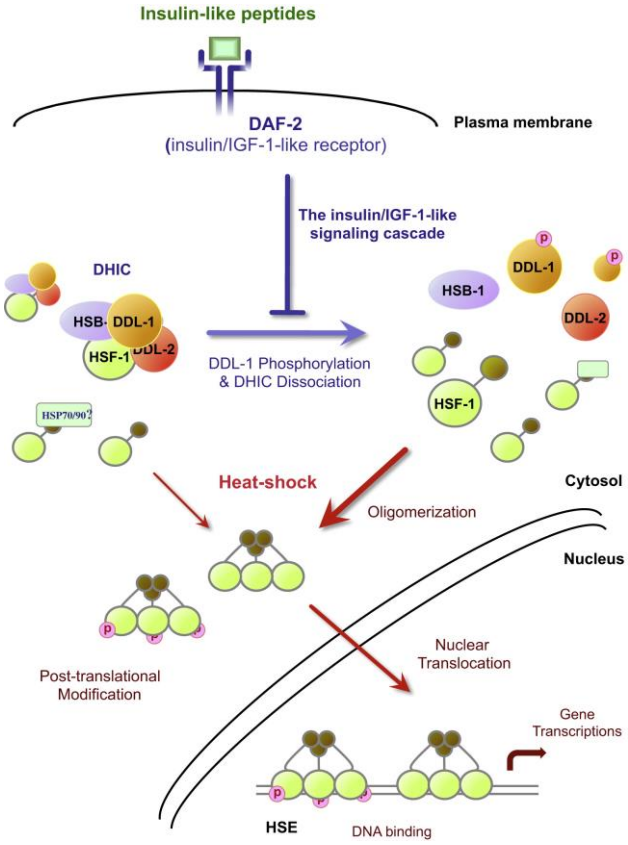

Figure 9. The HSF-1 mode of action regulated by IIS in C. elegans. *Upon heat stress HSF-1 is activated and undergoes translocation to the nucleus. The formation of the DHIC complex is disrupted upon DDL-1 phosphorylation, which subsequently increases HSF-1 activity. Upon translocation to the nucleus, HSF-1 oligomers bind heat shock elements to initiate Hsp and sHsp expression (retrieved from Li et al., (2017)).*

It was reported that age-related decline and the HSR are related. Interestingly, several studies stated a direct implication of sHsps in not only the HSR, but also in the regulation of longevity. It was reported that sHsps expression is increased in *daf-2* mutants that show a long-lived phenotype (Kenyon et al., 1993; Hsu et al., 2003; Murphy et al., 2003), in particular, the Hsp16 family.

Many molecular players downstream of HSF-1 and Daf-16 are not fully unveiled and details remain to be determined. Therefore, further details about the pathway components, specifically sHsps, are yet to be further investigated. The focus of this study is directed towards a sHsp family in *C. elegans* – the Hsp16s.

The Hsp16 family

There are 16 different sHsps in *C. elegans* (Figure 10.a), which is more than the 10 sHsps found in humans. The Hsp16 family consists of 4 “main” members, Hsp16.1, Hsp16.2, Hsp16.41 and Hsp16.48. There are also two related proteins that are assigned to the family – F08H9.3 and F08H9.4. They are named after their ORFs and are not given any protein name yet (Shim et al., 2003; Wormbase). To this time, little is known about this family and its functions in the organism.

Having the canonical structure of small heat shock proteins, the Hsp16 family consists of a highly conserved α-crystallin domain (ACD), a variable N-terminal region (NTR) and a short C-terminal region (CTR) (Figure 10.b). All proteins carry an I-X-I/V motif in the CTR with exception of F08H9.3, which has an IPV motif in the NTR. The molecular masses of the protein monomers lie around 16 kDa. The polypeptides for Hsp16.1 and Hsp16.2 are 145 amino acid residues (aa) and are 93% identical. Likewise, Hsp16.41 and Hsp16.48 are 143aa in length and also share 93% identity. The differences are only 10 and 9 amino acid residues, accordingly. In contrast, the given pairs are 70% identical to each other. Such homology among the family is extraordinary and suggests an origin from the same ancestor gene.

Two members of the Hsp16 family, Hsp16.1 and Hsp16.48 were firstly identified in 1985 by Russnak and Candido (1985). They later identified *Hsp16.2* and *Hsp16.41* genes and highlighted the remarkable orientation of all genes of the family on a chromosome (Jones et al., 1986). F08H9.4 and F08H9.4 genes were identified much later in 2003 (Shim et al., 2003).

The location of sHsp16 genes is illustrated in Fig.10c. They all are located on chromosome V and spread over three different regions. The two genes *Hsp16.2* and *Hsp16.41* are arranged in divergent orientations at one end of the chromosome. The other locus of *Hsp16.1* and *Hsp16.48* genes downstream the chromosome consists of a highly repetitive structure. Each protein is encoded by two copies of the gene, referred in this study as *Hsp16.1a* and *Hsp16.1b*, *Hsp16.48a* and *Hsp16.48b*,

respectively. Each gene at this locus arranged in opposite direction to another. The gene regions of the *a*-copies are located within 1.9-kilobase patch which is duplicated accurately to form a 3.8-kilobase inverted repetitive region. In contrast, further downstream the chromosome *F09H9.3* and *F08H9.4* genes are orientated in the same direction. Unlike other Hsp16 genes, they do not share any promoter region and sequence homology between them is 46%. In total, eight genes at three loci of chromosome V encode the proteins of sHsp16 family.

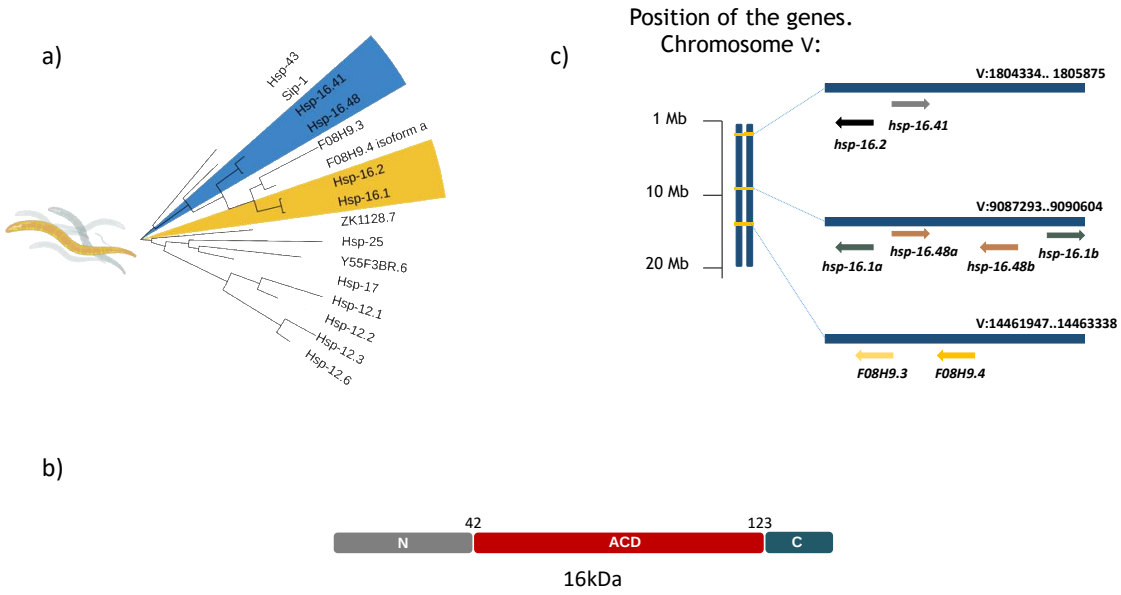

Figure 10. Genetic characteristics of the Hsp16 family. *A) a phylogenetic tree of all sHsps in C. elegans demonstrates their relationship. The main members of the family are indicated in blue and yellow. Phylogeny analysis was performed via the PhyML tool (Dereeper et al., 2008) and visualised by iTOL (Letunic and Bork, 2021). B) an illustration of the canonical sHsp structure of the Hsp16 family, which consists of the N-terminal region (NTR) highlighted in grey, an α-crystallin domain (ACD) in red and a short C-terminal region (CTR) in dark blue. The ACD is assigned to 42-123aa. Molecular mass of a monomer is around 16 kDa. C) an illustration of the chromosomal location of all genes that encode Hsp16s. The genes are located on V chromosome and distributed along it. The Hsp16.1 and Hsp16.48 proteins are encoded by 2 pairs of genes each.*

The genomic organisation of the Hsp16 genes is coherent with the idea that sHsp genes originated from duplication events. The duplication is of a high importance in providing genetic diversity and thus ability to obtain new gene functions. In the *C. elegans* genome the number of gene duplication exceeds the one in *Drosophila* by two times (Rubin et al., 2000; Woollard, 2005). The fate and consequences of gene duplication is yet unknown, however there are several theories. It is hypothesised that one gene copy loses the function due to accumulation of harmful mutations (non-functionalisation theory). Second scenario, neofunctionalization, is that one copy uptakes a novel function, which is later preserved during natural selection. This theory also suggests that both duplicates may obtain each a different function and also maintain the functional similarity. According to a third theory, subfunctionalisation, the duplicates inherit unique functions from their ancestor and divide a labour (Lynch and Conery, 2000).

In case of sHsp16 family, the hypothesis proposed in this study stands for the neofunctionalization. According to this hypothesis, sHsp16s have originated from the same ancestor and upon several duplication events have divided into a large family of homologous chaperones. It is hypothesised that they share functions and have gained the novel distinct roles to expand the chaperone network. Indeed, it is proposed that duplication of genes that are involved in responses to stress are usually favoured during natural selection (Lespinet et al., 2002; Cao et al., 2022).

What is known?

The duplication of these genes advocates the need for the expansion of a chaperone network in response to a variety of stress factors during the time of evolution. The functions of Hsp16s are not clearly known and remain a significant challenge in our understanding of the stress response. It is known, however, that Hsp16s are heat-induced (Russnak and Candido, 1985; Shim et al., 2003), which is a common feature of many sHsps. Interestingly, it was discovered that total mRNA levels of each gene locus are different following exposure to heat stress for 2 hours. *Hsp16.2* and

Hsp16.41 exceeded expression level of *Hsp16.1/16.48* in 7-folds (Candido et al., 1989).

In 1997 structural characterisation of Hsp16.2 (Leroux et al., 1997) revealed an estimated size of 550 kDa. The native protein was extracted from the heat-shocked nematode extract and compared to the recombinantly purified His-tagged protein. The sedimentation velocity data of that time further added that Hsp16.2 is asymmetrical. The functional analysis confirmed the holdase feature oh Hsp16.2 by demonstrating the prevention of thermally and chemically induced aggregation of citrate synthase (CS). Moreover, it was shown that Hsp16.2 can form a complex with unfolded actin and tubulin. The NTR truncations of Hsp16.2 resulted in the loss of large oligomeric complexes. Such mutants also lost the ability to suppress CS aggregation. The structural features of other Hsp16s were not characterised in detail.

At first it was assumed that Hsp16s act only upon heat stress, nonetheless sHsps can be induced by different stresses. For example, Hsp16.1 and Hsp16.2 were later reported to be induced by hypoxia (Hong et al., 2004; Lee and Lee, 2013). Hsp16.1 is also reported to mediate a cytoprotective effect during heat-stroke by localising to Golgi and cooperating with Pmr-1 ATPase (Kourtis et al., 2012). In the study, the authours showed that heat preconditioning of the worms before the heat-stroke stress supressed neurodegeneration. Cytoprection in this case is mediated by HSF-1 and Hsp16.1. In addition, Hsp16.1 co-localised to Golgi to stabilise heat-labile PMR-1 that regulate stress-induced Ca^{2+} overload in a cytoplasm. Kourtis and colleagues (2012) also reported that Hsp16.41 together with Dnj-19 are required for the tolerance towards heat stroke. Heavy metal exposure is reported to lead to an increase in Hsp16.2 expression (Roh et al., 2006). In addition, sHsp16s may be involved in a regulation of a lifespan by assisting bmk-1 (Qian et al., 2015) or modulating the long lifespan of ribosomal protein rsks-1 mutants (Seo et al., 2013). In this perspective, ageing is considered as a stress factor.

Hsp16s are reported to be expressed in many structures and organs in *C. elegans*, such as muscle, intestine, pharynx, neurons and ventral nerve cord (Wormbase). Their expression is notably ubiquitous and spread across the body. As mentioned

above, the expression is not limited to any specific stage of development – Hsp16s are expressed during nematode growth starting from embryos, during all larva stages (L1-L4) and in adulthood. The express levels vary across the stages, the highest level is reported in L1s (Figure 11).

Expression of F08H9.3 was reported in the pharynx, while F08H9.4 was found in the excretory canal and several neurons. Their expression upon heat exposure was reported as slow and mild. Upon RNAi knockdown of F08H9s, the general thermotolerance of worms was reduced. The level of expression for F08H9s has not been identified (Shim et al., 2003) due to possible tissue-specific expression of the proteins independent of developmental stage.

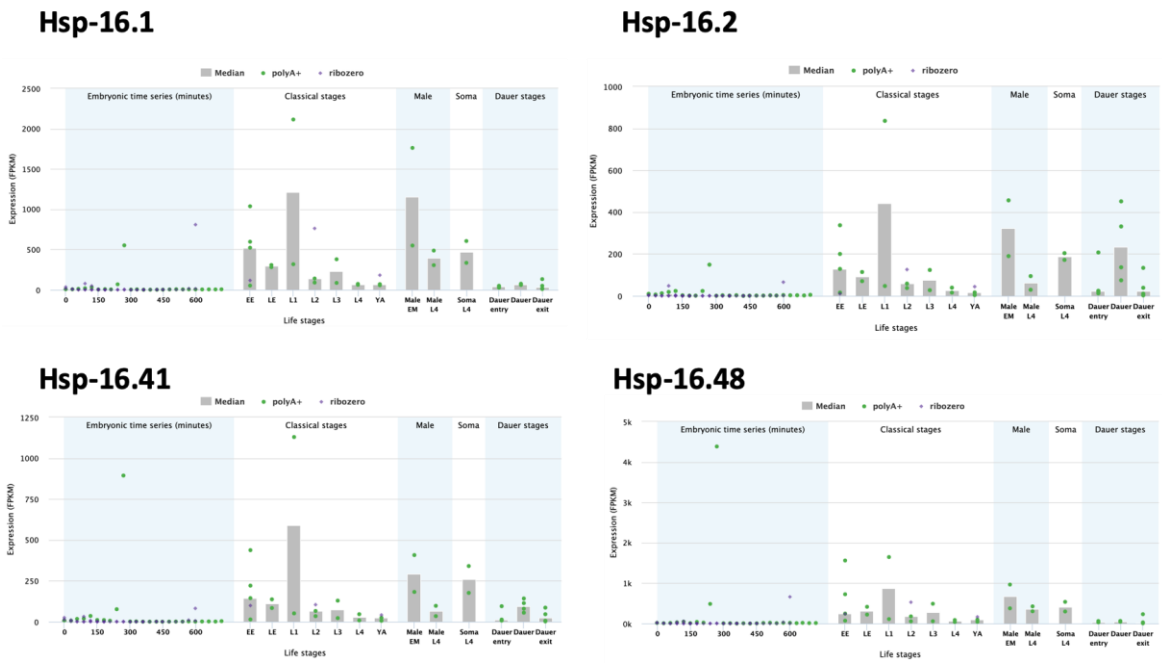

Figure 11. Representation of the expression values of sHsp16s across life stages of C. elegans from the early minutes through larva stages and till young adulthood (YA). *The data is derived from PolyA+ and Ribozero modENCODE libraries. The bars demonstrate the median value of data of the three libraries (adapted from WormBase).*

The cellular localisation of Hsp16s is considered as cytoplasmic. However, it is also reported that Hsp16.1 and Hsp16.41 localise to Golgi, and to the neuronal cell body for Hsp16.41 (Ding and Candido, 2000; Kourtis et al., 2012).

The gathered information about the Hsp16 family is full of discrepancies and lacks a structured and complete characterisation of the molecular functions of all members. The characterisation should also be aligned with the remarkable feature of this family – duplication and subsequently high homology between family members. Therefore, the functional and structural analysis of Hsp16s was covered in this study.

Central question, aim and objectives

sHsps are a conserved and ubiquitous group of molecular chaperones. With 16 of them found in *C. elegans*, the molecular mechanisms of their cellular functions and information about their structure remain mostly elusive. Yet, they are considered as major players in stress response, including the HSR, oxidative stress and ageing. A systematic and comprehensive data set on members of Hsp16 family in a comparative manner has not been reported.

Although some information was published about Hsp16s, it was limited to one or two members of the family and a particular function. In this study, the family of Hsp16 chaperones in *C. elegans* was systematically characterised. Several hypotheses were formed to unravel the main research question – what is the necessity to evolve such a large chaperone network that includes a family of highly homologous chaperones, like the Hsp16s? To answer this question, the approach was focused on the characterisation of protein structure and functions of the Hsp16 family members.

The Hsp16s were investigated with a focus on their characteristics as chaperones, such as typical oligomer structure and suppression of aggregation. The oligomer structure was analysed by methods, such as CD spectroscopy, AUC, HPLC, SEC-MALS and H/DX-MS. In addition, stability of sHsp16 oligomers was analysed by thermal denaturation monitored by CD spectroscopy. Functional analysis of chaperones was done via chaperone activity assays with several model substrates at permissive and elevated temperature. This was complemented by TEM micrographs.

Due to the high homology, sHsp16s were hypothesised to cooperate and communicate in a cell by forming hetero-oligomers. This was tested *in vitro* by establishing a FRET system and subsequent a subunit-exchange assay. Moreover, the hypothesis expanded to the cooperation between different CEsHsp families, which was also tested via FRET subunit-exchange assay.

The major goal was to investigate functional divergence of Hsp16s, especially with regards to their high homology. It was hypothesised that the Hsp16 proteins have

evolved into distinct functional units and preserved the functions of the ancestor gene, from which they originated. To test this, co-IP/MS analysis was performed to detect protein-protein interactions of individual Hsp16 and subsequently analyse divergence between them. Moreover, protein-protein interaction networks were built for both elevated (stress) and permissive (non-stress) conditions to get an overview of functional plasticity and promiscuity of Hsp16s.

II. Results

1. Biochemical and biophysical characterisation of sHsp16s

Structural homology of sHsp16s

The sHsp16 family consists of 4 “main” members (Hsp16.1, Hsp16.2, Hsp16.41 and Hsp16.48) and two related (F08H9.3 and F08H9.4). The BLAST analysis revealed the high homology between these proteins, which indicates that they have originated form one ancestor (Figure 1.1). The highest homology lies in the ACD and the I/V-X-I/V motif in the CTR of all proteins, except F08H9.3, which seems to miss this motif in the CTR and has instead a VPI motif in the NTR. In total, the homology between F08H9.3 and F08H9.4 is the smallest among the family – 46%. The highest similarity of 93% is shared between Hsp16.1 and Hsp16.2, the same identity of 93% is also shared between Hsp16.41 and Hsp16.48. The identity between Hsp16.1 and Hsp16.41/16.48 is 70% as well as between Hsp16.2 and Hsp16.41/16.48. Such sequence similarity allows to allocate Hsp16.1 and Hsp16.2, Hsp16.41 and Hsp16.48 into homologous pairs and hypothesise that behind this feature stands a putative divergence of functions.

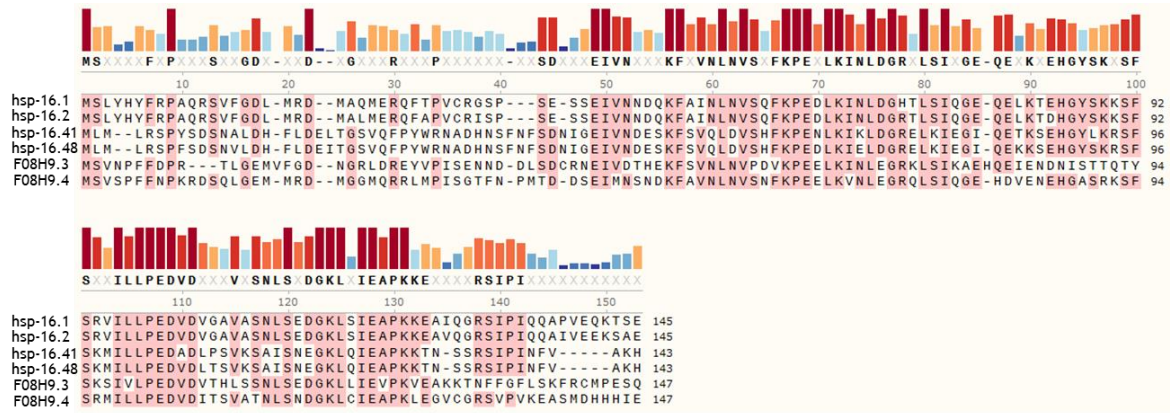

Figure 1.1. Sequence alignment of sHsp16s from C. elegans reveals high identity between the family members. *The protein sequences were aligned using Mafft-G-INS-i with the default parameters and viewed and edited with Jalview and SnapGene. The bar colour intensity corresponds to the degree of conservation and completely conserved residues are marked with dark red bars, dark blue with the least conserved.*

The amino acid content of main sHsp16 members is poor for aromatic amino acid residues, such as Trp and Tyr. Hsp16.41 and Hsp16.48 have only 1 Trp residue each, while Hsp16.1 and Hsp16.2 lack this residue. Each of the protein contains 3 Tyr residues. In addition, only Hsp16.1 and Hsp16.2 contains one Cys residue at position 33. The Asp and Glu-rich content in sHsp16s results in pI values between 4.7-5.94. The intracellular pH in adult *C. elegans* is around 7.5 (Nehrke, 2003), making sHsp16s negatively charged *in vivo*.

IUPred2A context-dependent prediction of protein disorder (Erdős and Dosztányi, 2020) proposed a low level of disorder for main sHsp16s members with a primarily disordered short CTR (Figure 1.2).

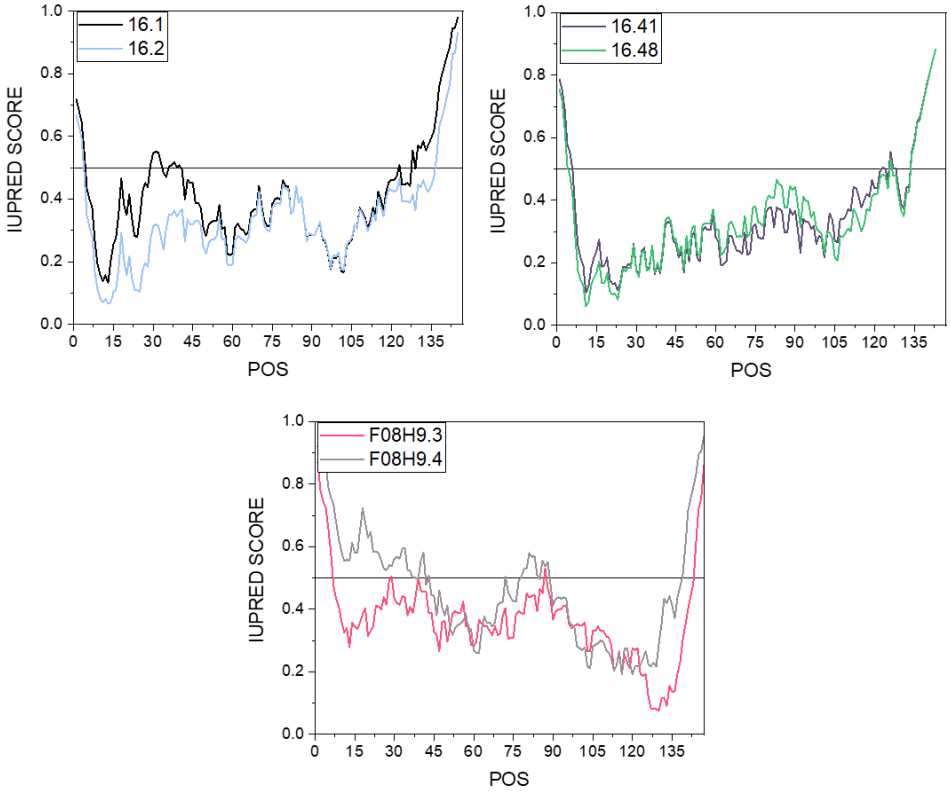

Figure 1.2. Prediction of disordered regions in sHsp16s. *The disorder prediction score plotted against amino acid sequence highlights the ordered nature of the ACD in all proteins and the disordered nature of the CTR of main members. The NTR in F08H9s displays enhanced disorder tendency.*

The very end of the NTR for "core" members is predicted to be highly disordered, while it becomes more structured towards ACD. F08H9.3 and F08H9.4 had several regions of disorder, mainly in the CTR. The highest score of up to 0.7 was predicted for F08H9.4 NTR. Interestingly, CTR of F08H9s was predicted to be more structured compared to CTR of other sHsp16s with a score lower than 0.1. The ACD regions were characterised as least disordered ones.

Purification of sHsp16s

To characterise their structure and functions, the main members of sHsp16 family (Hsp16.1, Hsp16.2, Hsp16.41, Hsp16.48) were overexpressed in BL21 (DE3) cells and purified from inclusion bodies as follows in Figure 1.3:

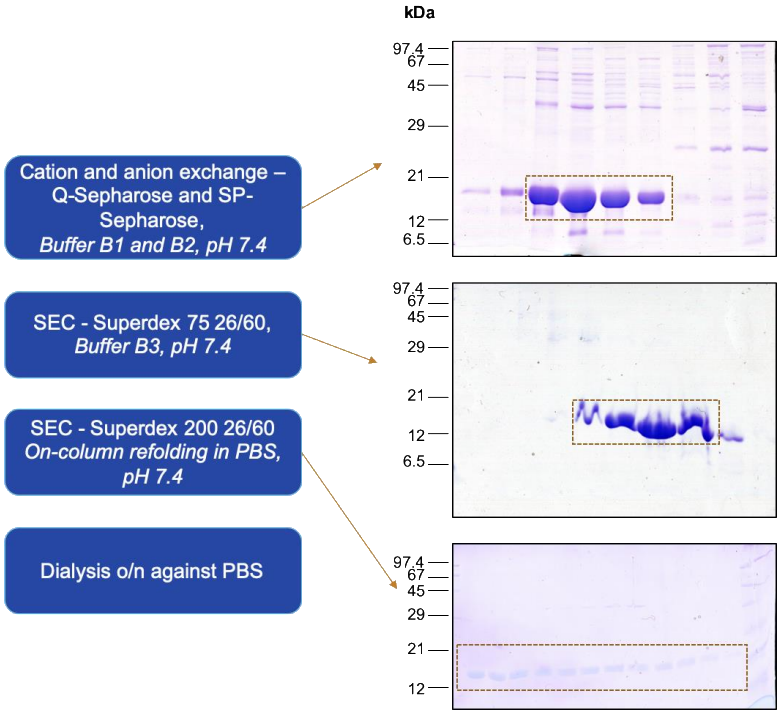

Figure 1.3. Purification strategy for sHsp16s (Hsp16.1, Hsp16.2, Hsp16.41, Hsp16.48). *All four proteins were purified from inclusion bodies via ion-exchange and size exclusion chromatography followed by on-column refolding and overnight dialysis against PBS.*

Hsp16.1 and Hsp16.2 usually yielded 20 mg from 4 L cultures, for the two others the yields were significantly less (about 2-5 mg) and the proteins showed instability and tendency to aggregate at high concentrations. Extinction coefficients for the proteins were taken from UniProt, however upon oligomerisation they tended to change potentially due to the Tryptophan and Tyrosine residues being hidden in the oligomer structure.

After purification and refolding the proteins were analysed by far-UV CD spectroscopy (Figure 1.4) to investigate their secondary structure and confirm the successful refolding. The proteins were examined at the concentration 20 µM in 0.5 mm cuvettes in Chirascan CD Spectrometer. All proteins displayed CD spectra with a negative maximum at 217 nm for Hsp16.1, as well as Hsp16.41, 215 nm for Hsp16.2 and 218 nm for Hsp16.48. The values indicate the β-sheet-rich content and presence of a much smaller proportion of α-helices (Greenfield, 2006).

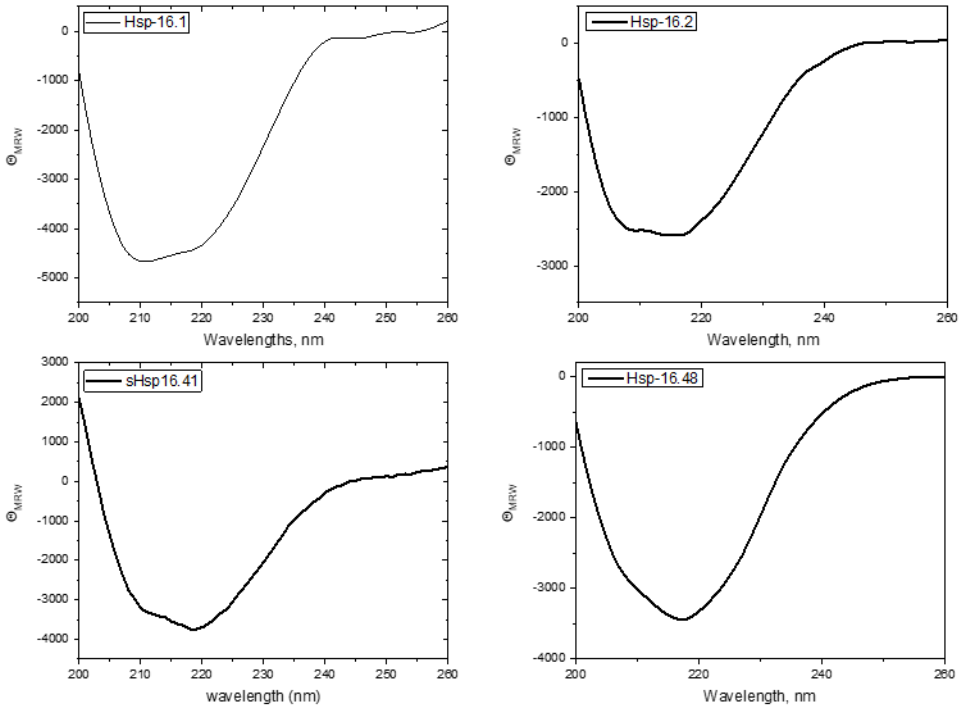

Figure 1.4. Analysis of the secondary structures of sHsp16s shows high β-sheet content. *The spectra were recorded in Chirascan CD spectrometer at 20 ℃ from 260 to 200 nm with a 1 nm step. The protein concentration was 0.3 mg/mL in PBS and measurements were taken in 0.5 mm cuvette. The spectrum was baseline substracted and normalised for protein concentration, path length and the peptide bonds number. The data were moderately smoothed by Savitzky-Golay filtering on the spectrum.*

The secondary structure composition was then evaluated by Beta Structure Selection (BeStSel) (Micsona et al., 2015). The advantage of the algorithm is an ability to distinguish between the parallel and antiparallel β-sheets. The spectra compositions

were estimated in a range from 200 nm to 260 nm (Table 1.1). Analysis showed a high content of antiparallel β-sheets for all Hsp16s. The highest content was estimated for Hsp16.2 (37.1 %). In contrast, homologous to Hsp16.2, Hsp16.1 showed the lowest content of antiparallel β-sheets (23.0 %). Only a very low proportion of parallel β-sheets (1.1 %) was estimated for Hsp16.48. In addition, a low number of α-helices was estimated for all four Hsp16s. Hsp16.1 contains 7.7 %, which is the highest among the family. Contrary to its homologous protein, Hsp16.2 contains only 2.2 % of α-helices. Hsp16.41 and Hsp16.48 have 5.8 % and 4.6 % of α-helices in their secondary structure. From 46.0 % to 54.4 % of the secondary structure were estimated as other types of structures, such as bends, irregular/loop and invisible regions of the structure.

Table 1.1. The estimated secondary structure content of Hsp16s.

	Hsp16.1	**Hsp16.2**	**Hsp16.41**	**Hsp16.48**
Helix	7.7 %	2.2 %	5.8 %	4.6 %
Antiparallel	23.0 %	37.1 %	32.0 %	34.8 %
Parallel	0.0 %	0.0 %	0.0 %	1.1 %
Turn	14.9 %	14.3 %	14.5 %	13.4 %
Others	54.4 %	46.4 %	47.7 %	46.0 %

In addition, fold prediction algorithm (Micsonai et al., 2021) estimated that the majority of antiparallel β-sheets in Hsp16s are denoted to the right-twisted and relaxed antiparallel β-sheets (Table 1.2). Interestingly, Hsp16.1 contains only 2.4 % of relaxed antiparallel β-sheets, while other proteins have 11.8 % - 17.4 %. In addition, a large proportion of α-helices was estimated as distorted ones (1.5% - 4.9 %).

Table 1.2. Fold architecture prediction of secondary structure of Hsp16s.

	Hsp16.1	**Hsp16.2**	**Hsp16.41**	**Hsp16.48**
Regular α-helix	2.8 %	0.8 %	1.8 %	2.0 %
Distorted α-helix	4.9 %	1.5 %	4.0 %	2.7 %
Left-twisted antiparallel β-strand	**2.7 %**	**2.6 %**	**3.1 %**	**4.0 %**
Relaxed antiparallel β-strand	**2.4 %**	**17.4 %**	**11.8 %**	**16.2 %**

	Hsp16.1	Hsp16.2	Hsp16.41	Hsp16.48
Right-twisted antiparallel β-strand	**17.8 %**	**17.2 %**	**17.1 %**	**14.6 %**
Parallel β-strand	0.0 %	0.0 %	0.0 %	1.1 %
Turn	14.9 %	14.3 %	14.5 %	13.4 %
Others	54.4 %	46.4 %	47.7 %	46.0 %

The secondary structures match with the predicted ones by AlphaFold in regards of their β-sheets content (Figure 1.5). According to AlphaFold, there is a high confidence that Hsp16s consist of antiparallel β-sheets and with a low confidence it is predicted that structure includes α-helices in the NTR and CTR. The CD data and the estimated secondary structure content shown above confirm the prediction.

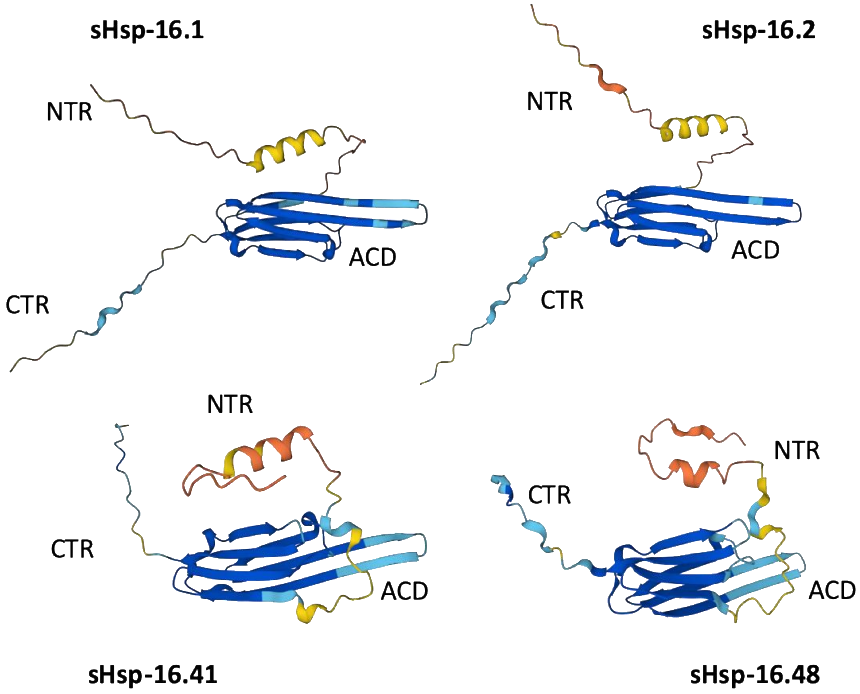

Figure 1.5. Predicted structures of sHsp16s by AlphaFold Protein Structure Database*. Dark Blue shows prediction confidence of "very high", light blue – "confident", yellow – "low", orange – "very low".*

Thermally induced denaturation of sHsp16s was followed to examine their stability. The unfolding was monitored by CD spectroscopy as a function of temperature. The unfolding curves induced by increasing temperatures (Figure 1.6) showed two

distinct transitions (with two mid-points, Tm) indicating the presence of intermediate species during unfolding. The data suggests oligomer subunit dissociation (first step) followed by irreversible monomer unfolding (second step).

All proteins showed a first step with a Tm ranging between 24 to 38°C and a second between 42 to 69°C. Hsp16.41 started oligomer dissociation already at 24°C which designates Hsp16.41 as the least stable within the family. Hsp16.2 is the most stable among the hsp16s with the highest melting mid-points at 38 and 61.6°C. The nature thermal unfolding of Hsp16.48 was different from the other Hsp16s. The unfolding curve shows a rapid unfolding already at 30°C, while the second mid-point possibly represents aggregation.

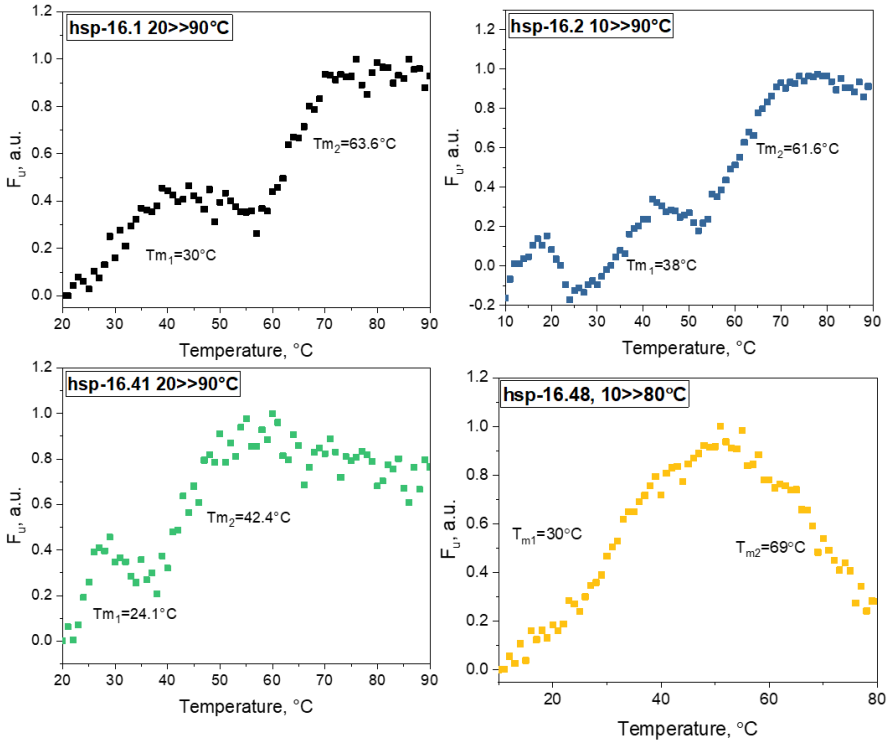

Figure 1.6. Analysis of thermal stability indicates a two-step unfolding for all sHsp16s. *All four sHsp16s were measured at a 0.3 mg/mL concentration. Thermal transition was recorded from 10 to 80 ℃ or 90 ℃ at 217 nm with a heating rate 1 ℃/min. All transition curves are fitted with a sigmoidal Boltzmann fit for each step of the transition to calculate Tm values. The data were normalised and plotted as F_u (fraction unfolded) against temperature points.*

In summary, CD spectroscopy confirmed that all Hsp16s were correctly re-folded. They share similar features in their secondary structure by displaying a rich antiparallel β-sheet structure and exhibit two-step thermal unfolding. From this point, a further characterisation of protein structure, specifically quaternary structure, was performed.

Structural heterogeneity of sHsp16s

To investigate the oligomeric nature of sHsp16 family, the proteins were analysed by SEC-HPLC, SEC-MALS and AUC. These methods allow to determine molecular weight and heterogenic nature of the molecules. Hsp16.41 and Hsp16.48 showed a tendency to aggregate on the SEC column and were studied only via AUC.

SEC-HPLC data were recorded at 230 nm to enable measurement of proteins with low content of Tyrosine and Tryptophan residues. As expected, Hsp16.1 and Hsp16.2 formed large oligomers up to 700 kDa (Figure 1.7), which correspond to the elution of thyroglobulin. These data correlate well with SEC-MALS results.

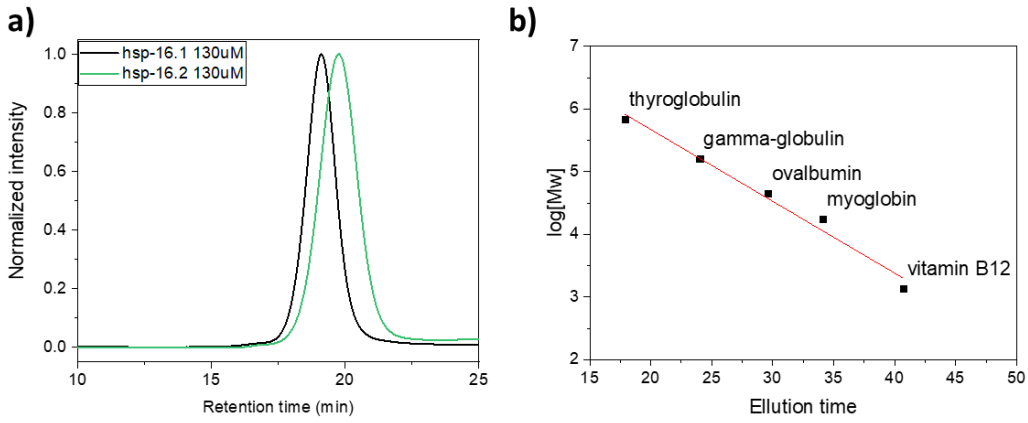

Figure 1.8. Hsp16.1 and Hsp16.2 form large oligomers. *HPLC-SEC chromatograms of Hsp16.1 and Hsp16.2 were recorded at 230 nm and separated at a 0. 5mL/min flowrate on Superdex200 increase 10/300 column. 50 µL of proteins were loaded in PBS. a) Elution chromatograms of Hsp16.1 and Hsp16.2, b) Standard curve was plotted for SEC-HPLC marker and used to determine the molecular weights of the oligomers.*

All members of the family have a low content of aromatic amino acid residues, therefore, for SEC-MALS analysis proteins were analysed with a RI detector. It allows to not only estimate the molecular mass but also extinction coefficient (ε) of a protein. SEC-MALS showed a major peak for Hsp16.1 and Hsp16.2 proteins at 21-24 mins which corresponds to 300-600 kDa molecules and indicates a high polydispersity of the proteins (Figure 1.8). The average of the peaks is ≈450 kDa. The polydispersity

index of 1.016 suggests polydispersity (the monodisperse value corresponds to 1.000). The software estimated for both proteins an extinction coefficient ε of 0.495 which is higher than the one calculated automatically by UniProt (0.275). SEC-MALS analysis indicates that oligomerisation of the proteins affects their absorption.

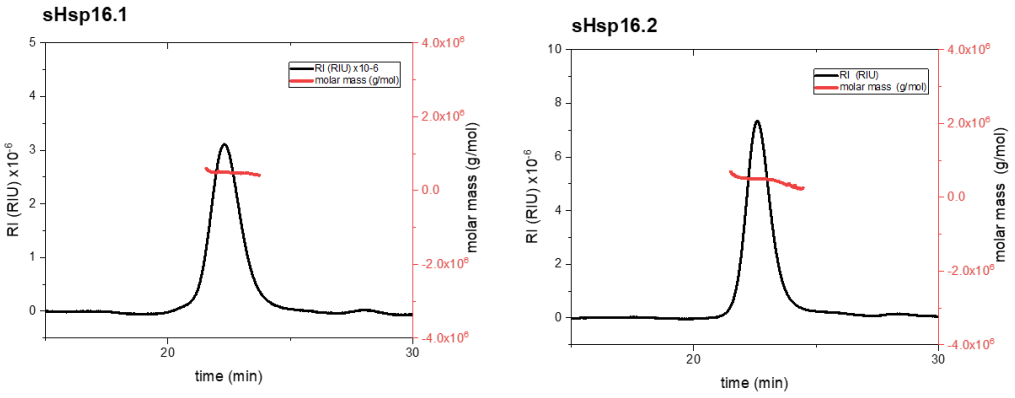

Figure 1.8. SEC-MALS chromatograms of sHsp16.1 and sHsp16.2 show polydispersity. *20 µM of sHsp16s were loaded on a Superdex200 increase 10/300GL column and eluted with PBS at 0.5 mL/min flowrate. Bovine serum albumin (BSA) was used as a standard for calculating the molecular masses.*

As an additional method, AUC was used to evaluate the size and nature of oligomers. It allowed to measure all four proteins. The data was recorded at 230 nm given the low content of aromatic amino acids (Figure 1.9).

As AUC does not involve any interaction with a column matrix, it was possible to get the oligomer sizes for Hsp16.41 and Hsp16.48 proteins, which usually aggregate on a SEC column. Broad peaks of sedimentation (Figure 1.9, A) for Hsp16.1 and Hsp16.2 speak for a wide distribution of oligomer sizes within a sample. Herewith up to 90 % of oligomers exhibit 30-36 subunit complexes (Figure 1.9, B). The distribution of Hsp16.41 and Hsp16.48 oligomers was different. Only half of the species were large oligomers with up to 53 % of them formed by 26-28 subunits (415-460 kDa) and nearly 50 % of small species (ranging from dimers to different multimers comprised of 12 subunits) were present in the sample. The shown profiles match the hypothesis that Hsp16s can be divided into homologous pairs regarding not only their sequence identity but, as shown above, also their structure.

In total, Hsp16 family members are present as large oligomers with up to 36 monomeric subunits. Hsp16.1/16.2 and Hsp16.41/16.48 show similar features in their structure. The oligomers are heterogeneous, which indicates the presence of various molecular species and potentially high dynamics

A

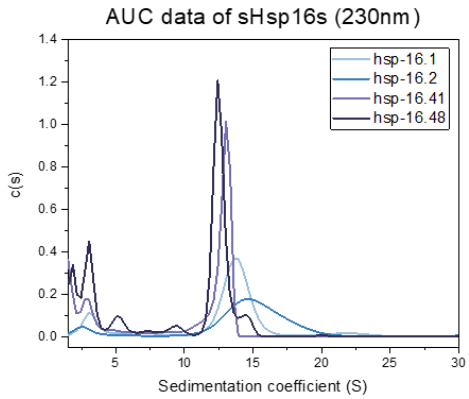

B

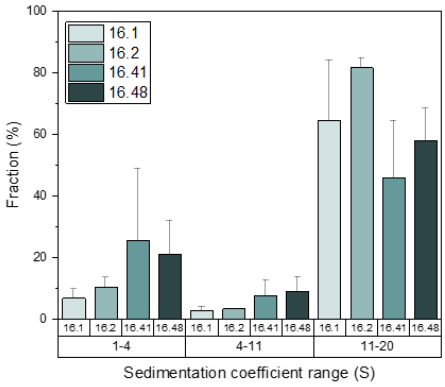

	Average S-value of a main peak	Percentage of the loading signal	
Hsp-16.1	13.5 S	up to 90%	≈480 kDa
Hsp-16.2	15.4 S	up to 84 %	≈580 kDa
Hsp-16.41	12.7 S	up to 53%	≈460 kDa
Hsp-16.48	13 S	up to 52 %	≈422 kDa

Figure 1.9. Homologous sHsp16s show same size pattern for oligomers. *Proteins were measured at 0.3 mg/mL concentration in PBS at 20℃ in triplicates. Sedimentation values were determined at 230 nm at 30 000 rpm. a) Sedimentation profiles of Hsp16.1, Hsp16.2, Hsp16.41, Hsp16.48 show large complexes, the peaks of the homologous Hsp16.1 and Hsp16.2 correspond to heterogenic oligomers, Hsp16.41 and Hsp16.48 have less pronounced heterogeneity of oligomers. b) Distribution of Svedberg values indicates the presence of mostly large oligomers in the samples.*

.

The chaperone activity of Hsp16s *in vitro* comprises holdase and aggregase functions independent of temperature

Hsp16s are molecular chaperones that act in an ATP-independent manner. To investigate their chaperone activity *in vitro*, the proteins were tested for their ability to suppress aggregation of model substrates such as MDH, CS and Insulin. The first two substrates were thermally aggregated at 42°C, which is a lethal heat stress for worms. Also, the chemical aggregation of insulin was used as a model for a milder type of aggregation that would be closer to *in vivo* conditions.

Although the aggregation for MDH and CS was performed at elevated temperature, Hsp16.1 and Hsp16.2 in the similar pattern demonstrated holdase activity by supressing their aggregation (Figure 1.10). Hsp16.2 showed higher activity with both substrates compared to Hsp16.1. While 1 µM of Hsp16.2 supressed aggregation of 2 µM MDH by 85%, Hsp16.1 reached the point only at 1:2 ratio. According to the CD data (Figure 1.4), 43°C would correspond to the dissociation of the Hsp16.1 and Hsp16.2 oligomers and this might assist in their holdase activity. Both chaperones were successful in supressing chemical denaturation of insulin performed at 37°C, however, Hsp16.1 showed higher activity (Figure 1.10). Insulin aggregation was suppressed by 50% with 0.5 µM Hsp16.1, in contrast, Hsp16.2 showed the same activity at twice higher concentration. 4 µM of either hsp16.1 or Hsp16.2 were enough to completely reduce the aggregation of insulin. In contrast, Hsp16.41 and Hsp16.48 demonstrated a tendency towards aggregase activity at elevated temperatures (Figure 1.11). With the increase of Hsp concentration the aggregation was accelerated rapidly for Hsp16.41 and Hsp16.48 with MDH. In the CS aggregation assay complexes showed a less rapid co-aggregation compared to the MDH assay and neither holdase nor aggregase activities were noted. With insulin, however, Hsp16.48 at a concentration 4 µM suppressed aggregation by nearly 50%. Its homologous protein Hsp16.41 showed high suppression at 1 µM concentration by supressing aggregation by 30% and the highest co-aggregation at 4 µM.

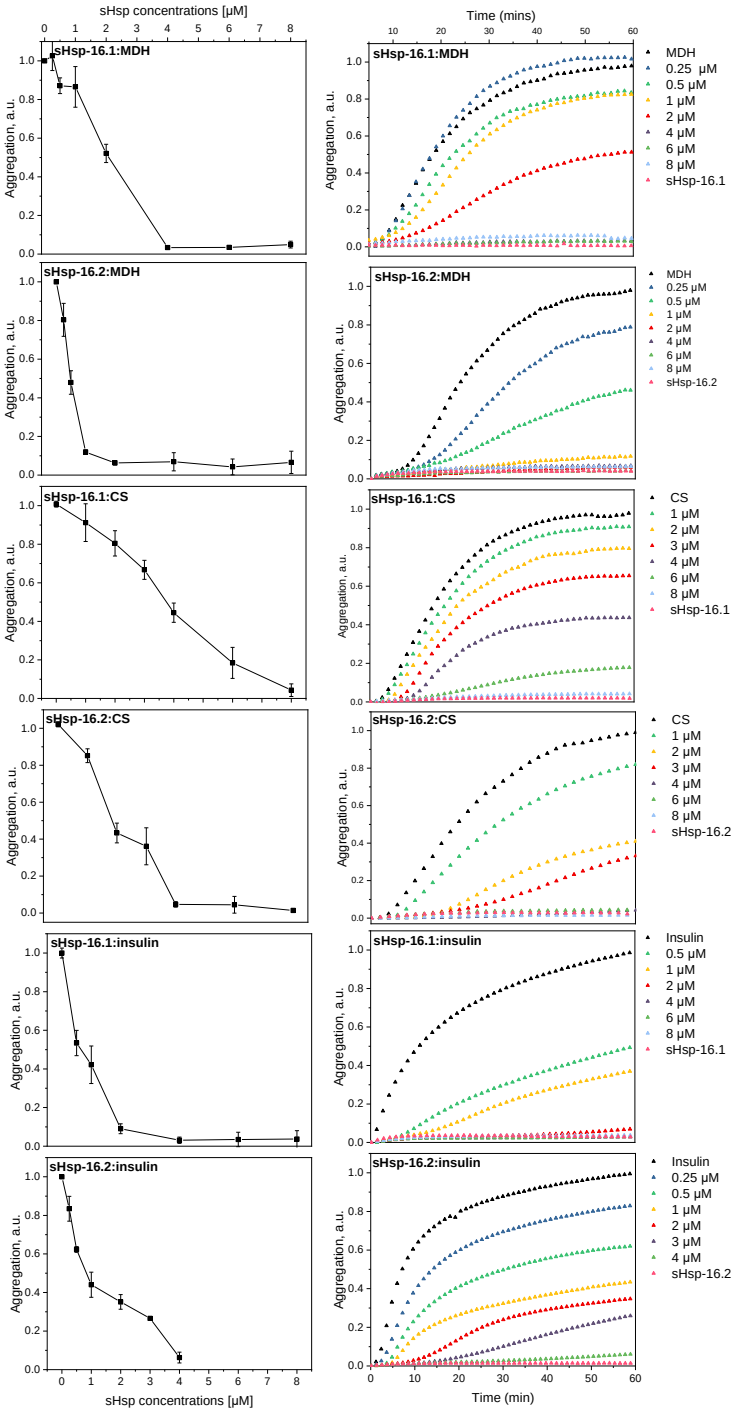

Figure 1.10. Hsp16.1 and Hsp16.2 show similar holdase activity towards model substrates at elevated temperatures. *The proteins were added at different concentrations (0.25 μM, 0.5 μM, 1 μM, 2 μM, 3 μM, 4 μM, 6 μM, 8 μM) to either 2 μM of MDH, 1 μM CS or 40 μM insulin. 8μM of chaperone alone were used as a control for the MDH and CS assays, 4 μM in the insulin assay. Aggregation was monitored at 42 ℃ at 360 nm in a photometer for the MDH as well as CS, and at 37 ℃ with insulin. Level of aggregation at the maximal point (a.u.) is plotted against the concentration of the chaperone added (left), the aggregation curves were plotted against the respective time point (right). Standard deviations were calculated from at least 3 replicates.*

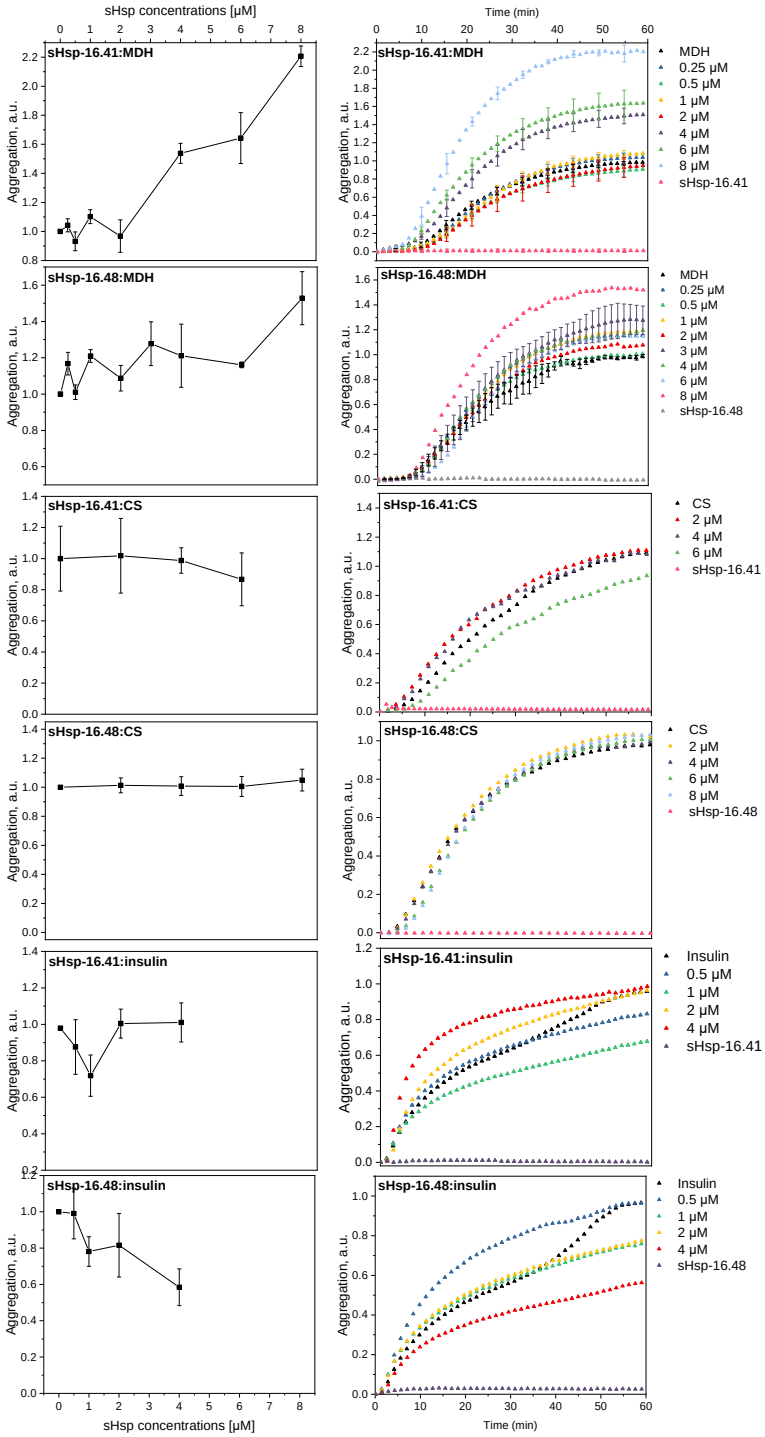

Figure 1.11. Hsp16.41 and Hsp16.48 show similar aggregase activity towards model substrates at elevated temperatures. *The proteins were added at different concentrations (0.25 μM, 0.5 μM, 1 μM, 2 μM, 3 μM, 4 μM, 6 μM, 8 μM) to either 2 μM of MDH, 1 μM CS or 40 μM insulin. 8 μM of chaperone alone were used as a control for MDH assay, 4 μM in CS and insulin assays. Aggregation was monitored at 42 ℃ at 360 nm in a photometer for the MDH as well as CS, and at 37 ℃ with insulin. Level of aggregation at maximal point (a.u.) is plotted against the concentration of the chaperone added (left), the aggregation curves were plotted against the respective time point (right). Standard deviations were calculated from at least 3 replicates.*

From the above graphs it is clear that the Hsp16 family shows pairwise similar chaperone activity mechanisms. Hsp16.1 and Hsp16.2 demonstrate clear holdase activity, whereas Hsp16.41 and Hsp16.48 show aggregase features.

Since chaperones are often associated with activation by heat stress and sHsp16s are not an exception (Ritosssa, 1962; Candido et al., 1989), the aggregation of insulin was then monitored at permissive temperature (15°C). Furthermore, *C. elegans* usually live at 15-20°C, while 37°C is considered an extreme stress (Zevian and Yanovitz, 2014). The question is whether these chaperones need heat to activate their chaperone function. It was hypothesised that the Hsp16 family may not require heat to prevent/promote aggregation of the unfolding substrate. In addition, their chaperone function may be not limited by heat stress but driven by a variety of other cellular stresses.

Hsp16.1 and Hsp16.2 showed high holdase activity with insulin at 15°C (Figure 1.12). Both chaperones supressed aggregation of insulin by 90% at 2 µM concentration. Hsp16.1 showed the same effect at 37°C only at 4 µM. Hsp16.2 was more effective at elevated temperature by suppressing aggregation by 90% at 1 µM. Nonetheless, both chaperones clearly show holdase activity independent of the temperature.

Hsp16.41 and Hsp16.48 showed relatively low holdase activity towards insulin at 15°C. The highest activity (about 20% of aggregation suppression) of Hsp16.41 was at 1 µM, which complements the experiment at 37°C. Hsp16.48 at concentration 4µM suppressed aggregation by nearly 30%, which is similar to its activity at 37°C. These two chaperones were more active at 37°C than at 15°C.

In summary, all Hsp16 proteins showed chaperone activity. Hsp16.1 and Hsp16.2 clearly demonstrate holdase activity with all tested substrates, while Hsp16.41 and Hsp16.48 displayed tendency to aggregase function with MDH and CS and minor holdase activity with insulin.

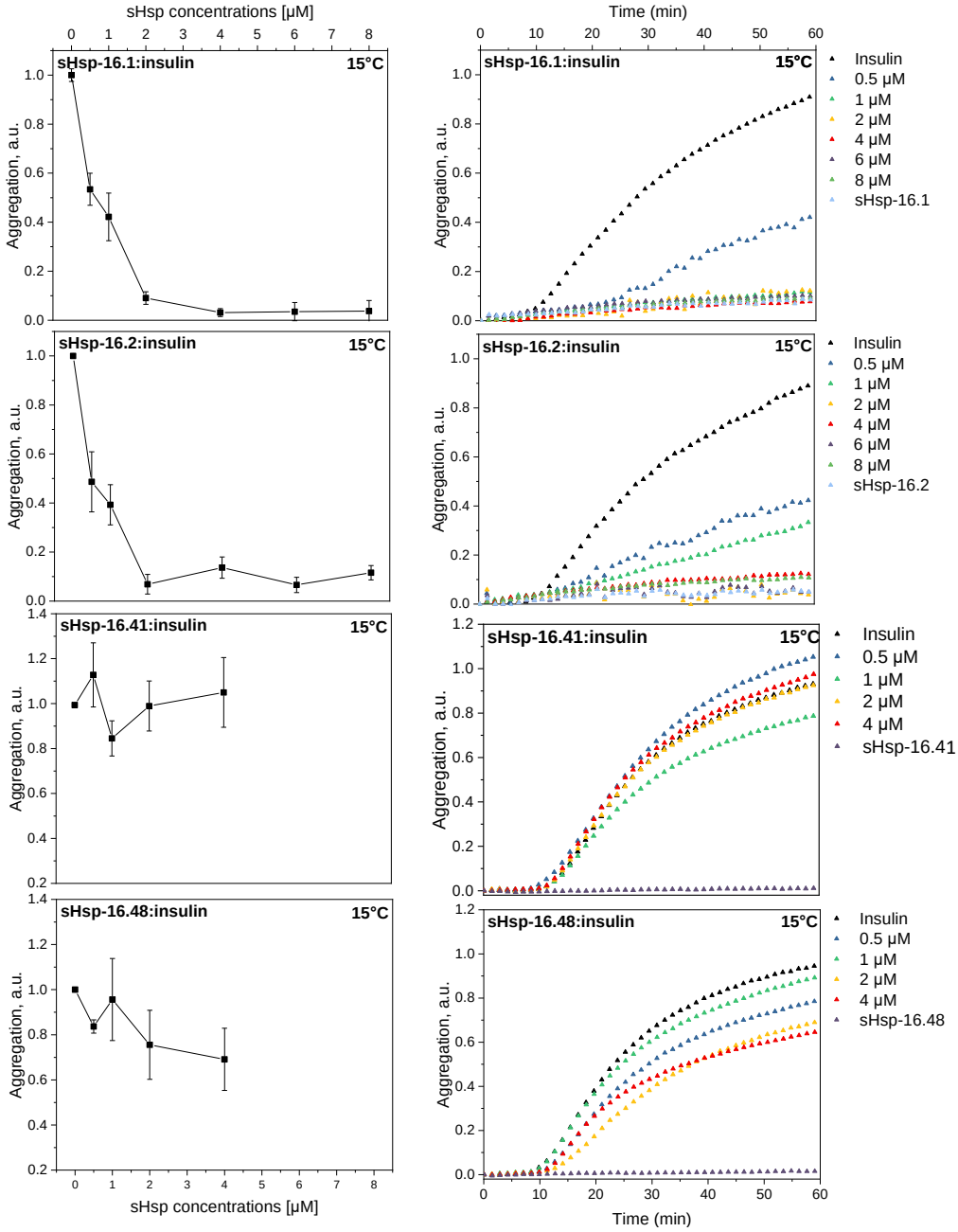

Figure 1.12. Hsp16.1 and Hsp16.2 are active chaperones at permissive temperatures. *The proteins were added at different concentrations (0.5µM, 1µM, 2µM, 4µM, 6µM, 8µM) to 40µM insulin. 8µM or 4µM of chaperone alone were used as a control. Aggregation was monitored at 15 ℃ at 360nm in a photometer. Level of aggregation at maximal point (a.u.) is plotted against the concentration of the chaperone added (left), the aggregation curves were plotted against the respective time point (right). Standard deviations were calculated from at least 3 replicates.*

As shown above, Hsp16.1 and 16.2 supress the formation of amorphous aggregates during a heat stress. To take a closer look at the mechanism of the holdase action of Hsp16.1 and Hsp16.2, the interaction between them and aggregating substrates (MDH and insulin) was monitored by TEM at the timepoints between 0 and 50 min. In aggregation assays 8 µM of Hsp16s is enough to suppress MDH aggregation (2 µM MDH), and 4 µM of 40 µM insulin. These ratios were chosen as a starting point for TEM.

The micrographs show that Hsp16.1 oligomers are stable during the 50 min of exposure to heat and keep the same size without visible dissociation to smaller species (Figure 1.13. A-E). This indicates that heat stress alone may not influence dissociation of Hsp16.1 to smaller species to become an active chaperone.

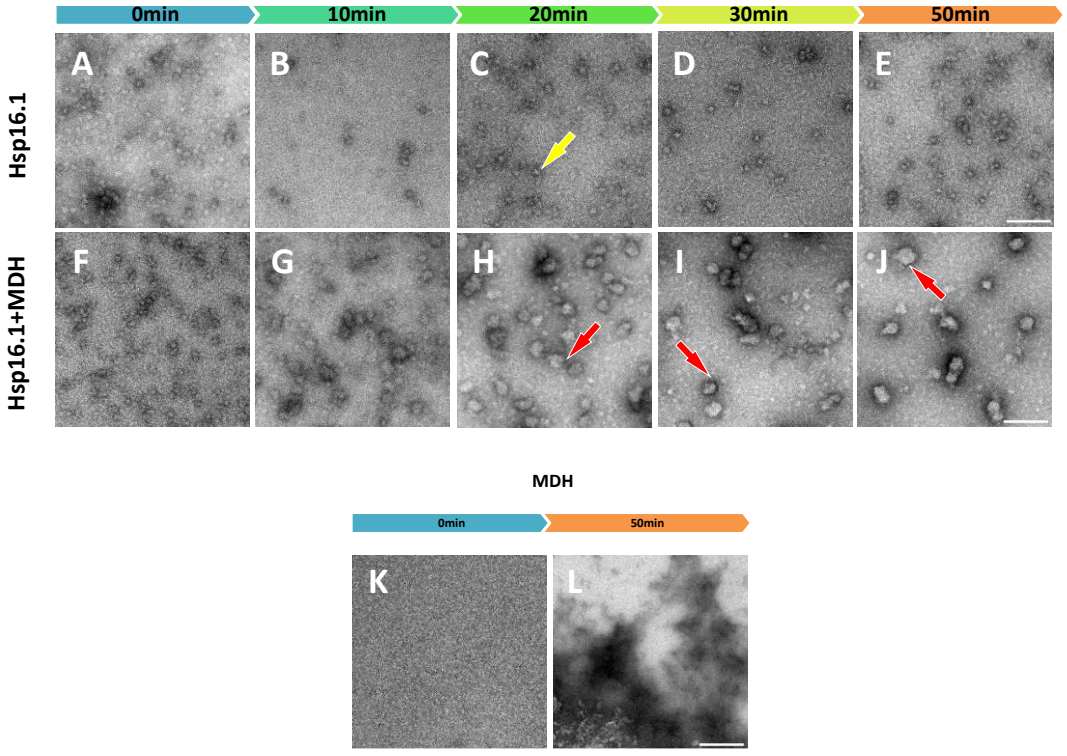

Figure 1.13. Hsp16.1 forms complex with an aggregating MDH to prevent forming of amorphous aggregates*. A-E) TEM micrographs of Hsp16.1 incubated at 42 ℃ for 0 min (A), 10 min (B), 20 min (C), 30 min (D), 50 min (E). F-J) TEM micrographs of Hsp16.1 incubated with aggregating MDH at 42 ℃ for 0 min (F), 10 min (G), 20 min (H), 30 min (I), 5 0min (J). K and L correspond to MDH alone at 0 and 50 min after incubation at 42 ℃ respectively. The scale bars correspond to 100 nm. Red arrows indicate the growing substrate:Hsp complexes, yellow – stable oligomers of Hsp16.1. TEM images were taken by Dr. Carsten Peters.*

Once Hsp16.1 is exposed to an aggregating substrate, it shows a canonical holdase feature by forming a complex with the aggregating MDH (Figure XF-J). These substrate:Hsp complexes grow in size and become at least twice larger than hsp16.1 alone already after 10min of aggregation (Figure 1.13. B, G). MDH alone shows a clear sign of amorphous aggregates in the absence of the chaperone (Figure 1.13. K, L).

As expected, Hsp16.2 showed the same pattern of preventing MDH from amorphous aggregation. The only difference was that the substrate:Hsp complexes demonstrated at least a twice large size compared to Hsp16.2 alone at the 20 min timepoint (Figure 1.14.C, H). As Hsp16.1, Hsp16.2 remained stable during the 50 min incubation at 42°C with no sign of a complete dissociation into smaller species (Figure 1.14. A-E).

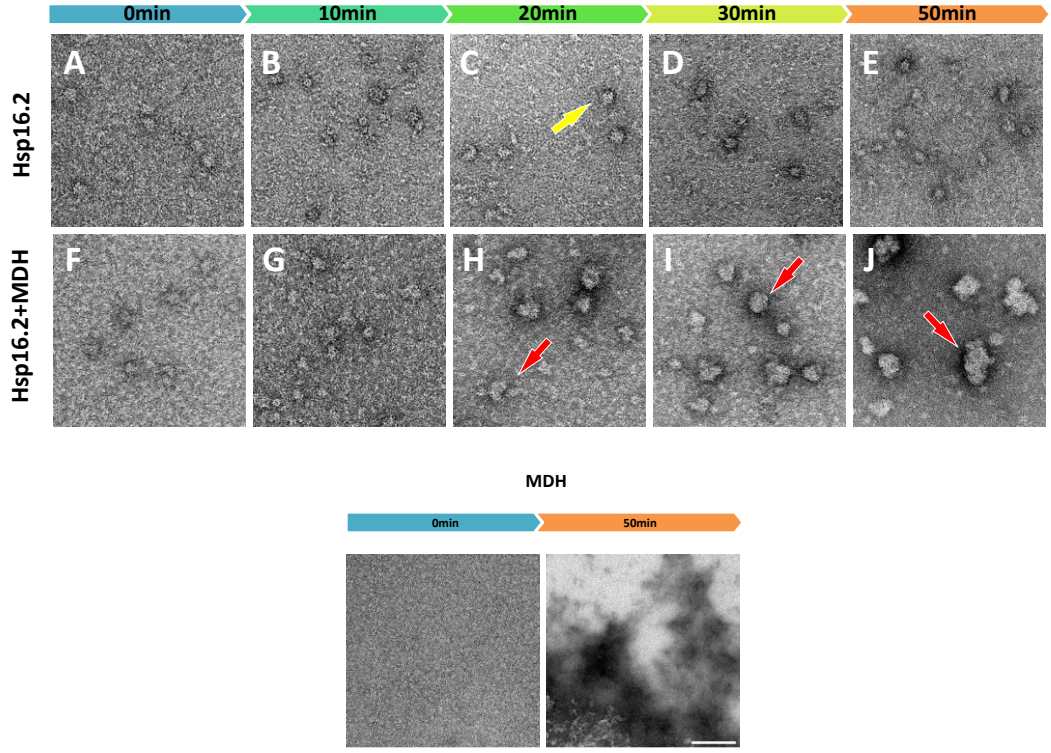

Figure 1.14. Hsp16.2 forms a complex with an aggregating MDH to prevent forming of amorphous aggregates*. A-E) TEM micrographs of 8 µM Hsp16.2 incubated at 42 ℃ for 0 min (A), 10 min (B), 20 min (C), 30 min (D), 50 min (E). F-J) TEM micrographs of Hsp16.1 incubated with aggregating 2 µM MDH at 42 ℃ for 0 min (F), 10 min (G), 20 min (H), 30 min (I), 50 min (J). K and L correspond to 2 µM MDH alone at 0 and 50min after incubation at 42 ℃ respectively. The scale bars correspond to 100 nm. Red arrows indicate the growing substrate:Hsp complexes, yellow – stable oligomers of Hsp16.2. TEM images were taken by Dr. Carsten Peters.*

Hsp16.1 and Hsp16.2 show similar mechanisms of suppression of insulin aggregation (Figure 1.15 and 1.16). Insulin was reduced with DTT and after 50 min showed amorphous aggregates (Figure 1.15, L). Starting at 10min of incubation (Figure 1.15, G), the complexes were visibly larger compared to Hsp16.1 and Hsp16.2 alone. However, unlike MDH, the insulin:Hsp complexes appeared morphologically different, mostly forming smaller complexes of different shapes. Although aggregation is clearly supressed and insulin aggregates were smaller in the presence of Hsp16s, they looked less structured compared to MDH:Hsp.

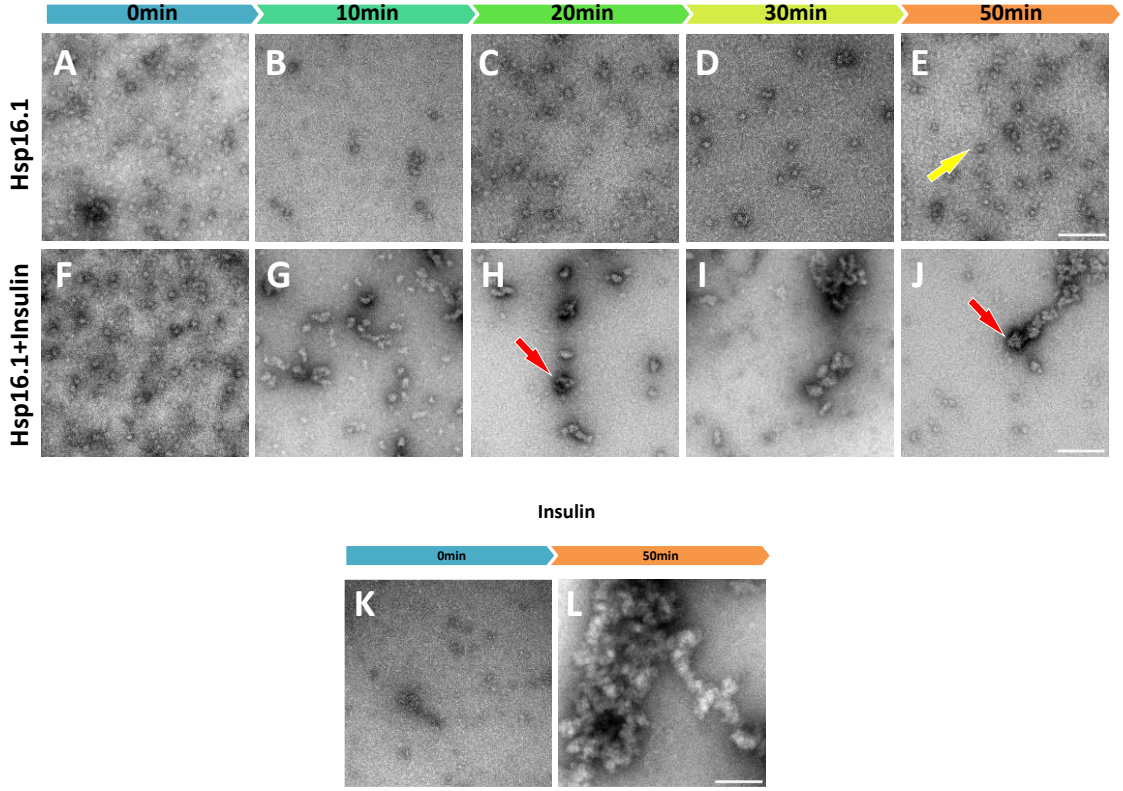

Figure 1.15. Hsp16.1 forms a complex with chemically aggregated insulin to prevent forming of amorphous aggregates*. A-E) TEM micrographs of 4 µM Hsp16.1 incubated at 37℃ for 0 min (A), 10 min (B), 20 min (C), 30 min (D), 50 min (E). F-J) TEM micrographs of 4 µM Hsp16.1 incubated with aggregating 40 µM insulin at 37℃ for 0 min (F), 10 min (G), 20 min (H), 30 min (I), 50 min (J). K and L correspond to 40 µM insulin alone at 0 and 50 min after incubation at 37℃ respectively. Scalebar corresponds to 100 nm. Red arrows indicate the growing substrate:Hsp complexes, yellow – stable oligomers of Hsp16.1. TEM images were taken by Dr. Carsten Peters.*

In addition, it can be concluded that 4 µM of Hsp16.1 do not supress insulin aggregation completely. In contrast, 8 µM of Hsp16.2 (Figure 16, F-J) showed a evident suppression of amorphous aggregation by forming structured Hsp:substrate complexes. The complexes appear larger compared to Hsp only control (Figure 1.16, A-E) but smaller than observed for MDH complexes (Figure 1.14, F-J).

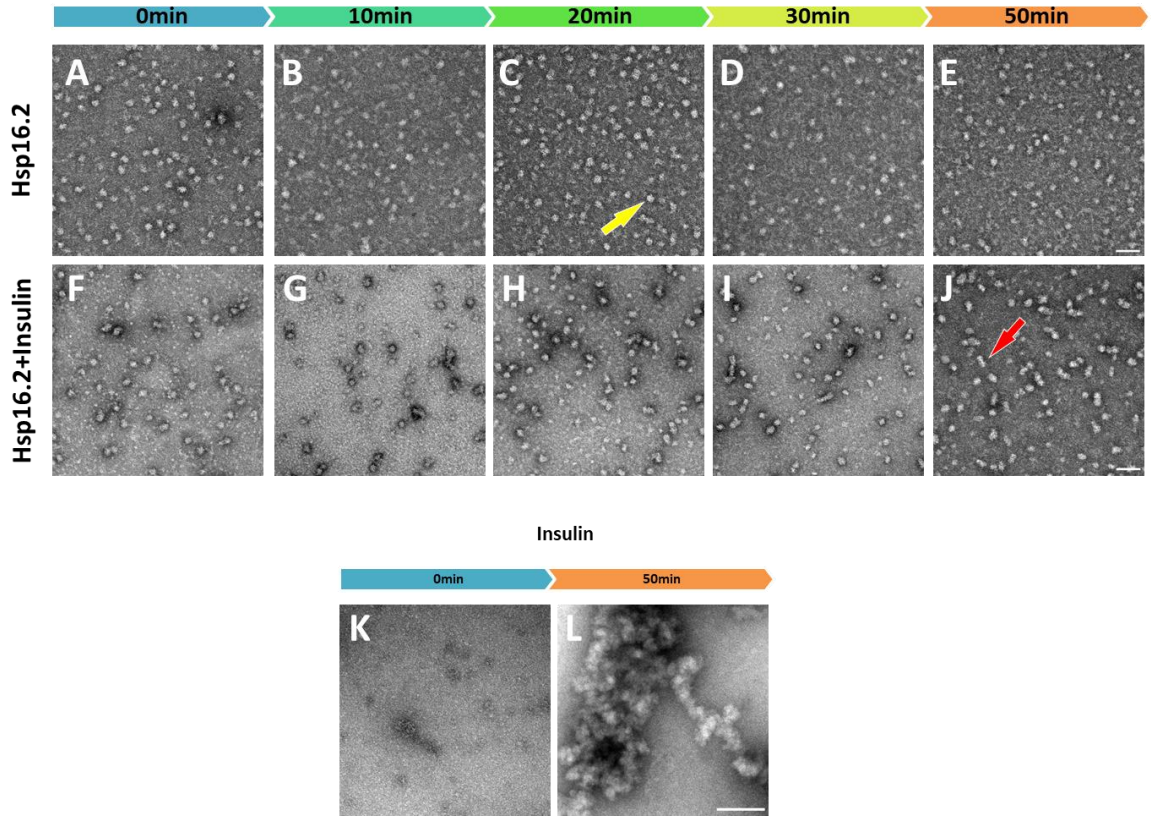

Figure 1.16. Hsp16.2 forms a complex with chemically aggregated insulin to prevent forming of amorphous aggregates*. A-E) TEM micrographs of 4 µM Hsp16.2 incubated at 37℃ for 0 min (A), 10 min (B), 20 min (C), 30 min (D), 50 min (E). F-J) TEM micrographs of 8 µM Hsp16.2 incubated with aggregating 40 µM insulin at 37℃ for 0 min (F), 10 min (G), 20 min (H), 30 min (I), 50 min (J). K and L correspond to 40 µM insulin alone at 0 and 50min after incubation at 37℃ respectively. The scalebar corresponds to 50 nm for assay and 100 nm for insulin control. Red arrows indicate the substrate:Hsp complexes, yellow – stable oligomers of Hsp16.2. TEM images were taken by Dr. Carsten Peters.*

According to the thermal transitions (Figure 1.6), at 37°C and 42°C both chaperones still retain their oligomeric structure and dissociate at temperatures above 50°C. This

corresponds to the observations made in TEM, where Hsp16.1 and Hsp16.2 do not dissociate during the 50 min of incubation. Thus, they do not dissociate into smaller species to become active chaperones and excel their holdase function. They act independently of a heat stress, although *in vivo* they are expressed under stress conditions, including heat stress. The mechanism of their action looks as if they are recruited to unfolding MDH and keep it in a structured form in soluble oligomers without changing their own oligomeric size. Unlike MDH, the insulin:Hsp complexes were less structured, more heterogenous and smaller in size.

In summary, the chaperones displayed a concentration-dependent holdase and aggregase activity with the tested substrates – MDH, CS and insulin under denaturing conditions. They are active at permissive and elevated temperatures as shown in chaperone assays. TEM micrographs specifically illustrated the inhibition of amorphous aggregates at early time points after the induction of aggregation without dissociation of Hsp16.1 or Hsp16.2 into smaller species.

Dynamics of sHsp16s. H/DX-MS

H/DX-MS allows to investigate the structure of sHsp16s by evaluating the dynamics of the molecule. This method allows to analyse the accessibility of hydrogen atoms of amino acid residues (aa) to deuterium and thus evaluate the flexibility or rigidity of proteins on a peptide level. The exchange of hydrogen atoms of each oligomer was measured. The mass spectra were monitored at several time points of exchange (10s, 1min, 10min, 30min, 120min) and visualised via heat maps (Figure 1.17). The peptide coverage is between 84.6% to 97.2% (Figure S1). Hsp16.1 and Hsp16.2 were covered from residue 2 to 145, while residues 16-19 in Hsp16.1, as well as 34-42 and 138 for Hsp16.2 were missing (Figure 1.17, A and B). MS spectra for Hsp16.41 miss residues at the positions 68 and 77, as well as 93-99 peptide, as well as 55-59, 85-89, 123-130 peptides for Hsp16.48 (Figure 1.17, C and D). The NTR of sHsp16s is allocated to 1-42 residues, the ACD to 42-123 and the CTR is 124 to 143/145.

sHsp16s share the same canonical β-fold core structure of the ACD. The B-factor profiles indicate an enhanced rigidity in the ACD region of all proteins (Figure 1.18). However, Hsp16.1 and Hsp16.2 exhibit greater flexibility in the NTR and CTR. Interestingly, the sequence difference between Hsp16.1 and Hsp16.2 is only 10 amino acid residues. Those differences are distributed over all domains - the NTR, ACD and CTR (highlighted in light blue, Figure 1.18, B). This feature may have granted a deviation in flexibility of the NTR and CTR but surprisingly not in the ACD. Switch of hydrophobic residues in Hsp16.1 to more hydrophilic in Hsp16.2 introduced higher plasticity at the position 26-29aa (highlighted in red, Figure 1.18, B). Typical for sHsps (Haslbeck et al., 2019), the CTR at its very end was reported to be flexible. Isoleucine-valine substitution influenced CTR exposure by making this region more flexible in Hsp16.2. Interestingly, alanine-isoleucine cluster (51-52) in the beginning of the ACD showed the same highest rigidity in both proteins and might serve as a stability core.

Hsp16.41 and Hsp16.48 have 93% homology of their protein sequences with a difference in only 9 aa. H/DX-MS showed similar pattern of rigidity in the ACD as in Hsp16.1/16.2, from which they differ in 70%. The highest difference between two

protein pairs lies in NTR and CTR. For Hsp16.41, the first part of the NTR was flexible except a “pocket” at 18-20 L-D-E residues. The same pattern is seen for Hsp16.48. Aspartic residue (D) and Glutamic residues (E) are negatively charged and tend to be exposed on the surface of proteins, unless they are crucial for stability of the protein (Betts and Russel, 2003). The rest of the NTR is moderately exposed in Hsp16.41, even more in Hsp16.48. The NTR of Hsp16.48 was slightly more flexible at the position 13-17aa, where Alanine is replaced by Valine, which is more hydrophobic (underlined red, Figure 1.18, B). Nevertheless, the presence of hidden patterns is surprising as the NTR is considered to be involved in the interaction with unfolding substrate. Another difference between homologous Hsp16.41 and Hsp16.48 lies at another place of variability at the end of the ACD, 110-113aa (SVKS), where Proline is exchanged to the Threonine at the position 109.

The highest flexibility within ACD and in total for Hsp16.41 was at 115-118 aa (ISNE), this region is mostly polar and such residues tend to be exposed to the aqueous environment. The most flexible region of Hsp16.48 is at 78-83aa and 110-113aa regions located in ACD. The CTR of Hsp16.48 was slightly less rigid compared to Hsp16.41, although they both share the identical sequence in the CTRs.

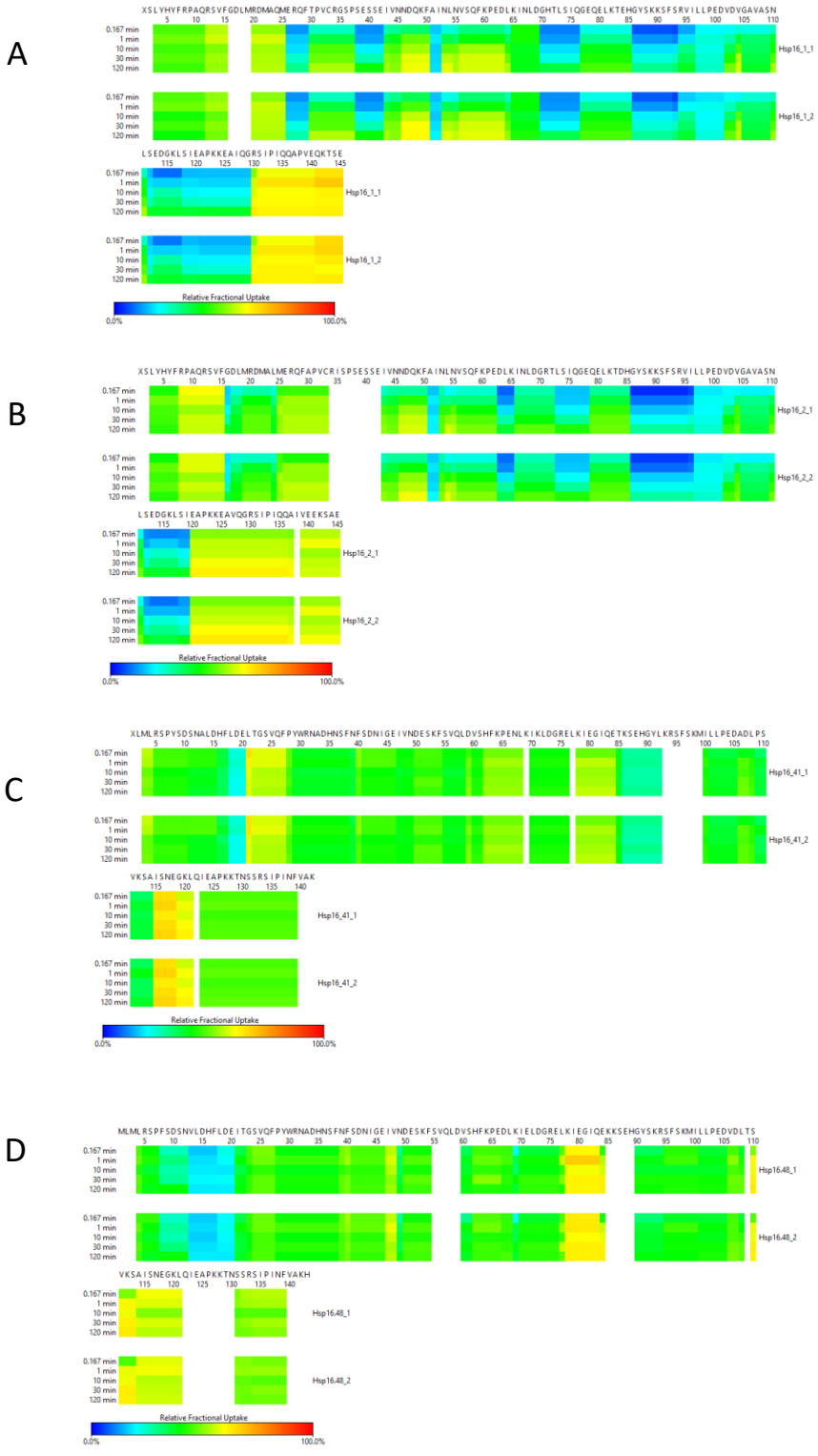

Figure 1.17. sHsp16s show pairwise division in flexibility. *HDX-MS was measured at 10 s, 1 min, 10 min, 30 min and 120 min. Heat maps represent the exchange for amino acid residues with indication of the least flexible (blue) and the most flexible (red) regions A). Heat map for Hsp16.41 B) Heat map for Hsp16.2. C) Heat map for Hsp16.41. D) Heat map for Hsp16.48.*

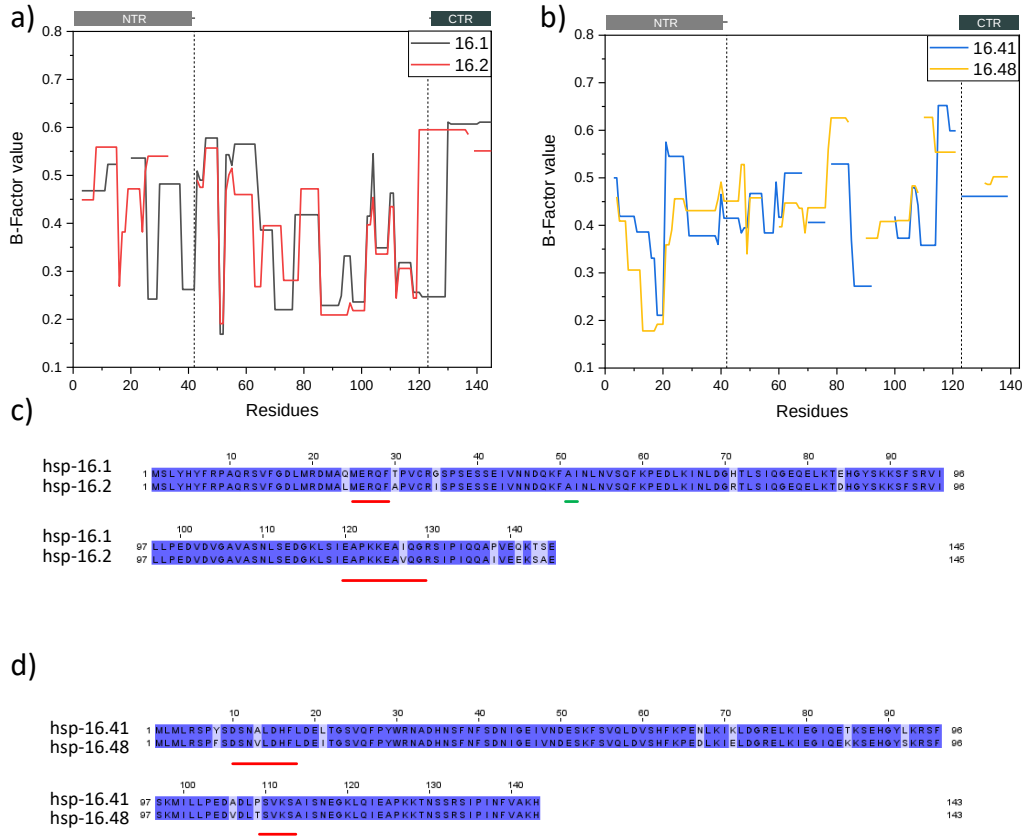

Figure 1.18. Hsp16.1 and Hsp16.2 show differences in the flexibility at the interchange of hydrophillic/hydrophobic residues in the NTR. *A) Comparison of Hsp16.1/Hsp16.2 and Hsp16.41/Hsp16.48 b-factor values that represent the level of flexibility for a protein region. B) Sequence alignment of Hsp16.1/ Hsp16.2 and 16.41/Hsp16.48 with an indication of the most striking differences (red) and one noticeable similarity (green). Differences in amino acid residues are highlighted in light blue.*

FRET shows that homologous sHsp16s cooperate *in vitro*

Given the high homology between sHsp16s and their oligomer size with up to 32 subunits, it was hypothesised that proteins may cooperate and exchange their subunits. The formation of such hetero-oligomers may have a functional advantage *in vivo* (Mymrikov et al., 2020). To test the hypothesis, a Förster resonance energy transfer (FRET) system was established for Hsp16.2. The chaperone contains a single Cys residue at the position 33 (NTR), which makes it an attractive target for labelling. At this position the protein was labelled with Atto550 or Atto647N dyes. First, the FRET complex was formed between Hsp16.2-Atto550 and Hsp16.2-Atto647N at 15°C for 30 min (Figure 1.19, a). FRET was measured for donor (Atto550) and acceptor (Atto647N) at 555 nm and 666 nm, respectively. The gain in acceptor fluorescence resulted in loss of donor fluorescence. This suggests that protein subunits are in a close proximity, which enables transfer of energy from donor to acceptor.

After successfully establishing the FRET system, the interaction of Hsp16.2 with other family members was evaluated by a subunit-exchange assay. For this purpose, a 10-fold excess of unlabelled Hsp16 was added to the pre-formed FRET complex. The exchange was monitored at 15°C by following the change in donor fluorescence. The gain in donor fluorescence would suggest an active subunit exchange between oligomers. The reduction of acceptor signal was not followed due to high dynamic of Hsp16s and generally low acceptor signal at the given concentration.

According to the results shown in Fig.1.19(B), the highest rate of exchange was between Hsp16.2 and Hsp16.1 (56%). This indicates that high homology of these proteins motivates the interaction and possibly leads to interchangeability of Hsp16.1 and Hsp16.2. The disruption of Hsp16.2 FRET complex was less pronounced with Hsp16.41 (38%) and even lower with Hsp16.48 (30%). These findings match well with the expectations built on the assumption that Hsp16.1 and Hsp16.2 may share features due to their similarity.

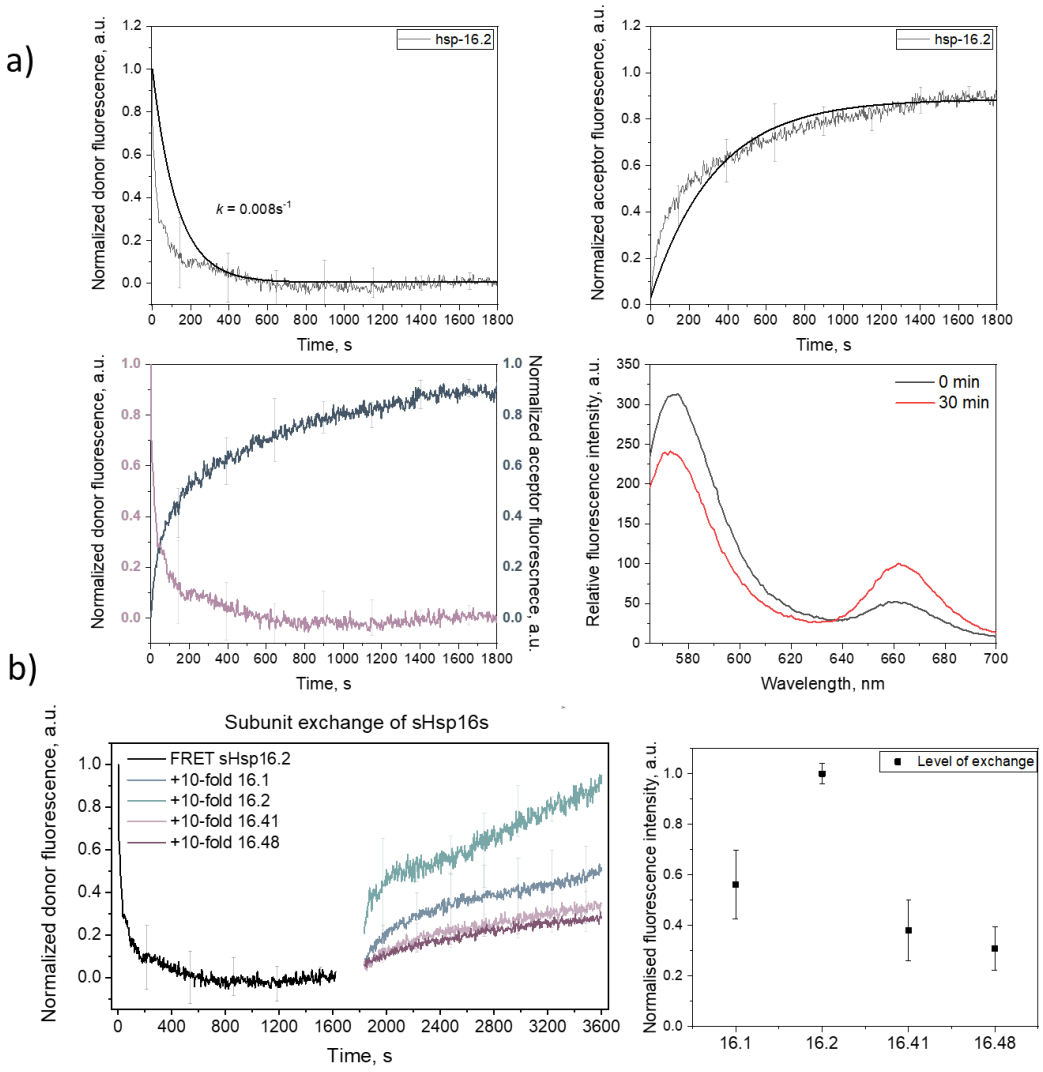

Figure 1.19. sHsp16s interaction in vitro studied by FRET*. A) Formation of the Hsp16.2 FRET pair. Atto550 and Atto647N labelled Hsp16.2 were mixed at 1:1 ratio, to result in 5µM total protein concentration. The change in donor and acceptor fluorescence was measured at 15°C for 30 min at 555 nm excitation and 575/666 nm emission wavelengths. The change in spectra at 0 min and 30 min was followed at 555 nm excitation and 575-700 nm emission range. B) Subunit-exchange was measured by addition of 10-fold excess of unlabelled protein with a final protein concentration 5 µM. The dissociation of a FRET pair complex was monitored by change in donor signal at 15°C for 30 min at 555 nm excitation and 575 nm emission (left). The relative level of exchange with FRET pair was plotted for each of the unlabelled protein (right) by normalizing the end-point of exchange to Hsp16.2. The experiment was performed at least in triplicates and the mean values and the standard deviation are shown.*

To test subunit exchange via FRET with at least one of other homologous proteins, either Hsp16.41 or Hsp16.48, two Cys mutant constructs were ordered from GeneArt (Figure 1.20). The sequences were codon optimised for *E. coli* expression and the genes were cloned in the pET21(+) vector. The plasmids for the Hsp16.41 (A33C) and Hsp16.48 (A33C) mutants were transformed into JM109 (DE3), BL21 (DE3) and Shuffle cells. To optimise expression and later purification of the mutant proteins a pool of test expressions was done at 30°C and 37°C (Figure 1.20) with addition of 1 mM IPTG (final concentration). The test expression of cysteine mutants indicates the optimal system for protein expression as BL21(DE3) at 30°C for Hsp16.41(A33C) and JM109(DE3) at 30°C or 37°C for Hsp16.48(A33C) overnight. Under all tested conditions, the proteins were expressed as inclusion bodies, which requires refolding and purification protocol.

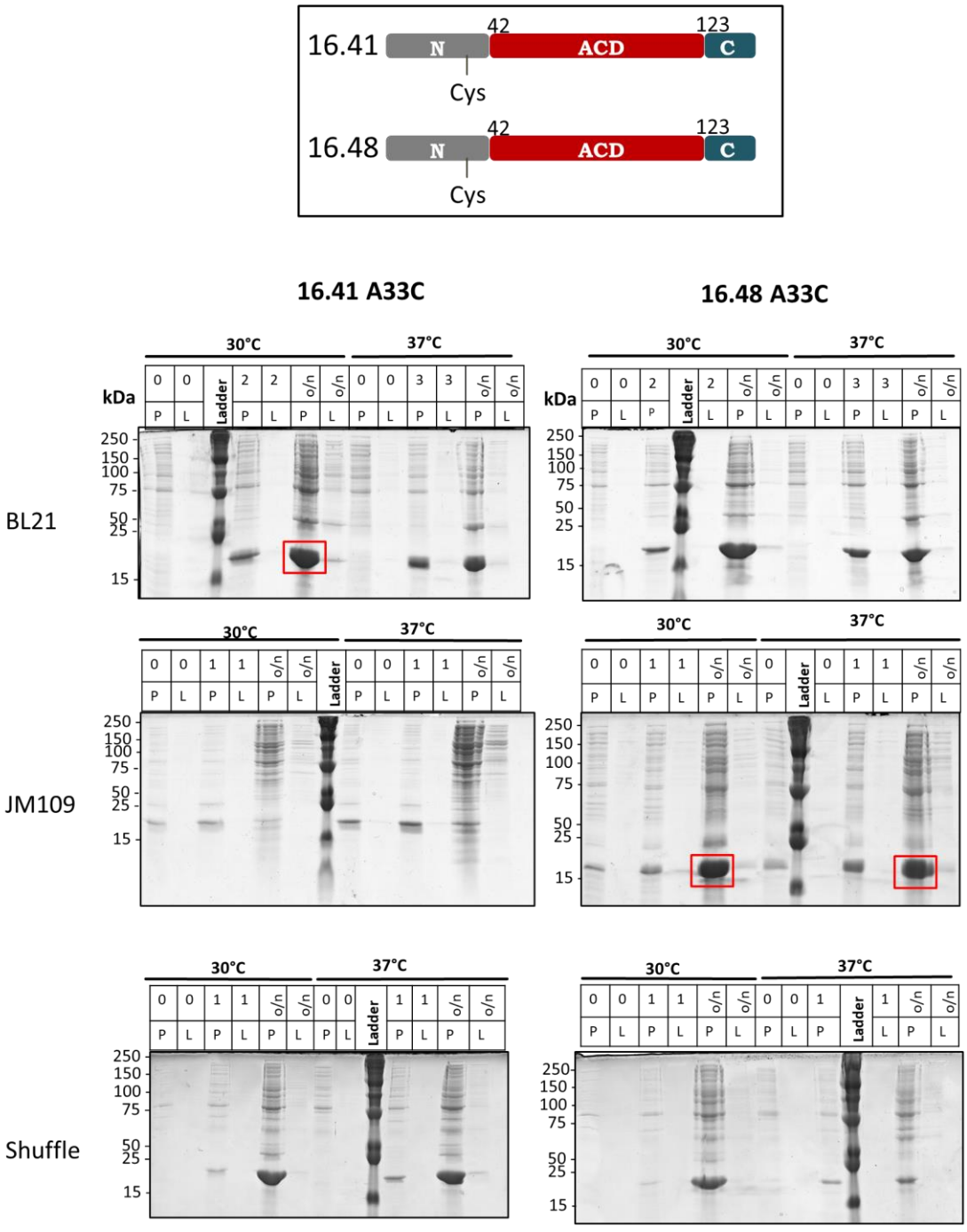

Figure 1.20. Test expression of Hsp16.41 and Hsp16.48 cysteine mutants. *The scheme at the top illustrates a position in NTR at which Alanine was substituted to Cysteine for later fluorescent labelling. SDS-PAGE gels (15%) below show expression of Hsps in the insoluble pellet fraction (P) and in soluble lysate fraction (L) at different time points (0 h, 1 h, 2 h, 3 h or overnight (o/n)). As a reference, pre-stained dual colour protein ladder (Serva) was used. The molecular weights are indicated on the left panel in kDa. The test expressions were carried in three expression E. coli systems, such as BL21 (DE3), JM109 (DE3) and Shuffle cells at 30°C and 37°C. The highest expression for each protein is highlighted in the red boxes.*

2. Interactome profiling of sHsp16s

The feature of sHsps is their ability to prevent aggregation of their substrates. Given the high homology of Hsp16s, it was hypothesised that they act cooperatively in the cell (as shown in FRET experiments). However, the differences in their sequences allow to assume that the interaction network may include Hsp-specific interactors. To investigate this hypothesis and to examine substrate specificity, co-immunoprecipitation coupled to mass spectrometry (co-IP/MS) was performed for all 4 proteins to determine the protein-protein interaction (PPI) network. The chosen workflow is depicted in Figure 2.1:

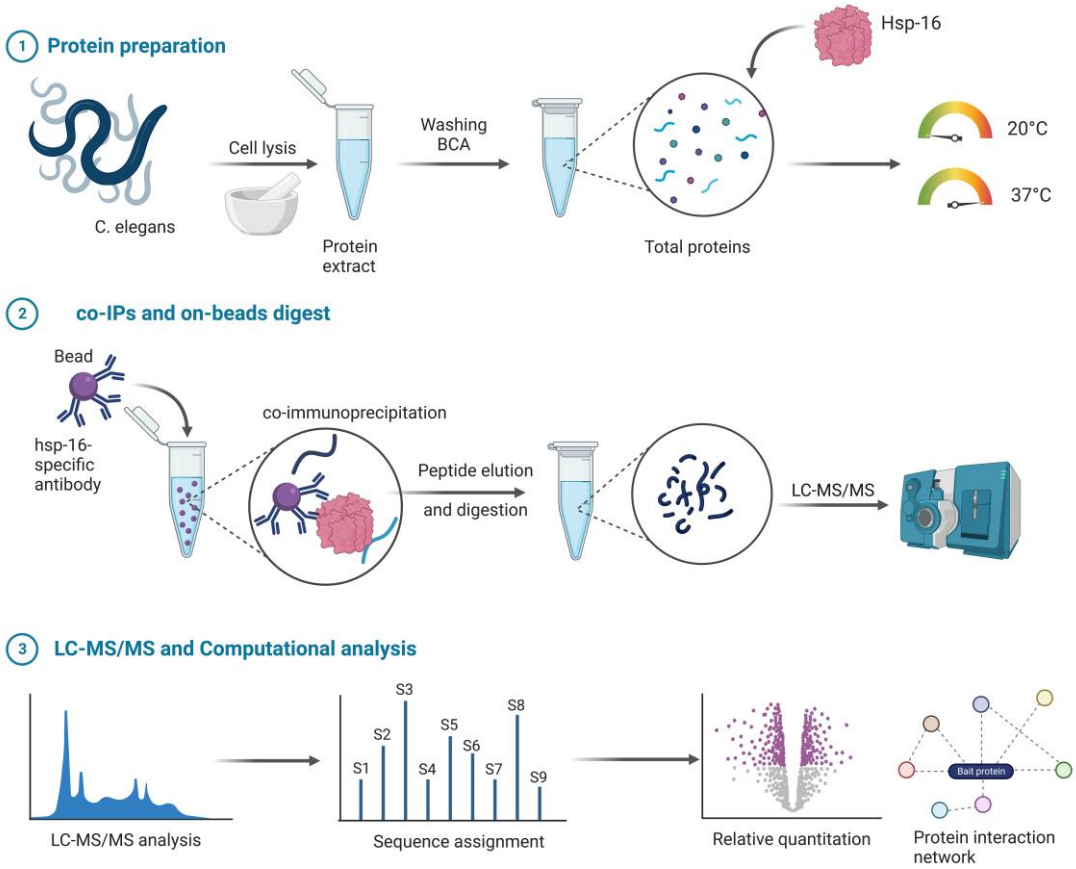

Figure 2.1. The workflow of co-IP/MS for ppi network of Hsp16s. *The three major steps include the protein extraction from worms, co-immunoprecipitation on the beads and mass spectrometry analysis followed by statistical analysis. The workflow is illustrated in BioRender.*

The Hsp16s were added to the protein extract of the wild type (N2 Bristol) *C. elegans* strain and incubated at 20°C and 37°C to mimic regular and stress conditions. Then the formed complexes were captured on the G-sepharose beads coupled to a specific antibody. As a control and to remove false-positive interactions, the complexes were also incubated with a pre-serum. An anti-Hsp16.41 antibody was used for capturing each of sHsp16 as it was tested to be reactive with all four members of the family (Figure. 2.2). The complexes were immobilised on the beads and subjected to the on-bead digest with Trypsin followed by mass spectrometry analysis on the Orbitrap Fusion Mass Spectrometer. Data analysis was performed in MaxQuant v.1.6.2 with a label-free quantification approach (LFQ). The filtering and statistical analysis were done in Perseus v.1.6.2.1. To increase statistical significance, the experiment was performed in quadruplicates with a false discovery rate (FDR) of 0.05.

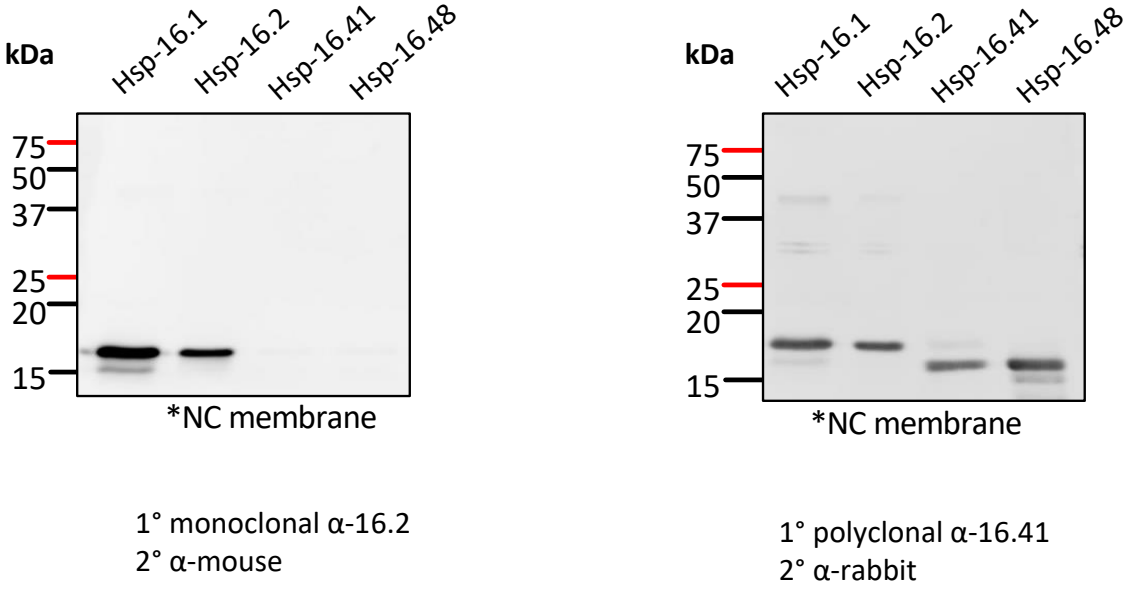

Figure 2.2. Western Blots show low antibody specificity towards sHsp16s. *The anti-Hsp16.2 monoclonal antibody reacts with the two homologous Hsp16.1 and Hsp16.2 proteins, but not with Hsp16.41 and Hsp16.48 (left). The anti-Hsp16.41 polyclonal antibody cross-reacted with all Hsp16s (right).*

In total, over 3000 interactors were identified for each of the four proteins. Around 400 of those were selected after filtering as statistically significant (FDR<0.05) with at least 2-fold change in the abundance compared to the control (Table S1). The Venn diagrams present a visual summary of protein interactors of Hsp16s identified at 20°C and 37°C. The highest number of substrates for each chaperone was noted at 20°C, with exception of Hsp16.48, which showed a slightly higher number of interactors at elevated temperature. Specifically, the highest number of hits were found for Hsp16.1 at 20°C and for Hsp16.48 at 37°C as 477 and 466, respectively (Figure 2.3, A). The lowest number of interactors was found for Hsp16.48 at 20°C and Hsp16.41 at 37°C, 445 and 397 hits respectively.

Interestingly, data showed that the substrate specificity is different at elevated and regular temperatures for each Hsp16. The chaperones show high activity at both conditions, which suggests that they may not act only upon heat stress. This statement was supported by the *in vitro* chaperone assays shown above. In particular, 230 proteins were found at 37°C in all the samples, while at 20°C this number is even higher as 270 hits were shared. Against expectations, a high number of the matching interactors was found for nonhomologous Hsp16s, such as Hsp16.1 and Hsp16.41 (18 hits at 37°C and 25 at 37°C, Figure 2.3, A, in yellow).

Interestingly, when individual Hsp16's interactome at 20°C and 37°C compared, the overlap of interactors is only slightly over 20 % (Figure 2.3, B). For example, only 22% of Hsp16.1 substrates were found at both 20°C and 37°C. In the case of Hsp16.2, this proportion is 23 %, Hsp16.41 is 24% and Hsp16.48 is 24%.

In general, the pattern of overlaps between different Hsp16s is similar at both temperatures. However, when the same Hsp16 is compared at two different temperatures, there is a low number of the same interactors. It appears that the interactomes are affected by temperature.

Protein name	Number of interactors at 20 °C	Number of interactors at 37 °C
Hsp16.1	477	441
Hsp16.2	448	423
Hsp16.41	468	397
Hsp16.48	445	466

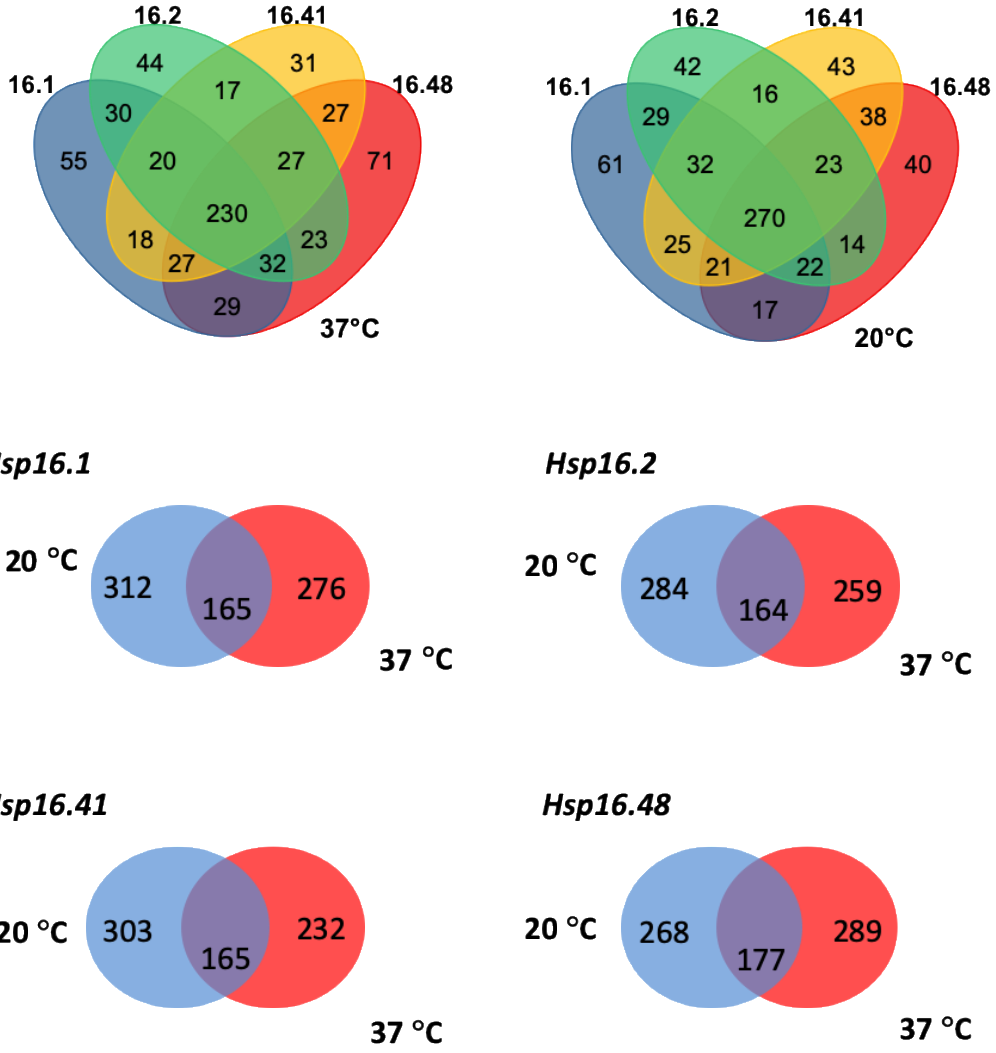

Figure 2.3. Characteristics of the interactome. *A) The table on top summarises the total amount of significant interactors for each chaperone at 20°C and 37°C. Venn diagrams of interactors identified at 20℃ and 37℃ show the total number of hits for each of the samples and an overlap between them derived from the filtered data set. B) The overlap of the hits identified for each Hsp16 at both temperatures was compared.*

The interactors were visualised as volcano plots (Figure 2.4 and 2.5) and the top 15 interactors with the highest abundance were highlighted. These interactors varied among the sHsp16s, however, several of them were found in all four pull-downs.

Hsp16s share many highly abundant interactors at 37°C (Figure 2.4). For example, among the interactors with highest abundance was tost-1, responsible for cell division (Cordeiro Rodriges et al, 2019). Spd-5 is another specific example of a top interactor. However, it was not found among the top scored for Hsp16.41. This protein is involved in regulation of miotic cycle and protein localisation to organelles (Erpf et al, 2019). Interestingly, unc-26 was among the top interactors for all four Hsp16s but only at 37°C. This protein is responsible for locomotion, a phosphatase activity and is also implicated in the Down syndrome. It is considered to be an ortholog of a human protein involved in Parkinson's disease (Yemini et al, 2013; Kim et al., 2018). An exclusive hit for Hsp16.1, Hsp16.41 and Hsp16.48 was the mlc-2 interactor, which is involved in muscle contraction and hypothesised to be a part of myosin complex (Rushforth et al, 1998). In addition, it is an ortholog of several human genes, such as MYL10, MYL2 and MYL7 (Kim et al., 2018). Highly abundant in Hsp16.41 and Hsp16.48 pull-downs at 37°C was raga-1 that has GTPase activity and determinates the adult lifespan (Heintz et al, 2017). Found among the Hsp16.2, Hsp16.41 and Hsp16.48 top-15 interactors a sel-11 protein, is predicted to facilitate ubiquitin protein ligase activity, it is also an ortholog of human SYVN1 (Choi et al, 2010). As can be seen, at 37°C the interaction network of sHsp16s overlaps, including the top-15 of the most abundant interactors.

In the top-15 interactors of Hsp16.2 at 37°C (Figure 2.4, b) trpp-6 protein was found, which is a member of the trafficking protein family in *C. elegans*. Interestingly, this protein is predicted to be involved in ER/Golgi vesicle-mediated transport. Hsp16.41 and Hsp16.48 were also identified as interactors of trpp-6 at 37°C, however at lower abundance. At 20°C, however, trpp-6 was among the Hsp16.2 interactors only. Several other trpp family members were identified, such as trpp-5, trpp-8 and trpp-11. In addition, at 20 trpp-1 and trpp-4 were found to interact with Hsp16.48 and Hsp16.2/Hsp16.41 respectively.

Hsp16.41's unique top-15 interactor (Figure 2.4, c) imp-2 is involved in proteolysis (Grigorenko et al, 2017). It was also found to be interactor of other sHsp16s but at lower abundance. In addition, in the top-15 of Hsp16.41 was also found epg-7, which is a scaffold protein that is reported to be implicated in autophagy (Zhang et al., 2013). Human ortholog of this gene RB1CC1 is reported to be involved in breast cancer (Ki, et al., 2018; Konstantinidis and Tavernarakis, 2021). The epg-7 was among interactors of all sHsp16s with exception of Hsp16.1.

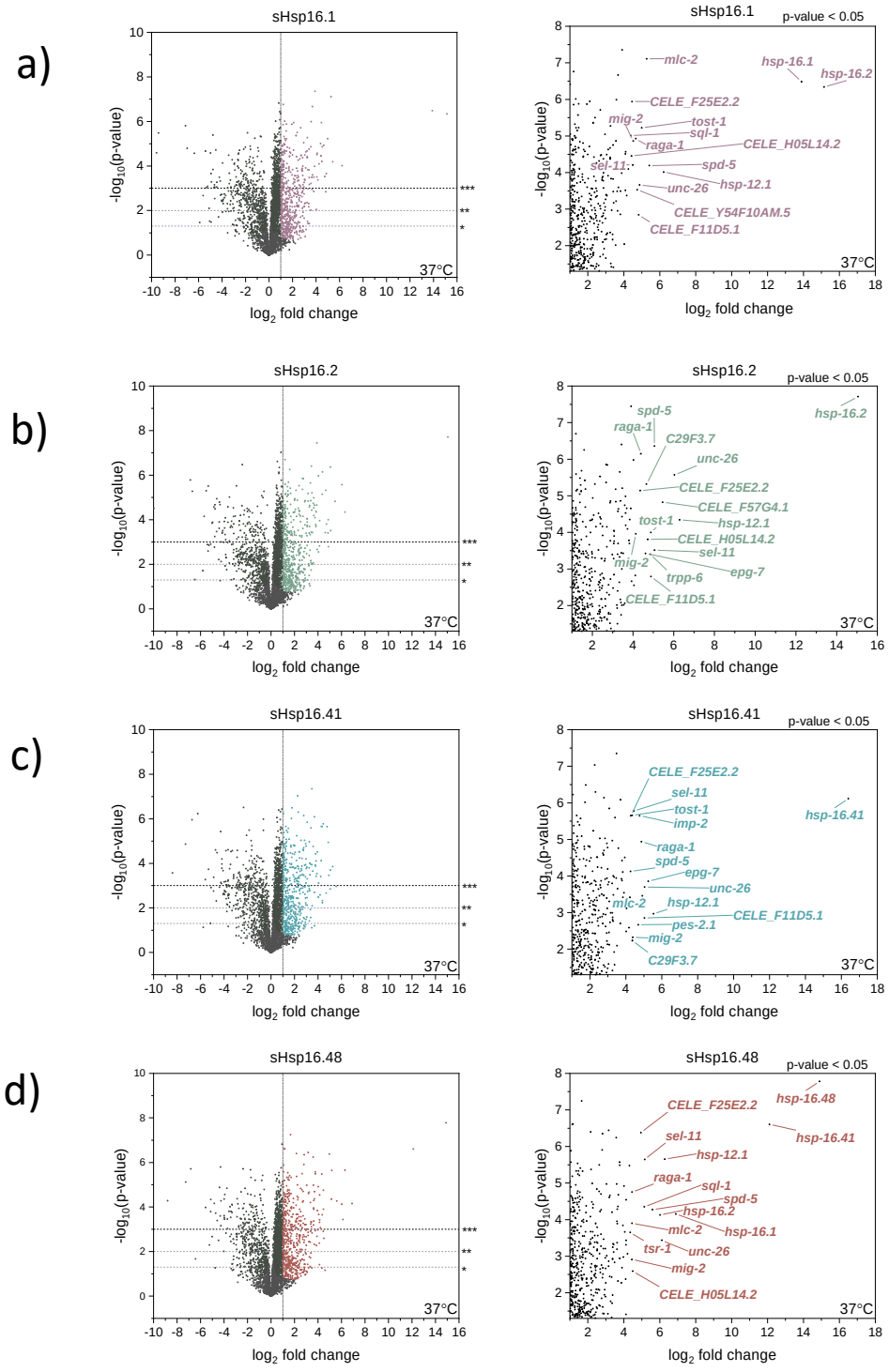

Figure 2.4. Volcano plots illustrate the interactors of Hsp16s at 37°C. *A-D) Volcano plots that represent the interactors of Hsp16.1, Hsp16.2, Hsp16.41 and Hsp16.48 respectively. The most significant interactors were visualised in colour, the parameters were FDR<0.05 and at least 2-fold change of abundance (* corresponds to FDR<0.05, ** to FDR<0.01, *** to FDR<0.001). The top-15 interactors were chosen based on their abundance and are presented on the right.*

In the interaction network of Hsp16.48 (Figure 2.4, d) sql-1 was found at high abundance compared to other Hsp16s. Interestingly, it is predicted to participate in ER/Golgi vesicle-mediated transport and small GTPase activity (Broekhuis et al, 2013), likewise trpp family. Sql-1 was identified as an interactor of all Hsp16s, however at the highest level in PPI network of Hsp16.48. Mig-2 and tsr-1 are both assigned as interactors of all fours Hsp16s but were enriched the most for Hsp16.48.

The most striking interaction that is found in the data is one with the members of another small heat shock family in *C. elegans* – Hsp12s. Hsp12.1 was listed in top-15 of all Hsp16s at both temperatures. In addition, Hsp12.2 was found among the hits of all Hsp16s as well, however at a lower abundance. The other two members of Hsp12 family – Hsp12.3 and Hsp12.6 – were not found.

In summary, the top-15 interactors of Hsp16s at 37°C overlap, however, the list also includes unique proteins. On the other hand, most top-15 interactors are allocated to more than one Hsp16 but at lower abundance, which excluded them from the top-15 list.

To check the hypothesis that homologous Hsp16s may share functions and therefore substrates, the obtained data sets were plotted against each other to estimate the correlation between them (Figure 2.5). Unsurprisingly, the homologous chaperones showed strikingly high correlation. Pearson's coefficients (*r)* were 0.93 and 0.91 for Hsp16.1/Hsp16.2 and Hsp16.41/Hsp16.48 pairs respectively. This means that chaperones share a significant proportion of substrates at 37°C, which confirms the initial hypothesis.

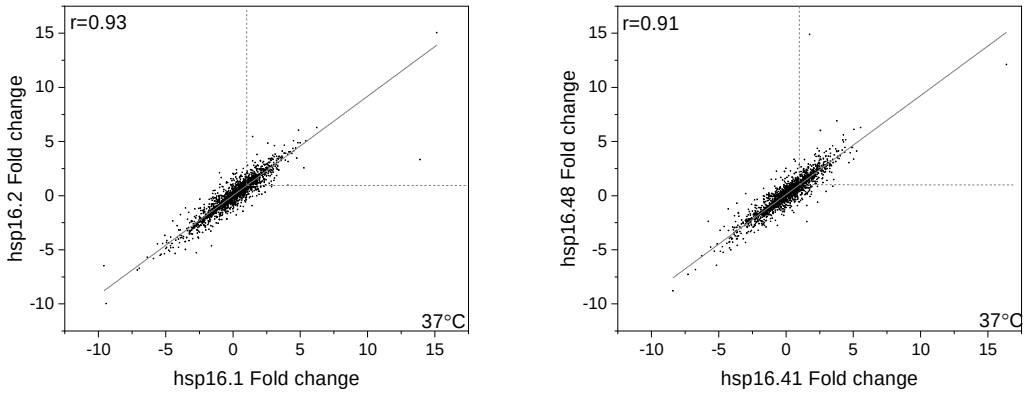

Figure 2.5. Correlation between homologous sHsp16s regarding their interactors is high at 37℃. *The fold change in abundance of interactors of homologous proteins (Hsp16.1 to Hsp16.2, Hsp16.41 to Hsp16.48) were plotted against each other and Pearson's correlation coefficient was calculated to determine the linear correlation between two sets of data.*

The correlation between nonhomologous chaperones was estimated in the same manner by calculating the Pearson's coefficients (Figure 2.6). The correlation between Hsp16.41 and Hsp16.1 or Hsp16.2 is 0.86. The correlation between Hsp16.48 and Hsp16.1 or Hsp16.2 is 0.85. Although the correlation was lower compared to homologous chaperones, it is nonetheless high. This suggests that a homology of 70% between nonhomologous proteins allows the proteins to share substrates.

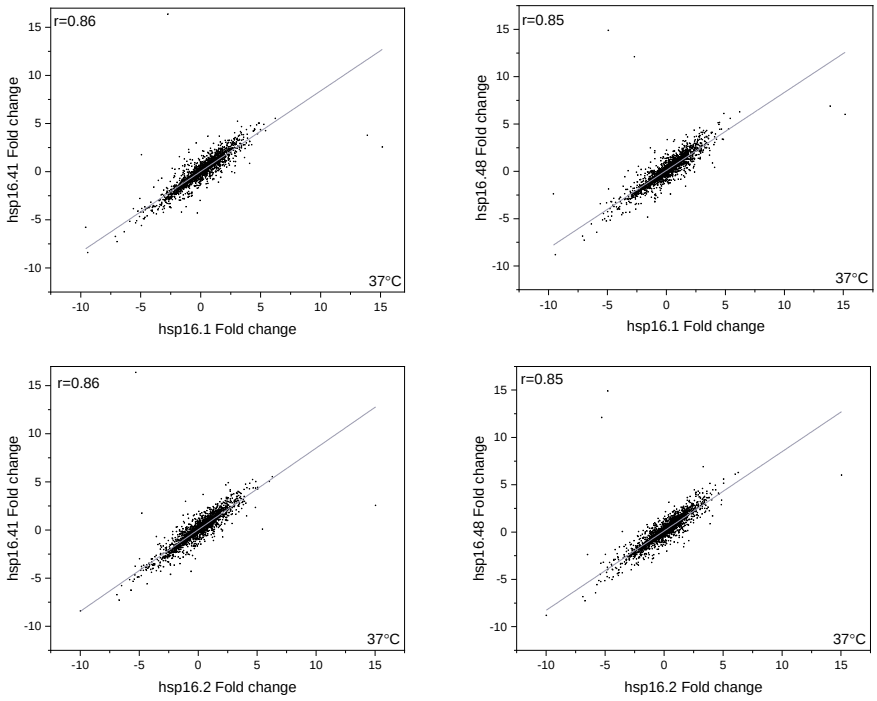

Figure 2.6. Correlation between nonhomologous sHsp16s in regards of their interactors is lower than between homologous ones at 37°C. *All interactors of nonhomologous proteins (Hsp16.1 to Hsp16.41, Hsp16.1 to Hsp16.48, Hsp16.2 to Hsp16.41, Hsp16.2 to Hsp16.48) were plotted and Pearson's correlation coefficient was calculated to determine the linear correlation between two sets of data.*

Then the correlation between interactors of each chaperone at different temperatures was estimated via Pearson's correlation coefficient (Figure 2.7). For Hsp16.1 the correlation between identified substrates at 20°C and 37°C is *r*=0.59, for Hsp16.2 *r*=0.57, for Hsp16.41 it is slightly lower and is estimated as *r*=0.56, for Hsp16.48 is *r*=0.58. The correlations are similar among the protein family. Interestingly, there is more correlation between substrates at 37°C among different chaperones than between the interactome of the same chaperone at different temperatures.

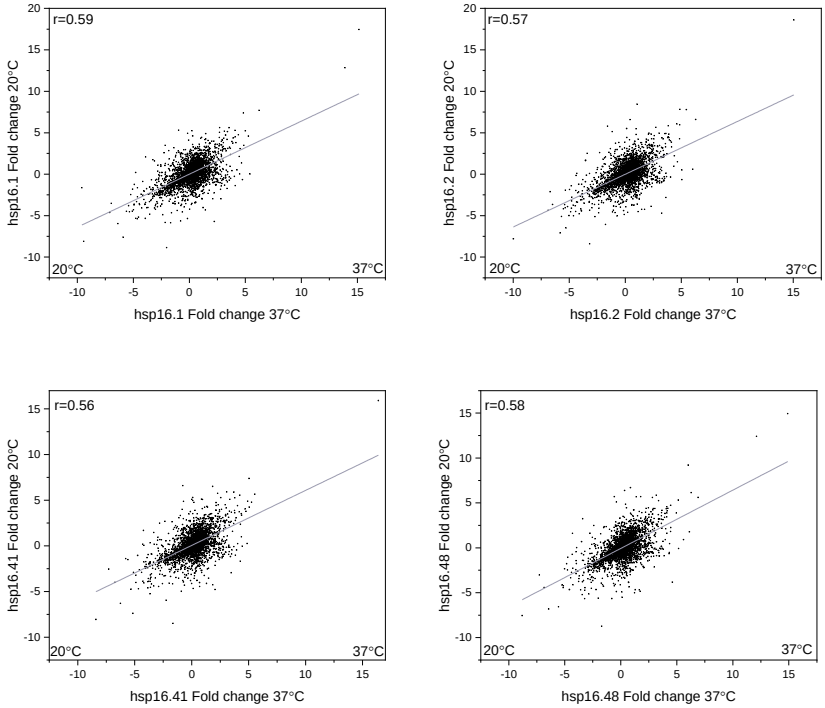

Figure 2.7. Correlation between PPIs at 20°C and 37°C. *The fold change of interactors 20°C and 37°C were plotted against each other and Pearson's correlation coefficient was calculated to determine the linear correlation between two sets of data.*

This leads to the analysis of interactome at 20°C. Almost 40% of PPIs are shared between each chaperone at 20°C and 37°C (Figure 2.3). Nonetheless, the majority of interactors change upon different temperatures. The volcano plots (Figure 2.8) indicate a high number of significant hits (p-value<0.05) with over 400 of them at 2-fold change compared to the control.

The top-15 list of the hits with the most pronounced fold change were plotted for all four Hsp16s. The plots that represent the 20°C data set showed noticeable difference from the ones at 37°C. For example, among the interactors with the highest fold change appeared Hsp17, which is another small heat shock protein of *C. elega*ns. It was found among interactors of Hsp16s at 37°C at low abundance, however, upon permissive temperature the abundance of the protein increased.

Hsp12.1 was also found in the top-15 of interactors of all Hsp16s. Another member of the Hsp12 family, Hsp12.2, was found in the interactome of all Hsp16s as well but

at a much lower abundance. Interestingly, two other members of Hsp12 group were not detected in any of pull-downs.

A striking hit found for all Hsp16s at 20°C is hum-6. This protein is considered as a heavy chain of an unconventional myosin (Baker and Titus, 1997). It is predicted to enable microfilament motor activity. The human ortholog MYO7A is implicated in several diseases, such as Usher syndrome (Kim et al., 2018). Another common interactor, sql-1, was allocated to the top-15 list for Hsp16.41 and Hsp16.48. At a lower abundance it was also found among Hsp16.1 and Hsp16.2's interactors. The protein is located in the Golgi apparatus and predicted to be involved in ER to Golgi vesicle-mediated transport (Broekhuis et al., 2013).

Another transport component found was hpo-12, which is involved in transmembrane transport. However, hpo-12 was found exclusively in the Hsp16.1 interactome. Among the top-15 interactors of Hsp16.2 and Hsp16.48 is trr-1. This protein is involved in negative regulation of vulva development and regulation of reproduction (Ceol and Horovitz, 2004). Interestingly, Trr-1 was not identified as interactor of any sHsp16 at 37°C. A common for 20°C and 37°C interactomes is epg-7 which was identified among the interactors of all four Hsp16s at 20°C, and among all Hsp16s at 37°C with the exception of Hsp16.1. As stated above, it is involved in autophagy. Interestingly, sHsp16s were found among PPIs of each other at both temperatures. This leads to the assumption that they communicate with each other and form hetero-oligomers.

Many interactors that appeared in top-15 list are not yet characterised, thus, the type of interaction between them and sHsp16s remains elusive. Overall, the interactome of sHsp16s is impressively large and notably changes upon different temperatures. Almost 25% of interactors are shared between the interactomes at two conditions, however, a large part of the interaction network shifts towards unique substrates. The interactors of the Hsp16 family are involved in various cellular processes, including vesicle-mediated transport, apoptosis, development and locomotion. These findings reveal a functional plasticity of sHsp16 family.

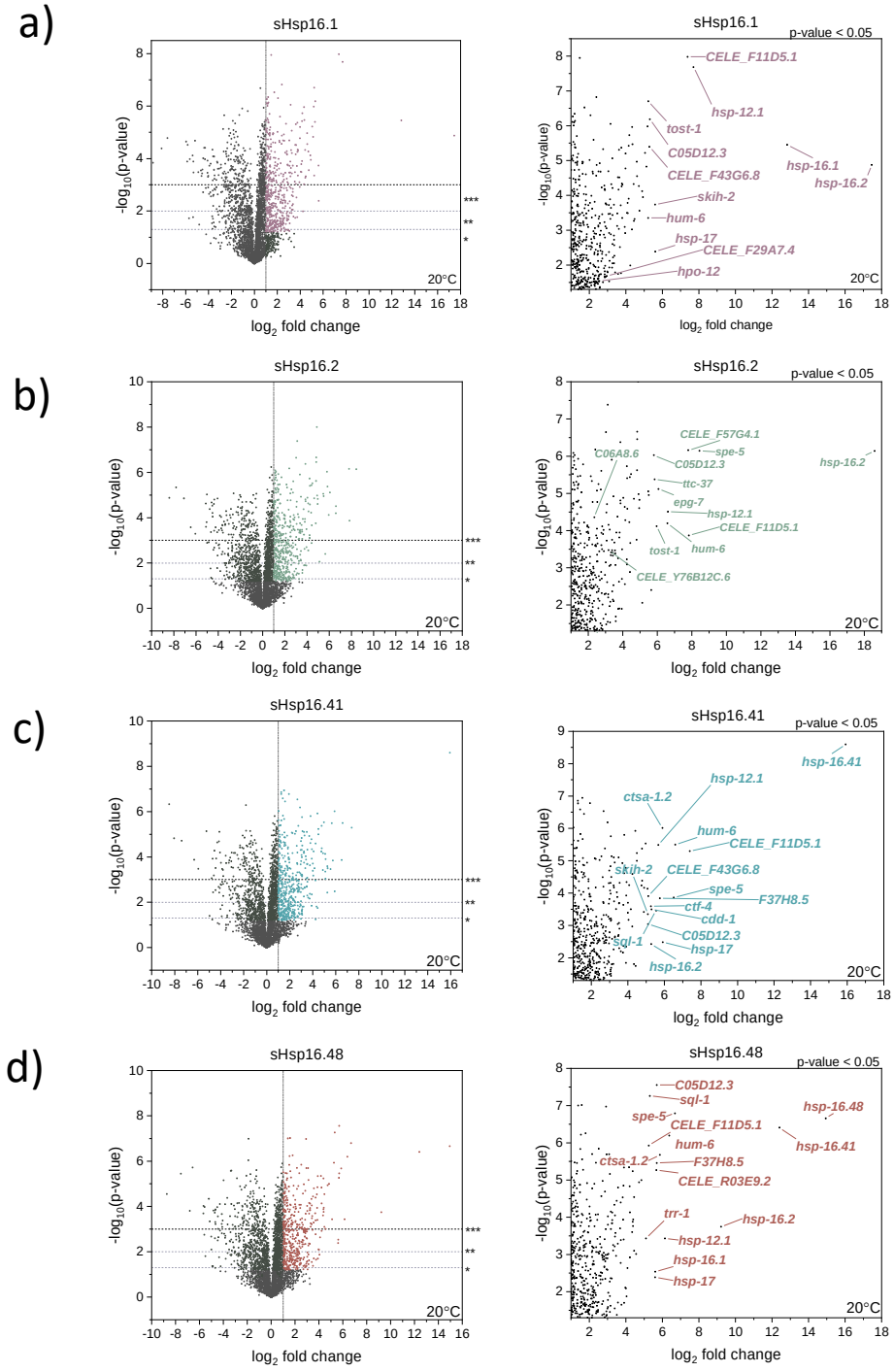

Figure 2.8. Volcano plots illustrate the interactors of Hsp16s at 37°C. *A-D) Volcano plots that represent the interactors of Hsp16.1, Hsp16.2, Hsp16.41 and Hsp16.48 respectively. The most significant interactors were visualised in colour, the parameters were FDR<0.05 and at least 2-fold change of abundance (* corresponds to FDR<0.05, ** to FDR<0.01, *** to FDR<0.001). The top-15 interactors were chosen based on their abundance (fold change) and presented on the right.*

The correlation between the set of interactors of homologous chaperones is, as expected, high. The Pearson's correlations were estimated by linear fit and are *r* = 0.90 and 0.91 for Hsp16.1/16.2 and Hsp16.41/16.48, respectively (Figure 2.9). The correlation matches with the one at 37°C and shows the large proportion of shared substrates between chaperones.

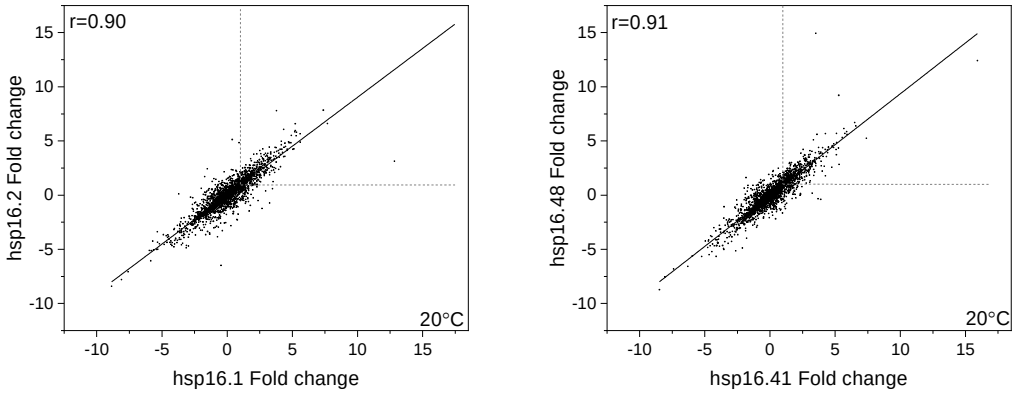

Figure 2.9. Correlation between homologous sHsp16s regarding their interactors is high at 20°C. *The fold change in abundance of interactors of homologous proteins (Hsp16.1 to Hsp16.2, Hsp16.41 to Hsp16.48) were plotted against each other and Pearson's correlation coefficient was calculated to determine the linear correlation between two sets of data.*

Statistical analysis of the Hsp16's interactome shows that pI values, molecular masses and hydrophobicity of the interactors differ from the characteristics of the total worm proteome (Figure 2.10). The mean hydrophobicity of total proteome is -0.28, which is slightly hydrophilic. Hsp16s interact with slightly more hydrophilic proteins at both 20°C and 37°C. The mean of GRAVY distributions range from -0.35 to -0.33. The most hydrophobic interactors with value 0.94 were at 20°C. At elevated temperature the maximum hydrophobicity is only 0.62 (Table S2).

pI values of the Hsp16's interactors also differed from the ones of a total proteome, which are around 6.4 and 7.3, accordingly. The means of the molecular masses distributions were close to 70 kDa for both temperatures. The largest interactors are 79 kDa, which is calculated for 20°C pull-downs. The maximum for 37°C is slightly lower – from 55 to 86 kDa.

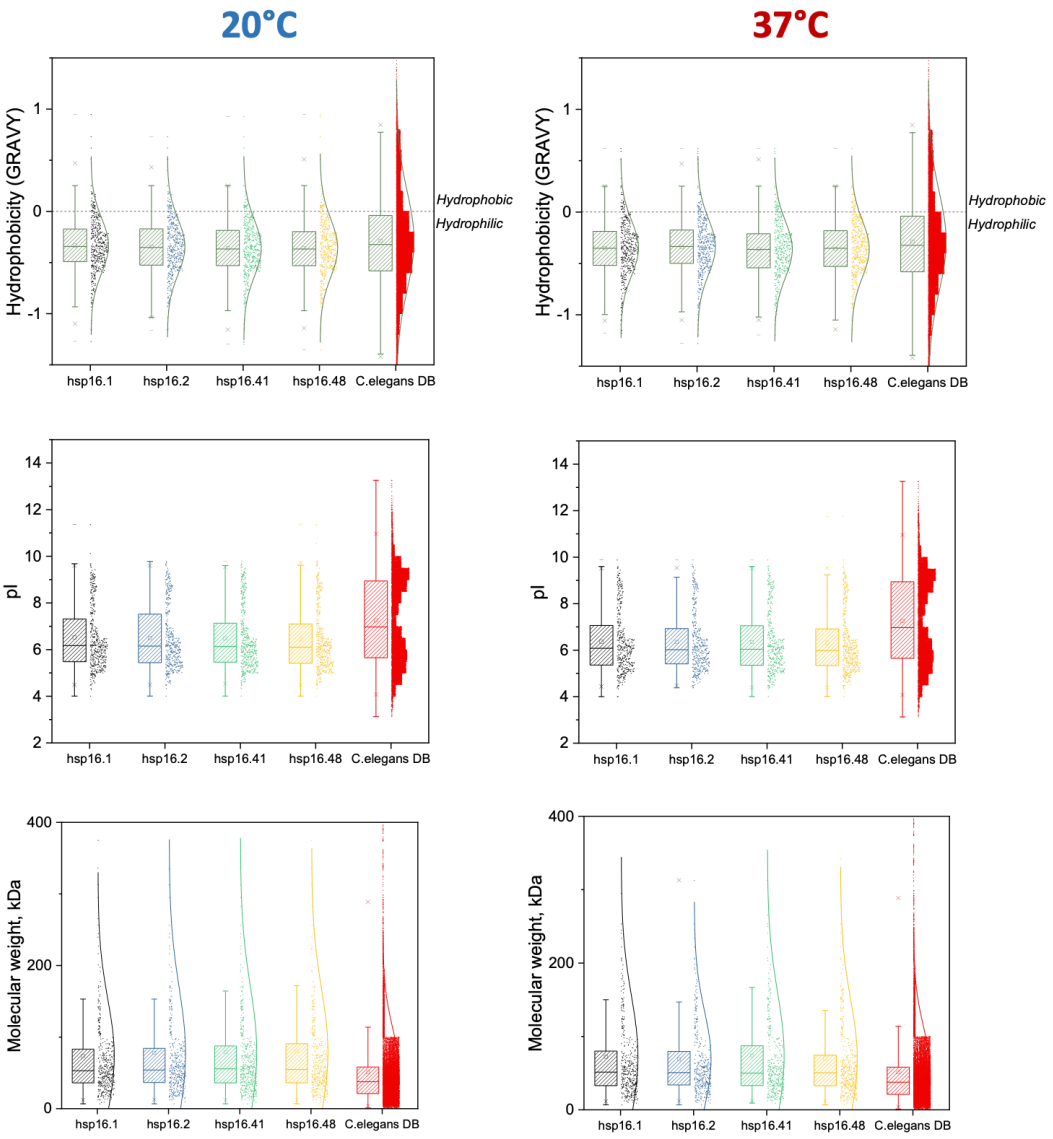

Figure 2.10. Statistical analysis of the pIs, molecular masses (Mw) and GRAVY indexes of the Hsp16 interactome at 20 ℃ and 37 ℃. *The sequences were matched to the values and the meansof the distributions were calculated in Expasy and GRAVY calculator. The interactors of Hsp16s were compared to the proteome of C. elegans (DB, database).*

sHsp families cooperate *in vitro*

Hsp16s showed signs of cooperation with each other *in vitro.* In FRET SUX experiments subunit exchange between Hsp16s was observed. This was shown via disruption of FRET pair of Hsp16.2 by unlabelled Hsp16.1, Hsp16.41 or Hsp16.48. In addition, co-IP/MS analysis revealed many shared substrates of sHsp16s. Interestingly, protein-protein interaction mapping also revealed high abundance of another sHsp family – Hsp12s – specifically, Hsp12.1 and Hsp12.2. This led to the idea that sHsp12s may communicate with sHsp16s. To further investigate the interaction between Hsp16s and Hsp12s, they were analysed by FRET SUX. As FRET system, a pair of labelled Hsp16.2 proteins was used. To disrupt the Hsp16.2 FRET complex and follow the change in donor signal, an excess of unlabelled Hsp12.1 and Hsp12.2 was added so that the total protein concentration was 5µM. The change in signal was monitored at 555 nm excitation and 575 nm emission at 15°C (Figure 2.11).

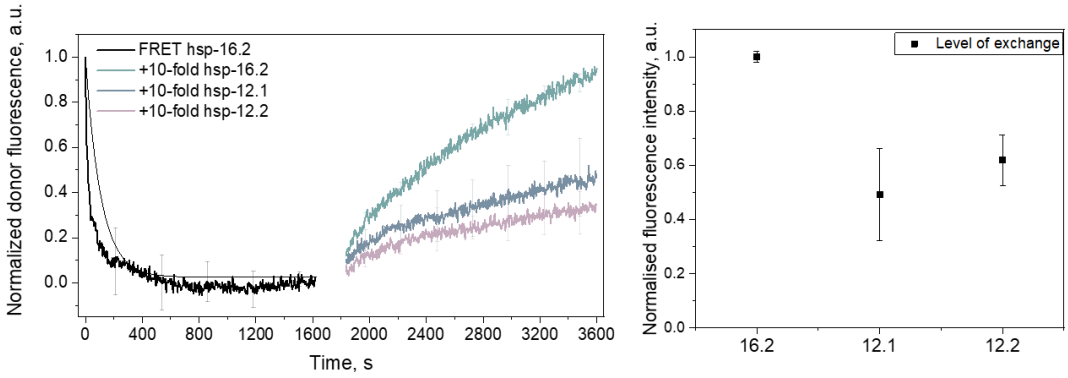

Figure 2.11. Interaction of Hsp16.2 with Hsp12 family members measured by FRET SUX. *Subunit-exchange was measured by addition of 10-fold excess of unlabelled protein with a total concentration of proteins in the sample of 5 µM. The dissociation of a FRET pair complex was monitored by change in donor signal at 15°C for 30 min at 555 nm excitation and 575 nm emission wavelengths (left). The data was normalised to the exchange of labelled Hsp16.2 with unlabelled Hsp16.2. The relative level of exchange of the FRET pair was plotted for each of the unlabelled protein (right) by normalizing the endpoint of exchange to Hsp16.2. The experiment was performed at least in triplicates, the mean values and the standard deviation are shown. Experiment was performed together with Katerina Slanska.*

Subunit-exchange experiment showed that Hsp16.2 cooperates with both Hsp12s. The level of exchange was the highest for Hsp12.2 with 62%±0.09 dissociation of the

complex, while level of exchange between Hsp16.2 and Hsp12.1 was notably lower at 49%±0.17. Such a relatively high level of exchange indicates that sHsp16s interact specifically with members of Hsp12 family. Further analysis of labelled Hsp16s with Hsp12s and vice versa are required.

3. The in vivo role of sHsp16s

To investigate the role of sHsp16 family *in vivo,* the deletion mutants were examined for phenotypes in combination with RNAi knockdown. First, the mutants VC475 (ΔHsp16.2), tm1093 (ΔHsp16.41), tm1221 (ΔHsp16.1b/16.48b), and RB791 (ΔHsp16.1a/16.48a) were tested for mutation via PCR genotyping (Figure 3.1, A) and then backcrossed to the wild type at least twice to eliminate presence of unwanted mutations in the background. The single worm of each mutant was lysed and its genomic DNA was used to confirm the presence of the mutation at the respective site (Figure 3.1, B).

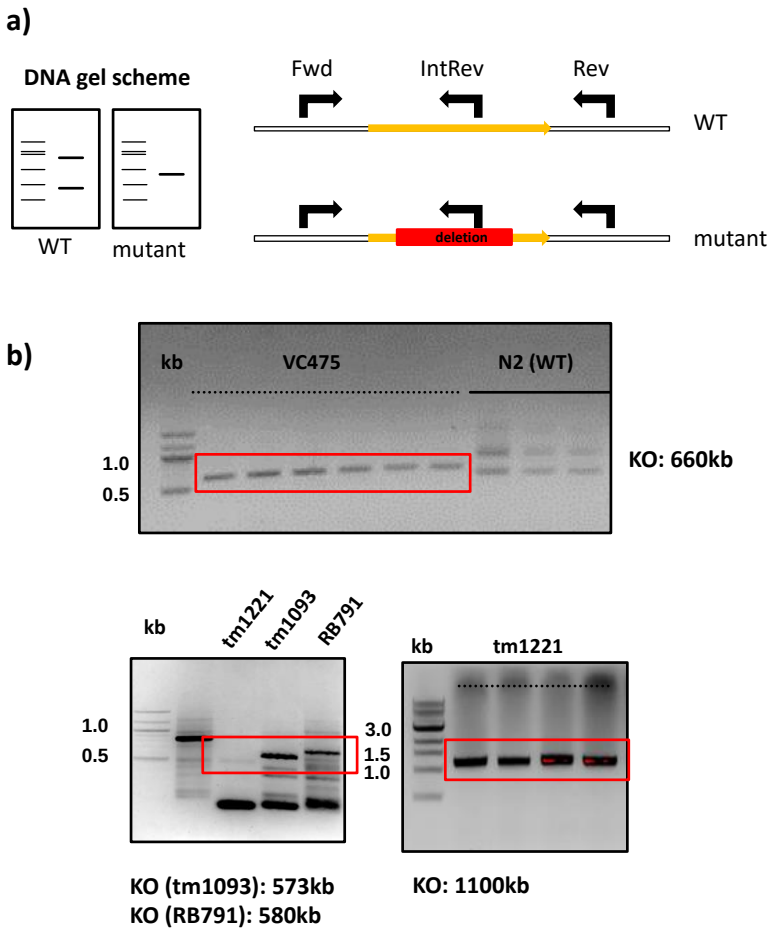

Figure 3.1. Strategy of genotyping. Each mutant C. elegans strain was tested for the respective mutation by genotyping. *A) an illustration of the expected DNA agarose gel for mutant and wild type strains. The forward, reverse and internal reverse PCR primers were designed for each mutation. B) 1% agarose DNA gels, the size of the DNA fragments expected for each mutant strain confirmed the carried mutation (red box).*

Each mutation was confirmed by PCR genotyping. The primers were designed to target Hsp16s upstream and downstream the respective gene of interest. In addition, one internal primer was designed to target the expected mutated region for each of the mutant strains (tm1221, RB791, tm1093 and VC475). In the wild type PCR, the internal primer, as well as upstream and downstream primers bind to gDNA, which results in two PCR products. In case of the mutant strain, internal primer would not target the missing region, which results in only one PCR product. In case of the tm1093, VC475 and RB791, the mutations were confirmed by PCR and matched the

information provided by CGC (Caenorhabditis Genetics Center) and NBRP (National Bioresource Project) (Figure S2). The expected sizes of PCR products were 660 kb, 573 kb and 580 kb for VC475, tm1093 and RB791, respectively.

The tm1221 strain, however, was identified to carry mutation at the different position than stated in Wormbase and NBRP. The mutated region is stated to cover T27E4.9 (*Hsp16.49*) and T27E4.2 (*Hsp16.11*) genes (Figure 3.2, highlighted in yellow). For the simplicity, these two genes are referred in this study as *Hsp16.48b* and *Hsp16.1b*. The designed primers for T27E4.9 and T27E4.2 region indicated the presence of the genes in the gDNA of tm1221 strain. The further PCR analysis targeted two other copies of the genes (PCR product of 1100 kb long, Figure 3.1) and confirmed that the position of the mutation is actually upstream from the one stated by NBRP. PCR genotyping showed that the mutation covers *Hsp16.48a* (*T27E4.3*) and *Hsp16.1a* (*T27E4.8*) genes (Figure 3.1, highlighted in green).

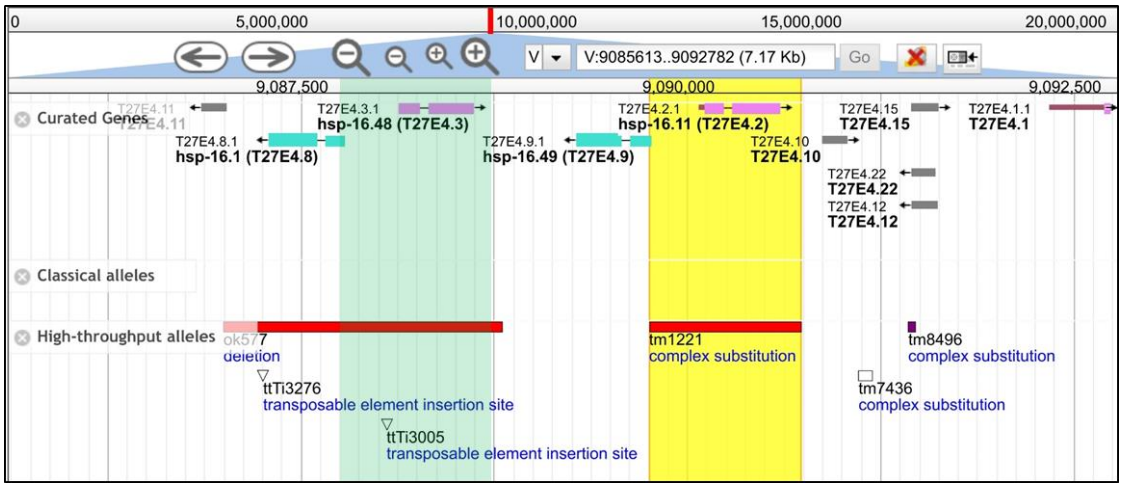

Figure 3.2. The position of the mutation for tm1221. *The complex substitution is stated to cover T27E4.9 (Hsp16.49) and T27E4.2 (Hsp16.11) genes (yellow). The actual mutation position was confirmed by PCR genotyping (green) (adapted from WormBase)*

Mutant strains were analysed for lifespan compared to the wild type. As all available mutants do not cover all sHsp16s, RNAi knock-downs in combination with knock-out strains were used. The worms were grown on RNAi plates for the duration of their lifespan. The experiment was performed in two trials (Figure 3.3, A) with total amount of nematodes N = 1667. The average from two trials showed (Figure 3.3, B) a slight decrease in the mean lifespan of tm1093 (ΔHsp16.41) and VC475 (ΔHsp16.2) compared to the wild type. Other mutants showed a slight deviation from the mean lifespan of the wild type as well. In contrast, additional knock-downs of Hsp16.1 and Hsp16.48 genes showed a slight increase in the mean lifespan, as well as the crossed mutant (tm1093xRB791) that carries knock-out of Hsp16.41 and single copies of Hsp16.1 and Hsp16.48 genes. In general, the alteration of Hsp16s only moderately influenced the mean lifespan of the worms. The data should be interpreted carefully and more trials should be performed.

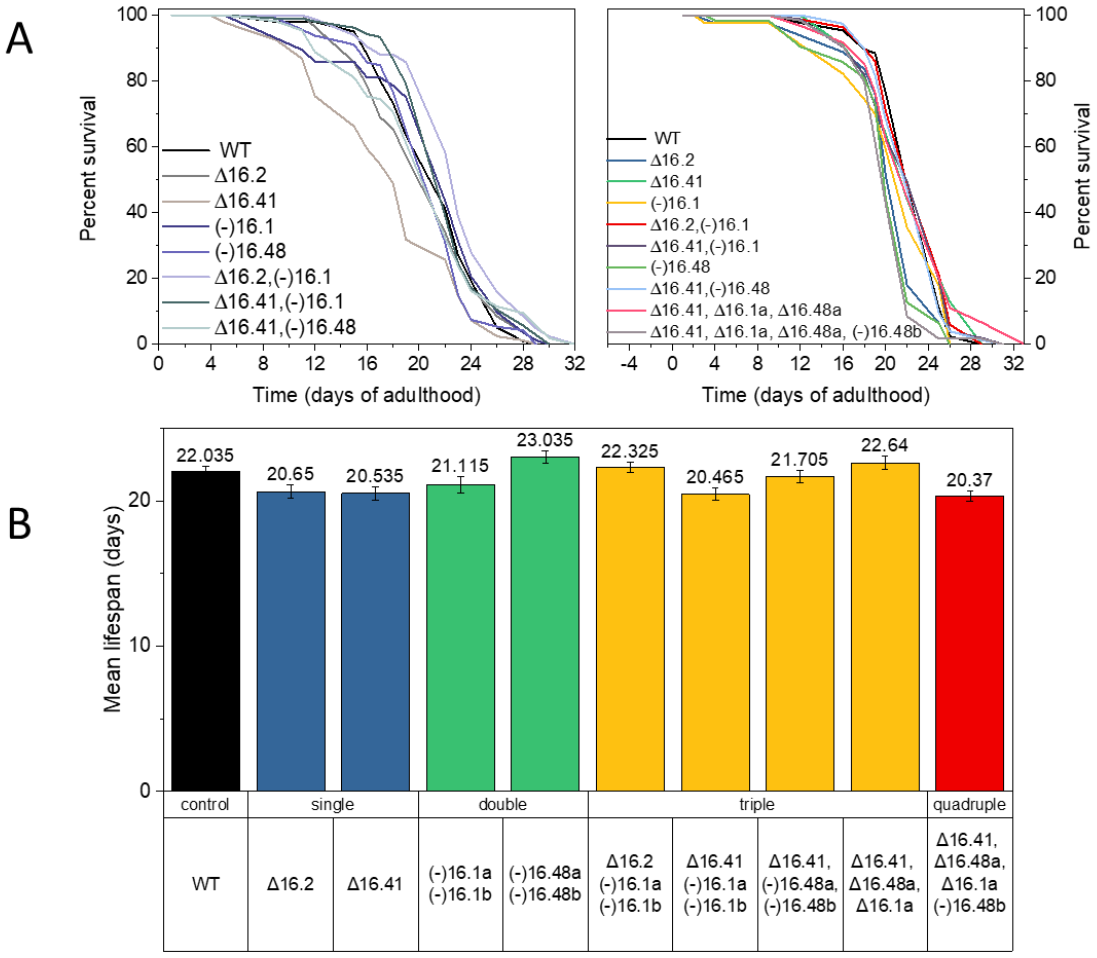

Figure 3.3. Effect of gene silencing on the mean lifespan in C. elegans. *A) The survival curve represents the percent survival of each population with a respective combination of the gene knock-out and knock-down of Hsp16s at each time point. The assay was performed in two independent trials (left and right). Knock-out of the gene (Δ) and knock-down via RNAi (-) are indicated. B) The influence of the gene alteration on the mean lifespan value is visualised as a bar chart (right) from average of two independent trials. The combinations of the gene knock-out and knock-down are grouped as control (WT, wild type, in black), single (alteration of one gene, in blue), double (alteration of two genes, in green), triple (alteration of three genes, in yellow) and quadruple (alteration of four genes, in red). The standard deviations are estimated in OASIS2.*

During the assessment of the lifespan tm1093 showed alteration in its healthspan, which is life-limiting and, therefore, potentially affected the lifespan. It appeared that the strain developed age-related vulval integrity disorder, which is stated to be a marker of a nematode healthspan and associated with early death (Leiser et al, 2016). It is reported, however, that a high percentage of vulval protrusions in *C. elega*ns

results from premature utilisation of FUdR (Floxuridine, 5'-fluorodeoxyuridine), which was also used in a current study. The chemical is often utilized to inhibit a reproductive cycle of adult worms and allows maintenance of synchronous worm populations (Mitchel et al., 1979; Gadhi et al., 1980; Rahman et al., 2020). Interestingly, that such abnormality occurred in tm1093 strain only (Figure 3.4), which means that such disorder might be influenced by the mutation in Hsp16.41 as well.

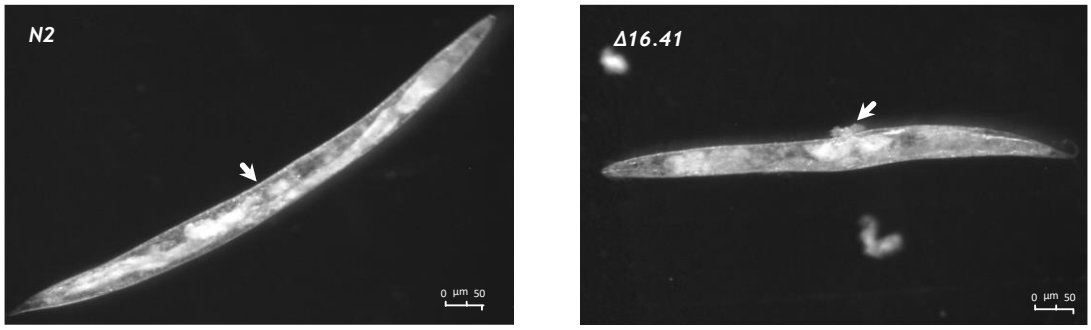

Figure 3.4. Loss in vulva integrity in nematodes during ageing. *Representative worm images showing wild type worm (N2, left) with no defects and mutant strain tm1093 with developed vulva-integrity defect during lifespan experiments.*

Worms exhibited different levels of protrusions, including level I, II and III (Leiser et al., 2016). In Figure 3.4 the level I is represented – herniated vulva. In addition, the size of the tm1093 nematodes that underwent protrusions was visually smaller compared to the wild type by day 9 of adulthood. In general, the most striking effect was noticed in the tm1093 mutant, which exhibited life-limiting age-associated pathology.

III. Discussion

The small heat shock proteins are a ubiquitous family of molecular chaperones. They have evolved into a large group of 16 members in *C. elegans*. Six of them are combined in the Hsp16 family. Although the first mentions about the family were reported in 1985, to this time, little is known about them. In this study, I systematically investigated the structure and functions of the core Hsp16s (Hsp16.1, Hsp16.2, Hsp16.41 and Hsp14.48) in a comparative manner. Of special interest was homology of up to 93% between the family members. The findings of the study were aimed on answering the central question – what is the necessity to have a family of highly homologous chaperones in *C. elegans*?

Functional plasticity of Hsp16s is dictated by temperature

This study presents evidence of a high promiscuity of the Hsp16s towards their substrates. The sequence features of the Hsp16s allow them to explore a broad range of interaction partners. As duplicated genes that have arose in response to stress are usually preserved as a form of adaptivity (Cao et al., 2022), the genomic organisation and duplication of Hsp16s support this statement.

From co-IP/MS analysis it is evident that the interactions of the Hsp16s with the substrates are dictated by a temperature. The overlap of the protein interactors for the same Hsp16 is only 20% (Figure 2.3). For example, for Hsp16.1, in total 753 hits were found at 20°C and 37°C with only 165 of them were shared, while other 588 were split between the two pull-downs. Moreover, the correlation between protein-

protein interactors of non-homologous Hsp16s at the same temperature was more pronounced (r = 0.85-0.86) than between the interactors of the same chaperone at the same temperature (r = 0.56 – 0.59) (Figure 2.6, Figure 2.7).

The proteomics findings suggest that Hsp16s exhibit a functional plasticity at different temperatures, thus Hsp16s can adapt their chaperone function depending on the temperature of the environment. At the same time, an activation of their chaperone function is independent of a temperature. Chaperone assays with insulin support this conclusion as Hsp16.1 and Hsp16.2 showed a high activity not only at 37°C but also at 15°C (Figure 1.10 and Figure 1.12). As the results confidently indicate that these two Hsp16s are the temperature-independent chaperones, this raises the question whether Hsp16s need other types of activation. In the case of the homologous Hsp16.41 and Hsp16.48 this might be the case, since they both showed no evident holdase activity with the tested substrates. Instead, they rather promoted an aggregation of the substrates, which could be an indication of the aggregase activity, like the one of the Hsp42 in yeast (Mogk and Bukau, 2017).

Protein-protein interaction network

All Hsp16s were linked by their common interaction partners. In total, between 397 to 477 interactors were identified for each Hsp16 at 20°C and 37°C, many of which were shared between the chaperones. Notably, the temperature factor shaped the PPI networks of Hsp16 family differently (Figure 3.1 and Figure 3.2). Analysis of the interaction maps at the given temperatures revealed differences in the interactors when searched for the greatest number of a certain protein family. In particular, at 20°C Hsp16s were associated with five members of the sHsp class – Hsp12.1, Hsp12.2, Hsp25, Hsp17 and Sip1 (Figure 3.1, in red). In the 37°C pull-downs Sip1 was not identified among the interactors, potentially because it is reported to be a crucial player itself in the heat shock survival of adult *C. elegans* (Fleckenstein et al., 2015). In addition, at 20°C a group of the stress response proteins interactors daf-21 (Hsp90 ortholog) and its co-chaperones Sti1 and Nud1, as well as a family of Hsp40s (dnj-8, dnj-11, dnj-16, dnj-25) is identified. At 37°C, however, only one DnaJ protein was

identified – dnj-16. At 37°C, Hsp16s shifted their interaction network from stress response proteins to other targets.

Another change in the PPI network of the Hsp16s is the ATG family, which consists of proteins involved in autophagy. While atg-4.1 was identified at 37°C, several members, including atg-2, atg-7, atg-16.1, atg-16.2 and atg-18, were identified at 20°C. Additionally, the Hsp40s and Hsp70s are reported to be involved in chaperone-mediated autophagy (Agarraberes and Dice, 2001; Venugopal et al., 2008; Kaushik and Cuervo, 2019). Although ATG proteins and Hsps are involved in the separate cascades of autophagy, this may be an evidence that they intersect. For example, ATG8 was reported to co-immunoprecipitate with different Hsp classes in plants (Sedaghatmehr et al., 2019). As several Hsp40 proteins were identified among Hsp16s' interactors, Hsp16s might not directly interact with autophagy-related proteins but stabilise autophagy clients. Nonetheless, the reason for the difference between the PPI network at 20°C and 37°C in regards of ATG interactors is yet elusive.

Interestingly, Hsp16s interact with four muscle-related components (myo-1, myo-2, myo-5 and myo-6) only at 20°C. The presence of these interactors is not surprising, as sHsps were reported to participate in the crucial steps of muscle differentiation (Sugiyama et al., 2000; Singh et al., 2010; Middleton and Shelden, 2013). According to the recent findings, Dr. Benesch proposed that apart from canonical functions, sHsps may also interact with mechanosensitice proteins to affect contraction and extensions (Carra et al., 2019). However, the absence of the MYO proteins hits in 37*°C* pull-downs of Hsp16s is surprising.

Several tRNA synthetases, such as sars-1, sars-2, dars-2, gars-1 were identified at 20°C (Figure 3.1), while only one members of this family, sars-2 was in 37°C pull-downs (Figure 3.2). It is known that under heat stress, tRNA synthetases can group in a complex and act along with a chaperone system (Riback et al., 2015), which would explain the lack of interaction between them and Hsp16s at 37°C.

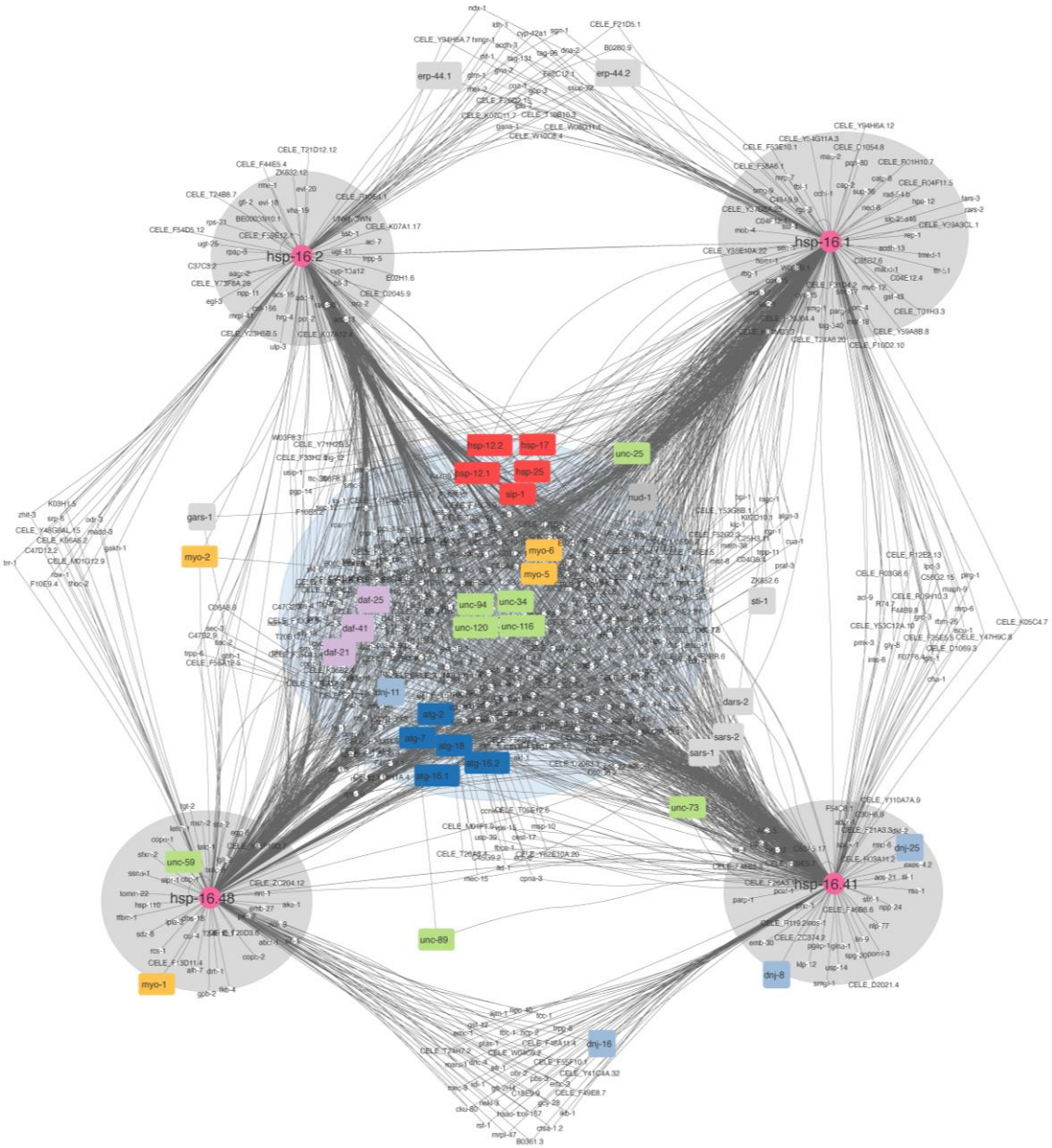

Figure 3.1. Protein-protein interaction map of Hsp16s at 20°C. *The interactors of interest are highlighted in different colours, Hsps in red, Unc group in green, Atg group in blue, Daf group in purple, Dnj - in blue, others - in grey. The network was built in Cytoscape based on the list of the significant interactors obtained after down-stream processing of the co-IP/MS data.*

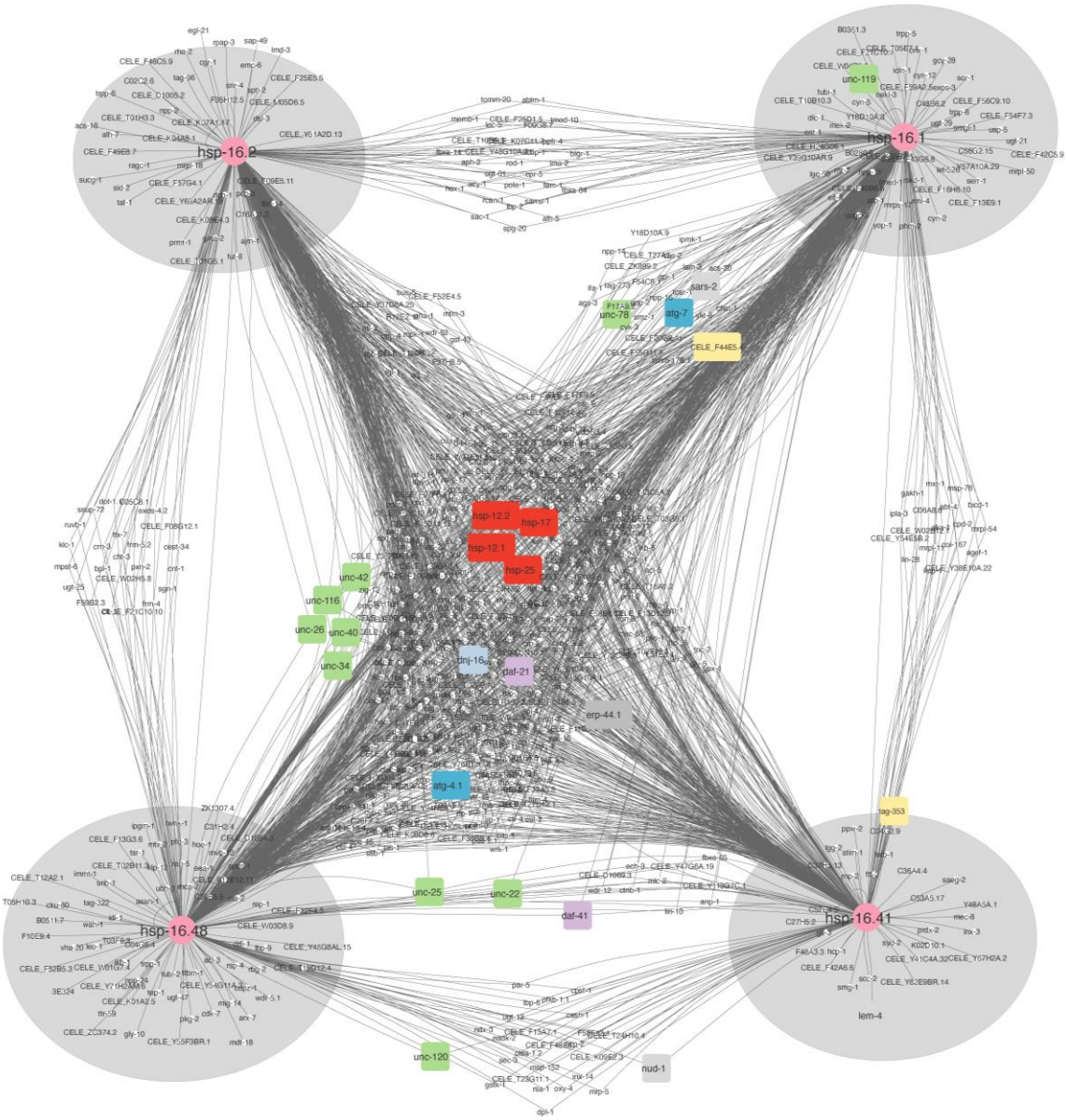

Figure 3.2. Protein-protein interaction map of Hsp16s at 37°C. *The interactors of interest are highlighted in different colours, Hsps in red, Unc group in green, Atg group in blue, Daf group in purple, Dnj - in blue, others - in grey. The network was built in Cytoscape based on the list of the significant interactors obtained after down-stream processing of the co-IP/MS data.*

Top-15 interactors

The factor of temperature has also shaped the top-15 interactors of Hsp16s. Several hits were identified at 20°C or 37°C exclusively for all Hsp16s (Table 3.1). The hits identified solely at 20°C for all Hsp16s are hum-6, Hsp17 and C05D12.3, which are related to microfilament motor activity, stress response and potentially cell adhesion, respectively (Baker and Titus, 1997; Iburg et al., 2020; Whittaker and Hynes, 2002). Exclusive for 37°C pull-downs spd-5, unc-26, raga-1, mig-2, sel-11 and CELE_F25E2.2 were identified as the top-15 interactors. All of them are involved in different cellular processes and localised differently in the cell, including cytoplasm, nucleus, and lysosome (WormBase). Although these interactors are functionally different, the temperature factor has shaped their presence among the top-15 interactors of all Hsp16s specifically at 37°C.

Table 3.1 Comparison of the top-15 interactors of Hsp16 family. *The proteins identified at 20°C only (blue) and at 37°C (pink) for all Hsp16s are highlighted, as well as the common interactor found in all pull-downs (black).*

Hsp16.1 20°C	*Hsp16.1 37°C*	*Hsp16.2 20°C*	*Hsp16.2 37°C*	*Hsp16.41 20°C*	*Hsp16.41 37°C*	*Hsp16.48 20°C*	*Hsp16.48 37°C*
gene name							
Hsp16.2	Hsp16.2	Hsp16.2	Hsp16.2	Hsp16.41	Hsp16.41	Hsp16.48	Hsp16.48
Hsp16.1	Hsp16.1	spe-5	**Hsp12.1**	CELE_F11D5.1	**Hsp12.1**	Hsp16.41	Hsp16.41
Hsp12.1	**Hsp12.1**	CELE_F11D5.1	unc-26	**hum-6**	epg-7	Hsp16.2	Hsp16.1
CELE_F11D5.1	spd-5	CELE_F57G4.1	CELE_F57G4.1	spe-5	unc-26	spe-5	**Hsp12.1**
Hsp17	mlc-2	**Hsp12.1**	sel-11	**Hsp17**	CELE_F11D5.1	**hum-6**	unc-26
skih-2	tost-1	**hum-6**	spd-5	ctsa-1.2	mlc-2	**Hsp12.1**	Hsp16.2
C05D12.3	unc-26	epg-7	CELE_F11D5.1	F37H8.5	raga-1	ctsa-1.2	spd-5
CELE_F43G6.8	CELE_F11D5.1	tost-1	tost-1	**Hsp12.1**	imp-2	C05D12.3	sel-11
tost-1	CELE_Y54F10AM.5	ttc-37	trpp-6	sql-1	pes-2.1	F37H8.5	sql-1
hum-6	raga-1	C05D12.3	CELE_H05L14.2	cdd-1	sel-11	CELE_R03E9.2	CELE_F25E2.2
ttc-37	mig-2	**Hsp17**	C29F3.7	Hsp16.2	mig-2	Hsp16.1	CELE_H05L14.2

Hsp16.1 20°C	*Hsp16.1 37°C*	*Hsp16.2 20°C*	*Hsp16.2 37°C*	*Hsp16.41 20°C*	*Hsp16.41 37°C*	*Hsp16.48 20°C*	*Hsp16.48 37°C*
pes-2.1	sel-11	cdd-1	epg-7	ctf-4	C29F3.7	Hsp17	raga-1
CELE_R03E9.2	CELE_F25E2.2	CELE_F43G6.8	raga-1	CELE_F43G6.8	tost-1	sql-1	mlc-2
cdd-1	CELE_H05L14.2	gfi-2	CELE_F25E2.2	C05D12.3	CELE_F25E2.2	CELE_F11D5.1	mig-2
F37H8.5	sql-1	CELE_F21C10.10	mig-2	skih-2	spd-5	trr-1	tsr-1

Interestingly, Hsp12.1 was found among the top-15 interactors independently of the temperature. This interaction seems particularly unique, which is why this encouraged us to investigate this interaction between Hsp16 family and Hsp12s with subunit-exchange experiment.

Interactors and their biological processes

Gene ontology (GO) annotation (Bindea et al., 2009; Carbon et al., 2021) by biological process (BP) underlines the functional ubiquity of Hsp16s at both temperatures (Figure 3.3). The Hsp16s interaction partners are involved in various biological processes. The most represented group at both temperatures are proteins that are involved in the "metabolic processes", including organonitrogen at 20°C and 37°C and organophosphate metabolic processes at 37°C. These include such processes like catabolism, anabolism, DNA repair, protein synthesis and degradation (Carbon et al., 2021). At this point the similarity between the pull-downs is decreasing.

A large group of interactors identified at 20°C is allocated to "signal transduction", which at 37°C has transformed to a "response to stimulus" group. Both BPs start from the process that initiates a cascade of the molecular events, which end with a change of a cell activity. However, signal transduction is initiated by the molecular events, such as ligand binding, whereas response to stimulus is a reaction to an environmental influence, such as temperature, electricity, or another organism.

A group of interactors involved in vesicle-mediate transport was represented more at 20°C than at 37°C. Whereas, the second large group of interactors at 37°C was

“establishment of localisation in cell”, that is not represented at 20°C. Those interactors are involved in a direct movement of a substance to a specific location in a cell, while during vesicle-mediated transport the substance is firstly coated in the vesicle. Although it is self-evident, the temperature has contributed to the shift from one group of interactors to another. Interestingly, Hsp-16.1 was reported to localise to the Golgi to tolerate heat stroke and act together with pmr-1 to maintain Ca^{2+} homeostasis (Kourtis et al, 2012). Although current analysis showed no direct interaction between Hsp16.1 and pmr-1, interaction with several transport proteins that are responsible for transport to the Golgi, such as Trpp-6, was confirmed.

The largest groups of interactors at 20°C were those involved in organelle organisation, cellular catabolic processes as well as organismal development and reproduction. In contrast, those groups were slightly underrepresented at 37°C, especially organelle organisation and catabolic processes. The organelle organisation process identified at 20°C correlates well with the identified vesicle-mediated transport process, as both imply an involvement of the vesicles.

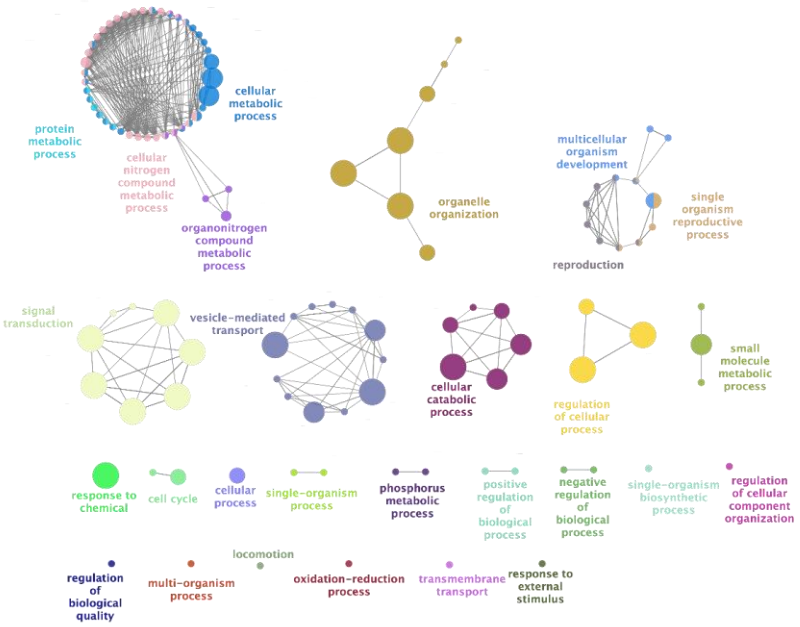

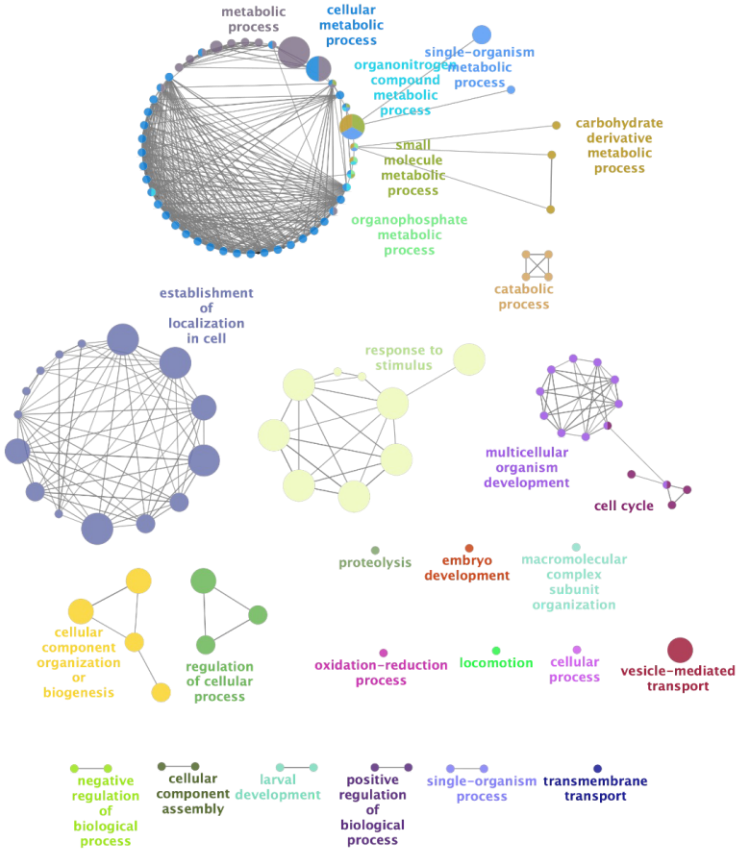

Figure 3.3. Gene ontology terms by biological process for interactors of Hsp16s. *The groups for 20℃ (top) and 37C (bottom) are illustrated. The GO terms were searched and visualised in Cytoscape.*

With this, it is suggested that temperature underlies the shift of the PPI network. The total interactors of Hsp16s are different but there is an evident temperature-dependent pattern among the top-15 interactors that are present in the pull-downs of all Hsp16s. They may exhibit multiple functions depending on the tissue or cell they are expressed as well as environment conditions. In addition, the interactomes showed potential additional functions of Hsp16s that can be targeted in future experiments.

The chaperone activity of the Hsp16s is temperature independent

In addition to shaping the type of interactors, often temperature is a key factor in regulating chaperone activity, like in the case of yeast Hsp26 or human αA- and αB-crystallins (Haslbeck et al., 1999; Reddy et al., 2000). Usually, temperature induces a dissociation of Hsp oligomers into smaller species, which is typically the active form of sHsps (Haslbeck et al., 2019). Nonetheless, the TEM micrographs of Hsp16.1 and Hsp16.2 (Figure 1.13, Figure 1.14) indicate that the chaperones exhibit holdase activity without visible dissociation into the smaller species. This may be beneficial for a cell to rapidly respond to a stress and subsequent protein unfolding.

The other factors that can modulate chaperone activity include pH and post-translational modifications (PTMs). It has been found that chaperone activity of the Hsp16s is not improved by changes in pH, like in the case of their closely related sHsp - Sip1 (Fleckenstein, 2014; Fleckenstein et al., 2015). In the case of Hsp26, its activity at the permissive temperature is regulated by phosphorylation (Mühlhofer et al., 2021). Yet, no evidence of PTMs regulation of Hsp16s' chaperone activity was reported. Although phosphorylation is a fundamental mechanism in *C. elegans*, especially the IIS pathway (Murphy and Hu, 2013), the number of the identified phosphorylation sites in the nematode is only 15 443, while over 119 000 sites were identified in human (Li et al., 2021). By taking advantage of the proteomics, influence of PTMs can be revealed. Bottom-up MS approaches allow to identify the sites of

PTMs in proteins (Larsen et al., 2006; Sinha and Mann, 2020). In addition, by using an *in vivo* model to investigate the chaperone function of Hsp16.41 and Hsp16.48, we can be confident that the conclusion regarding their aggregase activity is correct. For example, the protein lysates from worms can be used to examine the fraction of these chaperones in the insoluble fraction.

Hsp16s communicate with each other and two Hsp12 members

Another source of modulation of the chaperone activity are the interactions between molecular chaperones. Indeed, they do not exist in isolation, like Hsp70 functions with the Hsp40 family or Hsp90 with its co-chaperones (Laufen et al., 1999; Johnson and Brown, 2009; Frumkin et al., 2014; Nillegoda et al., 2015). The sequence homology of Hsp16s motivated us to investigate the interaction between the Hsp16 members.

The HPLC, SEC-MALS and AUC assays demonstrate the presence of large oligomer species of the Hsp16s. The chaperones form heterogeneous and large oligomers of 420-700 kDa consisting numerous subunits (Fig. 1.7-1.9). With this, a large proportion of oligomers (up to 48%) was ascribed to the variable in size smaller species (Figure 1.9). Such heterogeneity implies that Hsp16s are dynamic, thus, may exchange subunits and affect activity of each other. Subunit-exchange assays confirmed that Hsp16s communicate by exchanging subunits *in vitro* (Figure 1.19). The interaction between homologous Hsp16.1 and Hsp16.2 was the most pronounced (56%). The interaction between Hsp16.2 and the non-homologous to it Hsp16.41 or Hsp16.48 was less prominent (38% and 30%, respectively), as expected. In this case, the subunit-exchange between Hsp16s looks like a homology-based interaction. Hochberg and colleagues (2018) showed that two duplicated plant sHsps tend to assemble into homo-oligomers, avoiding co-assembly. In the case of Hsp16s, it seems that the most homologous of them tend to co-assemble (Hsp16.1 with Hsp16.2). As hsp40s cooperate with hsp70 in a form of an interactive flexible network (Kirstein et al., 2017), the sHsp16s cooperate with each other.

Proteomic data revealed two members of Hsp12 family among the interactors of Hsp16s at 20°C and 37°C. Hsp12.1 was among the top-15 interactors of all Hsp16s at both temperatures. Due to such a high abundance of Hsp12 proteins compared to other interactors, the interaction between Hsp16s and Hsp12s was investigated in more details. The results of the subunit-exchange assay show that Hsp16.2 exchange subunits with Hsp12.1 and Hsp12.2 *in vitro*, however, the mechanisms behind this interaction are elusive. Dr. Benesch and Dr. E. Vierling state that interaction between sHsps may drive the functional evolution (Carra et al., 2019).

The possible scenario (Figure 3.4) involves the formation of hetero-oligomers between Hsp16s and Hsp12.1 or Hsp12.2 as a functional cooperation. Alternatively, Hsp12s may not function together with Hsp16s as a very little chaperone activity for Hsp12s was reported (Kokke et al., 1998; Fu et al., 2021). Instead, Hsp12s may modulate activity of Hsp16s. The nature of the relationship between these two families should be further studied via subunit-exchange assay. In addition, it would be advantageous to examine the chaperone activity of Hsp16s in the presence of Hsp12s. In total, the results unravelled a potential evolutionary advantage of the divergence of Hsp16s and subsequent cooperation between Hsp16s and two members of Hsp12 family.

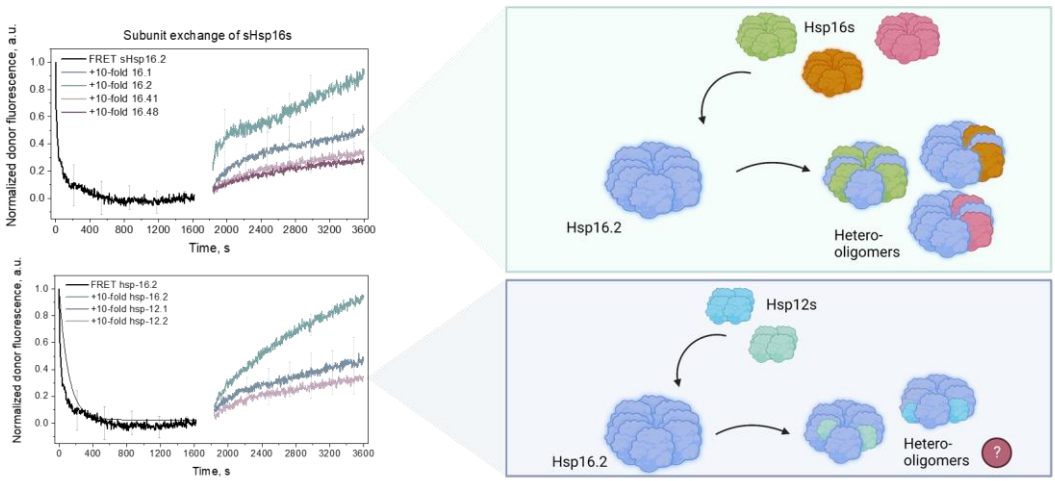

Figure 3.4. An illustration of the mechanisms of the interaction between Hsp16s and Hsp12s. A proposed scheme of the interaction between *Hsp16.2 and other Hsp16s (on the top). Hsp12.1 and Hsp12.2 interact with Hsp16.2 (on the bottom). In both cases it is proposed that chaperones form hetero-oligomers. Illustrated in BioRender.*

Pairwise homology of Hsp16s is reflected in their structure and functions

A homology of up to 93% between Hsp16.1 and Hsp16.2 or Hsp16.41 and Hsp16.48 is a striking feature of Hsp16s. Heterogeneity of the Hsp16s, as well as the chaperone activity or their protein interactome are similar between the homologous proteins (Hsp16.1/Hsp16.2 or Hsp16.41/Hsp16.48). The pattern of homology is seen throughout the assays. For example, a size distribution of the Hsp16s oligomers was similar for homologous proteins (Figure 1.9). Proportion of the large oligomer species for Hsp16.1 and Hsp16.2 was 84 - 90%, while Hsp16.41 and Hsp16.48 have 52 - 53% of species allocated to the group of large oligomers. HDX analysis supported the structural homology of the Hsp16s. Hsp16.1/Hsp16.2 exhibit same flexibility patterns, rigidity in the ACD and flexibility in the CTR (Figure 1.17, A and B). In contrast, both Hsp16.41 and Hsp16.48 were more flexible in the ACDs and slightly more rigid in the NTRs compared to Hsp16.1/Hsp16.2 pair (Figure 1.17, C and D). Although deviation in the amino acid content of each homologous pair introduced some structural differences, the general flexibility patterns of each pair remain similar.

Moreover, chaperone activity assays support the similar pair-wise behaviour of the Hsp16s. Hsp16.1 and Hsp16.2 show holdase activity towards CS, MDH and insulin at both permissive and elevated temperature. In contrast, Hsp16.41 and Hsp16.48 showed a similar aggregase behaviour towards tested substrates. In addition, the correlation between the interactomes of homologous proteins was higher than between non-homologous ones (Figure 2.5 and Figure 2.6). Furthermore, the subunit exchange was the most pronounced also between the homologous Hsp16.2 and Hsp16.1.

The high sequence identity and origin from the same ancestor have shaped the structural and functional features of the Hsp16s. It was reported that homologues tend to have similar or even shared biological functions. It was found that PPIs of a known protein can be transferred to its homologue when two proteins share over 80% of joint sequence identity (Yu et al., 2004). As we proved the communication of

Hsp16s *in vitro*, it is of high interest to investigate their homologous behaviour in an *in vivo* model.

It is reported that RNAi knock-down of Hsp16.1 and Hsp16.48 shortened the lifespan of a long-lived *daf-2* mutant (Hsu et al., 2003). In this study, combination of knock-down and knock-out of the Hsp16s showed a very little influence on the lifespan. To investigate the cooperative roles of Hsp16s in the genetic background of *daf-2* (or other IIS proteins) mutant may be advantageous as well as application of a stress.

Conclusion

The Hsp16 family of molecular chaperones have evolved into a large group of homologous proteins. We state that based on the sequence homology, and, as shown in this study, functional and structural homology, Hsp16s are divided into homologous pairs Hsp16.1/Hsp16.2 and Hsp16.41/Hsp16.48. Diversification and expansion of the Hsp16 family have also expanded their PPI map. A measurement of Hsp16s PPIs provides an in-depth view of the composition of their interactome, which is shaped by the temperature. At the same time, the chaperone activity of the Hsp16s is temperature-independent. Moreover, Hsp16.1 and Hsp16.2 exhibit a chaperone activity without dissociating into smaller species. In addition to a large interaction network, Hsp16s also communicate with each other in the cell. Such feature may contribute to the cytoprotective function of the Hsp16s. In total, this study provides an in-depth characterisation of the structure and functions of the Hsp16s in a comparative manner with a special interest in the homology of these proteins.

IV. Materials and Methods

Materials

Primers

Table 4.1. The list of primers generated in current work.

Name	Sequence	Provider	Purpose
L4440 Fwd #8	TGTAAAACGACGGCCAGT	Eurofins	RNAi
L4440 Rev #10	AGCGAGTCAGTGAGCGAG	Eurofins	RNAi
VC475 Fwd AH #14	CTTTTCCATGTACCGAATGTG	Eurofins	Genotyping VC475
VC475 IntRev AH #15	CTTCTTTCTTTGGCGCTTC	Eurofins	Genotyping VC475
VC475 Rev AH #16	TCCGGGAAATTAATATCTGGC	Eurofins	Genotyping VC475
Int Fwd Uni 16.11 #40	AAGATCTATTCCAATTCAGCAAGCGC	Eurofins	Genotyping tm1221
Fwd 16.1 copy #42	TTTAACAGGGACTCCTACGGCAAC	Eurofins	Genotyping tm1221
Rev 16.1 copy #43	GCAGTTGATCAACACAGTTGTGAG	Eurofins	Genotyping tm1221
Hsp16.41 Fwd #47	CAACACGCTTTGTTCTAGTGCATC	Eurofins	Genotyping tm1093
Hsp16.41 Rev #49	CTTGCCGCCCACTTCTGGTAT	Eurofins	Genotyping tm1093
Hsp16.41 IntRev opt #50	GACAGAAGGTAAATCAGCATCTTCTGG	Eurofins	Genotyping tm1093
Hsp16.48 Fwd #44	CATGGAATGGGTGTACGAGTGTCC	Eurofins	Genotyping RB791
Hsp16.48 IntRev #45	CAGAAAATGGAGAACGGAGCATGAGC	Eurofins	Genotyping RB791
Hsp16.48 Rev #46	CCCTGTAGAAGTTGCACGCACTG	Eurofins	Genotyping RB791

Plasmids and RNAi vectors

Table 4.2. The list of plasmids and RNAi vectors used in this work.

Plasmid name	Resistance	Provider	Comment
pET-21a(+)	Amp	Novagen	Insert: Hsp16s were cloned via NdeI / XhoI with STOP, no C-terminal Tag
L4440	Amp	Julie Ahringer's group at The Wellcome CRC Institute	Inserts: Hsp16s

Strains

Table 4.3. The list of the bacterial and worm strains used in this work

Name	Organism	Genotype	Provider
JM109(DE3)	*E. coli*	endA1, recA1, gyrA96, thi, hsdR17 (rk–, mk+), relA1, supE44, λ-, Δ(lac–proAB), [F' traD36, proAB, laqIqZΔM15], IDE3	Novagen
Shuffle	*E. coli*	fhuA2 lacZ::T7 gene1 [lon] ompT ahpC gal λatt::pNEB3-r1-cDsbC (SpecR, lacIq) ΔtrxB sulA11 R(mcr-73::miniTn10--TetS)2 [dcm] R(zgb-210::Tn10 --TetS) endA1 Δgor Δ(mcrC-mrr)114::IS10	NEB
BL21 DE3 CodonPlus-RIL	*E. coli*	F– ompT hsdS(rB- mB-) dcm+ TetR gal λ(DE3) endA Hte [argU ileY leuW CamR]	Stratagene
HT115 DE3	*E. coli*	E. coli [F-, mcrA, mcrB, IN(rrnD-rrnE)1, rnc14::Tn10(DE3 lysogen: lacUV5 promoter -T7 polymerase]	CGC
OP50	*E. coli*	Uracil auxotroph	CGC
XL1 Blue	*E. coli*	recA1 endA1 gyrA96 thi-1 hsdR17 supE44 relA1 lac [F proAB lacIqZΔM15 Tn10 (Tetr)]	Agilent
N2 (WT)	*C. elegans*	*C. elegans* wild isolate	CGC
tm1221	*C. elegans*	26615/26616-C-27604/27605 (989 bp deletion) V	NBPR
tm1093	*C. elegans*	4185/4186-CTTTCAAATGATT-4457/4458 (272 bp deletion + 13 bp insertion)	NBPR
VC475	*C. elegans*	Hsp16.2(gk249) V	CGC
RB791	*C. elegans*	Hsp16.48(ok577) V	CGC

Chemicals

Table 4.4. The list of the chemical that were used in this work.

Chemical	Provider
2-Mercaptoethanol (β-ME)	Sigma
Acetic acid	Roth
Acetonitrile	Sigma
Acrylamide/Bis solution 38:2 (40% w:v)	Serva
Agar Agar	Serva
Agarose	Serva
Ammonium persulfate (APS)	Roth
Ampicillin sodium salt	Roth
Calcium chloride	Merck
Citric acid monohydrate	Merck
Cholesterol	Sigma
Coomassie Brilliant Blue R-250	Serva
Coomassie Quick Stain	Serva
Deoxynucleoside triphosphates (dNTPs)	Roche
Dimethyl sulfoxide (DMSO)	Sigma
Dipotassium phosphate	Merck
Disodium phosphate	Roth
Dithiothreitol (DTT)	Roth
Ethanol	Merck
Ethylenediaminetetraacetic acid (EDTA)	Merck
Formic acid	Sigma
Glycerol	Roth
Glycin	Roth
Guanidine hydrochloride	Roth
Hydrochlorid acid 32 %	Merck
Iodoacetamide	Merck
Isopropanol	Roth
Isopropyl β-d-1-thiogalactopyranoside (IPTG)	Serva
LB medium	Serva
Magnesium chloride	Merck
Magnesium sulfate	Sigma
Methanol	Sigma
Milk powder	Roth
Monopotassium phosphate	Merck
N,N,N',N'-Tetramethylethylendiamine (TEMED)	Roth
Nonidet P-40 substitute	Sigma
Peptone	BD
Phenylmethanesulfonyl fluoride (PMSF)	Sigma
Potassium chloride	Roth
Potassium hydroxide	Roth
Protease inhibitor Mix HP, G	Serva
Sodium acetate	Roth
Sodium chloride	Roth

Chemical	Provider
Sodium deoxycholate	Merck
Sodium dodecylsulfate (SDS)	Serva
Sodium hydroxide	Roth
TCEP	Sigma
Trifluoroacetic acid	Sigma
Trizma Base	Sigma
Triton X-100	Merck
Tween-20	Merck
Uranyl acetate	Sigma
Urea	Merck
Water (MS)	Merck
WesternBright™ ECL-Spray	Advansta

Kits, enzymes and standards

Table 4.5. The list of the kits, enzymes and standards (protein and DNA) used in current work.

Product name	Provider
100 bp DNA ladder	NEB
1 kb DNA ladder	NEB
Gel Filtration Standard	BioRad
Lmw SDS PAGE standard test mixture 6	Serva
Dual color protein standard	Serva
PierceTM BCA Protein Assay Kit	Thermo Scientific
WizardR Plus SV Minipreps DNA Purification System	Promega
Trypsin (Sequencing Grade Modified Trypsin)	Promega
PolyQ DNA polymerase	NEB

Antibodies

Table 4.6. The list of the antibodies used in this work in western blot and co-immunoprecipitation.

Antibody	Host	Provider
anti-Hsp16.2	mouse	Pineda
anti-Hsp16.41	rabbit	Pineda
anti-Hsp16.48	rabbit	Pineda
anti-rabbit IgG- Peroxidase	goat	Sigma- Aldrich
anti-mouse IgG-Peroxidase	rabbit	Sigma- Aldrich

Substrate proteins

- Malate dehydrogenase (MDH) from pig heart mitochondria, Roche
- Citrate synthase (CS), Sigma
- Insulin drom bovine pancreas, Sigma

Equipment

Table 4.7. The list of the devices that were used in this work.

Name of the device	**Provider**
ÄKTA FPLC P-920	GE Healthcare
ÄKTA PURE	GE Healthcare
Amicon Bioseparations Stirred Cells	EMD Millipore
Bead Mill MM400	Retsch
Cell Disruption Apparatus Basic Z	Constant Systems
Centrifuge Avanti J25 and J26 XP	Beckman Coulter
Centrifuge Optima XL-I	Beckman Coulter
Centrifuge Rotina 420R	Hettich
Centrifuge Tabletop centrifuge 5415 C	Eppendorf
Centrifuge Tabletop centrifuge 5418	Eppendorf
Chirascan™ - Circular Dichroism Spectrometer	Applied PhotoPhysics
Gel electrophoresis and blotting devices	Hoefer
Glass slides	Marienfeld
Homogeniser Ultra Turrax DIAX900	Heidolph
HPLC system	Shimadzu
Ice machine	Ziegra
ImageQuant LAS4000 system	GE Healthcare
Incubator	mytrom/New Brunswick Scientific
Magnetic stirrer Heidolph Hei-Standard	Heidolph
MALS detector Dawn Heleos II MALS detector	Wyatt
Microscope Stemi 2000 with a CL1500 Eco cold light source	Zeiss
Orbitrap Fusion Mass Spectrometer	ThermoFisher Scientific
pH meter	WTW
Pherastar plate reader	BMG Labtech
Pipettes (2.5, 10, 20, 200, 1000, 5000 µl)	Eppendorf
Rotator SB3	Stuart
SavantTM DNA120 SpeedVacTM Concentrator	ThermoFisher Scientific

Name of the device	Provider
Scales SI-234	Denver Instrument
Scales SI-4002	Denver Instrument
SDS-PAGE Running Chamber	Serva
Superloop	GE Healthcare
Thermomixer comfort, compact	Eppendorf
Typhoon Scanner	GE Healthcare
Ultrasonic cleaner USC-T	VWR
Ultrospec 1100 pro spectrometer	Amersham Biosciences
UV-Vis spectrophotometer NanoDrop1000	Peqlab
Varian Cary 50 Bio spectrometer	Agilent
Vortex Genie 2	Scientific Industries
Western Blotting Apparatus Fasblot B34	Biometra

Consumables

Table 4.8. The list of the consumables used in this work.

Name	Provider
200-mesh copper grids	Merck
Amicon Ultra-15 centrifugal filter units	Merck
Blotting paper	Whatmann
Centrifuge Filter, 0.22 µm	Merck
Chromacol Closures, 9mm, white Silicone/Red PTFE	ThermoFisher Scientific
Chromacol vials, 9mm, Polypropylene, 300 µl	ThermoFisher Scientific
Cuvettes	Brand
Dialysis membranes Spectra/Por	Spectrum Laboratories
Empore C18 extraction discs	ThermoFisher Scientific
Glass pasteur pipettes	Labsolute
Nitrocellulose Membrane Roti® NC	Roth
Parafilm	Roth
PCR tubes	BioRad Laboratories
Petri dishes	Greiner Bio One
Pipette tips	Eppendorf
Protein G Sepharose 4 Fast Flow	GE Healthcare
Protein LoBind tubes	Eppenforf
Q Sepharose Fast Flow	GE Healthcare
Reaction tubes, 0.5, 1.5 mL and 2 mL	Sarstedt
Serological pipettes 1 mL, 2 mL, 5 mL, 10 mL, 15 mL	Sarstedt
SP Sepharose Fast Flow	GE Healthcare
Superdex 200 26/60	GE Healthcare

Name	Provider
Superdex 200 6/60	GE Healthcare
Superdex 75 16/60	GE Healthcare
Superdex75 26/60	GE Healthcare
Ultracel Ultrafiltration disc 3 kDa NMWL	Millipore
Xpress Micro Dialyzer MD300	Scienova

Software and online resources

Origin lab	version 2018b, TUM license
PyMOL Schrodinger, LLC	http://pymol.sourceforge.net/
GdmCl] and [Urea] Calculator	http://sosnick.uchicago.edu/gdmcl.html
ExPASy Prot Param tool	http://web.expasy.org/protparam/
CLUSTAL W2	http://www.clustal.org/
BLAST	http://blast.ncbi.nlm.nih.gov/Blast.cgi
PDB	http://www.rcsb.org/pdb/home/home.do
PubMed	http://www.ncbi.nlm.nih.gov/pubmed
SnapGene Viewer	www.snapgene.com
New England Biolabs Tm Calculator	https://tmcalculator.neb.com
Astra	Wyatt
MaxQuant	Cox et al., 2011
Perseus	Sinitcyn et al., 2018
Cytoscape	v. 3.9.1, https://cytoscape.org/
Deuteros	https://github.com/andymlau/Deuteros
Sedfit	https://sedfitsedphat.github.io/
BestSel	https://bestsel.elte.hu/extcoeff.php
Adobe Illustrator	Adobe Inc.
UniProt	www.uniprot.org
Wormbase	https://wormbase.org/#012-34-5
WormBook	http://www.wormbook.org/
Jalview	https://www.jalview.org/

Methods

Molecular biology

Transformation of bacterial cells

50µL of chemically competent *E. coli* cells were thawed on ice. 1µL of DNA was added and cells were incubated on ice for 15min. Afterwards, the cells were heat shocked at 42°C for 10sec and incubated on ice for 5min. then 950µL of LB-medium were added and cells were further incubated for 60min at 37°C while shaking at 300rpm. After incubation, 100µL of transformed cells were plated out on a selection plate (Ampicillin, 100 µg/mL) and incubated overnight at 37°C.

Minipreps for DNA isolation

Bacterial plasmid DNA was isolated via WizardR Plus SV DNA Purification System (Promega) was used according to the manufacturer's manuals. The DNA was usually eluted in 20 µL of pre-warmed nuclease free water and stored at -20°C.

Polymerase chain reaction (PCR)

Polymerase chain reaction (PCR) was used to amplify DNA fragments. DNA template was amplified by DNA polymerase (NEB) (Taq polymerase). Two primers were designed and ordered from Eurofins. The annealing temperature was calculated in SnapGene or NEB Tm Calculator (NEB). dNTPs (nucleotides of bases A, T, G and C) were added to the reaction as well as DNA template. The pipetting scheme is given in Table 4.9. The reaction was carried in a thermal cycler under the conditions described in Table 4.10.

Table 4.9. Pipetting scheme of Master Mix for PCR reaction. *The Master Mixes were prepared in access for N+1 reactions.*

	Volume
Primer Fwd	0.8 µL
Primer Rev	0.8 µL
10mM dNTPs	0.5 µL
Polymerase buffer	2 µL
Polymerase	0.2 µL
ddH_2O	14.7 µL
DNA template (100ng/µL for plasmid)	1 µL

Table 4.10. Cycling parameters for PCR reactions.

	Parameters	
Denaturation	95°C, 3 min	
Melting	94°C, 30 sec	x35 cycles
Annealing	Based on primers	
Extension	68°C, 60 sec/kb	
Final extension	68°C, 5 min	
	16°C, ∞	

Agarose gel electrophoresis

To evaluate DNA samples, they were analysed by DNA gel electrophoresis. For this, 1% agarose solution in 100 mL 1x TAE buffer (40 mM Tris/Acetate pH 8.0, 50 mM EDTA) was prepared. Agarose was slowly melted avoiding boiling via gentle heating until the solution looked clear. Then solution was cooled at room temperature and 3µL of Stain G (Serva) were added so that DNA is visible under UV light. DNA samples were diluted with 5x Loading DNA buffer (Serva) and loaded onto the gel. A reference 1 kb or 100 bp ladder (Serva) were loaded as well. Gel was running in 1x TAE buffer at 120 V for 30 mins and visualised under UV light in ImageQuant 300 Imager (GE).

PCR product purification

The products of PCR were purified with Promega PCR purification kit (Wizard® SV Gel and PCR Clean-Up System) according to the manufacturer guide. Briefly, the

amplification product was placed in SV Minicolumn and incubated for 1 min at room temperature, then centrifuged at 16 000 g for 1min. the column was washed with 700 µL of Membrane Wash Solution by centrifugation at 16 000 g for 1min. the washing step was repeated with 500 µL of Membrane Wash Solution and the column was centrifuged for 5min. The residual ethanol was removed by additional 1min centrifugation. The column was transferred to an empty 1.5 mL tube and 50 µL of Nuclease-free water were applied. After 1min incubation at room temperature, the assembly was centrifuged at 16 000 g for 1min. the eluted DNA was stored at -20°C. 15 µL were sent for sequencing to Eurofins to validate PCR.

DNA sequencing

Purified plasmids or PCR products were sent to Eurofins Sanger sequencing for validation at the concentrations 50-100 ng/µL and 10-50 ng/µL respectively as recommended by Eurofins.

Protein analytical methods

Determination of recombinant protein concentration

The concentration of purified proteins and substrates was usually determined by UV spectroscopy at NanoDrop1000. The concentration of the protein is estimated and calculated by the software as follows:

$$A = \varepsilon \times c \times d,$$

where

A is the absorption measured at 280 nm,
ε is the molar absorption coefficient ($M^{-1} \cdot cm^{-1}$),
c is the molar concentration (M),
d is the path length of the light through the cuvette (cm).

The molar absorption coefficient of the respective protein was predicted by Expasy´s ProtParam tool (Gasteiger et al., 2005). The measurements were corrected to the respective buffer.

BCA assay

To determine the concentration of complex protein mixtures or proteins with low spectroscopic characteristics BCA assay was applied according to the manufacturer's manual (Pierce BCA Assay Kit, ThermoFisher Scientific). The assay employs the process of reduction Cu^{2+} to Cu^{1+} by the protein in an alkaline environment and allows colorimetric detection due to reaction of bicinchonic acid (BCA) with reduced copper cations (Smith et al., 1985). The reaction is known as biuret reaction.

The assay was performed in 1 mL cuvettes or 96-well plate. The reagent:protein mixtures were incubated at 37°C for 30 min, cooled down at RT and measured in a photometer or Pherastar plate reader (BMG LAbtech) at 562 nm. The concentration of the protein of interest was derived from the calibration curve of BSA standards.

Sodium dodecyl sulphate polyacrylamide gel electrophoresis (SDS-PAGE)

SDS-PAGE was used for analytical separation and visualisation of protein of interest according to its molecular weight (Laemmli, 1970). The proteins were analysed on 15% gels with 5% stacking gel due o low molecular weight of the proteins of interest. The composition of the gels is as follows:

Table 4.11. The recipe for 15% SDS-PAGE gel. *The volumes of reagents are given for 15% running gel and 5% stacking gel.*

15%	Volume	5%	Volume
4xTG (1.5 M Tris/HCl, pH 8.8, 0.8 % w/v SDS)	2.5 mL	2xSG (250 mM TRIS/HCl, pH 6.8, 0.4% w/v SDS)	2.5 mL
40% Acrylamide	3.75 mL	40% Acrylamide	0.625 mL
H_2O	3.75 mL	H_2O	1.875 mL
10% APS	100 µL	10% APS	100 µL
TEMED	10 µL	TEMED	10 µL
Total	10 mL		10 mL

The first step was to prepare separation gel. On the top of it was poured isopropanol to flatten the top of the gel. After the removal of isopropanol, the stacking gel was made on the top of the already polymerised separation one.

The proteins were mixed with 5x Laemmli buffer and incubated at 95°C for 5 min to unfold the proteins and bound them to SDS. The samples were briefly centrifuged and loaded onto the gel. As a protein standard, 7 µL of either low molecular weight marker (Serva test mixture 6) or pre-stained dual colour protein ladder (Serva) was used. The electrophoresis was carried out usually at 35 mA per gel for 40 min in SDS running buffer (25 mM TRIS, pH 8.3, 0.2 M Glycine, 0.1% w/v SDS). The gels were stained with Fairbanks A (25% v/v isopropanol, 10% v/v acetic acid, 0.05% m/v Coomassie Brilliant Blue R-250) and de-stained with Fairbanks D (10% v/v acetic acid) based on Fairbanks et al., 1971.

Western Blot

For identification of specific proteins, the western blot was performed. Protein samples were examined on SDS-PAGE 15% gels using pre-stained molecular weight marker. Then skipping staining process proteins were transferred onto nitrocellulose membrane (NC) by semi-dry transfer. The gel was placed on a membrane, and then they both were put between three layers of a filter paper from each side. The transfer was done at 75mA per gel for at least 2h in transfer buffer (48 mM Tris, pH 9.0, 39 mM Glycine, 20% v/v Methanol, 0.037% w/v SDS). The NC with transferred proteins was incubated in the blocking solution (5% w/v milk powder in TBST: 20 mM Tris, 150 mM NaCl, 0.1% w/v Tween20) for 1 hour at RT while slowly shaking to block any unspecific protein binding sites. The membrane was washed three times in TBST, cut if necessary to separate different proteins, and then incubated overnight with the respective primary antibody at the following dilutions in TBST: α16.2 at 1:1000, α16.41 at 1:250, and α16.48 at 1:250. The membranes were then washed 2 times for 5 min in TBST then incubated with the respective secondary antibody (Hsp16.2 with

α-mouse, Hsp16.41 and Hsp16.48 with α-rabbit) for 45-60 min at the 1:10 000 dilutions. The membranes were washed again two times in TBST for 5 min and finally one time in TBS (no Tween20) for 10 min. To visualise the result, membranes were sprayed with chemiluminescence detection spray WesternBright ECL Spray (Advansta) and visualised via ImageQuant LAS 4000 System (GE Healthcare).

Protein expression and purification

Test expression

Two mutant expression vectors, Hsp16.41 (A33C) and Hsp16.48 (A33C), were tested for optimal protein over-expression at different conditions. The constructs were transformed into three expression systems, such as JM109 (DE3), SHuffle and BL21-CodonPlus (DE3). The expression was induced by 1mM IPTG and carried at 30°C and 37°C overnight. 1 mL of expression culture were taken every other hour for further analysis by SDS-PAGE. The cells were separated by centrifugation at 16 900 g for 5 min and washed three times in IB Buffer (50 mM Tris (pH 7.4), 10 mM EDTA, 50 mM NaCl, Protease Inhibitor Mix G (Serva)). Cell disruption was done with 0.25-0.5 mm glass beads in a bead mill at 30 s^{-1} for 1 min 3 times at 8°C. Cells were separated from glass beads into fresh tube. The inclusion bodies were separated from soluble fraction via centrifugation at 16 900 g for 5 min. The pellet and lysate were analysed by SDS-PAGE on 15% gels.

Expression and purification of the “core” hsp16s

Recombinant sHsp16s were purified under denaturing conditions. The genes were sub-cloned into NdeI/XhoI sites of the vector pET-21a(+) (Novagen-Merck Biosciences, Ltd., Nottingham, UK). The plasmids were transformed into *E. coli* strain BL21-CodonPlus (DE3). The transformed cells were cultured at 37°C overnight in 50 mL Luria-Bertani (LB) medium containing 100 µg/mL ampicillin and used to inoculate 2 L LB medium for further protein expression. The protein expression was induced by 1 mM isopropyl-1-thio-β-D-galactopyranoside (IPTG) once cells reached OD600 = 0.6-

0.7 (approximately after 4-5 h) and carried out overnight at 37°C. Cells were harvested by centrifugation at 6 000 rpm at 4°C and re-suspended in 50 ml ice-cold IB-Buffer (50 mM Tris (pH 7.4), 10 mM EDTA, 50 mM NaCl, Protease Inhibitor Mix G (Serva)). Cell disruption was performed by sonication in a high pressure cell disruption system BasicZ (ConstantSystems, Daventry, United Kingdom). 1% Triton X-100 was added to the lysate and stirred for 1 h at 4°C. The inclusion bodies were harvested by centrifugation at 20 000 rpm at 8°C and washed with IB buffer at least three times. The inclusion bodies were re-suspended in IB-dissolving buffer (50 mM Tris (pH 7.4), 5 mM EDTA, 4 M Urea, 10 mM β-Mercaptoethanol) and dissolved by stirring for 2 h at room temperature. Insoluble parts were separated by centrifugation at 20 000 rpm at 25°C. The supernatant was applied to an ion-exchange Q-sepharose column equilibrated in Buffer B1 (50 mM Tris (pH 7.4), 5 mM EDTA, 50 mM NaCl, 5 mM DTT, 4 M Urea) and eluted using a gradient of 0-100 % Buffer B2 (50 mM Tris (pH 7.4), 5 mM EDTA, 1 M NaCl, 5 mM DTT, 4 M Urea). Fractions containing the protein of interest were loaded on an ion-exchange SP-sepharose equilibrated in Buffer B1 and were eluted using a gradient of 0-100 % Buffer B2.

The fractions of interest were concentrated to 10 ml with Amicon Stirred Ultrafiltration Cells (EMD Millipore, Billerica, MA, USA) using ultrafiltration disc membranes with a 3 kDa molecular weight cutoff. The concentrated sample was loaded on a size-exclusion Superdex75 26/60 column equilibrated in Buffer B3 (50 mM Tris, pH 7.4, 5 mM EDTA, 150 mM NaCl, 5 mM DTT, 4 M Guanidinhydrochloride) and eluted.

Refolding was performed on a size-exclusion column Superdex200 26/60 equilibrated in PBS (8.1 mM $Na_2HPO_4x2H_2O$ (pH 7.4), 1.76 mM KH_2PO_4, 137 mM NaCl, 2.7 mM KCl). Fractions containing refolded protein were dialyzed overnight in 5 L of PBS (pH 7.4) at 4°C in Spectra/Por dialysis tubes (Spectrum Laboratories, Inc, USA) with a molecular weight cutoff of 6-8 kDa. The purity was confirmed by 15% sodium dodecyl sulphate polyacrylamide gel electrophoresis. Purified proteins were concentrated again at 4°C, flash-frozen in liquid nitrogen and stored at -80°C.

Protein concentrating

The proteins were concentrated in Amicon Stirred Ultrafiltration Cells (EMD Millipore, Billerica, MA, USA) using ultrafiltration disc membranes with a 3 kDa molecular weight cutoff. For smaller amounts, Amicon Ultra Centrifugal Filter Units (Merck) with a 3 kDa cut-off were used for concentration via centrifugation at 4,000 x g and 8°C.

Protein dialysis

The buffer exchange was done against 100-fold excess of a fresh buffer overnight at 8°C with a gentle stirring. The proteins were poured into a Spectra/Por dialysis tube (Spectrum Laboratories) with a 3 kDa cutoff. For small amount (0.5-1 mL), the proteins were dialysed in Slide-A-Lyzer™ Dialysis Cassettes (Thermo Scientific) with a 3 or 10 kDa cutoff.

In vitro structural assays

CD spectroscopy

To characterise the secondary protein structures Far-UV CD measurements were carried out in a Chirascan – Circular Dichroism Spectrometer (Applied PhotoPhysics). The protein samples were diluted in PBS (pH 7.4) and loaded into 0.1 or 0.5mm cuvettes (Hellma) at 10-25 µM concentration. CD signals were collected ten times from 260 nm to 200 nm, using a scanning rate of 1 nm/sec at 10°C. The spectra were corrected by the background spectra from PBS. The molecular ellipticities were calculated for the mean residue weight (MRW) due to macromolecular structure of the chaperones as follows (Venyaminov and Yang, 1996):

$$\theta_{\mathrm{MRW}} = \frac{\theta_{\lambda} \times \mathrm{MRW}}{c \times l \times 10}$$

where

θ_{MRW} = mean residue ellipticity [deg cm2 dmol-1];

MRW = mean residue molecular weight;

θλ = ellipticity [deg];

l= path length of the cuvette [cm];

c = protein concentration [M];

Thermal unfolding and refolding

To test thermal stability of the proteins their thermal transitions from 10°C to 80 °C and backwards were analysed (Greenfield, 2006). The heating/cooling rate of 1°C/min with stepped ramp was applied. The change in molar ellipticity was recorded by the Chirascan coupled to the water bath and Peltier element (Quantum Northwest) in a range of 210-225 nm wavelengths. The protein concentrations were 20 µM and the transitions are shown at specific wavelengths indicated for each plot separately.

High performance liquid chromatography (HPLC)

HPLC is a method used to analyse the size of complex biological samples by separating them on a size-exclusion column according to their size. The retention time of the analysed complex is compared to the standard (BioRad) which in this case contained thyroglobulin (670 kDa), γ-Globulin (158 kDa), Ovalbumin (44 kDa), Myoglobin (17 kDa) and Vitamin B12 (1.35 Da). HPLC system (Shimadzu) was equipped with analytical size exclusion column Superdex200 increase 10/300GL (GE), which was chosen due to the ability of sHsp16s to form oligomers up to 500 kDa. In addition, HPLC was equipped with SPD-20A UV/VIS detector, RF-10A XL fluorescent detection system, SIL-20AC auto sampler, DGU-20A degassing unit and FRC-10A fractionation collector. The proteins were separated in PBS (pH 7.4) at a flow rate 0.5 mL/min at RT. Injection volume was usually 100 µL with various protein concentrations. Prior analysis the protein samples were centrifuged at 16 000 rpm for 20 min at 8°C to

remove any possible artefacts. In case of fractionation, the fractionation volume was set to 500 µL.

To complement the transmission electron microscopy experiment with chaperone:substrate complexes, 8 µM of the respective chaperone were incubated with aggregating 2 µM MDH, 1 µM CS or 40 µM insulin at the respective aggregation inducing conditions to track complex formation. The formed complexes were loaded on the column after 30 min of incubation and compared with the sizes of the control samples (chaperone and aggregating substrate alone).

Analytical size exclusion chromatography-multi-angle light scattering (SEC-MALS)

Another method to assess the molecular weight of proteins is SEC-MALS. The HPLC system is equipped with a refractive index (RI) detector (Shimadzu) and multi-angle light scattering (MALS) detector (Wyatt). 80 µM of protein were applies onto a Superdex200 increase 10/300GL (GE) column equilibrated in PBS, pH 7.4. The flow-rate was set to 1 mL/min with a separation time 60 min. BSA standard (ThermoFisher Scientific) was used for the calculation of molecular masses and extinction coefficient in ASTRA software (Wyatt).

Analytical ultracentrifugation (AUC)

The proteins were analysed by analytical ultracentrifugation to obtain their molecular weights. This is an advantageous method, especially for proteins that tend to interact with a column matrix (HPLC, SEC-MALS) and for proteins with low content of aromatic amino acid residues. The measurements were carried at 230 nm in ProteomeLab XL-I Beckman Coulter under sedimentation velocity mode. The 20 µM protein samples (in PBS) were analysed at 20°C at 30 000 rpm in a AN50Ti rotor. For this, 350 µL of a sample in triplicate was loaded in assembled double-sector cells with quartz windows. The scan counts were set to 250 with a rate 1 scan/min. The analysis was

carried out in SEDFIT software (Brown and Schmuck, 2006). The measurements were performed with Dr. Martin Haslbeck.

Hydrogen/deuterium exchange mass spectrometry (H/DX-MS)

The changes in molecule dynamics can be monitored by Hydrogen/deuterium exchange mass spectrometry (H/DX-MS). The principles of the method consist in measuring the time-dependent isotopic exchange of hydrogen atoms in the protein and the surrounding solvent (Masson et al., 2019). The tightly folded atoms are protected from the exchange, while unfolded or disordered regions are more accessible and thus are rapidly involved in the HDX (Konermann et al., 2011).

The measurements were done on the Synapt G2-S ESI-TOF mass spectrometer (Waters) equipped with Leap PAL RTC (robotic tool change) and ACQUITY M-Class UPLC (Waters) system for a high efficiency particle separation. 30 µM protein samples were diluted with deuterium oxide to 1.5 µM concentration in PBS, pH 7.4. The samples were incubated at 20°C for 0.167 min, 1 min, 10 min, 30 min and 120 min. The reaction was quenched by adding an equal amount of quenching buffer (50 mM Na_2HPO_4/NaH_2PO_4, pH 2.6, 35 mM TCEP, 4 M guanidine hydrochloride) at 1°C. The proteins were then digested on the Enzymate BEH Pepsin Column (2.1 x 30 mm; Waters) at 20 °C. The peptides were trapped and then separated on an ACQUITY UPLC BEH C18 column (1.7 µm, 1.0 x 100 mm; Waters) at 0°C by eluting with 0.1 % (v/v) formic acid in acetonitrile and 0.1 % (v/v) formic acid in water gradient. The peptides were additionally separated by drift time in the mobility cell and fragmented by MSE optimised approach (Boczek et al., 2015; Helm and Baginsky, 2018). The data was analysed in Protein Lynx Global Server PLGS and DynamX (Waters) and Deuteros (Lau et al., 2021).

Negative stain transmission electron microscopy (TEM)

5 µL of protein samples in PBS, pH 7.4, were applied on the 200-mesh activated copper grids (Merck) and incubated for 10 sec. The proteins were then washed with 10 µL of 50 mM Tris buffer and stained with 5 µL of 1.5 % (w/v) uranyl acetate solution for 30 sec. The access liquid was removed by a gentle touch with a filter paper. The

micrographs were taken on a JEOL JEM-1400 Plus transmission electron microscope (JEOL Germany GmbH) at 120 kV and a magnification of 50,000x by Dr. Carsten Peters.

In vitro functional assays

Chaperone activity assay

To assess a chaperone function of sHsp16s *in vitro*, they were examined for their ability to prevent (holdase) or promote (aggregase) the aggregation of induced unfolding of model substrates (Mymrikov et al., 2017). The aggregation of chaperone:substrate complexes was monitored via light scattering at 360 nm for 50-70 min in a Cary50 photometer (Agilent) equipped with waterbath for temperature control in 10mm quartz cuvettes (Hellma). The aggregation was induced either by elevated temperature or chemically. For thermal aggregation malate dehydrogenase (MDH, 2 µM) and citrate synthase (CS, 1 µM) were used and induced at 42°C and 44°C respectively. For chemical aggregation assay insulin (40 µM) was induced by 20 mM DTT and monitored at 37°C. Proteins were diluted in PBS (pH 7.4) to the final concentration of 0-8 µM. sHsp16.41 and sHsp16.48 were additionally analysed in HEPES buffer (pH 7.4) into which they were dialysed overnight before the measurement. To compare chaperone activity at different chaperone:substrate ratios, the endpoint of scattering data of experimental samples was normalised to the endpoint value of control sample (substrate alone) at respective chaperone concentration.

Protein labelling

Hsp16.2 was labelled with ATTO550 and ATTO647N fluorescent dyes (ATTO TEC) at the C33 position. The protein in PBS, pH 7.4, was incubated with 10-fold molar access of each dye for 1 h at 37°C in the dark while shaking. The unbound dye was removed with PD10 column.

Förster resonance energy transfer (FRET)

Förster resonance energy transfer (FRET) occurs between the excited state donor fluorophore and acceptor fluorophore. For the transfer to occur, the spectral overlap and proximity of fluorophores up to 20 nm have to be satisfied (Algar et al., 2019). The chosen optimal FRET dyes were ATTO550 and ATTO647N.

For FRET measurements, 5 µM of ATTO550 and 5 µM of ATTO647N labelled Hsp16.2 (PBS, pH 7.4) were mixed in a 200 µL cuvette at 1:1 ratio resulting in 5 µM total concentration. The experiment was performed at 15°C on Jasco FP-8550 spectrofluorometer equipped with a temperature control. The donor (ATTO550) was excited at 555 nm. The bandwidth was set to 2.5 mm. Sensitivity was set to medium and the response to 0.1 sec. The scan speed was 500 nm/min with 1 nm data intervals. For kinetics measurement, the change in fluorescence was recorded at 575 nm for donor and at 666 nm for acceptor for 1800 sec. For spectra measurement, the emission was monitored from 565 to 700 nm.

Subunit exchange

To investigate the relationship between Hsp16 family members and their ability to freely associate and dissociate subunits, they were examined by a FRET subunit exchange assay (Bova et al., 1997). For this, a pre-formed for 1800 sec Hsp16.2 FRET complex (5 µM) was diluted with a 10-fold molar access of unlabelled Hsp16. The total protein concentration was kept constant at 5 µM, as this was important for Hsp16s due to their heterogeneity and dynamic. For this, 15 µL of 5 µM pre-formed FRET complex were diluted with 135 µL of an unlabelled protein and PBS, pH 7.4, so that the total protein concentration in the cuvette was still 5 µM. The dissociation of a FRET pair complex was monitored as a change in donor signal at 15°C for 1800 sec at 555 nm excitation and 575 nm emission.

In vivo assays

C. elegans growth and maintenance

The worms were normally maintained at 20˚C on the Nematode Growth Medium (NGM) plates (3 g NaCl, 2.5 g peptone, 20 g agar, 1 mL of 5 mg/mL cholesterol in ethanol, 1 mL of 1 M $CaCl_2$, 1 mL of 1 M $MgSO_4$ and 25 mL of 1 M KH_2PO_4 pH 6.0 in 1 L ddH_2O) as recommended in Wormbook (Eisenmann, 2005). The agar contained a lawn of OP50 *E. coli* as a food source. Bacterial cultures were grown in B-broth (10 g Tryptone, 5 g NaCl in 1 L ddH_2O) at 37˚C without shaking overnight or at RT for 24 h. To keep culture running, worms were either picked twice a week or chunked once in 1-2 weeks. In case of a long-term storage, the worms were kept at 10-15˚C on starved plates (with no source of food) for several months. All strains were purchased either from Caenorhabditis Genetic Center (CGC) or National Biosource Project (NBPR, Mitani).

Generation and maintenance of males

For genetic manipulations, male (XO) animals were generated by heat shock. The purpose of generating males was to either backcross mutant strains and ensure that mutation is fixed in the population or generate a strain with multiple mutations (Fay, 2006) (Wormbook). Given that males occur at a low frequency in a wild-type population (~0.02%), they were generated by mild heat shock. 3-4 seeded NGM plates with 10-15 L4s were placed in a water bath for 4 h at 30˚C. In several days the F1 generation was checked for males. At least 10 males were then picked onto a fresh non-seeded NGM plate and mated with 5 hermaphrodites (XX). This should increase the frequency of males in next generation. A small dot of *E. coli* lawn was put in a centre of a plate as a source of food so that the chance of mating increases. The male plate was maintained by picking excess of males and mating them with hermaphrodites at least once a week.

C.elegans genotyping, backcrossing, and outcrossing

I. PCR genotyping

Firstly, to validate that the purchased mutant strains carry the correct mutation they were examined by PCR genotyping (Ahringer, 2006). Three primers were designed for each of the mutant strains: forward, reverse, and internal reverse so that they bind before, after and within the mutated region, respectively. The principle of this approach is as follows (Figure 4.1): if mutation is present, the internal primer does not bind which results in one type of PCR product made by forward and reverse primers; if the mutation is absent, then two PCR products are created; in case of heterozygous mutation, there are all three PCR products.

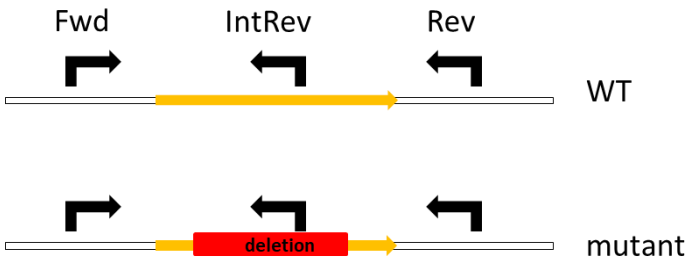

Figure 4.1. The principle of primer design for PCR genotyping. *For each mutant strain the forward, revers and internal reverse primers were designed.*

To get a DNA template, the genomic DNA (gDNA) was extracted from the mutants of interest via worm lysis. 10 µL of worm lysis buffer (50 mM KCl, 10 mM Tris pH 8.2, 2.5 mM $MgCl_2$, 0.45% NP-40, 0.45% Tween20, 0.01% Gelatine and 6 µL of 20 mg/mL Proteinase K per 1 mL added freshly) were put on a lid of PCR tube and 10 µL inside the tube. Then 10 gravid adults were picked and transferred in the drop of the buffer in the lid. The worms were briefly centrifuged down and placed to -80°C for 20 min to accelerate the breaking of a harsh cuticle of the worms. The next step was carried out in PCR cycler with the following method: 1 h at 60°C, then 20 min at 95°C to inactivate Proteinase K. For PCR genotyping, 1 µL of extracted gDNA was used in a

reaction. MasterMix composition for PCR contained 0.8 µL of each 10 µM primer, 0.5 µL of 10 mM dNTPs, 2 µL TaqBuffer, 0.3 µL Taq Polymerase and 13.8 µL ddH_2O.

The PCR genotyping was carried out in a PCR cycler using OneTaq PCR kit (NEB) as follows:

Table4.12. PCR cycling methods for genotyping

tm1221	VC475	tm1093	RB791	
95°C, 3 min				
94°C, 30 sec				x35 cycles
64.1°C, 30 sec	55,7°C, 1 min	62°C, 1 min	62°C	
68°C, 2.5 min	68°C, 45 sec	68°C, 45 sec	68°C, 2 min	
68°C, 5 min				
16°C, ∞				

PCR products were loaded on a 1% DNA agarose gel and subjected to a DNA electrophoresis. In this way all mutants were validated and matched the information provided by the manufacturer. However, tm1221 mutant that is supposed to have *hsp16.1b* and partially *hsp16.48b* genes mutated had mutation in other gene copies, *hsp16.1a* and *hsp16.48a,* instead.

II. Backcrossing

Given that mutant strains were heavily mutagenized by manufacturer and may contain several mutations in addition to the one of interest, it is crucial to backcross them to the wild-type strain (Ahringer, 2006). For this, 5 L4 hermaphrodites of the mutant strain were mated with 10 males of wild type (N2) overnight at 20°C. The next day adult hermaphrodites were singled out (each individual was put on a separate 3 cm NGM plate seeded with OP50). In 4 days, the progeny (L4s) was singled out on 16 plates and allowed to self-fertilize and lay eggs once reached adulthood (overnight). Then each of 16 “mothers” was used for single-worm lysis (SWL) and genotyped for heterozygous mutation. The progeny of those with heterozygosity was again singled out on 32 plates and once reached adulthood was again genotyped for homozygous mutation. By this stage, the strain was 3x backcrossed. Then mating with N2 males was again repeated to obtain 4-6x backcross.

III. Outcrossing

To generate double-mutant strains, they were genetically manipulated by the method similar to backcrossing. In *C. elegans,* hermaphrodites can only self-cross, so the outcrossing is carried out with males of one of the mutants and hermaphrodites of another one. However, as sHsps are heat sensitive proteins, generating mutant males via heat shock was rejected as a method of choice. Therefore, the first step of crossing was to mate 5 L4 hermaphrodites of mutant with 10 males of N2 wilt type instead of males of another mutant. This approach takes more time but might be safer for the strains with a mutation in heat-shock proteins.

Animals carrying mutation in one gene of interest (gene A) were mated with 10 wild type males to obtain males carrying mutation in gene A. Next, 5 L4 hermaphrodites of the second mutant of interest (gene B) were mated with 10 males of gene A mutant. The 16 F1 heterozygotes were singled out to lay eggs and then were subjected to SWL and PCR genotyping for gene A. The F2 progeny of those mothers with homozygosity in gene A were singled out (32 animals), allowed to self-fertilize, lay eggs, and then subjected to SWL and genotyping for gene B. In case if gene B was still heterozygous, the F3 animals were again singled out and genotyped until both genes of interest became homozygous (Huang, 2006).

In this project tm1093 (Δ*hsp16.41*) was crossed with RB791. The last strain carries mutation in *hsp16.1a* and *hsp16.48a* (CGC; WormBase). RB791 deletion is 1803bp long and covers both genes. The result of crossing was a double (technically triple) mutant strain named tm1093xRB791 that carries mutations in *hsp16.41*, *hsp16.1a* and *hsp16.48a* genes.

RNAi lifespan assay

To examine the role of Hsp16s in *C. elegans* ageing, animals were analysed via lifespan assay. The principle of this method is to monitor the time from day 1 adulthood of the worm and assess whether animal is alive or dead. The combination of gene knock-out in mutant strains and knock-down by RNAi bacteria were used.

All mutant (tm1221, tm1093, VC475, RB791, tm1093xtm1221, tm1093xRB791) and N2 wild type strains were bleached to synchronize the worm populations. The principle of bleaching technique is that adult worms are sensitive to the component of bleaching solution while egg shell protects embryos. For this 2-3 NGM plates of each strain with many gravid adults and little or no *E. coli* lawn were washed off the plates with M9 buffer. Worms were then washed at least 3 times by centrifugation at 2 000 rpm for 2 min to get rid of the bacteria. The M9 buffer was discarded and 2.5 mL of bleaching solution were added (300 µL of 12% Sodium Hypochlorite NaOCl, 250 µL of 10M NaCl, 1950 µL of ddH_2O). The samples were vigorously shaken for 2 min to break down the cuticula and release eggs. The solution was examined under the microscope in between of shaking and once worms "broke", it was centrifuged again, supernatant immediately discarded and 4 mL of M9 buffer were added to stop the bleaching reaction. The eggs were washed at least 3 times with M9 buffer via centrifugation (Porta-de-la-Riva et.al., 2012). After the last washing step, the pellet was concentrated to around 500 µL. Approximately 100 eggs were put per NGM plate and grown at 20°C for 4 days until worms reached L4 stage. Then 20-25 L4s of each strain were put on 3-5 RNAi plates (3 g NaCl, 2.5 g peptone, 20 g agar, 1 mL of 5 mg/mL cholesterol in ethanol, 1 mL of 1 M $CaCl_2$, 1 mL of 1 M $MgSO_4$ and 25 mL of 1 M KH_2PO_4 pH 6.0, 1 mM IPTG, Ampicillin 100 µg/mL, 25 µM FUdR in 1 L ddH_2O) seeded with *E. coli* strain HT115 that carried a respective RNAi vector. Floxuridine, 5'-fluorodeoxyuridine (FUdR) was used to inhibit reproduction in adult animals (Gandhi et.al., 1980). This approach eliminates the need to transfer adult worms on the fresh plates to separate adults from growing larva. To avoid any unnecessary effects of FUdR on the development, larvae were first grown on regular NGM plates and transferred onto RNAi plates only at L4 stage of their development. After day7 of adulthood all worms were transferred onto the fresh RNAi plates with freshly seeded RNAi bacteria and no FUdR. The animals were transferred onto the fresh plates every week to maintain effectiveness of RNAi constructs. The total number of nematodes per variation was between 67 to 117 worms.

The vectors used were L4440 (empty vector), L4440:16.1, L4440:16.48. N2 grown on L4440 RNAi vector was used as a control. To note, L4440:16.1 and L4440:16:48 vectors each target two gene copies *16.1a/16.1b* and *16.48a/16.48b,* respectively. All vectors were validated by sequencing and targeted the respective genes of interest. Worms were grown at 20 ±1°C throughout the assay and monitored under the microscope every 1-3 days. The status of the worm (alive or dead) was assessed by gentle touch with a pick. Those worms that crawled inside agar or on the edge of the plate and dried out were marked as censored. The survival data was analysed with online tool OASIS2 (Han et al., 2016), data was assessed by Kaplan-Meier estimates (to evaluate percent survival and survival time), log-rank test (to compare results between the experimental groups), mean lifespan and visualised by survival plots in Origin (2018b).

Proteomics

C.elegans solid culture cultivation and lysate preparation

Growing worm cultures

To obtain enough material at least 30 10-cm NGM plates were seeded with 1.5 mL OP50 *E. coli* (grown in B-broth). Approximately 40-60 animals of mixed age were transferred onto the plates and grown at 20°C for 4 days (until plates are full of mixed worm populations).

C. elegans lysate preparation

For worm lysis worms were washed off the plates with M9 buffer, then the pellet was washed with M9 buffer by centrifugation at 2 000 rpm for 2 min 3-5 times until supernatant is clear (to get rid of the bacteria). The final centrifugation was carried out at 3 000 rpm to form a packed worm pellet and the supernatant was discarded. The pellet was re-suspended with equal amount of IP-buffer and flash-frozen in liquid nitrogen. The freezing step was always carried out and samples were always stored

at -80°C at least overnight. The worm pellet was thawed on ice and transferred into an ice-cold mortar. Worms were grinded 40 times and transferred into new Protein LoBind tubes (Eppenforf). The 0.25-0.5 mm glass beads were added and pellets were frozen in liquid nitrogen. Pellet was then slowly thawed on ice and broken up in a bead mill at 30 s^{-1} for 1 min 3 times at 8°C. Glass beads and cell debris were separated by centrifugation at 16 900 g for 10 min. The supernatant was transferred to a new tube and centrifugation was repeated. At this point lysate can be frozen in liquid nitrogen until further downstream applications. The concentration of protein mixture was assessed via BCA assay.

Co-Immunoprecipitation

The G-sepharose beads (Protein G Sepharose 4 Fast Flow, GE Healthcare) were washed 2 times with 750 µL PBS + 0.1% NP-40 by centrifugation at 2 000rpm for 2 min. Hsps were incubated with lysate (in a ratio 10 µg/mL 200 µL: 1 mg/mL 200 µL) for 1 h at 4°C while slowly rotating. Crude lysate sample was saved for later SDS-PAGE. Samples were then moved to water-bath for 45 mins for incubation at 20°C and 37°C. The control samples contained lysate and buffer with no hsp. The lysate:sHsp complexes were added to 20 µL of pre-equilibrated beads. 5 µL of antibody (anti-hsp16.48) were added to experimental samples. Pre-immune serum was added to control (no Hsp) samples. Samples were incubated overnight at 4°C while slowly rotating. Samples were then washed 3 times with 750 µL PBS + 0.2% NP-40. Last wash was done with 750 µL PBS, the supernatant was removed carefully. Samples were then flash frozen in liquid nitrogen. Samples were prepared in quadruplicates.

On-bead digest and desalting

The Co-IP samples were thawed on ice, then 25 µL of Buffer I (50mM Tris/HCl, pH 7.5, 2 M urea, 1 mM DTT, 5 ng/µL Trypsin) were added and samples were incubated for

2h at RT. Then 100µL of Buffer II (50 mM Tris/HCl, pH 7.5, 2 M urea, 5 mM Iodacetamide) were added and samples were incubated overnight at RT while shaking (300rpm). The tubes were covered with foil to protect them from light. The reaction was stopped by adding 1.5 µL of formic acid (FA). The beads were separated via centrifugation at 2 000 rpm for 2 mins. Samples were applied to a previously washed in 70 µL of 70% methanol and then equilibrated with 70µL of 0.5% FA Stage Tips with double C_{18} layer (Rappsilber et al., 2007). Tips were washed with methanol once by applying pressure with syringe filled with air and equilibrated with FA 3 times by centrifugation at 960 g for 1.5 min. The liquid leftovers were pushed through with syringe. Supernatant from beads samples (≈150 µL) was applied onto Stage Tips and centrifuged at 960 g for 3 mins. Sampled were again washed 3 times with 70µL of 0.5% FA. The elution was done into the fresh tubes using 2x 30 µL of 80% acetonitrile (ACN) and 0.5% FA solution via centrifugation at 960 g for 1 min. Eluted samples were put in SpeedVac concentrator (ThermoFisher Scientific) for at least 1 h at AQ method with constant heating. Dried samples were stored at -80°C until further step.

Sample preparation for LC-MS/MS

Peptides were thawed and dissolved in 24 µL of 0.1% FA and sonicated for 15 mins in an ultrasonic bath at RT. While sonicating, the centrifugal filters (0.22 µm, Merck) were equilibrated with 300 µL of 0.1% FA by centrifuging at 10 000 g for 2 min. The dissolved peptides were applied onto filters and centrifuged at 2 000 g for 1 min. The flow-through was transferred into Chromacol vials (ThermoFisher Scientific) for the following MS measurements.

MS/MS measurements

The measurements were performed on an Orbitrap Fusion instrument (ThermoFisher Scientific) equipped with an UltiMate 3000 nano HPLC system (Dionex). The samples were applied with injection volume 7 µL onto separation columns PepMap RSLC C18 trap column 100 2 cm (75 µm ID) and Acclaim PepMap RSLC C18 50 cm (75µm ID)

with a flow rate of 5 µL/min using 0.1% TFA at constant 40°C. The samples were separated with a flow rate of 0.3 µL/min and a gradient for 152min as follows: 7 min 5% ACN, 105min increase to 22% ACN, in 10 min to 32% ACN, 10 min to 90% ACN, and 10 min wash at 90% ACN, then 10min equilibration at 5% ACN. Scans (m/z 300 - 1,500) with a resolution of 120 000 and automatic gain control (AGC) ion target value of $2x10^5$ were performed with a maximal injection time set to 50 ms. For MS2 scans, charge states from 2 to 7 and intensities more than $5x10^3$ were chosen. HCD collision energy of 30% was set for the fragmentation. The AGC target value was set to $1×10^4$ and the maximum injection time to 35 ms. The option to inject ions for all available parallelizable time was selected.

MaxQuant and Perseus MS data analysis

For protein and peptide identification, MS raw files were analysed by MaxQuant v.1.6.2.6a with Andromeda search engine with data-dependent acquisition (DDA) (Cox et al., 2011; Sinitcyn et al., 2018). The search was performed against the unreviewed *Caenorhabditis elegans* UniProt database (downloaded on the 20th January 2021, 6293, canonical version). Group-specific parameters were set to label free quantification (LFQ). Global parameters were set default. The label min. ratio count was changed to 1. The chosen modifications were oxidation (M) and acetylation (protein N-term) as variable and carbamido-methylation (C) as fixed. Match between runs function was enabled. Peptides for quantification unique+razor were picked. Proteins were identified with false discovery rate (FDR) set to 0.01 by default. The replicates were set to the same fraction to enable comparison between them and increase protein identification. To increase validity of results, the peptides were searched against a decoy database (reverse) generated by MaxQuant. The resulted protein groups with identified LFQ intensities were further analysed by Perseus software.

For the statistical analysis Perseus software (v.1.6.2.1) was used. The *protein groups* table in the *txt* folder was uploaded in the programme. LFQ intensities were $\log_2$ transformed; potential contaminants, reverse hits and hits only identified by site

were removed. All samples where categorically annotated based on the treatment conditions in co-immunoprecipitation step and number of the replicates. The rows were then filtered by at least 3 valid values in each group, so that the proteins were identified by at least 3 out of 4 replicates. Then missing values were replaced from normal distribution.

Data was evaluated by principal component analysis (PCA) to detect similarities among the samples. To evaluate the degree of correlation between the different and same replicates the Pearson correlation was calculated with a Multi scatter plot function.

Hits were visualised firstly by generating the volcano plots with a fold change difference plotted against –log(p-value) with FDR = 0.05 and s_0 = 0.01. The most significant protein hits were selected based on FC > 1 and -log(p-value) $<$ 1 which corresponds to p-value $<$ 0.05. The combinations and number of proteins identified were then calculated by Venn diagram plotter.

Visualisation of PPI networks and GO term analysis

The protein-protein interaction networks of the most significant interactors were constructed in Cytoscape v.3.9.1 (Shannon et al., 2003). GO term analysis by biological process was performed in Cytoscape with a built-in plugin ClueGO v.2.5.9. The marker list was set to *C. elegans* (6239). The network specificity was set to global level. Cluster number was increased to 26. The GO networks were visualised with yFile plugin as circular layout.

Supplementary information

Table S1. Gene names of sHsp16s protein interactors identified in co-IP/MS pull-downs at 20°C and 37°C. *The interactors were filtered by p-value<0.05 and at least 2-fold change in the abundance. The gene names are listed from the highest to the lowest fold change in the abundance.*

Hsp16.1 20°C	*Hsp16.1 37°C*	*Hsp16.2 20°C*	*Hsp16.2 37°C*	*Hsp16.41 20°C*	*Hsp16.41 37°C*	*Hsp16.48 20°C*	*Hsp16.48 37°C*
Hsp16.2	Hsp16.2	Hsp16.2	Hsp16.2	prdx-2	Hsp16.41	C05D12.3	Hsp16.48
Hsp16.1	Hsp16.1	spe-5	Hsp12.1	ajm-1	Hsp12.1	sql-1	Hsp16.41
Hsp12.1	Hsp12.1	CELE_F11D5.1	unc-26	tag-335	epg-7	CELE_F13H8.2	Hsp16.1
CELE_F11D5.1	spd-5	CELE_F57G4.1	CELE_F57G4.1	C53A5.17	unc-26	cct-1	Hsp12.1
Hsp17	mlc-2	Hsp12.1	sel-11	sao-1	CELE_F11D5.1	CELE_F35D11.4	unc-26
skih-2	tost-1	hum-6	spd-5	lin-35	mlc-2	spe-5	Hsp16.2
C05D12.3	unc-26	epg-7	CELE_F11D5.1	adbp-1	raga-1	Hsp16.48	spd-5
CELE_F43G6.8	CELE_F11D5.1	tost-1	tost-1	asd-2	imp-2	Hsp16.41	sel-11
tost-1	CELE_Y54F10AM.5	ttc-37	trpp-6	nekl-3	pes-2.1	daf-21	sql-1
hum-6	raga-1	C05D12.3	CELE_H05L14.2	map-2	sel-11	sars-1	CELE_F25E2.2
ttc-37	mig-2	Hsp17	C29F3.7	F36D4.5	mig-2	hum-6	CELE_H05L14.2
pes-2.1	sel-11	cdd-1	epg-7	clr-1	C29F3.7	CELE_F11D5.1	raga-1
CELE_R03E9.2	CELE_F25E2.2	CELE_F43G6.8	raga-1	unc-94	tost-1	unc-116	mlc-2
cdd-1	CELE_H05L14.2	gfi-2	CELE_F25E2.2	unc-89	CELE_F25E2.2	uba-2	mig-2
F37H8.5	sql-1	CELE_F21C10.10	mig-2	efk-1	spd-5	pacs-1	tsr-1
sql-1	unc-42	pgp-8	CELE_K07C11.7	rsa-1	sql-1	Hsp12.2	C27F2.10
ctf-4	imp-2	ctf-4	unc-42	F17A9.2	mars-1	frm-4	mars-1
daf-25	mpz-1	skih-2	imp-2	atg-18	dhs-15	ctsa-1.2	frl-1
mlc-2	CELE_F43G6.8	CELE_F59E12.1	mrp-3	ruvb-1	C01B4.6	enpl-1	pgp-8
CELE_F27C1.2	CELE_F27C1.2	F37H8.5	CELE_F49E2.5	sams-1	CELE_Y54F10AM.5	copb-2	slc-25a46
npp-14	CELE_W02B12.1	sql-1	sql-1	F37H8.5	frl-1	cct-3	epg-7
W03F8.3	CELE_F49E2.5	npp-14	ttc-37	strl-1	metl-17	Hsp25	mrp-3
CELE_F49E2.5	frl-1	CELE_F10G8.9	CELE_F27C1.2	copz-1	nhr-49	F37H8.5	ctf-4
epg-7	C29F3.7	CELE_F27C1.2	acl-5	timm-17B.1	ctf-4	mca-3	C29F3.7
cyp-35a2	mrp-3	trr-1	CELE_T27D12.1	pmk-3	Hsp16.1	C01B4.6	CELE_Y111B2A.12
C27H5.2	unc-119	acl-5	CELE_F08G12.1	mec-17	pgp-8	CELE_F27C1.2	imp-2
C01B4.6	ltrpc4/ced-11	CELE_F49E2.5	ppfr-4	gly-8	ctsa-1.2	ruvb-1	rha-1
CELE_F21C10.10	CELE_K07C11.7	frl-1	ctf-4	arrd-17	golg-2	CELE_R03E9.2	lbp-9
CELE_F10G8.9	ppfr-4	trpp-6	C27F2.10	dkf-2	CELE_M05D6.2	F27D4.1	dhs-15
CELE_Y48C3A.12	CELE_M05D6.2	pes-2.1	metl-17	rpn-10	ncs-2	trpp-6	ndx-3

Hsp16.1 20°C	*Hsp16.1 37°C*	*Hsp16.2 20°C*	*Hsp16.2 37°C*	*Hsp16.41 20°C*	*Hsp16.41 37°C*	*Hsp16.48 20°C*	*Hsp16.48 37°C*
mcu-1	nhr-49	mlc-2	mlt-3	wago-4	gfi-3	cct-2	CELE_M05D6.2
pnk-4	C07D10.5	C01B4.6	skih-2	Hsp16.48	CELE_F49E2.5	C08E8.4	CELE_R04B5.5
CELE_F07F6.8	skih-2	CELE_R03E9.2	ltrpc4/ced-11	msp-10	mlt-3	gpb-2	C01B4.6
n/a	metl-17	pnk-4	CELE_Y54F10AM.5	Hsp16.41	knl-1	CELE_F43G6.8	egg-6
CELE_K05C4.7	C27F2.10	daf-25	CELE_K05C4.7	Hsp16.2	C50F4.1	emc-1	oig-3
mrp-3	ttr-25	mrp-3	ttr-25	myo-2	clec-88	tfg-1	CELE_F27C1.2
rha-1	pes-2.1	crml-1	gly-7	fem-1	skih-2	mlc-2	metl-17
imp-2	faah-3	imp-2	CELE_M05D6.2	mlc-2	rha-1	sars-2	F46F11.1
CELE_F57G4.1	wrk-1	tep-1	C18F10.7	lin-9	F46F11.1	CELE_Y18H1A.4	acl-5
hda-3	C01B4.6	nud-1	CELE_D2063.1	tbp-1	CELE_F55D12.2	CELE_Y41C4A.32	CELE_F08G12.1
frl-1	mars-1	C27H5.2	smk-1	cha-1	arr-1	crn-3	hgap-2
haf-2	lin-10	n/a	rabn-5	vps-33.1	C27F2.10	sams-1	nhr-49
cpn-1	C18F10.7	arrd-17	C01B4.6	C02C2.6	pxn-1	bre-1	C07D10.5
acl-5	CELE_F13E9.1	CELE_K07C11.7	F46F11.1	C02F5.3	dhs-4	gars-1	CELE_T02B11.3
CELE_D2063.1	hgap-2	wdr-4	CELE_Y76B12C.6	Hsp12.2	CELE_Y47G6A.19	pgp-8	CELE_Y54F10AM.5
bus-5	CELE_F55D12.2	CELE_F38B6.4	Hsp16.1	ced-7	spr-5	npp-14	unc-42
nud-1	gad-1	erp-44.1	frl-1	F44B9.2	CELE_F27C1.2	rpn-5	CELE_F11D5.1
pks-1	ctf-4	mec-17	CELE_F55D12.2	F44B9.8	mpz-1	tep-1	rabn-5
bcs-1	clec-88	CELE_Y48C3A.12	nhr-49	F54C8.1	cul-4	wdr-4	smk-1
mrp-1	tbp-1	atg-16.2	fusm-2	emb-30	Hsp17	eef-1B.2	F10E9.4
CELE_K05B2.4	ttc-37	mlt-3	C07D10.5	unc-116	CELE_Y76B12C.6	hda-3	mlt-3
fusm-2	dhs-4	mrp-1	pxn-1	ltrpc4/ced-11	smk-1	mca-2	atg-4.1
smk-1	CELE_F17E9.5	haf-2	prp-38	Hsp16.1	rig-3	dli-1	ikb-1
CELE_T23G11.7	mlt-3	dnc-1	CELE_F56B3.4	pgp-3	bus-5	unc-73	CELE_D2063.1
ags-3	rha-1	npp-11	CELE_T07A9.10	T20B12.7	T09A5.5	CELE_Y53C12B.1	cul-4
CELE_T07A9.10	ugt-21	W03F8.3	mpz-1	lgc-50	fusm-2	iglr-2	CELE_F21C10.10
CELE_F38B6.4	rbx-1	cyp-35a2	egg-6	cct-1	mrp-3	usip-1	CELE_F55D12.2
rbx-1	Y57A10A.29	CELE_F07F6.8	hgap-2	sds-22	CELE_T07A9.10	daf-25	ctsa-1.2
tep-1	phm-2	CELE_T03G6.1	wrk-1	cct-2	K02D10.1	imp-2	golg-2
CELE_T08G11.4	C50F4.1	rbx-1	CELE_W02H5.8	mag-1	egg-6	pyk-1	C18F10.7
mpdu-1	B0361.3	ndx-3	cul-4	imp-2	CELE_F10G8.9	math-33	crn-2
C08E8.4	CELE_Y76B12C.6	rha-1	wdr-62	ctsa-1.2	acl-5	mlcd-1	mpz-1
CELE_R03G8.6	CELE_T27D12.1	CELE_K02F6.7	rbx-1	F31E3.4	C18F10.7	apg-1	pes-2.1
CELE_M05D6.2	mcu-1	mpst-6	CELE_F45H11.8	sucg-1	cyp-25a3	atg-16.2	adr-2
slc-25a46	slc-25a46	CELE_T08G11.4	pgp-8	alh-13	C47E8.4	prmt-1	faah-3
CELE_T03G6.1	CELE_F10G8.9	bus-5	CELE_R04B5.5	F46F11.1	nish-1	prg-1	CELE_Y62E10A.20
gut-2	gly-7	C08E8.4	rha-2	wdr-12	ceeh-2	dhs-4	CELE_Y76B12C.6
C55A6.3	CELE_K05B2.4	erp-44.2	mics-1	coq-4	wrk-1	Hsp110	arr-1

Hsp16.1 20°C	*Hsp16.1 37°C*	*Hsp16.2 20°C*	*Hsp16.2 37°C*	*Hsp16.41 20°C*	*Hsp16.41 37°C*	*Hsp16.48 20°C*	*Hsp16.48 37°C*
lin-35	ncs-2	CELE_F35D11.4	CELE_F35D11.4	hum-6	CELE_Y111B2A.12	syf-1	gly-7
Hsp12.2	acs-20	mpdu-1	tbp-1	rgr-1	CELE_T27D12.1	pcs-1	CELE_F56B3.4
CELE_K02F6.7	adr-2	metl-17	rha-1	T23G5.2	crn-2	npp-23	lin-10
cash-1	CELE_K05C4.7	tba-5	CELE_F25D1.5	lrp-1	ltrpc4/ced-11	alh-13	T09A5.5
CELE_K07C11.7	CELE_T26A8.4	cogc-5	CELE_F42G10.1	C13B9.2	adr-2	B0250.5	C13B9.2
metl-17	CELE_Y71H2B.5	fusm-2	hrg-7	glod-4	C07D10.5	CELE_F52G2.3	CELE_T07A9.10
dnc-1	dhs-15	lin-35	ncs-2	npp-24	unc-40	ketn-1	CELE_F42G10.1
homt-1	fusm-2	CELE_T23G11.7	cyp-25a3	fzy-1	CELE_W02B12.1	clh-6	spr-5
CELE_F33H2.2	rabn-5	mlcd-1	golg-2	atg-16.2	CELE_W03F11.4	pks-1	skih-2
dhs-4	F46F11.1	CELE_Y76B12C.6	Hsp17	C45G9.2	C33G3.4	C13B9.2	Hsp17
asd-2	CELE_Y111B2A.12	F10B5.2	dhs-4	E02H1.2	ugt-13	CELE_Y76B12C.6	clec-88
mlt-3	C48B6.2	F10E9.4	sqv-6	F07F6.4	CELE_F07F6.8	CELE_F42G10.1	tbp-1
tbp-1	knl-1	Hsp16.1	ceeh-2	disl-2	tnt-3	upb-1	C50F4.1
ppt-1	chd-3	Hsp12.2	mars-1	tnc-2	C04G2.9	rad-8	rbx-1
sco-1	egg-6	lgc-50	CELE_Y111B2A.12	CELE_K02C4.3	wdr-62	lact-3	CELE_Y47G6A.19
CELE_F29A7.4	Hsp17	C55A6.3	dhs-15	lin-23	ttr-25	fzy-1	mrp-1
arrd-17	ptpn-22	cash-1	slc-25a46	prp-19	CELE_F17E9.5	trm-2a	pad-2
mrp-2	CELE_F45H11.8	hda-3	ptpn-22	dhs-5	memo-1	mrp-1	set-29
mlcd-1	CELE_D2063.1	C08B6.8	pad-2	pacs-1	ttc-37	copz-1	gad-1
cogc-3	W03F8.3	C13B9.2	mpst-6	usp-14	ftt-2	pmt-2	fusm-2
rabn-5	smk-1	acs-20	CELE_R74.8	cul-1	atg-4.1	CELE_Y38F2AR.12	itx-1
efk-1	crn-2	CELE_F33H2.2	aipr-1	AC3.5	C06A8.6	unc-34	rsa-1
cyp-25a3	C47E8.4	rgr-1	ssup-72	B0024.11	cpd-2	disl-2	CELE_F35D11.4
CELE_T04C9.1	CELE_F42G10.1	vrk-1	CELE_F10G8.9	npp-14	Hsp16.2	cyp-35a2	vps-15
rbc-1	aipr-1	pudl-1	atg-4.1	C08B6.8	tfg-1	CELE_Y48C3A.12	CELE_T27D12.1
fzy-1	unc-40	bub-1	mec-17	aos-1	hgap-2	CELE_T04C9.1	ugt-13
smg-1	spr-5	CELE_T04C9.1	spr-5	akt-1	rabn-5	cash-1	CELE_T13G4.4
prp-38	CELE_R04B5.5	cogc-3	CELE_T01H3.3	dpyd-1	CELE_Y62E10A.20	C47E8.4	CELE_K07C5.3
fbxa-14	mics-1	rabn-5	lin-13	C31H2.4	gad-1	dnj-11	CELE_F13D12.9
CELE_F58F9.3	CELE_R74.8	zig-12	acn-1	sphk-1	W03F8.3	CELE_F52C12.6	CELE_R74.8
pmt-2	T09A5.5	CELE_F57C2.5	memo-1	maph-9	gly-7	pes-2.1	rcs-1
atg-16.2	agef-1	pap-1	bub-1	coq-8	CELE_D2063.1	abcf-1	lrp-2
CELE_F42F12.4	memo-1	pmt-2	C50F4.1	mel-28	faah-3	cope-1	pkg-2
ten-1	pks-1	cyp-25a3	CELE_Y62E10A.20	dhp-2	lrp-2	ced-7	rgs-3
CELE_T27D12.1	itx-1	cdkr-3	nish-1	sars-1	CELE_R04B5.5	pmp-3	cyp-25a3
CELE_F35D11.4	mec-17	dars-2	T09A5.5	daf-21	F42H10.6	rabn-5	rig-3
mtp-18	CELE_F46B6.6	ech-8	CELE_F07F6.8	C47E8.4	rbx-1	CELE_K02F6.7	ttr-25

Hsp16.1 20°C	*Hsp16.1 37°C*	*Hsp16.2 20°C*	*Hsp16.2 37°C*	*Hsp16.41 20°C*	*Hsp16.41 37°C*	*Hsp16.48 20°C*	*Hsp16.48 37°C*
bub-1	lin-35	trpp-5	CELE_W09G3.7	bre-1	fntb-1	CELE_W04C9.2	ifa-1
dhp-2	atg-4.1	efk-1	CELE_W07E11.1	gst-42	CELE_F13H8.3	CELE_F33H2.6	wrk-1
mpst-6	CELE_F48E8.3	adr-2	arr-1	gbh-1	tbb-6	efk-1	nish-1
frm-4	ech-3	sec-6	spe-46	pho-1	CELE_F45H11.8	myo-2	CELE_F10G8.9
ned-8	dhs-23	CELE_T07A9.10	gst-43	atg-16.1	hrg-7	alh-7	acn-1
pudl-1	abt-4	tbp-1	unc-40	sec-6	oig-3	haao-1	gut-2
zig-12	CELE_F25D1.5	mtp-18	vps-15	pfas-1	itx-1	mars-1	W03F8.3
lgc-50	acs-21	rbc-1	knl-1	haao-1	rsa-1	fcp-1	F42H10.6
fbxa-65	ugt-29	C39D10.8	itx-1	rfl-1	agef-1	sds-22	hacd-1
tfg-1	arr-1	ldh-1	C13B9.2	vrk-1	trpp-4	arp-11	ttc-36
cchl-1	oig-3	ags-3	faah-3	mpdu-1	acn-1	abcf-3	frm-5.2
ced-12	ttc-36	mcu-1	adr-2	sip-1	CELE_Y41C4A.32	Hsp16.2	CELE_W02H5.8
wdr-4	hrg-7	ykt-6	pes-2.1	ppt-1	CELE_F13D12.9	mlt-3	memo-1
CELE_R08C7.8	memb-1	tfg-1	CELE_K02F6.7	haly-1	mrpl-11	metl-17	sqv-6
maoc-1	ifa-1	spr-5	acs-21	sec-3	mrp-1	CELE_F07F6.8	dhs-23
rbg-2	CELE_W07E11.1	ppt-1	bus-5	mcu-1	tbp-1	spe-46	ptpn-22
C31H2.4	tfg-1	pyk-1	W03F8.3	cogc-6	Hsp12.2	mvk-1	lin-35
ipla-7	F31E3.4	pks-1	pis-1	gpcp-1	ten-1	ctf-4	CELE_F45H11.8
lin-23	CELE_F13D11.4	ttc-36	clec-83	atg-2	CELE_R74.8	B0024.11	mcu-1
spr-5	gop-2	CELE_F45H11.8	rig-3	wago-1	ech-3	pud-4	tnt-3
hpo-12	Hsp12.2	asd-2	mcu-1	bub-1	syd-2	myo-5	CELE_M116.5
haly-1	CELE_F35D11.4	CELE_R08C7.8	snap-1	R74.7	CELE_K02F6.7	pyk-1	ipmk-1
CELE_F02D8.4	CELE_Y54E5B.2	CELE_F42F12.4	srp-3	mec-15	F37H8.5	mrp-3	tfg-1
crml-1	mrp-1	coa-1	Hsp12.2	enpl-1	tag-353	tald-1	npp-21
C47G2.3	CELE_Y47G6A.19	CELE_Y18H1A.4	crn-2	rha-1	Hsp25	C37H5.13	Hsp12.2
CELE_F57C2.5	CELE_T07A9.10	spe-46	taf-1	adr-2	lin-35	sip-1	gop-2
szy-2	col-167	rbg-2	tfg-1	rbg-2	ttc-36	srp-6	cest-1.2
E02H1.2	snap-1	ccnk-1	haf-2	soc-2	aka-1	cyp-25a3	CELE_R193.2
vrk-1	CELE_W09G3.7	dhp-2	CELE_T01G5.1	ife-4	ptpn-22	gut-2	unc-40
ykt-6	ugt-61	cpn-1	dhs-23	sbds-1	pad-2	fem-1	CELE_T26A8.4
unc-25	tcer-1	gut-2	lin-35	wdr-4	CELE_F48E8.3	elpc-2	CELE_T14G8.3
C47E8.4	dhps-1	CELE_T27D12.1	CELE_T26A8.4	ndx-3	col-167	trr-1	C03G6.17
tba-5	CELE_H24G06.1	haly-1	frm-5.2	pbs-3	snap-1	Hsp12.1	pyk-1
cogc-5	CELE_F07F6.8	CELE_Y55F3BR.6	dhp-2	daf-41	dhps-1	emc-3	dhs-4
pbrm-1	lrp-2	smc-5	CELE_F21C10.10	mmcm-1	bub-1	mrpl-47	haf-2
CELE_W03F11.4	cua-1	ssb-1	ten-1	rbx-1	lin-13	eri-1	CELE_W07E11.1
orc-4	acn-1	unc-116	unc-34	zyg-12	lin-10	CELE_F25E2.2	C47E8.4
pyk-1	CELE_Y113G7C.1	asps-1	pat-6	hpo-40	rnp-2	skih-2	ltrpc4/ced-11
atg-2	C33G3.4	rpap-3	F37H8.5	rad-8	CELE_T07F12.1	sfxn-2	inx-14
CELE_F44E7.4	serr-1	dhs-4	CELE_W03F11.4	dot-1.1	C04E12.4	fbxa-65	ssup-72

Hsp16.1 20°C	*Hsp16.1 37°C*	*Hsp16.2 20°C*	*Hsp16.2 37°C*	*Hsp16.41 20°C*	*Hsp16.41 37°C*	*Hsp16.48 20°C*	*Hsp16.48 37°C*
C08B6.8	sqv-6	ipla-7	CELE_K07C5.3	math-33	dnc-1	math-20	ech-3
abtm-1	lgc-50	ssup-72	ajm-1	B0361.3	C27H5.2	gbh-1	cyp-42a1
CELE_Y71H2B.5	C24G6.8	C06A8.6	Hsp25	gcy-28	ndx-3	aipl-1	CELE_F48E8.3
unc-116	F42H10.6	CELE_Y67H2A.7	rgs-3	gls-1	tnc-2	him-4	CELE_K02F6.7
cap-2	rgs-3	CELE_F02D8.4	C33G3.4	ced-12	gst-43	CELE_T20F5.6	bub-1
ltrpc4/ced-11	rig-3	CELE_F44E7.4	tnt-3	mtp-18	mec-17	txdc-9	ceeh-2
ints-6	dhp-2	mrpl-41	aqp-7	F27D4.1	inx-14	acl-5	mpst-6
trpp-11	CELE_F16H6.10	mrp-2	CELE_R193.2	fcp-1	CELE_R193.2	rfl-1	smz-1
CELE_Y94H6A.7	pad-2	bcs-1	clec-47	C56C10.7	rcs-1	prdx-2	Hsp25
CELE_M106.3	lin-13	cyp-13a12	lrp-2	gly-5	prp-38	lrp-2	hcp-2
F10B5.2	lam-3	ptpn-22	oig-3	daf-25	adpr-1	soc-2	CELE_T24H10.4
tnc-2	pxn-1	CELE_M01G12.9	CELE_F48E8.3	spg-7	pks-1	pnk-4	knl-1
CELE_Y67H2A.7	CELE_R193.2	mel-28	C24G6.8	parp-1	npp-21	prp-19	dpl-1
cdkr-3	vps-15	smk-1	C04E12.4	cct-3	rgs-3	unc-59	pks-1
pap-1	pyk-1	row-1	gst-5	pas-3	CELE_K07C5.3	ntl-9	CELE_F22F4.5
F52C12.1	rcs-1	lrp-2	CELE_W04C9.2	uba-2	F31E3.4	CELE_M01G12.9	AC3.5
C25H3.11	C06A8.6	abtm-1	memb-1	C47G2.3	dhs-23	rha-1	C24G6.8
CELE_Y37D8A.25	CELE_M116.5	CELE_K04A8.1	CELE_Y48G10A.2	tfg-1	CELE_T12D8.9	hpo-40	CELE_K05C4.7
gst-43	wdr-12	hpo-11	CELE_T10B5.3	eef-1B.2	hcp-2	myo-1	CELE_W09G3.7
dpf-3	CELE_Y62E10A.20	golg-2	pha-1	Y37H9A.3	clec-47	ppat-1	tcer-1
gly-5	gst-5	ints-7	CELE_T14G8.3	prmt-1	pha-1	CELE_H20J04.9	clr-1
C36B7.6	CELE_T13G4.4	unc-120	F42H10.6	cdkr-3	CELE_T14G8.3	acs-20	CELE_D1054.3
tag-340	Hsp25	CELE_T16G1.4	pmp-3	B0250.5	ketn-1	wago-4	cyp-13a12
erp-44.1	smz-1	mmcm-1	cyn-15	pbs-5	C24G6.8	bus-5	acl-3
ldh-1	pole-1	fzy-1	cyp-13a12	spr-5	pyk-1	rpn-10	dhps-1
cox-15	ints-6	madd-3	alh-5	bicd-1	stim-1	CELE_Y55F3BR.6	ten-1
C39D10.8	dnc-1	frm-4	cua-1	pps-1	sqv-6	T23G5.2	pat-6
spe-46	haf-2	CELE_Y94H6A.7	gad-1	lpd-3	aqp-7	wdr-4	spe-46
cua-1	CELE_T10B5.3	apm-3	C47E8.4	etr-1	ntl-3	atg-16.1	clec-83
mmcm-1	bub-1	CELE_F29A7.4	n/a	fbxa-72	mics-1	ubr-4	dcap-1
rcan-1	CELE_W04C9.2	CELE_F58F9.3	CELE_T24H7.2	unc-34	CELE_T26A8.4	sbds-1	ctnb-1
acs-20	mrpl-11	ugt-41	CELE_M116.5	ubr-4	unc-120	CELE_T21D9.2	map-2
asps-1	CELE_T14G8.3	Hsp25	chd-3	ltd-1	CELE_F23B12.4	cku-80	snap-1
CELE_K07A12.1	ttr-5	cest-2.2	trpp-4	let-711	pmp-3	haf-3	lrp-1
ints-8	cpd-2	atg-2	rpap-3	CELE_Y41C4A.32	set-29	rgr-1	msp-152
ubr-4	cyn-15	sec-3	CELE_F42F12.4	CELE_Y55F3BR.6	CELE_M116.5	CELE_F10G8.9	CELE_W03F11.4
smc-5	CELE_Y62E10A.13	CELE_F56B3.4	lmd-3	CELE_F45H11.8	pmt-2	atg-18	CELE_T24H7.2
git-1	alh-5	git-1	dnc-1	rbm-26	CELE_Y38E10A.22	daf-41	prp-38
CELE_F25E2.2	ipla-3	rad-50	ints-6	klp-12	CELE_Y94H6A.7	C02C2.6	F59B2.3

Hsp16.1 20°C	*Hsp16.1 37°C*	*Hsp16.2 20°C*	*Hsp16.2 37°C*	*Hsp16.41 20°C*	*Hsp16.41 37°C*	*Hsp16.48 20°C*	*Hsp16.48 37°C*
R74.7	acl-5	ppw-2	CELE_Y94H6A.7	dnj-25	lrp-1	dpf-3	dnc-1
praf-3	mrps-17	ten-1	dnc-5	cash-1	CELE_F42F12.4	CELE_T26A5.6	pps-1
adr-2	CELE_Y48G10A.2	CELE_W03F11.4	ntl-3	CELE_F49E2.5	CELE_Y113G7C.1	szy-2	dhp-2
CELE_D1054.8	adpr-1	CELE_M05D6.2	dhps-1	him-4	unc-25	cul-4	ketn-1
pcyt-2.1	mrp-4	CELE_F13D12.5	fbxa-72	rbc-1	mrpl-54	CELE_Y92H12BL.7	F31E3.4
C13B9.2	mrpl-50	ints-6	gut-2	CELE_Y92H12BL.7	CELE_W09G3.7	smc-5	lgg-1
snap-1	hacd-1	F46F11.1	snr-4	CELE_Y38F2AR.12	lgg-2	vrk-1	mrp-4
CELE_F13D12.5	tag-273	dnj-11	map-2	C44E4.5	AC3.5	dhs-18	CELE_F48E8.4
eef-1B.2	CELE_T16A1.2	CELE_T24B8.7	fem-1	C05C8.1	pps-1	mcu-1	B0491.7
CELE_F56B3.4	cyp-33c9	sco-1	mrp-4	CELE_T08G11.4	aipr-1	epg-7	tag-322
CELE_K04A8.1	CELE_T24H7.2	tag-335	zig-12	glna-1	abt-4	CELE_Y48G8AL.15	frm-4
ssup-72	map-2	CELE_F42G10.1	ugt-61	poml-3	ipla-3	CELE_Y45F10D.7	mrp-6
dnj-11	ipmk-1	acs-16	rnst-2	obr-2	cyp-33c9	cpn-1	CELE_W04C9.2
C56C10.7	F54C8.1	prp-38	tin-44	dnj-8	sfxn-2	W03F8.3	sec-3
pyk-1	CELE_K02F6.7	fcp-1	acs-16	CELE_F52C12.6	unc-116	F10E9.4	fbxa-65
CELE_M116.5	pps-1	lgl-1	pyk-1	ints-6	CELE_F13D11.4	F46F11.1	CELE_F23B12.4
rbm-26	zig-12	scp-1	sym-1	CELE_Y53C12A.10	CELE_W04C9.2	pgp-3	cyn-15
math-38	npp-1	C47B2.9	rcs-1	dnj-16	spe-46	tag-335	CELE_F58E6.13
mel-28	ceeh-2	cest-17	sfxn-2	CELE_F56B3.4	pis-1	F31E3.4	chd-3
lgl-1	dnc-5	snx-6	set-29	sql-1	ppw-2	crml-1	C04E12.4
ints-7	tin-44	mut-14	pmt-2	mars-1	CELE_T24H7.2	C08F8.3	aipr-1
CELE_Y47H9C.8	pmp-3	vps-15	BE0003N10.1	snx-6	hpo-11	kcc-1	npp-1
fcp-1	CELE_T07F12.1	eef-1B.2	rab-33	gut-2	gst-5	C02F5.3	unc-25
snx-6	mxt-1	CELE_T26A8.4	ttr-5	dnc-1	npp-1	usp-50	snb-1
coq-4	cogc-3	clr-1	rtcb-1	sac-2	inx-3	dars-2	tnc-2
C02G6.2	ver-3	pcyt-2.1	CELE_D1005.2	pmp-3	zig-12	CELE_F45H11.8	mics-1
aos-1	CELE_Y38E10A.22	lin-23	F59B2.3	CELE_F25E2.2	sym-1	mpdu-1	rfp-1
lrp-2	CELE_F13D12.9	miro-1	hpo-11	abtm-1	dnc-5	ssna-1	tfbm-1
glod-4	CELE_F59A2.5	ugt-25	tbb-6	atg-7	pho-1	nud-1	srp-7
pbs-5	sym-1	C47E8.4	CELE_F17E9.5	usp-50	cpsf-1	trpp-8	CELE_Y43C5A.2
CELE_Y94H6A.12	tnt-3	pcs-1	vps-26	crn-3	mrp-4	npp-12	hpo-11
mag-1	moc-1	msh-6	ketn-1	clh-6	bicd-1	asd-2	T05H10.3
apm-3	cest-1.2	mag-1	fbxa-14	CELE_F02D8.4	daf-41	ltrpc4/ced-11	pmt-2
CELE_T01H3.3	B0280.9	gly-5	prp-19	mpst-6	msp-152	pycr-1	sym-1
serr-1	tmed-1	CELE_Y62E10A.20	dcap-1	hda-3	CELE_F35D11.4	sec-12	pmk-3
atg-16.1	ketn-1	vha-19	fcp-1	mec-8	CELE_T16A1.2	msh-6	sgn-1
CELE_Y76B12C.6	CELE_F54F7.3	usp-39	adpr-1	dli-1	pat-6	F10B5.2	prp-19

Hsp16.1 20°C	*Hsp16.1 37°C*	*Hsp16.2 20°C*	*Hsp16.2 37°C*	*Hsp16.41 20°C*	*Hsp16.41 37°C*	*Hsp16.48 20°C*	*Hsp16.48 37°C*
ppat-1	fbxa-14	F31E3.4	CELE_F52E4.5	CELE_M05D6.2	hcp-1	ced-12	mec-17
sgn-1	ile-2	tnc-2	pps-1	pes-2.1	CELE_F56B3.4	asps-1	cua-1
sac-1	fbxa-72	CELE_M106.3	cest-1.2	C01B4.6	eef-1B.2	sao-1	cul-2
wdr-12	rfp-1	E02H1.2	C16A11.2	inos-1	F40A3.3	mlst-8	pis-1
catp-8	pat-6	C47D12.2	CELE_Y43C5A.2	hpo-11	dhp-2	nekl-3	CELE_Y94H6A.7
maph-9	dhs-5	smz-1	dsl-3	unc-25	mcu-1	C06A8.6	dot-1.1
pycr-1	cyp-13a12	CELE_M116.5	C03G6.17	CELE_R05H10.3	CELE_F52E4.5	cest-2.2	CELE_F13H8.3
CELE_F42G10.1	lrp-1	coq-4	pgp-14	ints-7	map-2	bpl-1	unc-120
daf-41	exos-3	unc-25	CELE_Y37D8A.25	nud-1	vps-26	CELE_Y77E11A.7	fcp-1
W03F9.1	lgg-1	snap-1	disl-2	plrg-1	dcap-1	madd-3	CELE_Y62E10A.13
sao-1	CELE_T05E7.1	glod-4	CELE_F23B12.4	pbrm-1	prp-19	CELE_Y41D4A.6	wdr-12
tag-335	hex-1	fem-1	CELE_F25E5.5	sars-2	rgl-1	cul-1	CELE_F07F6.8
Hsp25	fcp-1	wago-4	rme-1	cpn-1	fis-2	pcyt-2.1	arp-11
erp-44.2	yop-1	ced-12	rcan-1	CELE_F46C5.9	smg-1	C04G6.4	adpr-1
acy-1	CELE_T03G6.1	fbxa-14	pxn-2	CELE_H03A11.2	fcp-1	ints-6	wah-1
clr-1	lin-28	CELE_K07A12.4	lgg-1	C08E8.4	sec-3	wago-1	disl-2
wago-4	rbbp-5	pbrm-1	dnj-16	mrp-4	rnst-2	K03H1.5	ttr-59
CELE_Y92H12BL.7	fem-1	ppat-1	cgr-1	idi-1	cyp-13a12	bub-1	twnk-1
smz-1	ags-3	pyk-1	fis-2	ikb-1	moc-1	tbp-1	CELE_D1069.3
mdt-17	pmt-2	lrp-1	CELE_K09E4.3	pgp-8	haf-2	CELE_K04A8.1	unc-116
sec-6	prp-19	hmgr-1	arp-11	wdr-4	rme-1	frl-1	daf-41
Y37H9A.3	dnj-16	rcan-1	CELE_T12D8.9	ten-1	hacd-1	ttc-36	CELE_T16A1.2
CELE_Y55F3BR.6	msp-78	sac-2	moc-1	ints-8	CELE_Y80D3A.9	mec-17	gst-5
pacs-1	C49A9.9	aagr-2	mrp-6	C39D10.8	scc-2	timm-17B.1	cdk-7
mau-2	CELE_F42F12.4	kcc-1	enpl-1	smk-1	fbxa-72	ptpn-22	F54C8.1
mvk-1	rab-33	pacs-1	CELE_ZK154.1	frm-4	ptc-1	fbxa-72	tag-273
golg-2	cus-2	CELE_F54D5.12	ile-2	C27H5.2	snx-6	hcp-2	C31H2.4
hpo-11	uda-1	him-4	lrp-1	CELE_Y110A7A.9	CELE_ZK154.1	sti-1	anp-1
miro-1	CELE_ZK154.1	CELE_R144.11	npp-1	dpf-3	lgg-1	coq-4	moc-1
CELE_R144.11	CELE_W03F11.4	pycr-1	CELE_F38B6.4	CELE_F11D5.1	CELE_T24H10.4	CELE_K02C4.3	ubh-3
atg-18	mmcm-1	sgn-1	mmcm-1	CELE_T04C9.1	mxt-1	Hsp16.1	CELE_F52B5.3
lact-3	fbxa-64	C44E4.5	CELE_T13G4.4	CELE_F49E8.7	gpx-1	CELE_Y87G2A.2	pho-14
F44B9.8	C05D11.1	C47G2.3	CELE_Y66D12A.10	trpp-8	srp-6	spr-5	klc-1
ptpn-22	bigr-1	dpyd-1	C05D11.1	emc-1	CELE_Y54E5B.2	CELE_Y55F3BR.6	mig-14
CELE_F45H11.8	nekl-3	npp-12	hmgr-1	CELE_Y77E11A.7	fbxa-65	CELE_F44E7.4	him-4
pole-1	pho-1	dna-2	F35H12.5	cest-2.2	rfl-1	ragc-1	clec-47
soc-2	sor-1	atg-18	B0491.7	gft-2H4	cyn-15	snap-1	snx-6
C44E4.5	tnc-2	F36D4.5	aph-2	CELE_F55F10.1	T20B12.7	pfkb-1.1	tin-44
CELE_Y53C12A.10	cul-2	daf-41	CELE_Y73C8B.3	pud-4	disl-2	map-2	CELE_Y66D12A.10

Hsp16.1 20°C	*Hsp16.1 37°C*	*Hsp16.2 20°C*	*Hsp16.2 37°C*	*Hsp16.41 20°C*	*Hsp16.41 37°C*	*Hsp16.48 20°C*	*Hsp16.48 37°C*
gpcp-1	srp-7	gpcp-1	frm-4	Hsp12.1	CELE_Y67H2A.2	CELE_T07A9.10	hmgr-1
kcc-1	CELE_Y43C5A.2	soc-2	exc-4	CELE_F55A12.5	dhs-5	gst-42	ugt-25
CELE_R04F11.5	fbxa-65	arp-11	CELE_F46C5.9	lrp-2	gpb-2	CELE_K05B2.4	haf-6
fem-1	unc-116	cyp-42a1	snx-6	CELE_W03F11.4	enpl-1	CELE_D2063.1	CELE_F55G11.8
exos-3	gut-2	mca-2	cul-2	ari-1.3	n/a	CELE_F48A11.4	CELE_Y54G11A.3
disl-2	CELE_F20G2.1	haf-3	unc-116	smz-1	dpl-1	zhit-3	fbxa-72
tag-131	cha-1	ari-1.3	erp-44.1	haf-2	CELE_F42A6.6	pas-3	CELE_T03G6.1
CELE_R05H10.3	CELE_F23B12.4	fbxa-65	mrpl-18	cyp-35a2	CELE_Y66D12A.10	rcan-1	uda-1
C05C8.1	cnx-1	tbce-1	ugt-2	CELE_F29A7.4	arp-11	Hsp17	CELE_Y47G6A.5
mut-14	trpp-5	aos-1	gpb-2	acs-21	tin-44	T20B12.7	hpo-40
CELE_ZK858.7	C03G6.17	disl-2	CELE_Y47G6A.5	CELE_K02F6.7	srp-7	letm-1	enpl-1
scp-1	enpl-1	CELE_Y55F3BR.6	fbxa-64	CELE_F48A11.4	CELE_Y43C5A.2	CELE_W03F11.4	ncs-2
C08F8.3	disl-2	wdr-12	haf-6	ech-8	C53A5.17	rbg-2	pmp-3
ZK652.6	rme-1	sip-1	sac-1	CELE_F21A3.3	gakh-1	CELE_Y53G8B.1	dhs-5
myo-6	ctnb-1	unc-89	klc-1	ccnk-1	lron-8	dot-1.1	mdt-18
arp-11	CELE_D1069.3	exos-3	efk-1	haf-3	aos-1	CELE_T25G3.3	srp-6
F44B9.2	mrpl-54	CELE_F13H8.2	CELE_R09H10.5	aipl-1	CELE_T03G6.1	C02G6.2	cpsf-1
klc-1	rcan-1	cpf-1	fut-8	dhs-4	pgp-14	smk-1	tald-1
coa-1	anp-1	B0024.11	CELE_F13D11.4	CELE_Y53C12B.1	CELE_D1069.3	dcap-1	CELE_F20G2.1
CELE_F31D4.2	gpb-2	myo-6	ver-3	CELE_T07A9.10	haao-1	lin-35	unc-22
CELE_F46C5.9	srp-6	ubr-4	CELE_M05D6.5	spg-20	tald-1	B0205.13	lbp-6
dna-2	cyk-3	CELE_K07A12.1	sgn-1	usp-39	cul-2	aos-1	cas-1
vps-33.1	CELE_Y39G10AR.9	C56C10.7	CELE_Y71H2B.5	fbxa-65	rfp-1	coq-8	dnc-5
F36D4.5	CELE_F58E6.13	egl-3	srp-7	CELE_R74.8	Y48A5A.1	mpst-6	cest-34
B0024.11	C13B9.2	rfl-1	ttx-7	CELE_T05E12.6	CELE_W07E11.1	tcc-1	CELE_F13A7.1
dpyd-1	CELE_F38B6.4	trm-2a	hex-1	CELE_T23G11.7	C05D11.1	golg-2	vps-26
rgs-3	erp-44.1	usp-50	npp-21	iscu-1	nadk-2	arrd-17	daf-21
CELE_K02C4.3	exc-4	C05C8.1	CELE_F58E6.13	tep-1	ints-6	CELE_T14B4.1	rme-1
CELE_T10B10.3	npp-21	unc-94	prmt-7	unc-73	haf-6	math-38	nadk-2
CELE_F53E10.1	AC3.5	vps-33.1	uda-1	CELE_R119.2	CELE_Y50D4B.4	fusm-2	gpb-2
usp-50	cas-1	E02H1.6	rgl-1	CELE_R12E2.13	CELE_F52C12.6	myo-6	CELE_F44E5.4
unc-34	CELE_F49C12.7	CELE_Y73F8A.26	CELE_K04A8.1	pole-1	C29F7.2	ikb-1	rab-33
cpf-1	snx-6	C08F8.3	dhs-30	CELE_F33H2.2	mmcm-1	gcy-28	zig-12
pud-4	aka-1	CELE_T21D12.12	haao-1	myo-6	coq-4	ykt-6	eef-1B.2
lpd-3	tald-1	prp-19	CELE_F13H8.3	CELE_F57C2.5	unc-22	msh-2	rfl-1
CELE_F13H8.2	spg-20	upb-1	pho-1	math-20	pho-14	cpf-1	lron-8
upb-1	hpo-11	CELE_K07A1.17	CELE_F45D11.15	CELE_F25E5.5	saeg-2	ipla-3	CELE_Y113G7C.1
CELE_W10C8.4	gakh-1	pgp-3	pmk-3	mca-2	R12E2.11	fbxa-14	exc-4

Hsp16.1 20°C	*Hsp16.1 37°C*	*Hsp16.2 20°C*	*Hsp16.2 37°C*	*Hsp16.41 20°C*	*Hsp16.41 37°C*	*Hsp16.48 20°C*	*Hsp16.48 37°C*
mvb-12	gss-1	pbs-5	daf-21	C55A6.3	efk-1	smz-1	CELE_F38B6.4
unc-120	Y18D10A.3	aipl-1	CELE_F32A5.8	prg-1	gly-5	unc-120	CELE_ZK154.1
CELE_Y38E10A.22	CELE_ZK550.5	lact-3	CELE_F49E8.7	dars-2	him-4	mrp-4	BE0003N10.1
acl-9	pud-2.1	pcyt-2.2	uba-2	smgl-1	CELE_Y38F2AR.12	atg-2	leo-1
him-4	T24H10.1	cpna-3	eef-1B.2	CELE_K07A12.1	wdr-12	C47D12.2	smo-1
bicd-1	aos-1	CELE_T26A5.6	CELE_F49C12.7	cogc-5	mec-8	ttc-37	fubl-2
CELE_T14B4.1	nra-4	CELE_Y71H2B.5	cest-34	syf-1	daf-21	CELE_F13D11.4	CELE_Y48G10A.1
T23G5.2	cyn-2	ruvb-1	mtm-3	CELE_T20F5.6	msp-78	C27H5.2	ugt-47
math-20	pmk-3	C02C2.6	CELE_ZK550.5	npp-12	BE0003N10.1	CELE_T23G11.7	coq-4
dars-2	npl-4.2	crn-3	lec-5	metl-17	uba-1	ajm-1	ttr-5
iscu-1	lbp-2	uba-2	rfp-1	CELE_F42G10.1	ugt-2	CELE_F02D8.4	CELE_Y38F2AR.12
smg-9	CELE_R09H10.5	snx-1	T20B12.7	C56G2.15	anp-1	pbs-3	acs-21
elpc-2	eef-1B.2	F44B9.2	srp-6	CELE_F48E8.3	pud-2.1	CELE_F55A12.5	mvb-12
msh-6	pgp-14	odr-3	AC3.5	CELE_M106.3	dnj-16	snx-1	CELE_F49C12.7
C04E12.4	CELE_Y38F2AR.12	clh-6	CELE_K07A1.17	asps-1	pfkb-1.1	tgt-2	eif-3.H
CELE_F26D2.15	F17A9.2	enpl-1	CELE_T16A1.2	rmd-6	hpo-40	pgp-14	cnt-1
ruvb-1	sac-1	CELE_F46C5.9	C02G6.2	cpna-3	cbs-1	gakh-1	CELE_T07F12.1
F31E3.4	aipl-1	pole-1	CELE_K08D8.6	C02G6.2	T24H10.1	ppt-1	CELE_Y71H2B.5
hmgr-1	bicd-1	thoc-2	tald-1	C06A8.6	smo-1	lrp-1	C05D11.1
R12E2.11	efk-1	pot-2	rfl-1	nlp-77	exc-4	CELE_F29A7.4	T20B12.7
sams-1	haf-6	npp-23	unc-25	Hsp25	CELE_F48E8.4	atg-7	acs-20
sucg-1	T20B12.7	T20B12.7	nra-4	npp-23	npp-12	cogc-6	thoc-2
ppw-2	CELE_W04B5.5	sams-1	tomm-20	mut-14	dpyd-1	tbc-1	dnj-16
tmed-1	B0491.7	T23G5.2	usp-14	C18E9.9	CELE_F49C12.7	egg-6	rbbp-5
abcf-3	CELE_Y48G10A.1	BE0003N10.1	uba-1	dnc-4	plrg-1	spg-7	letm-1
gly-8	CELE_Y50D4B.4	CELE_K02C4.3	ugt-25	ntl-9	C52E4.5	bicd-1	C49A9.9
gls-1	CELE_F21C10.7	eel-1	egl-21	tost-1	C36A4.4	K02D10.1	unc-34
mrp-6	unc-78	ulp-3	vem-1	pcyt-2.2	usp-14	gly-5	mtx-2
eel-1	lec-5	CELE_T25G3.3	pho-14	pks-1	CELE_Y82E9BR.14	tomm-22	ver-3
enpl-1	let-526	tag-131	fkb-6	pnk-4	CELE_Y48G10A.1	rcs-1	CELE_Y50D4B.4
pmk-3	lron-8	ntl-9	cyp-29a2	snap-1	ced-7	dnc-4	pud-2.1
CELE_F33H2.6	hmgr-1	Y37H9A.3	aos-1	prp-38	nud-1	pole-1	poml-3
pcyt-2.2	pho-14	evl-18	aipl-1	unc-120	lem-4	mrp-2	cku-80
copz-1	clec-47	C45G9.2	pole-1	scp-1	F58F12.1	CELE_F46C5.9	ptc-1
grd-3	fkb-6	R12E2.11	CELE_T03G6.1	mrp-3	mtm-3	akt-1	cbs-1
cest-2.2	daf-21	usip-1	cct-2	rabn-5	poml-3	etr-1	haao-1
cgr-1	poml-3	cogc-6	cas-1	skih-2	CELE_K08D8.6	mec-8	pxn-2
cul-1	daf-41	prmt-1	CELE_Y62E10A.13	CELE_F09E5.7	CELE_Y39G8B.1	pbrm-1	CELE_ZC374.2
C02C2.6	elpc-2	F27D4.1	lbp-2	CELE_F09E5.11	npl-4.2	snx-6	pgp-14

Hsp16.1 20°C	*Hsp16.1 37°C*	*Hsp16.2 20°C*	*Hsp16.2 37°C*	*Hsp16.41 20°C*	*Hsp16.41 37°C*	*Hsp16.48 20°C*	*Hsp16.48 37°C*
aipl-1	CELE_T10B10.3	sec-12	C29F7.2	rpn-5	C03G6.17	CELE_T24H7.2	fis-2
pqn-80	dhs-30	mec-15	exos-4.2	CELE_F13D12.5	mrp-6	adr-2	gly-5
dhs-5	CELE_Y66D12A.10	CELE_T10B10.3	glna-2	CELE_F13H8.2	CELE_F38B6.4	CELE_F38B6.4	uba-1
CELE_Y41D4A.6	ugt-2	CELE_F26D2.15	poml-3	upb-1	thoc-2	CELE_T08G11.4	W09C3.4
rep-1	dcap-1	sucg-1	coq-4	git-1	cct-2	scp-1	CELE_Y55F3BR.1
npp-12	bpnt-1	CELE_T05E12.6	pud-2.1	tba-5	vps-15	CELE_Y71H2B.5	nra-4
pfkb-1.1	CELE_ZK899.2	CELE_W08G11.1	cyp-42a1	ctf-4	C02G6.2	praf-3	lin-13
ttc-36	ula-1	mca-3	dhs-5	acy-1	selt-1.1	CELE_R08C7.8	gpx-1
prmt-1	C44E4.5	elpc-2	hpo-40	mrp-6	rml-5	drh-1	ile-2
C56G2.15	gly-5	dot-1.1	spg-20	CELE_F21C10.10	cash-1	hpo-11	aos-1
B0280.9	haao-1	copz-1	selt-1.1	cpf-1	haf-3	thoc-2	idi-1
C02F5.3	rskd-1	cul-1	ppat-1	acs-20	C37H5.13	dnj-16	C29F7.2
usip-1	aph-2	pfkb-1.1	C02C2.6	ags-3	CELE_F26D2.15	ten-1	hoe-1
clh-6	npp-12	atg-16.1	npl-4.2	golg-2	rbbp-5	miro-1	CELE_W01G7.4
trm-2a	CELE_F56C9.10	rme-1	let-754	cyp-25a3	lin-28	dhs-5	CELE_ZK550.5
npp-23	rnr-2	CELE_ZK858.7	mpk-1	CELE_D2021.4	mpk-1	CELE_F55F10.1	npp-12
B0205.13	rml-5	CELE_W10C8.4	bpl-1	acl-5	prmt-7	C44E4.5	ssb-1
CELE_Y54G11A.3	cct-2	ketn-1	CELE_Y50D4B.4	CELE_F35D11.4	kup-1	eel-1	bpnt-1
CELE_Y38F2AR.12	sds-22	ndx-1	sid-2	mlcd-1	oxy-4	sucg-1	CELE_K08D8.6
B0250.5	ced-7	bicd-1	B0024.11	tbce-1	CELE_Y54E10A.6	cogc-5	CELE_F32A5.8
mca-2	CELE_Y80D3A.9	rad-8	CELE_Y38F2AR.12	CELE_F38B6.4	cas-1	gft-2H4	sta-2
CELE_Y53G8B.1	prmt-7	ZK632.12	C44E4.5	abcf-3	ssb-1	mel-28	CELE_K09E2.3
T20B12.7	plrg-1	unc-34	C49A9.9	CELE_F42F12.4	uba-2	sac-2	elpc-2
pcs-1	ppat-1	acl-7	clr-1	CELE_F43G6.8	CELE_Y37D8A.25	lin-23	CELE_Y73C8B.3
mca-3	smgl-1	CELE_Y38F2AR.12	cyp-33c9	CELE_F46B6.6	letm-1	pcyt-2.2	B0024.11
ced-7	mrp-6	CELE_Y41D4A.6	CELE_Y54E10A.6	Hsp17	nra-4	rbc-1	pho-1
cyn-15	kup-1	C02F5.3	npp-12	bus-5	n/a	B0361.3	bpl-1
CELE_Y55F3BR.6	gly-8	gakh-1	elpc-2	apm-3	CELE_ZK550.5	CELE_T03G6.1	nud-1
ntl-9	rnst-2	timm-17B.1	dpyd-1	bcs-1	CELE_R09H10.5	C18E9.9	selt-1.1
snx-1	Y18D10A.9	ced-7	H24K24.3	mrp-2	CELE_F32A5.8	tfbm-1	CELE_T19D12.4
CELE_T21D9.2	tomm-20	CELE_Y87G2A.2	npp-2	CELE_F58F9.3	erp-44.1	row-1	CELE_T27A3.7
acdh-13	CELE_F45D11.15	akt-1	CELE_F26D2.15	myo-5	unc-34	dnc-1	cyp-29a2
CELE_D1069.3	eif-3.H	atg-7	pcp-3	cest-17	CELE_T23G11.1	zig-12	rml-5
CELE_F58A6.1	letm-1	cct-2	R12E2.11	crml-1	sds-22	cbp-1	chat-1
CELE_F10D2.10	chat-1	daf-21	ula-1	pycr-1	CELE_K09E2.3	R12E2.11	pfkb-1.1
sup-36	uba-1	CELE_F55A12.5	CELE_Y39G8B.1	lact-3	elpc-2	mag-1	T03F6.3
akt-1	gpx-1	evl-20	crn-3	CELE_R03E9.2	prdx-2	CELE_Y67H2A.7	cash-1

Hsp16.1 20°C	*Hsp16.1 37°C*	*Hsp16.2 20°C*	*Hsp16.2 37°C*	*Hsp16.41 20°C*	*Hsp16.41 37°C*	*Hsp16.48 20°C*	*Hsp16.48 37°C*
gop-3	cpr-5	C37H5.13	C05C8.1	cku-80	mrp-5	CELE_R144.11	ced-7
mrp-4	W09C3.4	pud-4	bpnt-1	CELE_R08C7.8	clec-83	F36D4.5	gstk-1
prdx-2	fubl-1	ltd-1	ima-2	CELE_T03G6.1	gstk-1	C08B6.8	ykt-6
cyp-42a1	CELE_F55G11.8	B0250.5	ptc-1	ppat-1	fkb-6	clr-1	erp-44.1
pmp-3	mek-2	bli-3	smo-1	hcp-2	lis-1	tnc-2	cct-2
adbp-1	thoc-2	coq-8	rml-5	epg-7	ctnb-1	CELE_K07A12.1	CELE_Y80D3A.9
suf-1	npp-14	cct-1	sap-49	col-167	CELE_Y73C8B.3	mtp-18	CELE_Y54E10A.6
algn-3	CELE_F44E5.4	sars-1	hacd-1	CELE_T14B4.1	B0491.7	dpyd-1	CELE_Y39G8B.1
rad-8	H24K24.3	gop-3	CELE_Y48G10A.1	pgap-1	aipl-1	cgr-1	npp-14
cct-2	him-4	alh-13	him-4	CELE_T21D9.2	CELE_F45D11.15	ags-3	usp-14
sip-1	CELE_Y39G8B.1	CELE_F33H2.6	gss-1	rsf-1	let-754	algn-3	ruvb-1
CELE_F09E5.11	usp-14	pgp-14	CELE_Y69A2AR.19	CELE_T24H7.2	lbp-6	nnt-1	cha-1
ndx-1	npp-11	CELE_T21D9.2	W09C3.4	CELE_T25G3.3	dhs-30	lgl-1	npp-16
uba-2	CELE_T27A3.7	col-166	cnt-1	CELE_T26A5.6	par-5	CELE_F33H2.2	sds-22
ragc-1	uba-2	apg-1	tmed-10	CELE_T26A8.4	CELE_H20J04.9	rsf-1	pap-1
F27D4.1	tmed-10	CELE_Y23H5B.5	cpr-5	CELE_T27D12.1	ula-1	idi-1	copz-1
prp-19	C56G2.15	CELE_M01F1.9	T24H10.1	cdd-1	CELE_F13A7.1	pbs-5	CELE_H20J04.9
ttr-51	gcy-28	abcf-3	acy-1	pmt-2	CELE_Y47G6A.5	T24H10.1	ppat-1
CELE_F52C12.6	cyn-12	CELE_R74.8	ncbp-1	acl-9	cyp-29a2	CELE_F49E8.7	T24H10.1
wdr-4	let-754	gana-1	eif-3.H	CELE_ZC374.2	H24K24.3	haf-2	vha-20
pgp-3	unc-34	fbxa-72	alh-7	vps-15	gly-8	cdkr-3	uba-2
CELE_F21D5.1	vem-1	rpn-5	F09G8.7	CELE_Y62E10A.20	B0024.11	haly-1	plrg-1
plrg-1	cyp-29a2	wdr-4	tbc-14	mrpl-47	cyp-42a1	ZK652.6	trpp-1
myo-5	selt-1.1	sars-2	sptl-2	C05D12.3		sdz-8	gly-8
bpl-1	unc-22	math-33	thoc-2	cogc-3		pfas-1	lam-3
CELE_T24A6.20	cbs-1	CELE_T20F5.6	ruvb-1	B0205.13		bcs-1	gly-10
gna-2	dpyd-1	bre-1	lis-1	pyk-1		cogc-3	efk-1
ketn-1	ima-2	prdx-2	abtm-1	mrp-1		adbp-1	haf-3
prg-1	C02G6.2	mrp-4	bigr-1	pudl-1		riok-3	exos-4.2
mek-2	BE0003N10.1	hrg-4	CELE_H20J04.9	adpr-1		ints-7	arx-7
C49A9.9	fis-2	CELE_F09E5.11	CELE_Y51A2D.13	CELE_H20J04.9		obr-2	CELE_F13G3.6
rbg-1	lis-1	dif-1	tag-96	mvk-1		pudl-1	ttx-7
mob-4	atg-7	CELE_K06A5.2	letm-1	CELE_F10G8.9		C31H2.4	npp-24
fbl-1	timm-17B.1	F17A9.2	CELE_F09E5.11	CELE_D1069.3		CELE_K06A5.2	klp-12
haf-3	CELE_Y54E10A.6	gna-2	ssb-1	CELE_F27C1.2		sec-3	C02G6.2
atg-7	CELE_F32A5.8	gbh-1	CELE_Y80D3A.9	pyk-1		aipr-1	ula-1
daf-21	acy-1	CELE_F21D5.1	emc-6	CELE_M01F1.9		prp-38	pfd-3
rars-2	sars-2	mek-2	ragc-1	CELE_F44E7.4		C47B2.9	cyk-3
CELE_Y87G2A.2	coq-4	cct-3	pap-1	apg-1		C39D10.8	unc-78
alh-13	srp-3	K03H1.5	ced-7	CELE_F07F6.8		pap-1	CELE_F45D11.15

Hsp16.1 20°C	*Hsp16.1 37°C*	*Hsp16.2 20°C*	*Hsp16.2 37°C*	*Hsp16.41 20°C*	*Hsp16.41 37°C*	*Hsp16.48 20°C*	*Hsp16.48 37°C*
cct-1	CELE_F42C5.9	prg-1	sds-22	tbc-1		CELE_ZK858.7	B0511.7
fbxa-72	rfl-1	dcap-1	cht-3	tli-1		CELE_T20D3.6	sars-2
sec-12	abtm-1	CELE_T14B4.1	sucg-1	CELE_F26A3.1		klc-1	tep-1
snx-17	smo-1	acy-1	dot-1.1	exos-3		fkb-4	CELE_T12A2.1
sars-1	CELE_Y73C8B.3	gfm-1	CELE_F52C12.6	dnj-11		C56C10.7	par-5
CELE_T20F5.6	B0024.11	mvk-1	sams-1	CELE_K04A8.1		sco-1	rbg-2
crn-3	dlc-1	CELE_D2045.9	cbs-1	CELE_ZK858.7		emb-27	cht-3
cct-3	trpp-8	spg-7	rod-1	CELE_Y67H2A.7		let-711	CELE_ZK899.2
CELE_R74.8	cyn-5	pas-3	prmt-1	C37H5.13		ndx-3	crn-3
dli-1	ent-1	nra-2		CELE_R144.11		unc-94	CELE_F52C12.6
CELE_H20J04.4	gpi-1	msp-10		mca-3		odr-3	vem-1
rfl-1	ykt-6	myo-5		fusm-2		CELE_M106.3	prmt-7
cha-1	CELE_F52C12.6	rpn-10		CELE_M116.5		CELE_F58F9.3	npl-4.2
syf-1	F09G8.7	syf-1		ttc-37		aka-1	C04G6.4
rad-54.b	rml-4	let-711		pcyt-2.1		CELE_F13D12.5	CELE_F12E12.11
F17A9.2	CELE_F26D2.15	B0280.9		frl-1		C25H3.11	Y18D10A.9
spg-7	sams-1	dli-1		CELE_Y18H1A.4		ari-1.3	timm-17B.1
math-33	rod-1	srp-6		fbxa-14		tba-5	CELE_W03D8.9
apg-1	haf-3	zhit-3		tcc-1		sec-6	srp-3
CELE_Y59A8B.8	usp-5	pmp-3		eel-1		sta-2	CELE_T23G11.1
rpn-5	eif-6	tag-96		snx-1		col-167	ipgm-1
unc-94	npp-16	math-20		CELE_K05B2.4		CELE_ZC204.12	F58F12.1
CELE_W08G11.1	ncbp-1	add-1		arp-11		CELE_T16G1.4	fkb-6
CELE_F25E5.5	pap-1	myo-2		CELE_Y55F3BR.6		rbx-1	aipl-1
F07F6.4	icln-1	rps-21		dcap-1		C47G2.3	C44E4.5
map-2	ath-1	gars-1		pcaf-1		CELE_F57C2.5	rsp-4
pgp-14		CELE_F44E5.4		msh-6		pes-7	CELE_Y71H2AM.6
bre-1		acs-13		exos-4.2		exos-3	rep-1
mdt-18		CELE_H20J04.9		szy-2		CELE_F56B3.4	atg-7
parg-1		CELE_Y48G8AL.15		ppw-2		cua-1	dpyd-1
pas-3		acdh-3		pfkb-1.1		trpp-11	immt-1
wago-1		F52C12.1		spe-5			gpi-1
timm-17B.1		CELE_R10E4.1		trm-2a			C39B5.5
let-711		C37C3.2		elpc-2			C05C8.1
sars-2				ykt-6			eea-1
acdh-3				grd-3			ags-3
CELE_Y77E11A.7				CELE_W04C9.2			mrp-5
gfm-1				emc-3			ZK1307.4
gana-1				CELE_Y48C3A.12			oxy-4
K02D10.1				CELE_Y47H9C.8			wdr-5.1
CELE_Y53C12B.1				pap-1			3E324
sds-22				C47B2.9			asah-1

Hsp16.1 20°C	*Hsp16.1 37°C*	*Hsp16.2 20°C*	*Hsp16.2 37°C*	*Hsp16.41 20°C*	*Hsp16.41 37°C*	*Hsp16.48 20°C*	*Hsp16.48 37°C*
dot-1.1				CELE_D2063.1			ddi-1
CELE_R12E2.13				trpp-6			CELE_K01A2.5
CELE_T26A5.6				CELE_T16G1.4			spds-1
C04F12.1				CELE_K05C4.7			ugt-2
cogc-6				CELE_F57G4.1			F17A9.2
CELE_R01H10.7				C30H6.9			cus-2
gars-1				CELE_R03G8.6			CELE_Y48G8AL.15
CELE_F52G2.3				spe-46			mca-2
coq-8				kcc-1			gss-1
C04G6.4				CELE_Y76B12C.6			ran-5
mlst-8				ketn-1			
dif-1							
fars-3							
unc-73							
mrp-7							
CELE_H04M03.3							
sti-1							
CELE_Y39A3CL.1							
sbds-1							
tag-96							
pyk-1							

Table S2. Results of the statistical analysis of the Hsp16's interactome. *The values were calculated for the significant interactors. The protein sequences were taken from UniProt and calculated in Expasy and GRAVY calculator.*

	Mean	**Min**	**Median**	**Max**		**Mean**	**Min**	**Median**	**Max**
hsp16.1	-0,33438	-1,2709	-0,34273	0,94699		-0,35037	-1,17633	-0,3525	0,62008
hsp16.2	-0,34505	-1,15993	-0,35259	0,73017		-0,33775	-1,27938	-0,33549	0,62008
hsp16.41	-0,35893	-1,29918	-0,36766	0,92704	**GRAVY**	-0,36264	-1,1961	-0,36357	0,62008
hsp16.48	-0,35787	-1,35333	-0,36781	0,94699		-0,35842	-1,77347	-0,35257	0,62008
C.elegans DB	-0,2871	-2,84256	-0,32366	2,77		-0,2871	-2,84256	-0,32366	2,77
hsp16.1	6,5197	4,01	6,17	11,36		6,36102	4	6,08	9,88
hsp16.2	6,49839	4,01	6,15	9,78		6,35055	4,38	6,02	9,88
hsp16.41	6,47452	4,01	6,13	9,79	**pI**	6,34467	4,01	6,04	9,88
hsp16.48	6,43602	4,01	6,1	11,36		6,32319	4,01	5,985	11,76
C.elegans DB	7,2491	3,13	6,97	13,26		7,2491	3,13	6,97	13,26
hsp16.1	73491,62	6837,91	52985,52	864990,2		72344,19	6837,91	51336,03	864990,2
hsp16.2	77891,47	6837,91	54028,52	891809,2		68948,95	6837,91	50662,72	557550,1
hsp16.41	78965,79	6837,91	55525,59	891809,2	**Mw**	73826,83	9146,41	50038,71	864990,2
hsp16.48	79659,57	6837,91	54720,84	864990,2		70009,48	6837,91	50505,83	864990,2
C.elegans DB	51065,14	922,98	37538	1680884		51065,14	922,98	37538	1680884
	20°C					37°C			

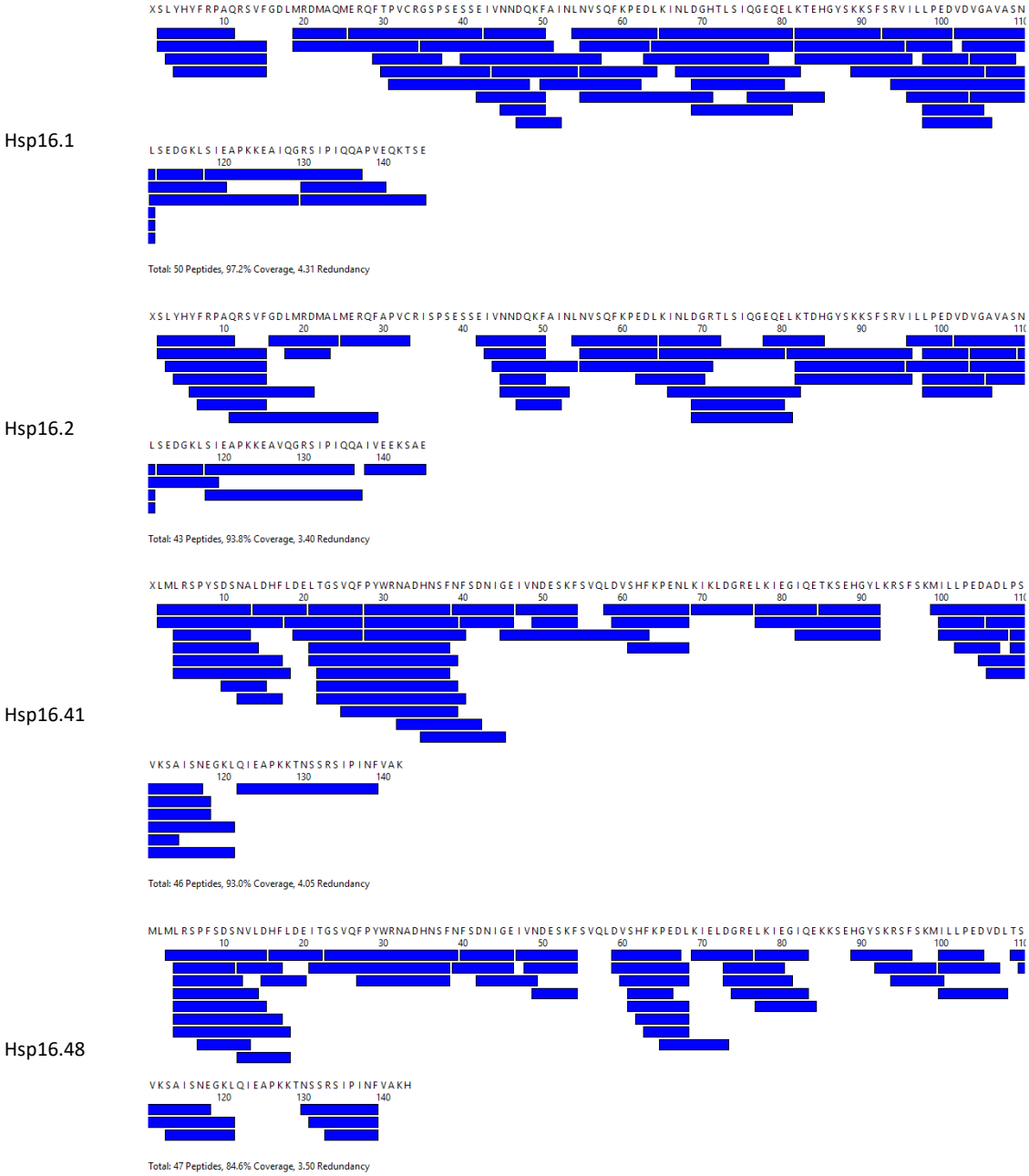

Figure S1. Peptide coverage maps of H/DX-MS analysis for Hsp16s. *The identified peptides are illustrated in blue. The sequence coverage ranges between 84.6% to 97.2%.*

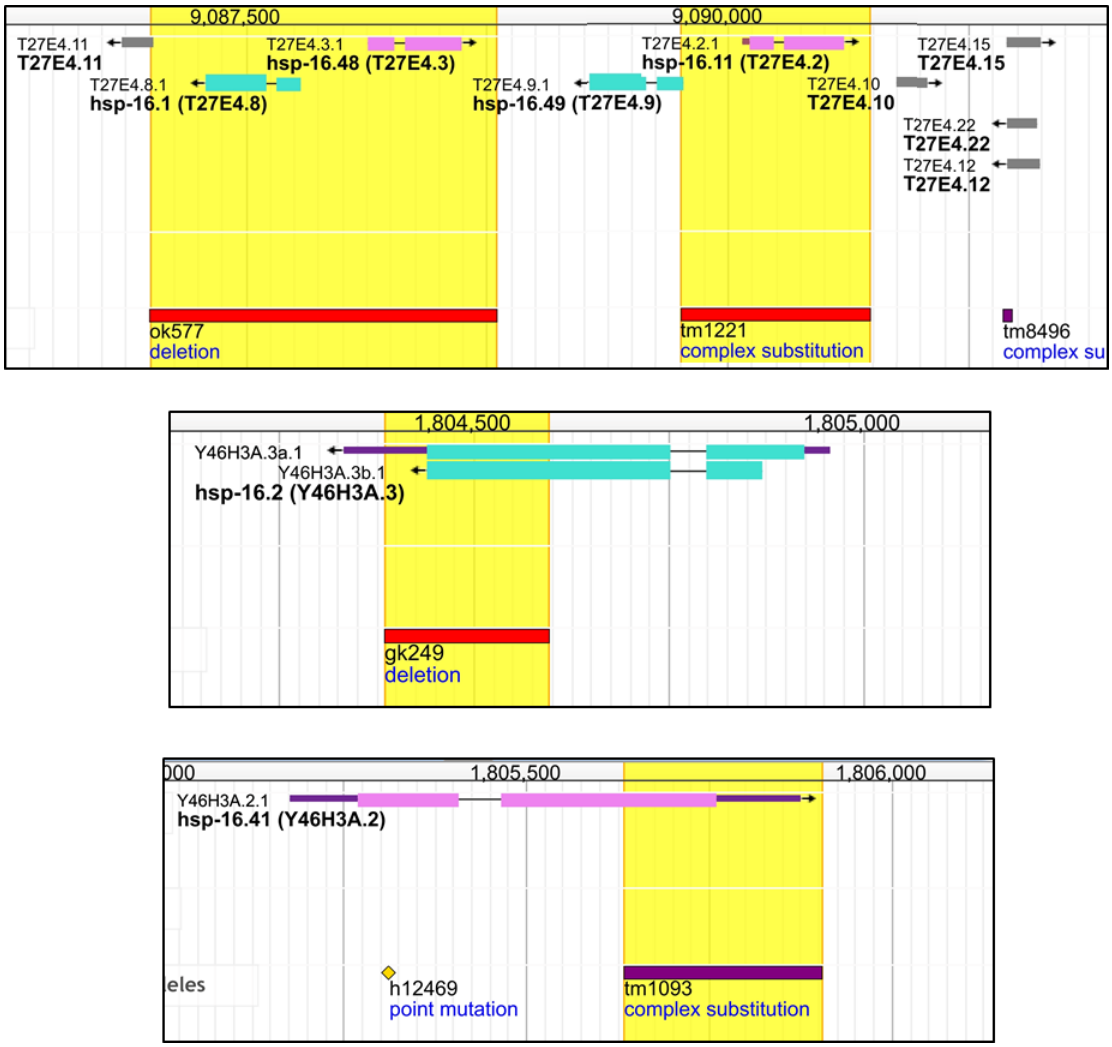

Figure S2. Genomic position of Hsp16 genes and the position of the mutations according. *The genes are illustrated in magenta or blue. The mutations (deletion or complex substitution) in the mutant strains are highlighted in yellow. Ok577 and gk249 are genetic variations of RB791 and VC475 strains, respectively, that are available from CGC. Tm1221 and tm1093 are genetic variations of strains with the same name that are available from NCBP. The data is adapted from Wormbase.*

List of abbreviations

sHsp	small heat shock protein
aa	amino acid
ACD	α-crystallin domain
ACN	acetonitrile
ADP	adenosindihosphate
ALP	autophagosomal-lysosomal pathway
Amp	ampicillin
ATP	adenosintriphosphate
AUC	analytical ultracentrifugation
BCA	bicinchoninic acid
bp	base pairs
BP	biological process
BSA	bovine serum albumin
Cys	cysteine
CD	circular dichroism
CE	*Caenorhabditis elegans*
Co-IP	co-immunoprecipitation
CS	citrate synthase
CTR	C-terminal region
Da	Dalton
DNA	deoxyribonucleic acid
DBD	DNA binding domain
dNTP	deoxynucleotide triphosphate
DHIC	DDL-1 containing HSF-1 inhibitory complex
DTT	dithiothreitol
ER	endoplasmic reclum
FA	formic acid
FC	fold change
FDR	false discovery rate
FRET	Förster resonance energy transfer
Fwd	Forward
FwdRev	Forward-Reverse (primer)
gDNA	genomic DNA
GO	gene ontology
H/DX	hydrogen deuterium exchange
HPLC	high performance liquid chromatography
HSE	heat shock element
HSF-1	heat-shock factor-1
HSR	heat shock response
IAA	iodoacetamide
IDR	intrinsically disordered region
IGF-1	insulin-like growth factor-1
IIS	insulin-like growth factor-1 signalling pathway

INS	insulin-like peptides
IPTG	isopropyl β-d-1-thiogalactopyranoside integrated stress response
KD	knock-down
KO	knock-out
LB0	lysogeny broth
LFQ	label-free quantification
MALS	multi angle light scattering
MD	middle domain
MDH	malate dehydrogenase
mRNA	messenger RNA
MS	mass spectrometry
MW	molecular weight
NBD	nucleotide binding domain
NC	nitrocellulose
NGM	Nematode Growth Medium
nt	nucleotide
NTR	N-terminal region
OD	optical density
PBS-T	phosphate buffered saline with tween
PCR	polymerase chain reaction
pI	isoelectric point
PTMs	post-translational modifications
PQC	protein quality control
Rev	reverse
RI	refractive index
RNAi	RNA interference
rpm	rotations per minute
RT	room temperature
S (AUC)	Svedberg
SBD	substrate binding domain
SD	standard deviation
SDS-PAGE	sodium dodecyl sulfate polyacrylamide gel electrophoresis
SEC	size exclusion chromatography
SG	stress granule
SWL	single worm lysis
TEM	transmission electron microscopy
Tris	Tris(hydroxymethyl)-aminomethane
UPS	ubiquitin-proteasome system
UV	ultra violet
WT	wild type
Δ	deletion

List of references

Agarraberes, Fernando A, and J.Fred Dice. 2001. “Protein Translocation across Membranes.” *Biochimica et Biophysica Acta (BBA) - Biomembranes* 1513 (1): 1–24. https://doi.org/10.1016/S0304-4157(01)00005-3.

Ahringer, Julie. 2006. “Reverse Genetics.” In *WormBook*, edited by The C. elegans Research Community. https://doi.org/10.1895/wormbook.1.47.1.

Alberti, Simon, and Serena Carra. 2018. “Quality Control of Membraneless Organelles.” *Journal of Molecular Biology* 430 (23): 4711–29. https://doi.org/10.1016/j.jmb.2018.05.013.

Algar, W. Russ, Niko Hildebrandt, Steven S. Vogel, and Igor L. Medintz. 2019. “FRET as a Biomolecular Research Tool — Understanding Its Potential While Avoiding Pitfalls.” *Nature Methods* 16 (9): 815–29. https://doi.org/10.1038/s41592-019-0530-8.

Anfinsen, C B, E Haber, M Selajf, and F H White. 1961. “The Kinetics of Formation Of Native Ribonuclease During Oxidation of The Reduced Polypeptide Chain.” *Proceedings of the NATIONAL ACADEMY OF SCIENCES*. Vol. 47.

Baker, Jeffrey P, and Margaret A Titus. 1997. “A Family of Unconventional Myosins from the Nematode Caenorhabditis Elegans.” *Journal of Molecular Biology*, no. 272: 523–35.

Balch, William E, Richard I Morimoto, Andrew Dillin, and Jeffery W Kelly. 2008. “Adapting Proteostasis for Disease Intervention.” *SCIENCE* 319 (5865): 916–20. https://www.science.org.

Bar-Lavan, Yael, Netta Shemesh, Shiran Dror, Rivka Ofir, Esti Yeger-Lotem, and Anat Ben-Zvi. 2016. “A Differentiation Transcription Factor Establishes Muscle-Specific Proteostasis in Caenorhabditis Elegans.” *PLOS Genetics* 12 (12): e1006531. https://doi.org/10.1371/journal.pgen.1006531.

Barral, José M., Alex H. Hutagalung, Achim Brinker, F. Ulrich Hartl, and Henry F. Epstein. 2002. “Role of the Myosin Assembly Protein UNC-45 as a Molecular Chaperone for Myosin.” *Science* 295 (5555): 669–71. https://doi.org/10.1126/science.1066648.

Bartlett, Alice I., and Sheena E. Radford. 2009. “An Expanding Arsenal of Experimental Methods Yields an Explosion of Insights into Protein Folding Mechanisms.” *Nature Structural and Molecular Biology*. https://doi.org/10.1038/nsmb.1592.

Bascos, Neil Andrew D., and Samuel J. Landry. 2019. “A History of Molecular Chaperone Structures in the Protein Data Bank.” *International Journal of Molecular Sciences* 20 (24): 6195. https://doi.org/10.3390/ijms20246195.

Basha, Eman, Christopher Jones, Anne E. Blackwell, Guilong Cheng, Elizabeth R. Waters, Kara A. Samsel, Masood Siddique, Virginia Pett, Vicki Wysocki, and Elizabeth Vierling. 2013. “An Unusual Dimeric Small Heat Shock Protein Provides Insight into the Mechanism of This Class of Chaperones.” *Journal of Molecular Biology* 425 (10): 1683–96. https://doi.org/10.1016/j.jmb.2013.02.011.

Basha, Eman, Heather O'Neill, and Elizabeth Vierling. 2012. "Small Heat Shock Proteins and α-Crystallins: Dynamic Proteins with Flexible Functions." *Trends in Biochemical Sciences* 37 (3): 106–17. https://doi.org/10.1016/j.tibs.2011.11.005.

Baughman, Hannah E. R., Thanh-Hau T. Pham, Chloe S. Adams, Abhinav Nath, and Rachel E. Klevit. 2020. "Release of a Disordered Domain Enhances HspB1 Chaperone Activity toward Tau." *Proceedings of the National Academy of Sciences* 117 (6): 2923–29. https://doi.org/10.1073/pnas.1915099117.

Behnke, Julia, Matthias J. Feige, and Linda M. Hendershot. 2015. "BiP and Its Nucleotide Exchange Factors Grp170 and Sil1: Mechanisms of Action and Biological Functions." *Journal of Molecular Biology* 427 (7): 1589–1608. https://doi.org/10.1016/j.jmb.2015.02.011.

Benesch, Justin L.P., Marina Ayoub, Carol v. Robinson, and J. Andrew Aquilina. 2008. "Small Heat Shock Protein Activity Is Regulated by Variable Oligomeric Substructure." *Journal of Biological Chemistry* 283 (42): 28513–17. https://doi.org/10.1074/jbc.M804729200.

Betts, Matthew J., and Robert B. Russell. 2003. "Amino Acid Properties and Consequences of Substitutions." In *Bioinformatics for Geneticists*, edited by R. M. Barners and I. C. Gray, 289–316. Chichester, UK: John Wiley & Sons, Ltd. https://doi.org/10.1002/0470867302.ch14.

Bie, Anne S., Paula Fernandez-Guerra, Rune I. D. Birkler, Shahar Nisemblat, Dita Pelnena, Xinping Lu, Joshua L. Deignan, et al. 2016. "Effects of a Mutation in the HSPE1 Gene Encoding the Mitochondrial Co-Chaperonin HSP10 and Its Potential Association with a Neurological and Developmental Disorder." *Frontiers in Molecular Biosciences* 3 (October). https://doi.org/10.3389/fmolb.2016.00065.

Biebl, Maximilian M., and Johannes Buchner. 2019. "Structure, Function, and Regulation of the Hsp90 Machinery." *Cold Spring Harbor Perspectives in Biology* 11 (9): a034017. https://doi.org/10.1101/cshperspect.a034017.

Bindea, Gabriela, Bernhard Mlecnik, Hubert Hackl, Pornpimol Charoentong, Marie Tosolini, Amos Kirilovsky, Wolf-Herman Fridman, Franck Pagès, Zlatko Trajanoski, and Jérôme Galon. 2009. "ClueGO: A Cytoscape Plug-in to Decipher Functionally Grouped Gene Ontology and Pathway Annotation Networks." *Bioinformatics (Oxford, England)* 25 (8): 1091–93. https://doi.org/10.1093/bioinformatics/btp101.

Blair, Laura J., Bryce A. Nordhues, Shannon E. Hill, K. Matthew Scaglione, John C. O'Leary, Sarah N. Fontaine, Leonid Breydo, et al. 2013. "Accelerated Neurodegeneration through Chaperone-Mediated Oligomerization of Tau." *Journal of Clinical Investigation* 123 (10): 4158–69. https://doi.org/10.1172/JCI69003.

Boczek, Edgar E, Julius Fürsch, Marie Laura Niedermeier, Louise Jawerth, Marcus Jahnel, Martine Ruer-Gruß, Kai-Michael Kammer, et al. 2021. "HspB8 Prevents Aberrant Phase Transitions of FUS by Chaperoning Its Folded RNA-Binding Domain." *ELife* 10 (September). https://doi.org/10.7554/eLife.69377.

Boczek, Edgar E., Lasse G. Reefschläger, Marco Dehling, Tobias J. Struller, Elisabeth Häusler, Andreas Seidl, Ville R. I. Kaila, and Johannes Buchner. 2015. "Conformational Processing of Oncogenic V-Src Kinase by the Molecular Chaperone Hsp90." *Proceedings of the National Academy of Sciences* 112 (25). https://doi.org/10.1073/pnas.1424342112.

Bouhy, Delphine, Manisha Juneja, Istvan Katona, Anne Holmgren, Bob Asselbergh, Vicky de Winter, Tino Hochepied, et al. 2018. “A Knock-in/Knock-out Mouse Model of HSPB8-Associated Distal Hereditary Motor Neuropathy and Myopathy Reveals Toxic Gain-of-Function of Mutant Hspb8.” *Acta Neuropathologica* 135 (1): 131–48. https://doi.org/10.1007/s00401-017-1756-0.

Bova, Michael P., Lin-Lin Ding, Joseph Horwitz, and Bernard K.-K. Fung. 1997. “Subunit Exchange of AA-Crystallin.” *Journal of Biological Chemistry* 272 (47): 29511–17. https://doi.org/10.1074/jbc.272.47.29511.

Bracher, Andreas, and Jacob Verghese. 2015a. “The Nucleotide Exchange Factors of Hsp70 Molecular Chaperones.” *Frontiers in Molecular Biosciences* 2 (April). https://doi.org/10.3389/fmolb.2015.00010.

Braig, K, M Simon, F Furuya, J F Hainfeld, and A L Horwich. 1993. “A Polypeptide Bound by the Chaperonin GroEL Is Localized within a Central Cavity.” *Proceedings of the National Academy of Sciences* 90 (9): 3978–82. https://doi.org/10.1073/pnas.90.9.3978.

Braig, Kerstin, Zbyszek Otwinowski, Rashmi Hegde, David C. Boisvert, Andrzej Joachimiak, Arthur L. Horwich, and Paul B. Sigler. 1994. “The Crystal Structure of the Bacterial Chaperonln GroEL at 2.8 Å.” *Nature* 371 (6498): 578–86. https://doi.org/10.1038/371578a0.

Brehme, Marc, Cindy Voisine, Thomas Rolland, Shinichiro Wachi, James H. Soper, Yitan Zhu, Kai Orton, et al. 2014. “A Chaperome Subnetwork Safeguards Proteostasis in Aging and Neurodegenerative Disease.” *Cell Reports* 9 (3): 1135–50. https://doi.org/10.1016/j.celrep.2014.09.042.

Brenner, S. 1974. “The Genetics of Caenorhabditis Elegans.” *Genetics* 77 (1): 71–94. https://doi.org/10.1093/genetics/77.1.71.

Brevet, Annie, Josiane Chen, Franoise Lévque, Sylvain Blanquet, and Pierre Plateau. 1995. “Comparison of the Enzymatic Properties of the Two Escherichia Coli Lysyl-TRNA Synthetase Species.” *Journal of Biological Chemistry* 270 (24): 14439–44. https://doi.org/10.1074/jbc.270.24.14439.

Bridges, Calvin B. 1936. “The Bar ‘Gene’ a Duplication.” *Science* 83 (2148): 210–11. https://doi.org/10.1126/science.83.2148.210.

Broekhuis, Joost R., Suzanne Rademakers, Jan Burghoorn, and Gert Jansen. 2013a. “SQL-1, Homologue of the Golgi Protein GMAP210, Modulates Intraflagellar Transport in *C. Elegans*.” *Journal of Cell Science*, January. https://doi.org/10.1242/jcs.116640.

Brown, Patrick H., and Peter Schuck. 2006. “Macromolecular Size-and-Shape Distributions by Sedimentation Velocity Analytical Ultracentrifugation.” *Biophysical Journal* 90 (12): 4651–61. https://doi.org/10.1529/biophysj.106.081372.

Bukach, Olesya v., Alim S. Seit-Nebi, Steven B. Marston, and Nikolai B. Gusev. 2004. “Some Properties of Human Small Heat Shock Protein Hsp20 (HspB6).” *European Journal of Biochemistry* 271 (2): 291–302. https://doi.org/10.1046/j.1432-1033.2003.03928.x.

Bukau, Bernd, Jonathan Weissman, and Arthur Horwich. 2006. “Molecular Chaperones and Protein Quality Control.” *Cell* 125 (3): 443–51. https://doi.org/10.1016/j.cell.2006.04.014.

Burston, Steven G., Neil A. Ranson, and Anthony R. Clarke. 1995. “The Origins and Consequences of Asymmetry in the Chaperonin Reaction Cycle.” *Journal of Molecular Biology* 249 (1): 138–52. https://doi.org/10.1006/jmbi.1995.0285.

C. elegans Sequencing Consortium. 1998. “Genome Sequence of the Nematode *C. Elegans* : A Platform for Investigating Biology.” *Science* 282 (5396): 2012–18. https://doi.org/10.1126/science.282.5396.2012.

Calloni, Giulia, and R. Martin Vabulas. 2020. “Proteome-Scale Studies of Protein Stability.” In *Protein Homeostasis Diseases*, 71–90. Elsevier. https://doi.org/10.1016/b978-0-12-819132-3.00004-x.

Candido, E. P. M., D. Jones, D. K. Dixon, R. W. Graham, R. H. Russnak, and R. J. Kay. 1989. “Structure, Organization, and Expression of the 16-KDa Heat Shock Gene Family of *Caenorhabditis Elegans*.” *Genome* 31 (2): 690–97. https://doi.org/10.1139/g89-126.

Cao, Ke, Zhen Peng, Xing Zhao, Yong Li, Kuozhan Liu, Pere Arus, Weichao Fang, et al. 2022. “Chromosome-Level Genome Assemblies of Four Wild Peach Species Provide Insights into Genome Evolution and Genetic Basis of Stress Resistance.” *BMC Biology* 20 (1). https://doi.org/10.1186/s12915-022-01342-y.

Carbon, Seth, Eric Douglass, Benjamin M Good, Deepak R Unni, Nomi L Harris, Christopher J Mungall, Siddartha Basu, et al. 2021. “The Gene Ontology Resource: Enriching a GOld Mine.” *Nucleic Acids Research* 49 (D1): D325–34. https://doi.org/10.1093/nar/gkaa1113.

Carra, Serena, Simon Alberti, Justin L. P. Benesch, Wilbert Boelens, Johannes Buchner, John A. Carver, Ciro Cecconi, et al. 2019. “Small Heat Shock Proteins: Multifaceted Proteins with Important Implications for Life.” *Cell Stress and Chaperones* 24 (2): 295–308. https://doi.org/10.1007/s12192-019-00979-z.

Caspers, Gert-Jan, Jack A. M. Leunissen, and Wilfried W. de Jong. 1995. “The Expanding Small Heat-Shock Protein Family, and Structure Predictions of the Conserved ‘α-Crystallin Domain.’” *Journal of Molecular Evolution* 40 (3): 238–48. https://doi.org/10.1007/BF00163229.

Ceol, Craig J, and H.R Horvitz. 2004. “A New Class of C. Elegans SynMuv Genes Implicates a Tip60/NuA4-like HAT Complex as a Negative Regulator of Ras Signaling.” *Developmental Cell* 6 (4): 563–75.

Chadli, Ahmed, Ilham Bouhouche, William Sullivan, Bridget Stensgard, Nancy McMahon, Maria G. Catelli, and David O. Toft. 2000. “Dimerization and N-Terminal Domain Proximity Underlie the Function of the Molecular Chaperone Heat Shock Protein 90.” *Proceedings of the National Academy of Sciences* 97 (23): 12524–29. https://doi.org/10.1073/pnas.220430297.

Cheng, Guilong, Eman Basha, Vicki H. Wysocki, and Elizabeth Vierling. 2008. “Insights into Small Heat Shock Protein and Substrate Structure during Chaperone Action Derived from Hydrogen/Deuterium Exchange and Mass Spectrometry.” *Journal of Biological Chemistry* 283 (39): 26634–42. https://doi.org/10.1074/jbc.M802946200.

Cherkasov, Valeria, Sarah Hofmann, Silke Druffel-Augustin, Axel Mogk, Jens Tyedmers, Georg Stoecklin, and Bernd Bukau. 2013. “Coordination of Translational Control and Protein Homeostasis during Severe Heat Stress.” *Current Biology* 23 (24): 2452–62. https://doi.org/10.1016/j.cub.2013.09.058.

Choi, Min Sung, Andrew S. Yoo, and Iva Greenwald. 2010. “Sel-11 and Cdc-42, Two Negative Modulators of LIN-12/Notch Activity in *C. Elegans*.” *PLoS ONE* 5 (7): e11885. https://doi.org/10.1371/journal.pone.0011885.

Clausen, Lene, Amanda B. Abildgaard, Sarah K. Gersing, Amelie Stein, Kresten Lindorff-Larsen, and Rasmus Hartmann-Petersen. 2019. “Protein Stability and Degradation in Health and Disease.” In *Advances in Protein Chemistry and Structural Biology*, 114:61–83. Academic Press Inc. https://doi.org/10.1016/bs.apcsb.2018.09.002.

Clouser, Amanda F, Hannah ER Baughman, Benjamin Basanta, Miklos Guttman, Abhinav Nath, and Rachel E Klevit. 2019. “Interplay of Disordered and Ordered Regions of a Human Small Heat Shock Protein Yields an Ensemble of ‘Quasi-Ordered’ States.” *ELife* 8 (October). https://doi.org/10.7554/eLife.50259.

Cook, Steven J., Travis A. Jarrell, Christopher A. Brittin, Yi Wang, Adam E. Bloniarz, Maksim A. Yakovlev, Ken C. Q. Nguyen, et al. 2019. “Whole-Animal Connectomes of Both *Caenorhabditis Elegans* Sexes.” *Nature* 571 (7763): 63–71. https://doi.org/10.1038/s41586-019-1352-7.

Coppinger, Judith A., Darren M. Hutt, Abbas Razvi, Atanas v. Koulov, Sandra Pankow, John R. Yates, and William E. Balch. 2012. “A Chaperone Trap Contributes to the Onset of Cystic Fibrosis.” *PLoS ONE* 7 (5): e37682. https://doi.org/10.1371/journal.pone.0037682.

Cordeiro Rodrigues, Ricardo J., António Miguel de Jesus Domingues, Svenja Hellmann, Sabrina Dietz, Bruno F.M. de Albuquerque, Christian Renz, Helle D. Ulrich, Peter Sarkies, Falk Butter, and René F. Ketting. 2019. “PETISCO Is a Novel Protein Complex Required for 21U RNA Biogenesis and Embryonic Viability.” *Genes & Development* 33 (13–14): 857–70. https://doi.org/10.1101/gad.322446.118.

Corsi, Ann K., B Wightmann, and M Chalfie. 2015. “A Transparent Window into Biology: A Primer on Caenorhabditis Elegans.” In *WormBook*, edited by E. A. de Stasio, 1–31. https://doi.org/10.1895/wormbook.1.177.1.

Cox, Jürgen, Nadin Neuhauser, Annette Michalski, Richard A. Scheltema, Jesper v. Olsen, and Matthias Mann. 2011. “Andromeda: A Peptide Search Engine Integrated into the MaxQuant Environment.” *Journal of Proteome Research* 10 (4): 1794–1805. https://doi.org/10.1021/pr101065j.

Craig, Elizabeth A. 2018. “Hsp70 at the Membrane: Driving Protein Translocation.” *BMC Biology* 16 (1): 11. https://doi.org/10.1186/s12915-017-0474-3.

Cristofani, Riccardo, Paola Rusmini, Mariarita Galbiati, Maria Elena Cicardi, Veronica Ferrari, Barbara Tedesco, Elena Casarotto, et al. 2019. “The Regulation of the Small Heat Shock Protein B8 in Misfolding Protein Diseases Causing Motoneuronal and Muscle Cell Death.” *Frontiers in Neuroscience* 13 (August). https://doi.org/10.3389/fnins.2019.00796.

Dahiya, Vinay, and Johannes Buchner. 2019. “Functional Principles and Regulation of Molecular Chaperones.” In *Advances in Protein Chemistry and Structural Biology*, 114:1–60. Academic Press Inc. https://doi.org/10.1016/bs.apcsb.2018.10.001.

Delbecq, Scott P, Stefan Jehle, and Rachel Klevit. 2012. “Binding Determinants of the Small Heat Shock Protein, AB-Crystallin: Recognition of the ‘IxI’ Motif.” *The EMBO Journal* 31 (24): 4587–94. https://doi.org/10.1038/emboj.2012.318.

Dereeper, A., V. Guignon, G. Blanc, S. Audic, S. Buffet, F. Chevenet, J.-F. Dufayard, et al. 2008. “Phylogeny.Fr: Robust Phylogenetic Analysis for the Non-Specialist.” *Nucleic Acids Research* 36 (Web Server): W465–69. https://doi.org/10.1093/nar/gkn180.

Dikic, Ivan. 2017. “Proteasomal and Autophagic Degradation Systems.” *Annual Review of Biochemistry* 86: 193–224. https://doi.org/10.1146/annurev-biochem.

Ding, Lily, and E. Peter M. Candido. 2000. “Association of Several Small Heat-Shock Proteins with Reproductive Tissues in the Nematode *Caenorhabditis Elegans*.” *Biochemical Journal* 351 (1): 13–17. https://doi.org/10.1042/bj3510013.

Dobson, C. M. 2001. “The Structural Basis of Protein Folding and Its Links with Human Disease.” *Philosophical Transactions of the Royal Society B: Biological Sciences* 356 (1406): 133–45. https://doi.org/10.1098/rstb.2000.0758.

Dutkiewicz, Rafal, Malgorzata Nowak, Elizabeth A. Craig, and Jaroslaw Marszalek. 2017. “Fe–S Cluster Hsp70 Chaperones: The ATPase Cycle and Protein Interactions.” In , 161–84. https://doi.org/10.1016/bs.mie.2017.07.004.

Eckl, Julia, Siyuan Sima, Katrin Marcus, Claudia Lindemann, and Klaus Richter. 2017. “Hsp90-Downregulation Influences the Heat-Shock Response, Innate Immune Response and Onset of Oocyte Development in Nematodes.” *PLOS ONE* 12 (10): e0186386. https://doi.org/10.1371/journal.pone.0186386.

Ehrnsperger, M. 1997. “Binding of Non-Native Protein to Hsp25 during Heat Shock Creates a Reservoir of Folding Intermediates for Reactivation.” *The EMBO Journal* 16 (2): 221–29. https://doi.org/10.1093/emboj/16.2.221.

Eisenmann, David M. 2005. “Wnt Signaling.” In *WormBook*, edited by The *C. elegans* Research Community. https://doi.org/10.1895/wormbook.1.7.1.

Ellis, R. John, and Allen P. Minton. 2006. “Protein Aggregation in Crowded Environments.” *Biological Chemistry*. https://doi.org/10.1515/BC.2006.064.

Erdős, Gábor, and Zsuzsanna Dosztányi. 2020. “Analyzing Protein Disorder with IUPred2A.” *Current Protocols in Bioinformatics* 70 (1). https://doi.org/10.1002/cpbi.99.

Erpf, Anna C., Lisa Stenzel, Nadin Memar, Martina Antoniolli, Mariam Osepashvili, Ralf Schnabel, Barbara Conradt, and Tamara Mikeladze-Dvali. 2019. “PCMD-1 Organizes Centrosome Matrix Assembly in C. Elegans.” *Current Biology* 29 (8): 1324-1336.e6. https://doi.org/10.1016/j.cub.2019.03.029.

Fairbanks, G., Theodore L. Steck, and D. F. H. Wallach. 1971. “Electrophoretic Analysis of the Major Polypeptides of the Human Erythrocyte Membrane.” *Biochemistry* 10 (13): 2606–17. https://doi.org/10.1021/bi00789a030.

Fay, David. 2006. “Genetic Mapping and Manipulation: Chapter 1-Introduction and Basics.” In *WormBook*, edited by The *C. elegans* Research Community. https://doi.org/10.1895/wormbook.1.90.1.

Fayet, O, T Ziegelhoffer, and C Georgopoulos. 1989. “The GroES and GroEL Heat Shock Gene Products of Escherichia Coli Are Essential for Bacterial Growth at All Temperatures.” *Journal of Bacteriology* 171 (3): 1379–85. https://doi.org/10.1128/jb.171.3.1379-1385.1989.

Feleciano, Diogo R., Katrin Juenemann, Manuel Iburg, Inês C. Brás, Carina I. Holmberg, and Janine Kirstein. 2019. “Crosstalk between Chaperone-Mediated Protein Disaggregation and Proteolytic Pathways in Aging and Disease.” *Frontiers in Aging Neuroscience* 11 (JAN). https://doi.org/10.3389/fnagi.2019.00009.

Fernández-Fernández, María Rosario, Marcos Gragera, Lissette Ochoa-Ibarrola, Lucía Quintana-Gallardo, and José María Valpuesta. 2017. “Hsp70 - a Master Regulator in Protein Degradation.” *FEBS Letters* 591 (17): 2648–60. https://doi.org/10.1002/1873-3468.12751.

Finka, Andrija, Vishal Sood, Manfredo Quadroni, Paolo De Los Rios, and Pierre Goloubinoff. 2015. “Quantitative Proteomics of Heat-Treated Human Cells Show an across-the-Board Mild Depletion of Housekeeping Proteins to Massively Accumulate Few HSPs.” *Cell Stress and Chaperones* 20 (4): 605–20. https://doi.org/10.1007/s12192-015-0583-2.

Fleckenstein, Tilly. 2014. “Sip1, a Unique Small Heat Shock Protein of the Nematode Caenorhabditis Elegans - a Structural and Functional Characterization.” TECHNISCHE UNIVERSITÄT MÜNCHEN.

Fleckenstein, Tilly, Andreas Kastenmüller, Martin Lorenz Stein, Carsten Peters, Marina Daake, Maike Krause, Daniel Weinfurtner, et al. 2015. “The Chaperone Activity of the Developmental Small Heat Shock Protein Sip1 Is Regulated by PH-Dependent Conformational Changes.” *Molecular Cell* 58 (6): 1067–78. https://doi.org/10.1016/j.molcel.2015.04.019.

Forslund, K., F. Schreiber, N. Thanintorn, and E. L. L. Sonnhammer. 2011. “OrthoDisease: Tracking Disease Gene Orthologs across 100 Species.” *Briefings in Bioinformatics* 12 (5): 463–73. https://doi.org/10.1093/bib/bbr024.

Fox, Leora M., and Ai Yamamoto. 2015. “Macroautophagy of Aggregation-Prone Proteins in Neurodegenerative Disease.” In *Autophagy: Cancer, Other Pathologies, Inflammation, Immunity, Infection, and Aging*, 7:117–37. Elsevier Inc. https://doi.org/10.1016/B978-0-12-801043-3.00007-8.

Friedrich, Kenneth L., Kim C. Giese, Nicole R. Buan, and Elizabeth Vierling. 2004. “Interactions between Small Heat Shock Protein Subunits and Substrate in Small Heat Shock Protein-Substrate Complexes.” *Journal of Biological Chemistry* 279 (2): 1080–89. https://doi.org/10.1074/jbc.M311104200.

Frumkin, Anna, Shiran Dror, Wojciech Pokrzywa, Yael Bar-Lavan, Ido Karady, Thorsten Hoppe, and Anat Ben-Zvi. 2014a. “Challenging Muscle Homeostasis Uncovers Novel Chaperone Interactions in Caenorhabditis Elegans.” *Frontiers in Molecular Biosciences* 1 (November). https://doi.org/10.3389/fmolb.2014.00021.

Fu, Xinmiao, Anastasia N. Ezemaduka, Xinping Lu, and Zengyi Chang. 2021. “The <scp> *Caenorhabditis Elegans* 12-kDa </Scp> Small Heat Shock Proteins with Little *in vitro* Chaperone Activity Play Crucial Roles for Its Dauer Formation, Longevity, and Reproduction.” *Protein Science* 30 (10): 2170–82. https://doi.org/10.1002/pro.4160.

Gaiser, Andreas M., Christoph J. O. Kaiser, Veronika Haslbeck, and Klaus Richter. 2011. "Downregulation of the Hsp90 System Causes Defects in Muscle Cells of Caenorhabditis Elegans." *PLoS ONE* 6 (9): e25485. https://doi.org/10.1371/journal.pone.0025485.

Gandhi, Schiva, John Santelli, David H. Mitchell, J. Wesley Stiles, and D. Rao Sanadi. 1980a. "A Simple Method for Maintaining Large, Aging Populations of Caenorhabditis Elegans." *Mechanisms of Ageing and Development* 12 (2): 137–50. https://doi.org/10.1016/0047-6374(80)90090-1.

Gasteiger, Elisabeth, Christine Hoogland, Alexandre Gattiker, S'everine Duvaud, Marc R. Wilkins, Ron D. Appel, and Amos Bairoch. 2005. "Protein Identification and Analysis Tools on the ExPASy Server." In *The Proteomics Protocols Handbook*, 571–607. Totowa, NJ: Humana Press. https://doi.org/10.1385/1-59259-890-0:571.

Gestaut, Daniel, Soung Hun Roh, Boxue Ma, Grigore Pintilie, Lukasz A. Joachimiak, Alexander Leitner, Thomas Walzthoeni, Ruedi Aebersold, Wah Chiu, and Judith Frydman. 2019. "The Chaperonin TRiC/CCT Associates with Prefoldin through a Conserved Electrostatic Interface Essential for Cellular Proteostasis." *Cell* 177 (3): 751-765.e15. https://doi.org/10.1016/j.cell.2019.03.012.

Gowda, Naveen K. C., Jayasankar M. Kaimal, Roman Kityk, Chammiran Daniel, Jobst Liebau, Marie Öhman, Matthias P. Mayer, and Claes Andréasson. 2018. "Nucleotide Exchange Factors Fes1 and HspBP1 Mimic Substrate to Release Misfolded Proteins from Hsp70." *Nature Structural & Molecular Biology* 25 (1): 83–89. https://doi.org/10.1038/s41594-017-0008-2.

Greenfield, Norma J. 2006a. "Using Circular Dichroism Spectra to Estimate Protein Secondary Structure." *Nature Protocols* 1 (6): 2876–90. https://doi.org/10.1038/nprot.2006.202.

Grigorenko, Anastasia P., Youri K. Moliaka, Olga v. Plotnikova, Alexander Smirnov, Vera A. Nikishina, Andrey Y. Goltsov, Fedor Gusev, et al. 2017. "Mutational Re-Modeling of Di-Aspartyl Intramembrane Proteases: Uncoupling Physiologically-Relevant Activities from Those Associated with Alzheimer's Disease." *Oncotarget* 8 (47): 82006–26. https://doi.org/10.18632/oncotarget.18299.

Grousl, Tomas, Sophia Ungelenk, Stephanie Miller, Chi-Ting Ho, Maria Khokhrina, Matthias P. Mayer, Bernd Bukau, and Axel Mogk. 2018. "A Prion-like Domain in Hsp42 Drives Chaperone-Facilitated Aggregation of Misfolded Proteins." *Journal of Cell Biology* 217 (4): 1269–85. https://doi.org/10.1083/jcb.201708116.

Gu, Jinge, Zhenying Liu, Shengnan Zhang, Yichen Li, Wencheng Xia, Chen Wang, Huaijiang Xiang, et al. 2020. "Hsp40 Proteins Phase Separate to Chaperone the Assembly and Maintenance of Membraneless Organelles." *Proceedings of the National Academy of Sciences* 117 (49): 31123–33. https://doi.org/10.1073/pnas.2002437117.

Guo, Huan, Yun Bai, Ping Xu, Zhibin Hu, Li Liu, Fang Wang, Guangfu Jin, et al. 2010. "Functional Promoter _1271G_C Variant of HSPB1 Predicts Lung Cancer Risk and Survival." *Journal of Clinical Oncology* 28 (11): 1928–35. https://doi.org/10.1200/JCO.2009.24.4954.

Hadizadeh Esfahani, Ali, Angelina Sverchkova, Julio Saez-Rodriguez, Andreas A. Schuppert, and Marc Brehme. 2018. "A Systematic Atlas of Chaperome Deregulation Topologies across the

Human Cancer Landscape." *PLOS Computational Biology* 14 (1): e1005890. https://doi.org/10.1371/journal.pcbi.1005890.

Han, Seong Kyu, Dongyeop Lee, Heetak Lee, Donghyo Kim, Heehwa G. Son, Jae-Seong Yang, Seung-Jae v. Lee, and Sanguk Kim. 2016. "OASIS 2: Online Application for Survival Analysis 2 with Features for the Analysis of Maximal Lifespan and Healthspan in Aging Research." *Oncotarget* 7 (35): 56147–52. https://doi.org/10.18632/oncotarget.11269.

Hartl, F. Ulrich, Andreas Bracher, and Manajit Hayer-Hartl. 2011. "Molecular Chaperones in Protein Folding and Proteostasis." *Nature*. https://doi.org/10.1038/nature10317.

Haslbeck, M., S. Walke, T. Sromerr, M Ehrnsperger, H White, S Chen, H Saibil, and J Buchner. 1999. "Hsp26: A Temperature-Regulated Chaperone." *The EMBO Journal* 18 (23): 6744–51. https://doi.org/10.1093/emboj/18.23.6744.

Haslbeck, M., S Walke, T Stromer, M Ehrnsperger, H. E. White, S Chen, H Saibil, and J Buchner. 1999. "Hsp26: A Temperature-Regulated Chaperone." *The EMBO Journal* 18 (23): 6744–51. https://doi.org/10.1093/emboj/18.23.6744.

Haslbeck, Martin, Jirka Peschek, Johannes Buchner, and Sevil Weinkauf. 2016. "Structure and Function of α-Crystallins: Traversing from in Vitro to in Vivo." *Biochimica et Biophysica Acta (BBA) - General Subjects* 1860 (1): 149–66. https://doi.org/10.1016/j.bbagen.2015.06.008.

Haslbeck, Martin, and Elizabeth Vierling. 2015. "A First Line of Stress Defense: Small Heat Shock Proteins and Their Function in Protein Homeostasis." *Journal of Molecular Biology* 427 (7): 1537–48. https://doi.org/10.1016/j.jmb.2015.02.002.

Haslbeck, Martin, Sevil Weinkauf, and Johannes Buchner. 2019. "Small Heat Shock Proteins: Simplicity Meets Complexity." *Journal of Biological Chemistry* 294 (6): 2121–32. https://doi.org/10.1074/jbc.REV118.002809.

Hayer-Hartl, Manajit, Andreas Bracher, and F. Ulrich Hartl. 2016. "The GroEL–GroES Chaperonin Machine: A Nano-Cage for Protein Folding." *Trends in Biochemical Sciences* 41 (1): 62–76. https://doi.org/10.1016/j.tibs.2015.07.009.

Hayes, Victoria H., Glyn Devlin, and Roy A. Quinlan. 2008. "Truncation of AB-Crystallin by the Myopathy-Causing Q151X Mutation Significantly Destabilizes the Protein Leading to Aggregate Formation in Transfected Cells." *Journal of Biological Chemistry* 283 (16): 10500–512. https://doi.org/10.1074/jbc.M706453200.

Heintz, Caroline, Thomas K. Doktor, Anne Lanjuin, Caroline C. Escoubas, Yue Zhang, Heather J. Weir, Sneha Dutta, et al. 2017. "Splicing Factor 1 Modulates Dietary Restriction and TORC1 Pathway Longevity in C. Elegans." *Nature* 541 (7635): 102–6. https://doi.org/10.1038/nature20789.

Helm, Stefan, and Sacha Baginsky. 2018. "MSE for Label-Free Absolute Protein Quantification in Complex Proteomes." In , 235–47. https://doi.org/10.1007/978-1-4939-7411-5_16.

Hochberg, Georg K. A., Dale A. Shepherd, Erik G. Marklund, Indu Santhanagoplan, Matteo T. Degiacomi, Arthur Laganowsky, Timothy M. Allison, et al. 2018. "Structural Principles That Enable Oligomeric Small Heat-Shock Protein Paralogs to Evolve Distinct Functions." *Science* 359 (6378): 930–35. https://doi.org/10.1126/science.aam7229.

Hong, Mingi, Jae Young Kwon, Jaegal Shim, and Junho Lee. 2004. “Differential Hypoxia Response of Hsp-16 Genes in the Nematode.” *Journal of Molecular Biology* 344 (2): 369–81. https://doi.org/10.1016/j.jmb.2004.09.077.

Horst, Reto, Eric B. Bertelsen, Jocelyne Fiaux, Gerhard Wider, Arthur L. Horwich, and Kurt Wüthrich. 2005. “Direct NMR Observation of a Substrate Protein Bound to the Chaperonin GroEL.” *Proceedings of the National Academy of Sciences* 102 (36): 12748–53. https://doi.org/10.1073/pnas.0505642102.

Horwich, Arthur L., Wayne A. Fenton, Eli Chapman, and George W. Farr. 2007. “Two Families of Chaperonin: Physiology and Mechanism.” *Annual Review of Cell and Developmental Biology* 23 (1): 115–45. https://doi.org/10.1146/annurev.cellbio.23.090506.123555.

Hsu, Ao-Lin, Coleen T. Murphy, and Cynthia Kenyon. 2003. “Regulation of Aging and Age-Related Disease by DAF-16 and Heat-Shock Factor.” *Science* 300 (5622): 1142–45. https://doi.org/10.1126/science.1083701.

Hu, Bin, Matthias P. Mayer, and Masaru Tomita. 2006. “Modeling Hsp70-Mediated Protein Folding.” *Biophysical Journal* 91 (2): 496–507. https://doi.org/10.1529/biophysj.106.083394.

Hua, Qing-xin, Satoe H. Nakagawa, Jill Wilken, Rowena R. Ramos, Wenhua Jia, Joseph Bass, and Michael A. Weiss. 2003. “A Divergent INS Protein in *Caenorhabditis Elegans* Structurally Resembles Human Insulin and Activates the Human Insulin Receptor.” *Genes & Development* 17 (7): 826–31. https://doi.org/10.1101/gad.1058003.

Huang, Linda, and Paul Sternberg. 2006. “Genetic Dissection of Developmental Pathways.” In *WormBook*, edited by The C. elegans Research Community. https://doi.org/10.1895/wormbook.1.88.2.

Hunt, John F., Arthur J. Weaver, Samuel J. Landry, Lila Gierasch, and Johann Deisenhofer. 1996. “The Crystal Structure of the GroES Co-Chaperonin at 2.8 Å Resolution.” *Nature* 379 (6560): 37–45. https://doi.org/10.1038/379037a0.

Iburg, Manuel, Dmytro Puchkov, Irving U. Rosas-Brugada, Linda Bergemann, Ulrike Rieprecht, and Janine Kirstein. 2020. “The Noncanonical Small Heat Shock Protein HSP-17 from Caenorhabditis Elegans Is a Selective Protein Aggregase.” *Journal of Biological Chemistry* 295 (10): 3064–79. https://doi.org/10.1074/jbc.RA119.011185.

Inoue, Tadao, Kazumasa Hirata, Yuichiro Kuwana, Masahiro Fujita, Johji Miwa, Richard Roy, and Yasunori Yamaguchi. 2006. “Cell Cycle Control by Daf-21/Hsp90 at the First Meiotic Prophase/Metaphase Boundary during Oogenesis in Caenorhabditis Elegans.” *Development, Growth and Differentiation* 48 (1): 25–32. https://doi.org/10.1111/j.1440-169X.2006.00841.x.

Jehle, Stefan, Breanna S. Vollmar, Benjamin Bardiaux, Katja K. Dove, Ponni Rajagopal, Tamir Gonen, Hartmut Oschkinat, and Rachel E. Klevit. 2011. “N-Terminal Domain of AB-Crystallin Provides a Conformational Switch for Multimerization and Structural Heterogeneity.” *Proceedings of the National Academy of Sciences* 108 (16): 6409–14. https://doi.org/10.1073/pnas.1014656108.

Jeong, Dae-Eun, Dongyeop Lee, Sun-Young Hwang, Yujin Lee, Jee-Eun Lee, Mihwa Seo, Wooseon Hwang, et al. 2017. “Mitochondrial Chaperone <scp>HSP</Scp> -60 Regulates Anti-bacterial

Immunity via P38 <scp>MAP</Scp> Kinase Signaling." *The EMBO Journal* 36 (8): 1046–65. https://doi.org/10.15252/embj.201694781.

Johnson, Jill L., and Celeste Brown. 2009. "Plasticity of the Hsp90 Chaperone Machine in Divergent Eukaryotic Organisms." *Cell Stress and Chaperones* 14 (1): 83–94. https://doi.org/10.1007/s12192-008-0058-9.

Jones, D, R H Russnak, R J Kay, and E P Candido. 1986. "Structure, Expression, and Evolution of a Heat Shock Gene Locus in *Caenorhabditis elegans* That Is Flanked by Repetitive Elements." *The Journal of Biological Chemistry* 261 (26): 12006–15.

Kaletta, Titus, and Michael O. Hengartner. 2006. "Finding Function in Novel Targets: *C. Elegans* as a Model Organism." *Nature Reviews Drug Discovery* 5 (5): 387–99. https://doi.org/10.1038/nrd2031.

Kampinga, Harm H., and Elizabeth A. Craig. 2010a. "The HSP70 Chaperone Machinery: J Proteins as Drivers of Functional Specificity." *Nature Reviews Molecular Cell Biology* 11 (8): 579–92. https://doi.org/10.1038/nrm2941.

Kanehisa, Minoru, Yoko Sato, Masayuki Kawashima, Miho Furumichi, and Mao Tanabe. 2016. "KEGG as a Reference Resource for Gene and Protein Annotation." *Nucleic Acids Research* 44 (D1): D457–62. https://doi.org/10.1093/nar/gkv1070.

Kappé, Guido, J. Andrew Aquilina, Lisa Wunderink, Bram Kamps, Carol v. Robinson, Teresa Garate, Wilbert C. Boelens, and Wilfried W. de Jong. 2004. "Tsp36, a Tapeworm Small Heat-Shock Protein with a Duplicated α-Crystallin Domain, Forms Dimers and Tetramers with Good Chaperone-like Activity." *Proteins: Structure, Function, and Bioinformatics* 57 (1): 109–17. https://doi.org/10.1002/prot.20220.

Kaushik, Susmita, and Ana Maria Cuervo. 2015. "Proteostasis and Aging." *Nature Medicine*. Nature Publishing Group. https://doi.org/10.1038/nm.4001.

Kazlauskas, Romas. 2018. "Engineering More Stable Proteins." *Chemical Society Reviews* 47 (24): 9026–45. https://doi.org/10.1039/c8cs00014j.

Kenyon, Cynthia, Jean Chang, Erin Gensch, Adam Rudner, and Ramon Tabtiang. 1993. "A *C. Elegans* Mutant That Lives Twice as Long as Wild Type." *Nature* 366 (6454): 461–64. https://doi.org/10.1038/366461a0.

Keramisanou, Dimitra, Adam Aboalroub, Ziming Zhang, Wenjun Liu, Devon Marshall, Andrea Diviney, Randy W. Larsen, Ralf Landgraf, and Ioannis Gelis. 2016. "Molecular Mechanism of Protein Kinase Recognition and Sorting by the Hsp90 Kinome-Specific Cochaperone Cdc37." *Molecular Cell* 62 (2): 260–71. https://doi.org/10.1016/j.molcel.2016.04.005.

Kim, Kyeong Kyu, Rosalind Kim, and Sung-Hou Kim. 1998. "Crystal Structure of a Small Heat-Shock Protein." *Nature* 394 (6693): 595–99. https://doi.org/10.1038/29106.

Kim, Woojin, Ryan S Underwood, Iva Greenwald, and Daniel D Shaye. 2018. "OrthoList 2: A New Comparative Genomic Analysis of Human and *Caenorhabditis Elegans* Genes." *Genetics* 210 (2): 445–61. https://doi.org/10.1534/genetics.118.301307.

Kirschke, Elaine, Devrishi Goswami, Daniel Southworth, Patrick R. Griffin, and David A. Agard. 2014. “Glucocorticoid Receptor Function Regulated by Coordinated Action of the Hsp90 and Hsp70 Chaperone Cycles.” *Cell* 157 (7): 1685–97. https://doi.org/10.1016/j.cell.2014.04.038.

Kirstein, Janine, Kristin Arnsburg, Annika Scior, Anna Szlachcic, D. Lys Guilbride, Richard I. Morimoto, Bernd Bukau, and Nadinath B. Nillegoda. 2017. “*In Vivo* Properties of the Disaggregase Function of J-proteins and Hsc70 in *Caenorhabditis Elegans* Stress and Aging.” *Aging Cell* 16 (6): 1414–24. https://doi.org/10.1111/acel.12686.

Kityk, Roman, Jürgen Kopp, and Matthias P. Mayer. 2018. “Molecular Mechanism of J-Domain-Triggered ATP Hydrolysis by Hsp70 Chaperones.” *Molecular Cell* 69 (2): 227-237.e4. https://doi.org/10.1016/j.molcel.2017.12.003.

Klevit, Rachel E. 2020. “Peeking from behind the Veil of Enigma: Emerging Insights on Small Heat Shock Protein Structure and Function.” *Cell Stress and Chaperones* 25 (4): 573–80. https://doi.org/10.1007/s12192-020-01092-2.

Kokke, Bas P.A., Michel R. Leroux, E.Peter M. Candido, Wilbert C. Boelens, and Wilfried W. de Jong. 1998a. “*Caenorhabditis Elegans* Small Heat-Shock Proteins Hsp12.2 and Hsp12.3 Form Tetramers and Have No Chaperone-like Activity.” *FEBS Letters* 433 (3): 228–32. https://doi.org/10.1016/S0014-5793(98)00917-X.

Kominek, Jacek, Jaroslaw Marszalek, Cécile Neuvéglise, Elizabeth A. Craig, and Barry L. Williams. 2013. “The Complex Evolutionary Dynamics of Hsp70s: A Genomic and Functional Perspective.” *Genome Biology and Evolution* 5 (12): 2460–77. https://doi.org/10.1093/gbe/evt192.

Konermann, Lars, Jingxi Pan, and Yu-Hong Liu. 2011. “Hydrogen Exchange Mass Spectrometry for Studying Protein Structure and Dynamics.” *Chem. Soc. Rev.* 40 (3): 1224–34. https://doi.org/10.1039/C0CS00113A.

Konstantinidis, Georgios, and Nektarios Tavernarakis. 2021. “Molecular Basis of Neuronal Autophagy in Ageing: Insights from Caenorhabditis Elegans.” *Cells* 10 (3): 694. https://doi.org/10.3390/cells10030694.

Kourtis, Nikos, Vassiliki Nikoletopoulou, and Nektarios Tavernarakis. 2012. “Small Heat-Shock Proteins Protect from Heat-Stroke-Associated Neurodegeneration.” *Nature* 490 (7419): 213–18. https://doi.org/10.1038/nature11417.

Kriehuber, Thomas, Thomas Rattei, Thomas Weinmaier, Alexander Bepperling, Martin Haslbeck, and Johannes Buchner. 2010a. “Independent Evolution of the Core Domain and Its Flanking Sequences in Small Heat Shock Proteins.” *The FASEB Journal* 24 (10): 3633–42. https://doi.org/10.1096/fj.10-156992.

Laemmli, U. K. 1970. “Cleavage of Structural Proteins during the Assembly of the Head of Bacteriophage T4.” *Nature* 227 (5259): 680–85. https://doi.org/10.1038/227680a0.

Langer, T., G. Pfeifer, J. Martin, W. Baumeister, and F.U. Hartl. 1992. “Chaperonin-Mediated Protein Folding: GroES Binds to One End of the GroEL Cylinder, Which Accommodates the Protein Substrate within Its Central Cavity.” *The EMBO Journal* 11 (13): 4757–65. https://doi.org/10.1002/j.1460-2075.1992.tb05581.x.

Larsen, Martin R., Morten B. Trelle, Tine E. Thingholm, and Ole N. Jensen. 2006. “Analysis of Posttranslational Modifications of Proteins by Tandem Mass Spectrometry.” *BioTechniques* 40 (6): 790–98. https://doi.org/10.2144/000112201.

Lau, Andy M, Jürgen Claesen, Kjetil Hansen, and Argyris Politis. 2021. “Deuteros 2.0: Peptide-Level Significance Testing of Data from Hydrogen Deuterium Exchange Mass Spectrometry.” *Bioinformatics* 37 (2): 270–72. https://doi.org/10.1093/bioinformatics/btaa677.

Laufen, Thomas, Matthias P. Mayer, Christian Beisel, Dagmar Klostermeier, Axel Mogk, Jochen Reinstein, and Bernd Bukau. 1999. “Mechanism of Regulation of Hsp70 Chaperones by DnaJ Cochaperones.” *Proceedings of the National Academy of Sciences* 96 (10): 5452–57. https://doi.org/10.1073/pnas.96.10.5452.

Lee, G. J., A.M. Roseman, H.R. Saibil, and E. Vierling. 1997. “A Small Heat Shock Protein Stably Binds Heat-Denatured Model Substrates and Can Maintain a Substrate in a Folding-Competent State.” *The EMBO Journal* 16 (3): 659–71. https://doi.org/10.1093/emboj/16.3.659.

Lee, Jihyun, and Junho Lee. 2013. “Hypoxia-Inducible Factor-1 (HIF-1)-Independent Hypoxia Response of the Small Heat Shock Protein Hsp-16.1 Gene Regulated by Chromatin-Remodeling Factors in the Nematode Caenorhabditis Elegans.” *Journal of Biological Chemistry* 288 (3): 1582–89. https://doi.org/10.1074/jbc.M112.401554.

Leiser, Scott F., Gholamali Jafari, Melissa Primitivo, George L. Sutphin, Jingyi Dong, Alison Leonard, Marissa Fletcher, and Matt Kaeberlein. 2016. “Age-Associated Vulval Integrity Is an Important Marker of Nematode Healthspan.” *AGE* 38 (5–6): 419–31. https://doi.org/10.1007/s11357-016-9936-8.

Leroux, M R., and Peter M. Candido. 1995. “Characterization of Four New *Tcp-1* -Related *Cct* Genes from the Nematode *Caenorhabditis Elegans*.” *DNA and Cell Biology* 14 (11): 951–60. https://doi.org/10.1089/dna.1995.14.951.

Leroux, Michel R., Ronald Melki, Bruce Gordon, Gérard Batelier, and E. Peter M. Candido. 1997. “Structure-Function Studies on Small Heat Shock Protein Oligomeric Assembly and Interaction with Unfolded Polypeptides.” *Journal of Biological Chemistry* 272 (39): 24646–56. https://doi.org/10.1074/jbc.272.39.24646.

Lespinet, Olivier, Yuri I. Wolf, Eugene v. Koonin, and L. Aravind. 2002. “The Role of Lineage-Specific Gene Family Expansion in the Evolution of Eukaryotes.” *Genome Research* 12 (7): 1048–59. https://doi.org/10.1101/gr.174302.

Letunic, Ivica, and Peer Bork. 2021. “Interactive Tree Of Life (ITOL) v5: An Online Tool for Phylogenetic Tree Display and Annotation.” *Nucleic Acids Research* 49 (W1): W293–96. https://doi.org/10.1093/nar/gkab301.

Li, Jian, Johnathan Labbadia, and Richard I. Morimoto. 2017. “Rethinking HSF1 in Stress, Development, and Organismal Health.” *Trends in Cell Biology* 27 (12): 895–905. https://doi.org/10.1016/j.tcb.2017.08.002.

Li, Jianbo, Jin Zhang, Huixia Jia, Yu Li, Xiangdong Xu, Lijuan Wang, and Mengzhu Lu. 2016. “The Populus Trichocarpa PtHSP17.8 Involved in Heat and Salt Stress Tolerances.” *Plant Cell Reports* 35 (8): 1587–99. https://doi.org/10.1007/s00299-016-1973-3.

Li, Wen-Jun, Chen-Wei Wang, Li Tao, Yong-Hong Yan, Mei-Jun Zhang, Ze-Xian Liu, Yu-Xin Li, et al. 2021. “Insulin Signaling Regulates Longevity through Protein Phosphorylation in *Caenorhabditis Elegans*.” *Nature Communications* 12 (1): 4568. https://doi.org/10.1038/s41467-021-24816-z.

Liu, Li, Rajani Srikakulam, and Donald A. Winkelmann. 2008. “Unc45 Activates Hsp90-Dependent Folding of the Myosin Motor Domain.” *Journal of Biological Chemistry* 283 (19): 13185–93. https://doi.org/10.1074/jbc.M800757200.

Liu, Peidang, Dan Li, Wenjie Li, and Dayong Wang. 2019. “Mitochondrial Unfolded Protein Response to Microgravity Stress in Nematode Caenorhabditis Elegans.” *Scientific Reports* 9 (1): 16474. https://doi.org/10.1038/s41598-019-53004-9.

Liu, Zhenying, Shengnan Zhang, Jinge Gu, Yilun Tong, Yichen Li, Xinrui Gui, Houfang Long, et al. 2020. “Hsp27 Chaperones FUS Phase Separation under the Modulation of Stress-Induced Phosphorylation.” *Nature Structural & Molecular Biology* 27 (4): 363–72. https://doi.org/10.1038/s41594-020-0399-3.

Los Rios, Paolo de, Anat Ben-Zvi, Olga Slutsky, Abdussalam Azem, and Pierre Goloubinoff. 2006. “Hsp70 Chaperones Accelerate Protein Translocation and the Unfolding of Stable Protein Aggregates by Entropic Pulling.” *Proceedings of the National Academy of Sciences* 103 (16): 6166–71. https://doi.org/10.1073/pnas.0510496103.

Lynch, Michael, and John S. Conery. 2000. “The Evolutionary Fate and Consequences of Duplicate Genes.” *Science* 290 (5494): 1151–55. https://doi.org/10.1126/science.290.5494.1151.

Mackenzie, Ian R., Alexandra M. Nicholson, Mohona Sarkar, James Messing, Maria D. Purice, Cyril Pottier, Kavya Annu, et al. 2017. “TIA1 Mutations in Amyotrophic Lateral Sclerosis and Frontotemporal Dementia Promote Phase Separation and Alter Stress Granule Dynamics.” *Neuron* 95 (4): 808-816.e9. https://doi.org/10.1016/j.neuron.2017.07.025.

Mainz, Andi, Jirka Peschek, Maria Stavropoulou, Katrin C Back, Benjamin Bardiaux, Sam Asami, Elke Prade, et al. 2015. “The Chaperone AB-Crystallin Uses Different Interfaces to Capture an Amorphous and an Amyloid Client.” *Nature Structural & Molecular Biology* 22 (11): 898–905. https://doi.org/10.1038/nsmb.3108.

Mallik, Saurav, Dan S Tawfik, and Emmanuel D Levy. 2022. “How Gene Duplication Diversifies the Landscape of Protein Oligomeric State and Function.” *Current Opinion in Genetics & Development* 76 (October): 101966. https://doi.org/10.1016/j.gde.2022.101966.

Marques, Ana C, Nicolas Vinckenbosch, David Brawand, and Henrik Kaessmann. 2008. “Functional Diversification of Duplicate Genes through Subcellular Adaptation of Encoded Proteins.” *Genome Biology* 9 (3): R54. https://doi.org/10.1186/gb-2008-9-3-r54.

Masson, Glenn R., John E. Burke, Natalie G. Ahn, Ganesh S. Anand, Christoph Borchers, Sébastien Brier, George M. Bou-Assaf, et al. 2019. “Recommendations for Performing, Interpreting and Reporting Hydrogen Deuterium Exchange Mass Spectrometry (HDX-MS) Experiments.” *Nature Methods* 16 (7): 595–602. https://doi.org/10.1038/s41592-019-0459-y.

McClellan, Amie J., Melissa D. Scott, and Judith Frydman. 2005. “Folding and Quality Control of the VHL Tumor Suppressor Proceed through Distinct Chaperone Pathways.” *Cell* 121 (5): 739–48. https://doi.org/10.1016/j.cell.2005.03.024.

McLaughlin, Stephen H., Frank Sobott, Zhong-ping Yao, Wei Zhang, Peter R. Nielsen, J. Günter Grossmann, Ernest D. Laue, Carol v. Robinson, and Sophie E. Jackson. 2006. "The Co-Chaperone P23 Arrests the Hsp90 ATPase Cycle to Trap Client Proteins." *Journal of Molecular Biology* 356 (3): 746–58. https://doi.org/10.1016/j.jmb.2005.11.085.

Meister-Broekema, Melanie, Rebecca Freilich, Chandhuru Jagadeesan, Jennifer N. Rauch, Rocio Bengoechea, William W. Motley, E. F. Elsiena Kuiper, et al. 2018. "Myopathy Associated BAG3 Mutations Lead to Protein Aggregation by Stalling Hsp70 Networks." *Nature Communications* 9 (1): 5342. https://doi.org/10.1038/s41467-018-07718-5.

Mendillo, Marc L., Sandro Santagata, Martina Koeva, George W. Bell, Rong Hu, Rulla M. Tamimi, Ernest Fraenkel, Tan A. Ince, Luke Whitesell, and Susan Lindquist. 2012. "HSF1 Drives a Transcriptional Program Distinct from Heat Shock to Support Highly Malignant Human Cancers." *Cell* 150 (3): 549–62. https://doi.org/10.1016/j.cell.2012.06.031.

Micsonai, András, Éva Bulyáki, and József Kardos. 2021. "BeStSel: From Secondary Structure Analysis to Protein Fold Prediction by Circular Dichroism Spectroscopy." In , 175–89. https://doi.org/10.1007/978-1-0716-0892-0_11.

Micsonai, András, Frank Wien, Linda Kernya, Young-Ho Lee, Yuji Goto, Matthieu Réfrégiers, and József Kardos. 2015. "Accurate Secondary Structure Prediction and Fold Recognition for Circular Dichroism Spectroscopy." *Proceedings of the National Academy of Sciences* 112 (24). https://doi.org/10.1073/pnas.1500851112.

Middleton, Ryan C., and Eric A. Shelden. 2013. "Small Heat Shock Protein HSPB1 Regulates Growth of Embryonic Zebrafish Craniofacial Muscles." *Experimental Cell Research* 319 (6): 860–74. https://doi.org/10.1016/j.yexcr.2013.01.002.

Mitchell, D. H., J. W. Stiles, J. Santelli, and D. R. Sanadi. 1979. "Synchronous Growth and Aging of Caenorhabditis Elegans in the Presence of Fluorodeoxyuridine." *Journal of Gerontology* 34 (1): 28–36. https://doi.org/10.1093/geronj/34.1.28.

Mogk, Axel, and Bernd Bukau. 2017. "Role of SHsps in Organizing Cytosolic Protein Aggregation and Disaggregation." *Cell Stress and Chaperones*. Cell Stress and Chaperones. https://doi.org/10.1007/s12192-017-0762-4.

Mogk, Axel, Christian Schlieker, Kenneth L. Friedrich, Hans-Joachim Schönfeld, Elizabeth Vierling, and Bernd Bukau. 2003. "Refolding of Substrates Bound to Small Hsps Relies on a Disaggregation Reaction Mediated Most Efficiently by ClpB/DnaK." *Journal of Biological Chemistry* 278 (33): 31033–42. https://doi.org/10.1074/jbc.M303587200.

Molliex, Amandine, Jamshid Temirov, Jihun Lee, Maura Coughlin, Anderson P. Kanagaraj, Hong Joo Kim, Tanja Mittag, and J. Paul Taylor. 2015. "Phase Separation by Low Complexity Domains Promotes Stress Granule Assembly and Drives Pathological Fibrillization." *Cell* 163 (1): 123–33. https://doi.org/10.1016/j.cell.2015.09.015.

Montfort, Rob L. M. van, Eman Basha, Kenneth L. Friedrich, Christine Slingsby, and Elizabeth Vierling. 2001. "Crystal Structure and Assembly of a Eukaryotic Small Heat Shock Protein." *Nature Structural Biology* 8 (12): 1025–30. https://doi.org/10.1038/nsb722.

Morelli, Federica F., Dineke S. Verbeek, Jessika Bertacchini, Jonathan Vinet, Laura Mediani, Sandra Marmiroli, Giovanna Cenacchi, et al. 2017. "Aberrant Compartment Formation by HSPB2

Mislocalizes Lamin A and Compromises Nuclear Integrity and Function." *Cell Reports* 20 (9): 2100–2115. https://doi.org/10.1016/j.celrep.2017.08.018.

Morley, James F., and Richard I. Morimoto. 2004. "Regulation of Longevity in *Caenorhabditis Elegans* by Heat Shock Factor and Molecular Chaperones." *Molecular Biology of the Cell* 15 (2): 657–64. https://doi.org/10.1091/mbc.e03-07-0532.

Morrow, Geneviève, Yutaka Inaguma, Kanefusa Kato, and Robert M. Tanguay. 2000. "The Small Heat Shock Protein Hsp22 of Drosophila Melanogaster Is a Mitochondrial Protein Displaying Oligomeric Organization." *Journal of Biological Chemistry* 275 (40): 31204–10. https://doi.org/10.1074/jbc.M002960200.

Mühlhofer, Moritz, Carsten Peters, Thomas Kriehuber, Marina Kreuzeder, Pamina Kazman, Natalia Rodina, Bernd Reif, Martin Haslbeck, Sevil Weinkauf, and Johannes Buchner. 2021. "Phosphorylation Activates the Yeast Small Heat Shock Protein Hsp26 by Weakening Domain Contacts in the Oligomer Ensemble." *Nature Communications* 12 (1): 6697. https://doi.org/10.1038/s41467-021-27036-7.

Muñoz-Lobato, Fernando, María Jesús Rodríguez-Palero, Francisco José Naranjo-Galindo, Freya Shephard, Christopher J. Gaffney, Nathaniel J. Szewczyk, Shusei Hamamichi, et al. 2014. "Protective Role of DNJ-27/ERdj5 in *Caenorhabditis Elegans* Models of Human Neurodegenerative Diseases." *Antioxidants & Redox Signaling* 20 (2): 217–35. https://doi.org/10.1089/ars.2012.5051.

Mymrikov, Evgeny v., Marina Daake, Bettina Richter, Martin Haslbeck, and Johannes Buchner. 2017. "The Chaperone Activity and Substrate Spectrum of Human Small Heat Shock Proteins." *Journal of Biological Chemistry* 292 (2): 672–84. https://doi.org/10.1074/jbc.M116.760413.

Mymrikov, Evgeny v., Mareike Riedl, Carsten Peters, Sevil Weinkauf, Martin Haslbeck, and Johannes Buchner. 2020. "Regulation of Small Heat-Shock Proteins by Hetero-Oligomer Formation." *Journal of Biological Chemistry* 295 (1): 158–69. https://doi.org/10.1074/jbc.RA119.011143.

Nehrke, Keith. 2003. "A Reduction in Intestinal Cell PHi Due to Loss of the *Caenorhabditis Elegans* Na+/H+ Exchanger NHX-2 Increases Life Span." *Journal of Biological Chemistry* 278 (45): 44657–66. https://doi.org/10.1074/jbc.M307351200.

Nikolaidis, Nikolas, and Masatoshi Nei. 2004. "Concerted and Nonconcerted Evolution of the Hsp70 Gene Superfamily in Two Sibling Species of Nematodes." *Molecular Biology and Evolution* 21 (3): 498–505. https://doi.org/10.1093/molbev/msh041.

Nillegoda, Nadinath B., Janine Kirstein, Anna Szlachcic, Mykhaylo Berynskyy, Antonia Stank, Florian Stengel, Kristin Arnsburg, et al. 2015a. "Crucial HSP70 Co-Chaperone Complex Unlocks Metazoan Protein Disaggregation." *Nature* 524 (7564): 247–51. https://doi.org/10.1038/nature14884.

Pagliuso, Delaney C., Devavrat M. Bodas, and Amy E. Pasquinelli. 2021. "Recovery from Heat Shock Requires the MicroRNA Pathway in Caenorhabditis Elegans." *PLOS Genetics* 17 (8): e1009734. https://doi.org/10.1371/journal.pgen.1009734.

Papsdorf, Katharina, Julia Sacherl, and Klaus Richter. 2014. “The Balanced Regulation of Hsc70 by DNJ-13 and UNC-23 Is Required for Muscle Functionality.” *Journal of Biological Chemistry* 289 (36): 25250–61. https://doi.org/10.1074/jbc.M114.565234.

Peña, Salvador, Teresa Sherman, Paul S. Brookes, and Keith Nehrke. 2016. “The Mitochondrial Unfolded Protein Response Protects against Anoxia in Caenorhabditis Elegans.” *PLOS ONE* 11 (7): e0159989. https://doi.org/10.1371/journal.pone.0159989.

Peter, E., and M. Candido. 2002. “The Small Heat Shock Proteins of the Nematode Caenorhabditis Elegans: Structure, Regulation and Biology.” In , 61–78. https://doi.org/10.1007/978-3-642-56348-5_4.

Piñero González, Janet, Olimpia Carrillo Farnés, Ana Tereza R. Vasconcelos, and Abel González Pérez. 2009. “Conservation of Key Members in the Course of the Evolution of the Insulin Signaling Pathway.” *Biosystems* 95 (1): 7–16. https://doi.org/10.1016/j.biosystems.2008.06.003.

Porta-de-la-Riva, Montserrat, Laura Fontrodona, Alberto Villanueva, and Julián Cerón. 2012. “Basic & *Caenorhabditis Elegans* Methods: Synchronization and Observation.” *Journal of Visualized Experiments*, no. 64 (June). https://doi.org/10.3791/4019.

Powers, Evan T., Richard I. Morimoto, Andrew Dillin, Jeffery W. Kelly, and William E. Balch. 2009. “Biological and Chemical Approaches to Diseases of Proteostasis Deficiency.” *Annual Review of Biochemistry*. https://doi.org/10.1146/annurev.biochem.052308.114844.

Protter, David S.W., and Roy Parker. 2016. “Principles and Properties of Stress Granules.” *Trends in Cell Biology* 26 (9): 668–79. https://doi.org/10.1016/j.tcb.2016.05.004.

Qian, Hong, Xiangru Xu, and Laura E. Niklason. 2015. “Bmk-1 Regulates Lifespan in *Caenorhabditis Elegans* by Activating Hsp-16.” *Oncotarget* 6 (22): 18790–99. https://doi.org/10.18632/oncotarget.4618.

Rahman, Mizanur, Hunter Edwards, Nikolajs Birze, Rebecca Gabrilska, Kendra P. Rumbaugh, Jerzy Blawzdziewicz, Nathaniel J. Szewczyk, Monica Driscoll, and Siva A. Vanapalli. 2020. “NemaLife Chip: A Micropillar-Based Microfluidic Culture Device Optimized for Aging Studies in Crawling C. Elegans.” *Scientific Reports* 10 (1): 16190. https://doi.org/10.1038/s41598-020-73002-6.

Ramsøe, Abigail, Melody S. Clark, and Victoria A. Sleight. 2020. “Gene Network Analyses Support Subfunctionalization Hypothesis for Duplicated Hsp70 Genes in the Antarctic Clam.” *Cell Stress and Chaperones* 25 (6): 1111–16. https://doi.org/10.1007/s12192-020-01118-9.

Rappsilber, Juri, Matthias Mann, and Yasushi Ishihama. 2007. “Protocol for Micro-Purification, Enrichment, Pre-Fractionation and Storage of Peptides for Proteomics Using StageTips.” *Nature Protocols* 2 (8): 1896–1906. https://doi.org/10.1038/nprot.2007.261.

Reddy, G.Bhanuprakash, Kali P. Das, J.Mark Petrash, and Witold K. Surewicz. 2000. “Temperature-Dependent Chaperone Activity and Structural Properties of Human AA- and AB-Crystallins.” *Journal of Biological Chemistry* 275 (7): 4565–70. https://doi.org/10.1074/jbc.275.7.4565.

Reinle, Kevin, Axel Mogk, and Bernd Bukau. 2022. “The Diverse Functions of Small Heat Shock Proteins in the Proteostasis Network.” *Journal of Molecular Biology* 434 (1): 167157. https://doi.org/10.1016/j.jmb.2021.167157.

Riback, Joshua, Pawel Laskowski, Jamie L. Scott, Edward W.J. Wallace, Alexandra E. Rojek, Michael H. Schwartz, Tobin R. Sosnick, and D. Allan Drummond. 2015. "Heat Shock Triggers Assembly of TRNA Synthetases into an Active Supercomplex." *Biophysical Journal* 108 (2): 221a. https://doi.org/10.1016/j.bpj.2014.11.1219.

Richter, Klaus, Paul Muschler, Otmar Hainzl, and Johannes Buchner. 2001. "Coordinated ATP Hydrolysis by the Hsp90 Dimer." *Journal of Biological Chemistry* 276 (36): 33689–96. https://doi.org/10.1074/jbc.M103832200.

Richter, Klaus, Paul Muschler, Otmar Hainzl, Jochen Reinstein, and Johannes Buchner. 2003. "Sti1 Is a Non-Competitive Inhibitor of the Hsp90 ATPase." *Journal of Biological Chemistry* 278 (12): 10328–33. https://doi.org/10.1074/jbc.M213094200.

Riedl, Mareike, Annika Strauch, Dragana A.M. Catici, and Martin Haslbeck. 2020. "Proteinaceous Transformers: Structural and Functional Variability of Human SHsps." *International Journal of Molecular Sciences* 21 (15): 5448. https://doi.org/10.3390/ijms21155448.

Ritossa, F. 1962. "A New Puffing Pattern Induced by Temperature Shock and DNP in Drosophila." *Experientia* 18 (12): 571–73. https://doi.org/10.1007/BF02172188.

Roh, Ji-Yeon, Junho Lee, and Jinhee Choi. 2006. "Assessment of Stress-Related Gene Expression In The Heavy Metal–Exposed Nematode *Caenorhabditis Elegans*: A Potential Biomarker For Metal-Induced Toxicity Monitoring And Environmental Risk Assessment." *Environmental Toxicology and Chemistry* 25 (11): 2946. https://doi.org/10.1897/05-676R.1.

Röhl, Alina, Daniela Wengler, Tobias Madl, Stephan Lagleder, Franziska Tippel, Monika Herrmann, Jelle Hendrix, et al. 2015. "Hsp90 Regulates the Dynamics of Its Cochaperone Sti1 and the Transfer of Hsp70 between Modules." *Nature Communications* 6 (1): 6655. https://doi.org/10.1038/ncomms7655.

Rosenzweig, Rina, Nadinath B. Nillegoda, Matthias P. Mayer, and Bernd Bukau. 2019. "The Hsp70 Chaperone Network." *Nature Reviews Molecular Cell Biology* 20 (11): 665–80. https://doi.org/10.1038/s41580-019-0133-3.

Rubin, Gerald M, Mark D Yandell, Jennifer R Wortman, George L Gabor Miklos, Catherine R Nelson, Iswar K Hariharan, Mark E Fortini, et al. 2000. "Comparative Genomics of the Eukaryotes." *Science*. Vol. 287.

Rusmini, Paola, Riccardo Cristofani, Mariarita Galbiati, Maria E. Cicardi, Marco Meroni, Veronica Ferrari, Giulia Vezzoli, et al. 2017. "The Role of the Heat Shock Protein B8 (HSPB8) in Motoneuron Diseases." *Frontiers in Molecular Neuroscience* 10 (June). https://doi.org/10.3389/fnmol.2017.00176.

Russnak, R H, and E P Candido. 1985. "Locus Encoding a Family of Small Heat Shock Genes in *Caenorhabditis Elegans*: Two Genes Duplicated to Form a 3.8-Kilobase Inverted Repeat." *Molecular and Cellular Biology* 5 (6): 1268–78. https://doi.org/10.1128/mcb.5.6.1268-1278.1985.

Saegusa, Keiko, Miyuki Sato, Katsuya Sato, Junko Nakajima-Shimada, Akihiro Harada, and Ken Sato. 2014. "*Caenorhabditis Elegans* Chaperonin CCT/TRiC Is Required for Actin and Tubulin Biogenesis and Microvillus Formation in Intestinal Epithelial Cells." *Molecular Biology of the Cell* 25 (20): 3095–3104. https://doi.org/10.1091/mbc.e13-09-0530.

Saibil, Helen. 2013. “Chaperone Machines for Protein Folding, Unfolding and Disaggregation.” *Nature Reviews Molecular Cell Biology* 14 (10): 630–42. https://doi.org/10.1038/nrm3658.

Samant, Rahul S., and Judith Frydman. 2019. “Methods for Measuring Misfolded Protein Clearance in the Budding Yeast *Saccharomyces Cerevisiae*.” In *Methods in Enzymology*, 619:27–45. Academic Press Inc. https://doi.org/10.1016/bs.mie.2018.12.039.

Schiene-Fischer, Cordelia. 2015. “Multidomain Peptidyl Prolyl Cis/Trans Isomerases.” *Biochimica et Biophysica Acta (BBA) - General Subjects* 1850 (10): 2005–16. https://doi.org/10.1016/j.bbagen.2014.11.012.

Schmauder, Lukas, and Klaus Richter. 2021. “Hsp-90 and Unc-45 Depletion Induce Characteristic Transcriptional Signatures in Coexpression Cliques of C. Elegans.” *Scientific Reports* 11 (1): 12852. https://doi.org/10.1038/s41598-021-91690-6.

Schmauder, Lukas, Siyuan Sima, Amira ben Hadj, Ricardo Cesar, and Klaus Richter. 2022. “Binding of the HSF-1 DNA-Binding Domain to Multimeric *C. Elegans* Consensus HSEs Is Guided by Cooperative Interactions.” *Scientific Reports* 12 (1): 8984. https://doi.org/10.1038/s41598-022-12736-x.

Schneider, Markus, Mathias Rosam, Manuel Glaser, Atanas Patronov, Harpreet Shah, Katrin Christiane Back, Marina Angelika Daake, Johannes Buchner, and Iris Antes. 2016. “BiPPred: Combined Sequence- and Structure-Based Prediction of Peptide Binding to the Hsp70 Chaperone BiP.” *Proteins: Structure, Function, and Bioinformatics* 84 (10): 1390–1407. https://doi.org/10.1002/prot.25084.

Schopf, Florian H., Maximilian M. Biebl, and Johannes Buchner. 2017. “The HSP90 Chaperone Machinery.” *Nature Reviews Molecular Cell Biology* 18 (6): 345–60. https://doi.org/10.1038/nrm.2017.20.

Sedaghatmehr, Mastoureh, Venkatesh P. Thirumalaikumar, Iman Kamranfar, Anne Marmagne, Celine Masclaux-Daubresse, and Salma Balazadeh. 2019. “A Regulatory Role of Autophagy for Resetting the Memory of Heat Stress in Plants.” *Plant, Cell & Environment* 42 (3): 1054–64. https://doi.org/10.1111/pce.13426.

Sekhar, Ashok, and Lewis E Kay. 2019. “An NMR View of Protein Dynamics in Health and Disease.” https://doi.org/10.1146/annurev-biophys-052118.

Seo, Keunhee, Eunseok Choi, Dongyeop Lee, Dae-Eun Jeong, Sung Key Jang, and Seung-Jae Lee. 2013. “Heat Shock Factor 1 Mediates the Longevity Conferred by Inhibition of TOR and Insulin/IGF-1 Signaling Pathways in *C. Elegans*.” *Aging Cell* 12 (6): 1073–81. https://doi.org/10.1111/acel.12140.

Servello, Francesco A., and Javier Apfeld. 2020. “The Heat Shock Transcription Factor HSF-1 Protects *Caenorhabditis Elegans* from Peroxide Stress.” *Translational Medicine of Aging* 4: 88–92. https://doi.org/10.1016/j.tma.2020.07.002.

Shannon, Paul, Andrew Markiel, Owen Ozier, Nitin S Baliga, Jonathan T Wang, Daniel Ramage, Nada Amin, Benno Schwikowski, and Trey Ideker. 2003. “Cytoscape: A Software Environment for Integrated Models of Biomolecular Interaction Networks.” *Genome Research* 13 (11): 2498–2504. https://doi.org/10.1101/gr.1239303.

Shaye, Daniel D., and Iva Greenwald. 2011. “OrthoList: A Compendium of C. Elegans Genes with Human Orthologs.” *PLoS ONE* 6 (5): e20085. https://doi.org/10.1371/journal.pone.0020085.

Shemesh, Netta, Juman Jubran, Shiran Dror, Eyal Simonovsky, Omer Basha, Chanan Argov, Idan Hekselman, et al. 2021. “The Landscape of Molecular Chaperones across Human Tissues Reveals a Layered Architecture of Core and Variable Chaperones.” *Nature Communications* 12 (1): 2180. https://doi.org/10.1038/s41467-021-22369-9.

Shen, Koning, and Judith Frydman. 2013. “The Interplay between the Chaperonin TRiC and N-Terminal Region of Huntingtin Mediates Huntington’s Disease Aggregation and Pathogenesis.” In , 121–32. https://doi.org/10.1007/978-3-642-27928-7_10.

Shiau, Andrew K., Seth F. Harris, Daniel R. Southworth, and David A. Agard. 2006a. “Structural Analysis of E. Coli Hsp90 Reveals Dramatic Nucleotide-Dependent Conformational Rearrangements.” *Cell* 127 (2): 329–40. https://doi.org/10.1016/j.cell.2006.09.027.

Shim, Jaegal, Seol Hee Im, and Junho Lee. 2003. “Tissue-Specific Expression, Heat Inducibility, and Biological Roles of Two *Hsp16* Genes in *Caenorhabditis Elegans*.” *FEBS Letters* 537 (1–3): 139–45. https://doi.org/10.1016/S0014-5793(03)00111-X.

Singh, Bhairab N., K. Sridhar Rao, and Ch Mohan Rao. 2010. “Ubiquitin–Proteasome-Mediated Degradation and Synthesis of MyoD Is Modulated by AB-Crystallin, a Small Heat Shock Protein, during Muscle Differentiation.” *Biochimica et Biophysica Acta (BBA) - Molecular Cell Research* 1803 (2): 288–99. https://doi.org/10.1016/j.bbamcr.2009.11.009.

Sinha, Ankit, and Matthias Mann. 2020. “A Beginner’s Guide to Mass Spectrometry–Based Proteomics.” *The Biochemist* 42 (5): 64–69. https://doi.org/10.1042/BIO20200057.

Sinitcyn, Pavel, Jan Daniel Rudolph, and Jürgen Cox. 2018. “Computational Methods for Understanding Mass Spectrometry–Based Shotgun Proteomics Data.” *Annual Review of Biomedical Data Science* 1 (1): 207–34. https://doi.org/10.1146/annurev-biodatasci-080917-013516.

Smith, P.K., R.I. Krohn, G.T. Hermanson, A.K. Mallia, F.H. Gartner, M.D. Provenzano, E.K. Fujimoto, N.M. Goeke, B.J. Olson, and D.C. Klenk. 1985. “Measurement of Protein Using Bicinchoninic Acid.” *Analytical Biochemistry* 150 (1): 76–85. https://doi.org/10.1016/0003-2697(85)90442-7.

Sobott, Frank, Justin L.P. Benesch, Elizabeth Vierling, and Carol v. Robinson. 2002. “Subunit Exchange of Multimeric Protein Complexes.” *Journal of Biological Chemistry* 277 (41): 38921–29. https://doi.org/10.1074/jbc.M206060200.

Somogyvári, Milán, Eszter Gecse, and Csaba Sőti. 2018. “DAF-21/Hsp90 Is Required for C. Elegans Longevity by Ensuring DAF-16/FOXO Isoform A Function.” *Scientific Reports* 8 (1): 12048. https://doi.org/10.1038/s41598-018-30592-6.

Specht, Sebastian, Stephanie B.M. Miller, Axel Mogk, and Bernd Bukau. 2011. “Hsp42 Is Required for Sequestration of Protein Aggregates into Deposition Sites in Saccharomyces Cerevisiae.” *Journal of Cell Biology* 195 (4): 617–29. https://doi.org/10.1083/jcb.201106037.

Srinivasan, Sharan R., Anne T. Gillies, Lyra Chang, Andrea D. Thompson, and Jason E. Gestwicki. 2012. “Molecular Chaperones DnaK and DnaJ Share Predicted Binding Sites on Most Proteins

in the E. Coli Proteome." *Molecular BioSystems* 8 (9): 2323. https://doi.org/10.1039/c2mb25145k.

Stamler, Robin, Guido Kappé, Wilbert Boelens, and Christine Slingsby. 2005. "Wrapping the α-Crystallin Domain Fold in a Chaperone Assembly." *Journal of Molecular Biology* 353 (1): 68–79. https://doi.org/10.1016/j.jmb.2005.08.025.

Stromer, Thusnelda, Monika Ehrnsperger, Matthias Gaestel, and Johannes Buchner. 2003. "Analysis of the Interaction of Small Heat Shock Proteins with Unfolding Proteins." *Journal of Biological Chemistry* 278 (20): 18015–21. https://doi.org/10.1074/jbc.M301640200.

Studer, Sonja, Markus Obrist, Nicolas Lentze, and Franz Narberhaus. 2002. "A Critical Motif for Oligomerization and Chaperone Activity of Bacterial α-Heat Shock Proteins." *European Journal of Biochemistry* 269 (14): 3578–86. https://doi.org/10.1046/j.1432-1033.2002.03049.x.

Sugiyama, Yuki, Atsushi Suzuki, Masaru Kishikawa, Rika Akutsu, Tomonori Hirose, Mary M.Y. Waye, Stephan K.W. Tsui, Shosei Yoshida, and Shigeo Ohno. 2000a. "Muscle Develops a Specific Form of Small Heat Shock Protein Complex Composed of MKBP/HSPB2 and HSPB3 during Myogenic Differentiation." *Journal of Biological Chemistry* 275 (2): 1095–1104. https://doi.org/10.1074/jbc.275.2.1095.

Sun, Li, Franziska T. Edelmann, Christoph J. O. Kaiser, Katharina Papsdorf, Andreas M. Gaiser, and Klaus Richter. 2012. "The Lid Domain of Caenorhabditis Elegans Hsc70 Influences ATP Turnover, Cofactor Binding and Protein Folding Activity." *PLoS ONE* 7 (3): e33980. https://doi.org/10.1371/journal.pone.0033980.

Sun, Yu, and Thomas H. MacRae. 2005. "The Small Heat Shock Proteins and Their Role in Human Disease." *FEBS Journal* 272 (11): 2613–27. https://doi.org/10.1111/j.1742-4658.2005.04708.x.

Sural, Surojit, Tzu-Chiao Lu, Seung Ah Jung, and Ao-Lin Hsu. 2019. "HSB-1 Inhibition and HSF-1 Overexpression Trigger Overlapping Transcriptional Changes to Promote Longevity in *Caenorhabditis Elegans*." *G3 Genes|Genomes|Genetics* 9 (5): 1679–92. https://doi.org/10.1534/g3.119.400044.

Taipale, Mikko, Daniel F. Jarosz, and Susan Lindquist. 2010a. "HSP90 at the Hub of Protein Homeostasis: Emerging Mechanistic Insights." *Nature Reviews Molecular Cell Biology* 11 (7): 515–28. https://doi.org/10.1038/nrm2918.

Taipale, Mikko, Irina Krykbaeva, Martina Koeva, Can Kayatekin, Kenneth D. Westover, Georgios I. Karras, and Susan Lindquist. 2012. "Quantitative Analysis of Hsp90-Client Interactions Reveals Principles of Substrate Recognition." *Cell* 150 (5): 987–1001. https://doi.org/10.1016/j.cell.2012.06.047.

Takeda, Shigeki, and David B. McKay. 1996. "Kinetics of Peptide Binding to the Bovine 70 KDa Heat Shock Cognate Protein, a Molecular Chaperone." *Biochemistry* 35 (14): 4636–44. https://doi.org/10.1021/bi952903o.

Thiyagarajan, P, SJ Henderson, and A Joachimiak. 1996. "Solution Structures of GroEL and Its Complex with Rhodanese from Small-Angle Neutron Scattering." *Structure* 4 (1): 79–88. https://doi.org/10.1016/S0969-2126(96)00011-1.

Tittelmeier, Jessica, Carl Alexander Sandhof, Heidrun Maja Ries, Silke Druffel-Augustin, Axel Mogk, Bernd Bukau, and Carmen Nussbaum-Krammer. 2020. “The HSP110/HSP70 Disaggregation System Generates Spreading-competent Toxic A-synuclein Species.” *The EMBO Journal* 39 (13). https://doi.org/10.15252/embj.2019103954.

Vendredy, Leen, Elias Adriaenssens, and Vincent Timmerman. 2020. “Small Heat Shock Proteins in Neurodegenerative Diseases.” *Cell Stress and Chaperones* 25 (4): 679–99. https://doi.org/10.1007/s12192-020-01101-4.

Venugopal, Bhuvarahamurthy, Nicholas T. Mesires, John C. Kennedy, Cyntia Curcio-Morelli, Janice M. LaPlante, J. Fred Dice, and Susan A. Slaugenhaupt. 2009. “Chaperone-Mediated Autophagy Is Defective in Mucolipidosis Type IV.” *Journal of Cellular Physiology* 219 (2): 344–53. https://doi.org/10.1002/jcp.21676.

Venyaminov, Sergei Yu., and Jen Tsi Yang. 1996. “Determination of Protein Secondary Structure.” In *Circular Dichroism and the Conformational Analysis of Biomolecules*, 69–107. Boston, MA: Springer US. https://doi.org/10.1007/978-1-4757-2508-7_3.

Voellmy, Richard, and Frank Boellmann. 2007. “Chaperone Regulation of the Heat Shock Protein Response.” In *Molecular Aspects of the Stress Response: Chaperones, Membranes and Networks*, 89–99. New York, NY: Springer New York. https://doi.org/10.1007/978-0-387-39975-1_9.

Walther, Dirk M., Prasad Kasturi, Min Zheng, Stefan Pinkert, Giulia Vecchi, Prajwal Ciryam, Richard I. Morimoto, et al. 2015. “Widespread Proteome Remodeling and Aggregation in Aging C. Elegans.” *Cell* 161 (4): 919–32. https://doi.org/10.1016/j.cell.2015.03.032.

Waters, Elizabeth R., and Elizabeth Vierling. 2020. “Plant Small Heat Shock Proteins – Evolutionary and Functional Diversity.” *New Phytologist* 227 (1): 24–37. https://doi.org/10.1111/nph.16536.

Whittaker, Charles A., and Richard O. Hynes. 2002. “Distribution and Evolution of von Willebrand/Integrin A Domains: Widely Dispersed Domains with Roles in Cell Adhesion and Elsewhere.” *Molecular Biology of the Cell* 13 (10): 3369–87. https://doi.org/10.1091/mbc.e02-05-0259.

Wintrode, Patrick L., Kenneth L. Friedrich, Elizabeth Vierling, Jean B. Smith, and David L. Smith. 2003. “Solution Structure and Dynamics of a Heat Shock Protein Assembly Probed by Hydrogen Exchange and Mass Spectrometry.” *Biochemistry* 42 (36): 10667–73. https://doi.org/10.1021/bi034117m.

Woollard, Alison. 2005. “Gene Duplications and Genetic Redundancy in *C. Elegans*.” *WormBook*. https://doi.org/10.1895/wormbook.1.2.1.

“WormBase.” 2022. 2022. https://wormbase.org/#012-34-5.

Yang, Jiao, Yinong Zong, Jiayue Su, Hongtao Li, Huanyu Zhu, Linda Columbus, Lei Zhou, and Qinglian Liu. 2017. “Conformation Transitions of the Polypeptide-Binding Pocket Support an Active Substrate Release from Hsp70s.” *Nature Communications* 8 (1): 1201. https://doi.org/10.1038/s41467-017-01310-z.

Yemini, Eviatar, Tadas Jucikas, Laura J Grundy, André E X Brown, and William R Schafer. 2013. “A Database of *Caenorhabditis Elegans* Behavioral Phenotypes.” *Nature Methods* 10 (9): 877–79. https://doi.org/10.1038/nmeth.2560.

Yokoyama, Ken, Keiji Fukumoto, Tatsuya Murakami, Shin-ichi Harada, Ryuji Hosono, Renu Wadhwa, Youji Mitsui, and Shoji Ohkuma. 2002. “Extended Longevity of *Caenorhabditis Elegans* by Knocking in Extra Copies of Hsp70F, a Homolog of Mot-2 (Mortalin)/Mthsp70/Grp75.” *FEBS Letters* 516 (1–3): 53–57. https://doi.org/10.1016/S0014-5793(02)02470-5.

Yoon, A-Rum, Renu Wadhwa, Sunil C Kaul, and Chae-Ok Yun. 2022. “Why Is Mortalin a Potential Therapeutic Target for Cancer?” *Frontiers in Cell and Developmental Biology* 10 (June). https://doi.org/10.3389/fcell.2022.914540.

Yu, Haiyuan, Nicholas M. Luscombe, Hao Xin Lu, Xiaowei Zhu, Yu Xia, Jing-Dong J. Han, Nicolas Bertin, Sambath Chung, Marc Vidal, and Mark Gerstein. 2004. “Annotation Transfer Between Genomes: Protein–Protein Interologs and Protein–DNA Regulogs.” *Genome Research* 14 (6): 1107–18. https://doi.org/10.1101/gr.1774904.

Zevian, Shannin C., and Judith L. Yanowitz. 2014. “Methodological Considerations for Heat Shock of the Nematode Caenorhabditis Elegans.” *Methods* 68 (3): 450–57. https://doi.org/10.1016/j.ymeth.2014.04.015.

Zhang, Gangming, Long Lin, Di Qi, and Hong Zhang. 2017. “The Composition of a Protein Aggregate Modulates the Specificity and Efficiency of Its Autophagic Degradation.” *Autophagy* 13 (9): 1487–95. https://doi.org/10.1080/15548627.2017.1339843.

Zhang, Hongli, Qianjin Zhou, Yi Yang, Xueqiu Chen, Baolong Yan, and AIFANG DU. 2013. “Characterization of Heat Shock Protein 70 Gene from *Haemonchus Contortus* and Its Expression and Promoter Analysis in *Caenorhabditis Elegans*.” *Parasitology* 140 (6): 683–94. https://doi.org/10.1017/S0031182012002168.

Zhang, Jin, Bobin Liu, Jianbo Li, Li Zhang, Yan Wang, Huanquan Zheng, Mengzhu Lu, and Jun Chen. 2015. “Hsf and Hsp Gene Families in Populus: Genome-Wide Identification, Organization and Correlated Expression during Development and in Stress Responses.” *BMC Genomics* 16 (1): 181. https://doi.org/10.1186/s12864-015-1398-3.

Zhang, William Hongyu, Seda Koyuncu, and David Vilchez. 2022. “Insights into the Links Between Proteostasis and Aging From *C. Elegans*.” *Frontiers in Aging* 3 (March). https://doi.org/10.3389/fragi.2022.854157.

Acknowledgements

I would like to thank my supervisor Prof. Dr. Johannes Buchner for his guidance during the research, valuable suggestions and giving me the opportunity to grow into an independent researcher. I would like to also express my gratitude to Dr. Martin Haslbeck for his scientific support, sharing his knowledge of the chaperone field and his help with many organisational matters. I would like to also acknowledge Prof. Dr. Bernd Reif for his scientific input into my PhD journey by being an active member of my IMPRS Thesis Advisory Committee.

IMPRS-LS provided me with a massive support, including finances, visa matters, various workshops, and lectures. They made it possible for me to meet Johannes and be selected for PhD programme in his lab. I would like to thank the coordination office of IMPRS for their encouragement, guidance and help with an adaptation as a foreigner. It is a big pleasure to be a part of an IMPRS community.

I am grateful to my mentor, Dr. Nicole Lim, who supported me not only as a scientist but was a true friend to me outside the working hours. In addition, it was a pleasure to work with the colleagues from Buchner lab and beyond. I would like to thank them for the distracting conversations, many cakes, to some of them for friendship outside the work and to all of them for an assistance in the lab. Thank you to those whom I shared office with. It was a great and fun atmosphere. In addition, I am grateful to the secretary office, Margot Rubinstein and Anna Semm, who were incredibly supportive in regards of the work contract and visa. It was great to have you on my side in the fight against bureaucracy. Additionally, Anna Hilber, who was also very helpful with SFB-related things and shared the office with me during the pandemic. I also would like to thank Dr. Carsten Peters for our TEM cooperation. Also all the students whom I supervised as well as Hiwis who contributed to the project.

I would like to specially acknowledge Laura Meier for her technical support in the lab and time spent in the practical course together, this made a supervision very fun and interesting. I am also thankful to Bettina Richter for the technical support, lab matters and for helping me with German.

On a less formal note, I am grateful to my last neurons and to my remained not-graying hair for still being with me. I am grateful to my husband, who agreed to join me in my scientific journey to pursue my dreams and who was ready to go through all the rough and marvellous times together, including learning German, Corona pandemic and war in our home country Ukraine. I am also grateful to my family, especially my wonderful mother, who sacrificed a lot so that I could get an education and pursue a scientific career, and who gave so much support, guidance, encouragement, presence and who listened to all my scientific rants with an interest. I am also thankful to the Ukrainian community in Munich and all Ukrainians in general for their/our fight for peace and independence.

Eidesstattliche Erklärung

Hiermit erkläre ich, Yevheniia Bushman, dass ich die vorliegende Arbeit selbständig verfasst habe und keine weiteren, außer den angegebenen Quellen und Hilfsmitteln, verwendet habe. Diese Arbeit wurde bisher keiner Prüfungskommission vorgelegt. Teile der Arbeit wurden bzw. werden in wissenschaftlichen Journalen veröffentlicht.

I, Yevheniia Bushman, hereby declare that this thesis was written by me independently and that only the stated resources and references were used. This work has not been submitted to any audit commission so far. Parts of the work already have been or will be published in scientific journals.

_____

Yevheniia Bushman